



University
of Glasgow

Cameron, Jenifer Mary (2013) Investigating the role of cofilin oxidation in cancer cell migration and invasion. PhD

<http://theses.gla.ac.uk/4770/>

Copyright and moral rights for this thesis are retained by the author

A copy can be downloaded for personal non-commercial research or study, without prior permission or charge

This thesis cannot be reproduced or quoted extensively from without first obtaining permission in writing from the Author

The content must not be changed in any way or sold commercially in any format or medium without the formal permission of the Author

When referring to this work, full bibliographic details including the author, title, awarding institution and date of the thesis must be given.

Investigating the role of cofilin oxidation in cancer cell migration and invasion

Jenifer Mary Cameron
BSc (Hons)

Submitted in fulfilment of the requirements for the
Degree of Doctor of Philosophy

September 2013

The Beatson Institute for Cancer Research
University of Glasgow

Abstract

Cancer cell invasion and metastasis is one of the hallmarks of cancer and is frequently the fatal stage in disease progression. One of the key cellular processes underlying invasion and metastasis is cell migration, which is highly dependent on dynamic changes in the actin cytoskeleton. Reactive oxygen species (ROS) are frequently found at elevated levels in cancer and promote disease progression particularly by increasing invasion and metastasis. Although it is known that ROS, specifically H₂O₂, mediate their downstream effects through the oxidation of proteins on key cysteine residues, very little is known about the direct protein targets of ROS and how the resulting protein oxidation might contribute to cell migration, invasion and metastasis.

I have demonstrated that the ROS, H₂O₂, is produced at increased levels in migrating cells, predominantly at the tips of cell protrusions. Furthermore, I established that protein oxidation is increased in migrating cells and identified the actin binding protein cofilin as one of these oxidised proteins. I have also provided evidence that, when oxidised, cofilin forms oligomers and has a reduced ability to decrease F-actin levels *in vitro*, which was dependent on cysteine residues 139 and 147. Moreover, I have shown that the oxidation of these cysteine residues is important for directional cell migration and adhesion.

Taken together my results provide a direct link between the increased production of ROS at the leading edge of migrating cells and dynamic changes in the actin cytoskeleton that take place in this region to enable cell migration. As the invasion and metastasis of cancer is largely dependent on cell migration, these findings could potentially lead to the development of new ways to target this stage in disease progression.

Table of Contents

Abstract.....	2
Table of Contents	3
List of Tables.....	8
List of Figures	9
Acknowledgements.....	11
Author's Declaration	12
Abbreviations	13
1 Introduction.....	16
1.1 Cancer invasion and metastasis	16
1.2 Cell migration	16
1.2.1 Individual cell migration	18
1.2.2 Collective cell migration.....	19
1.2.3 Flexibility in cell migration modes	19
1.3 Actin cytoskeleton dynamics in cell migration	22
1.4 ADF/cofilin family.....	25
1.5 Cofilin regulation of actin dynamics	25
1.6 Cofilin functions unrelated to actin dynamics	29
1.7 Regulation of cofilin activity	29
1.7.1 Phosphorylation of serine 3.....	29
1.7.2 pH and phosphatidylinositol (4,5) bisphosphate	33
1.7.3 Oxidation	33
1.7.4 Regulation by other proteins	34
1.8 Cofilin cellular functions.....	36
1.8.1 Cell migration.....	36
1.8.2 Cytokinesis	39
1.8.3 Endocytosis.....	39
1.8.4 Apoptosis	39
1.8.5 Cell specific cofilin functions.....	39
1.9 Cofilin in disease	40
1.9.1 Cancer	40
1.9.2 Neurodegenerative diseases	41
1.9.3 Other diseases	42
1.10 Reactive oxygen species	42
1.11 Cell signalling by ROS.....	45
1.11.1 Protein oxidation.....	45
1.12 ROS and cell migration	46
1.12.1 Regulation of cell migration by ROS.....	46

1.12.2	Sources of ROS in migrating cells	48
1.12.3	Localisation of ROS in migrating cells	48
1.12.4	Targets of ROS in migrating cells	49
1.13	ROS and cancer	50
1.13.1	ROS levels in cancer	50
1.13.2	Sources of increased ROS in cancer	51
1.13.3	ROS in cancer invasion and metastasis.....	51
1.14	Project aims	52
2	Materials and Methods.....	53
2.1	Materials.....	53
2.1.1	Reagents and chemicals.....	53
2.1.2	Kits	55
2.1.3	Solutions.....	55
2.1.4	Antibodies	56
2.1.5	Plasticware	57
2.2	Molecular cloning	57
2.2.1	Plasmids	57
2.2.2	Oligonucleotides and primers	58
2.2.3	Annealing oligonucleotides	60
2.2.4	PCR.....	60
2.2.5	Restriction enzyme digestion.....	61
2.2.6	DNA purification.....	61
2.2.7	Determination of DNA concentration.....	62
2.2.8	Ligation of DNA	62
2.2.9	Agarose gel electrophoresis	62
2.2.10	Bacterial transformation	62
2.2.11	Site-directed mutagenesis	63
2.2.12	Plasmid preparation	64
2.2.12.1	Small scale plasmid preparation	64
2.2.12.2	Large scale plasmid preparation	64
2.2.13	DNA Sequencing	64
2.3	Recombinant proteins and <i>in vitro</i> assays.....	65
2.3.1	Recombinant protein production	65
2.3.2	Oxidation of recombinant cofilin	65
2.3.3	Biotin-iodoacetamide labelling of recombinant cofilin.....	66
2.3.4	Preparation of G-actin.....	66
2.3.5	Actin depolymerisation assay.....	67
2.4	Cell culture techniques	67
2.4.1	Origin, maintenance and storage of cell lines	67

2.4.2	Tissue culture treatments.....	68
2.4.3	Transfection of plasmid DNA	68
2.4.4	Establishment of stable cell lines.....	69
2.4.5	Fluorescence activated cell sorting (FACS).....	70
2.4.6	Labelling and detection of oxidised proteins	70
2.4.6.1	Dimedone labelling following NAC treatment	70
2.4.6.2	Dimedone labelling following H ₂ O ₂ treatment	71
2.4.6.3	Dimedone labelling following wounding.....	71
2.4.7	Measurement of ROS production	71
2.4.8	Cell proliferation assay	71
2.4.9	Cell adhesion/spreading assay	72
2.4.10	Cell adhesion assay	72
2.4.11	Wound healing cell migration assay	72
2.4.12	Individual cell migration assay	73
2.4.13	Cell invasion assay	73
2.5	Microscopy	73
2.5.1	Fluorescence lifetime imaging microscopy	73
2.5.1.1	Baseline fluorescence lifetime imaging	74
2.5.1.2	Fluorescence lifetime imaging following H ₂ O ₂ treatment	74
2.5.1.3	Fluorescence lifetime imaging of <i>in vitro</i> wound healing assay.....	74
2.5.1.4	Fluorescence lifetime imaging of cell protrusions.....	74
2.6	Cellular protein extraction and analysis.....	75
2.6.1	Cell lysate preparation	75
2.6.2	Protein concentration determination	75
2.6.3	Immunoprecipitation	76
2.6.4	SDS-polyacrylamide gel electrophoresis	77
2.6.5	Gel staining	77
2.6.6	Western blotting	78
3	Reactive Oxygen Species and Cell Migration	79
3.1	Introduction.....	79
3.2	Results	79
3.2.1	NAC reduces cellular ROS levels in MDAMB231 cells	79
3.2.2	Reducing cellular ROS levels decreases cell migration	80
3.2.3	Establishment of MDAMB231 cell line stably expressing HyPer-cyto	83
3.2.4	Baseline fluorescence lifetime of MDAMB231 HyPer-cyto cells.....	87
3.2.5	HyPer-cyto fluorescence lifetime decreases after the addition of H ₂ O ₂	87

3.2.6	Change in fluorescence lifetime of HyPer-cyto after the addition of H ₂ O ₂ is reversible.....	91
3.2.7	H ₂ O ₂ levels are higher in migrating cells than stationary cells	94
3.2.8	Establishment of MDAMB231 cell line stably expressing HyPer-PM	94
3.2.9	Baseline fluorescence lifetime of MDAMB231 HyPer-PM cells	95
3.2.10	HyPer-PM fluorescence lifetime decreases upon the addition of H ₂ O ₂	95
3.2.11	Change in fluorescence lifetime of HyPer-PM upon H ₂ O ₂ addition is reversible	102
3.2.12	H ₂ O ₂ levels are higher at the plasma membrane in migrating cells than stationary cells.....	102
3.2.13	H ₂ O ₂ levels are elevated at the tips of cell protrusions	106
3.3	Conclusions.....	106
4	Protein Oxidation and Cell Migration	108
4.1	Introduction.....	108
4.2	Results	108
4.2.1	Cellular protein oxidation increases with H ₂ O ₂ treatment	108
4.2.2	Cellular protein oxidation decreases with NAC treatment	109
4.2.3	Cellular protein oxidation is higher in migrating than stationary cells	113
4.2.4	Cofilin is identified as a protein oxidised in cells	115
4.2.5	Cofilin oxidation is higher in migrating than stationary cells.....	117
4.3	Conclusions.....	117
5	Cofilin Oxidation and Actin Dynamics	119
5.1	Introduction.....	119
5.2	Results	119
5.2.1	Purification of actin and cofilin for <i>in vitro</i> actin depolymerisation assay.....	119
5.2.2	Oxidation of recombinant cofilin	120
5.2.3	Oxidation of recombinant cofilin reduces its ability to decrease F-actin levels	124
5.2.4	Generation of cofilin cysteine to alanine mutants	124
5.2.5	Cofilin cysteine residues 139 and 147 are responsible for the reduced ability of cofilin to decrease F-actin levels when oxidised.....	128
5.2.6	Generation of cofilin double cysteine to alanine mutants	129
5.2.7	Cofilin cysteine residue 147 appears to be the cysteine residue predominantly responsible for the reduced ability of cofilin to decrease F-actin levels when oxidised	129
5.2.8	Oxidation of recombinant cofilin results in a reduction in monomer levels and the formation of oligomers	143

5.2.9	Cofilin cysteine residue 147 is predominantly responsible for the reduction in monomer levels and oligomerisation of oxidised recombinant cofilin	145
5.2.10	Cofilin cysteine residues 139 and 147 are almost completely responsible for the reduction in monomer levels and oligomerisation of oxidised recombinant cofilin.....	147
5.3	Conclusions.....	150
6	Cofilin Oxidation and Cell Migration and Invasion.....	151
6.1	Introduction.....	151
6.2	Results	151
6.2.1	Establishment of MDAMB231 cell lines stably expressing mCh, mCh cofilin WT or mCh cofilin C139/147A	151
6.2.2	No difference in proliferation of MDAMB231 cell lines expressing mCh, mCh cofilin WT or mCh cofilin C139/147A	152
6.2.3	mCh cofilin WT and mCh cofilin C139/147A cells show slight decrease in migration	152
6.2.4	mCh cofilin C139/147A cells have reduced directionality	153
6.2.5	mCh cofilin C139/147A cells have reduced spreading/adhesion as measured by xCelligence system	160
6.2.6	mCh cofilin C139/147A cells have reduced adhesion	160
6.2.7	mCh cofilin WT and mCh cofilin C139/147A cells show no difference in invasion.....	163
6.3	Conclusions.....	163
7	Discussion	166
7.1	ROS and cell migration	166
7.2	Protein oxidation and cell migration.....	168
7.3	Cofilin oxidation and actin dynamics.....	169
7.4	Cofilin oxidation and cell migration and invasion	174
7.5	Final conclusions	176
	References.....	179

List of Tables

Table 2-1	List of reagents and chemicals	53
Table 2-2	List of kits	55
Table 2-3	List of solutions and their recipes	55
Table 2-4	List of primary antibodies.....	56
Table 2-5	List of secondary antibodies	56
Table 2-6	List of plasticware.....	57
Table 2-7	List of plasmids and their sources	57
Table 2-8	List of primers, their applications and sequences.....	58

List of Figures

Figure 1-1	Cancer cell metastasis	17
Figure 1-2	Different modes of cell migration	21
Figure 1-3	Proteins involved in mediating changes in the actin cytoskeleton ..	24
Figure 1-4	Model illustrating the regions of cofilin that interact with actin	28
Figure 1-5	Regulation of cofilin phosphorylation status	32
Figure 1-6	Regulation of cofilin activity	35
Figure 1-7	Cellular functions of cofilin.....	38
Figure 1-8	Potential protein products resulting from cysteine oxidation by ROS	47
Figure 3-1	The antioxidant NAC reduces cellular ROS levels	81
Figure 3-2	Decreasing cellular ROS levels with NAC reduces wound closure	82
Figure 3-3	Schematic diagram of H ₂ O ₂ sensing HyPer-cyto probe activation....	84
Figure 3-4	Creation of MDAMB231 cell line stably expressing HyPer-cyto	86
Figure 3-5	Expression and average fluorescence lifetime of HyPer-cyto	88
Figure 3-6	HyPer-cyto fluorescence lifetime decreases after addition of H ₂ O ₂	90
Figure 3-7	HyPer-cyto fluorescence lifetime recovers to baseline levels following H ₂ O ₂ treatment and can be reactivated following further H ₂ O ₂ addition	93
Figure 3-8	H ₂ O ₂ levels elevated in migrating compared to stationary cells	96
Figure 3-9	Schematic diagram of H ₂ O ₂ sensing HyPer-PM probe activation	97
Figure 3-10	Creation of MDAMB231 cell line stably expressing HyPer-PM.....	98
Figure 3-11	Expression and average fluorescence lifetime of HyPer-PM	99
Figure 3-12	HyPer-PM fluorescence lifetime decreases after addition of H ₂ O ₂	101
Figure 3-13	HyPer-PM lifetime recovers to baseline levels following H ₂ O ₂ treatment and can be reactivated following further H ₂ O ₂ addition.....	104
Figure 3-14	H ₂ O ₂ levels elevated at plasma membrane in migrating compared to stationary cells.....	105
Figure 3-15	H ₂ O ₂ levels elevated at tips of protrusions compared to cell bodies.....	107
Figure 4-1	Dimedone irreversibly reacts with oxidised cysteine in its sulfenic acid state.....	110
Figure 4-2	Cellular protein oxidation increases with H ₂ O ₂ treatment.....	111
Figure 4-3	Cellular protein oxidation decreases with NAC treatment.....	112
Figure 4-4	Protein oxidation is increased in migrating cells compared to stationary cells	114
Figure 4-5	Cofilin identified in oxidised state in cells	116
Figure 4-6	Cofilin oxidation increased in migrating cells compared to stationary cells	118
Figure 5-1	Schematic diagram of <i>in vitro</i> actin depolymerisation assay.....	121
Figure 5-2	Purification of cofilin and actin for <i>in vitro</i> assay	122

Figure 5-3	Oxidation of recombinant cofilin with H ₂ O ₂	123
Figure 5-4	Oxidation of cofilin reduces its ability to decrease F-actin levels..	125
Figure 5-5	Cofilin has four cysteine residues.....	126
Figure 5-6	Purification of cofilin cysteine to alanine mutants used for <i>in vitro</i> assay.....	127
Figure 5-7	Cofilin cysteine residues 139 and 147 are responsible for the reduced ability of cofilin to decrease F-actin levels when oxidised.....	130
Figure 5-8	Purification of cofilin double cysteine to alanine mutants for use in <i>in vitro</i> assay	132
Figure 5-9	Cofilin C39/147A mutant can rescue the inhibition in the ability of cofilin to decrease F-actin levels when oxidised.....	135
Figure 5-10	No cofilin cysteine to alanine mutants containing mutated cysteine 80 can rescue the inhibition in the ability of cofilin to decrease F-actin levels when oxidised.....	137
Figure 5-11	Cofilin C139A and C139/147A mutants can rescue the inhibition in the ability of cofilin to decrease F-actin levels when oxidised ..	140
Figure 5-12	Cofilin C147A, C39/147A and C139/147A mutants can rescue the inhibition in the ability of cofilin to decrease F-actin levels when oxidised.....	142
Figure 5-13	Oxidation of recombinant cofilin results in a reduction in cofilin monomer levels and the formation of oligomers.....	144
Figure 5-14	Monomer levels and oligomerisation before and following oxidation of cofilin cysteine to alanine mutants	146
Figure 5-15	Monomer levels and oligomerisation before and following oxidation of cofilin double cysteine to alanine mutants	149
Figure 6-1	Creation of MDAMB231 cell lines stably expressing mCh, mCh cofilin WT or mCh cofilin C139/147A	155
Figure 6-2	No difference in proliferation rate of stable cell lines expressing mCh, mCh cofilin WT or mCh cofilin C139/147A	156
Figure 6-3	Expression of mCh cofilin WT or mCh cofilin C139/147A results in a small decrease in wound closure	158
Figure 6-4	Cells expressing mCh cofilin C139/147A have reduced directionality	159
Figure 6-5	Cells expressing mCh cofilin C139/147A have reduced spreading/adhesion as measured by the xCelligence system.....	161
Figure 6-6	Cells expressing mCh cofilin C139/147A have reduced adhesion ...	162
Figure 6-7	No difference in invasion observed in cells expressing mCh cofilin WT or mCh cofilin C139/147A	165
Figure 7-1	Modelling of the interaction between oxidised cofilin and actin ...	173
Figure 7-2	Proposed model for the involvement of cofilin oxidation in cell migration	178

Acknowledgements

First and foremost, I would like to thank Mike Olson who has been a great supervisor; his constant guidance and encouragement have been really appreciated. Many thanks also to my advisor, Marcos Vidal, for the helpful discussions we have had during our meetings.

Special thanks should also go to the research services and support staff at the Beatson who really are a huge help to us all. Thanks to all R17 members, past and present, and to all the other friends I have made at the Beatson for making the last four years so enjoyable, it would not have been the same without you.

I would also like to thank my family for helping me get to where I am today and for always being there for me. I would especially like to thank my husband, Alasdair, for all his loving support and encouragement especially over the last few months.

Finally, I would like to thank Cancer Research UK for funding this research and all its supporters as without their generous donations this work would not have been possible.

Author's Declaration

I am the sole author of this thesis. All the work presented is entirely my own unless otherwise stated.

Abbreviations

$^1\text{O}_2$	Singlet oxygen
2D	Two-dimensional
3D	Three-dimensional
Ab	Antibody
ADF	Actin-depolymerising factor
ADP	Adenosine diphosphate
Aip1	Actin interacting protein 1
AMT	Amoeboid to mesenchymal transition
ATP	Adenosine triphosphate
BCA	Bicinchoninic acid
Ca^{2+}	Calcium
CAT	Collective-amoeboid transition
CFP	Cyan fluorescent protein
DCFDA	2',7'-dichlorofluorescein diacetate
dH ₂ O	Distilled water
Dimedone	5,5-dimethyl-1,3-cyclohexanedione
DMEM	Dulbecco's Modified Eagle Medium
DMSO	Dimethyl sulfoxide
DNA	Deoxyribonucleic acid
DUOX	Dual oxidase
ECM	Extracellular matrix
EGF	Epidermal growth factor
EMT	Epithelial to mesenchymal transition
FACS	Fluorescence activated cell sorting
F-actin	Filamentous actin
FAD	Flavin adenine dinucleotide
FAK	Focal adhesion kinase
FBS	Fetal bovine serum
FGF	Fibroblast growth factor
FLIM	Fluorescence lifetime imaging microscopy
G-actin	Globular actin
GFP	Green fluorescent protein
GPX	Glutathione peroxidase
GSH	Glutathione
H ₂ O	Water
H ₂ O ₂	Hydrogen peroxide
HGF	Hepatocyte growth factor
HIV	Human immunodeficiency virus
HNO ₄	Peroxynitrate
Hsp90	Heat shock protein 90
HUVEC	Human umbilical vein endothelial cells
IAA	Iodoacetamide
IPTG	Isopropyl B-D-1-thiogalactopyranoside

LIMK	LIM domain kinase
MAT	Mesenchymal to amoeboid transition
mCh	mCherry
MEFs	Mouse embryonic fibroblasts
MMP	Matrix metalloproteinases
MRCK	Myotonic dystrophy kinase-related Cdc42-binding kinase
NAC	N-acetylcysteine
NADPH	Nicotinamide adenine dinucleotide phosphate
NESK	Nck-interacting kinase-like embryo-specific kinase
NaOH	Sodium hydroxide
NLS	Nuclear localisation sequence
NO	Nitric oxide
NOX	NAPDH oxidase
O ₂	Oxygen
O ₂ ⁻	Superoxide
O ₃	Ozone
PA	Phosphatidic acid
PAGE	Polyacrylamide gel electrophoresis
PAK	p21-activated kinase
PC	Phosphatidylcholine
PCR	Polymerase chain reaction
PDGF	Platelet-derived growth factor
Pi	Inorganic phosphate
PIP ₂	Phosphatidylinositol (4,5) bisphosphate
PKD	Protein kinase D
PLC	Phospholipase C
PLD1	Phospholipase D1
PMSF	Phenylmethylsulfonyl fluoride
PP1	Protein phosphatase 1
PP2A	Protein phosphatase 2A
PTPs	Protein tyrosine phosphatases
RNA	Ribonucleic acid
ROCK	Rho-associated coiled-coil containing kinase
ROS	Reactive oxygen species
rpm	Revolutions per minute
SD	Standard deviation
SDM	Site-directed mutagenesis
SEM	Standard error of the mean
SF	Serum free
SOD	Superoxide dismutase
SSH	Slingshot
TESK	Testis-specific kinase
TnCl	Taurine chloramine
U	Units
V	Volts
VEGF	Vascular endothelial growth factor

WT
YFP

Wild type
Yellow fluorescent protein

1 Introduction

1.1 Cancer invasion and metastasis

Cancer cell invasion and metastasis, or the spread of cancer cells into surrounding tissues and eventually to distant sites in the body, is one of the hallmarks of cancer as described by Hanahan and Weinburg [1]. Metastasis is a multi-step process that involves invasion of cancer cells into tissues surrounding the primary tumour, intravasation into local blood and lymphatic vessels, dissemination to distant sites in the body, extravasation into tissues and finally the formation of secondary tumours (Figure 1-1) [2]. A number of cellular changes occur that enable a cancer cell to become invasive and metastasise, but the main consequences are cells have reduced cell-cell adhesion and increased migration. These changes closely mirror those frequently observed during embryonic development to allow the remodelling of tissues, a process known as epithelial to mesenchymal transition (EMT). Indeed, many transcription factors that are activated during EMT have been implicated in cancer invasion and metastasis [3]. As the growth of secondary tumours, metastases, is the cause of 90% of cancer deaths it is essential that we gain an extensive understanding of the molecular mechanisms that contribute to this process so we can develop ways to target and prevent this fatal step in cancer progression [4].

1.2 Cell migration

Cell migration is essential for many processes including embryonic development, wound healing and inflammation [5-7]. It also contributes to the development of diseases such as cardiovascular disease and cancer [8, 9]. All eukaryotic cells will undergo cell migration at some stage whether it is for a defined period such as during development and wound healing, or throughout its lifetime as is the case for leukocytes. There are a number of ways in which a cell can migrate, broadly categorised as individual or collective cell migration. Which method a cell adopts will depend on properties of the cell and the nature of the extracellular environment in which it is located [10, 11].

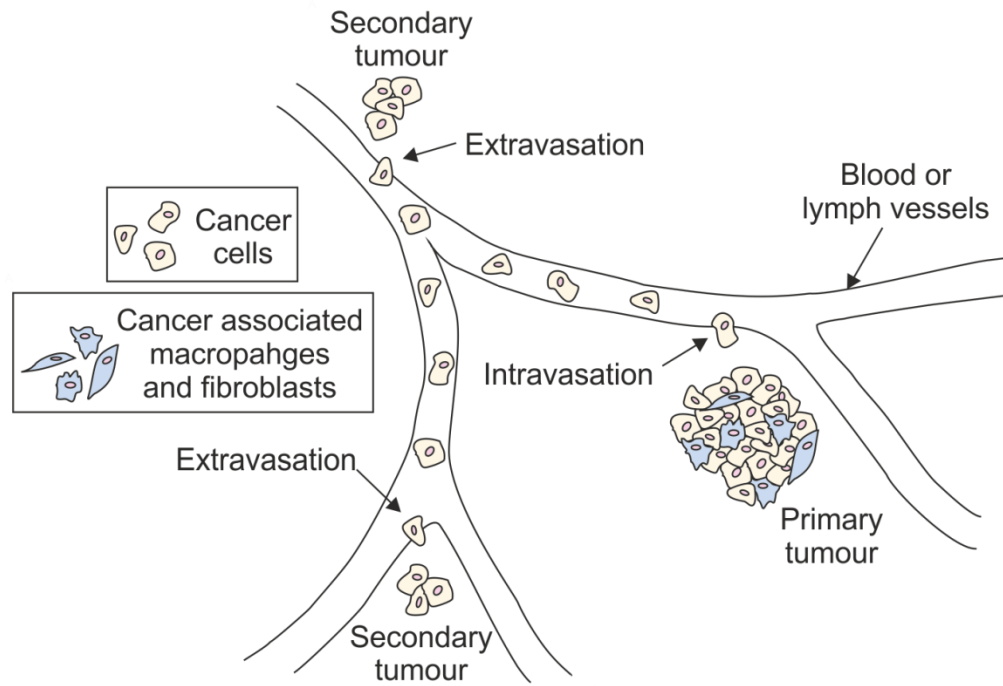


Figure 1-1 Cancer cell metastasis

Diagram illustrating cancer metastasis; the spread of cancer cells from the primary tumour to a distant site in the body where secondary tumours can form. Adapted from [12].

1.2.1 Individual cell migration

The migration of individual cells is important for a number of cell types including leukocytes and neural crest cells, and has also been observed to be used by some cancer cells [9, 13, 14]. There are two main types of individual cell migration; amoeboid and mesenchymal. These differ in a number of key ways including morphology, organisation of the actin cytoskeleton, interaction with the extracellular matrix (ECM), method of moving through the ECM and speed (Figure 1-2) [15] .

An amoeboid mode of cell migration is used by cells such as immune cells and cancer cells [13, 16, 17]. This type of cell migration is characterised by a rounded morphology, the presence of cortical actin and low levels of adhesion to the ECM [10]. These very weak interactions are thought to be the reason that cells utilising this mode of migration are able to move at high speeds of up to 25 $\mu\text{m}/\text{minute}$ [18]. Association of myosin with cortical actin gives these cells enhanced cortical actomyosin contractility and therefore allows cells to move through the ECM by changing their shape to squeeze through pre-existing spaces. This actomyosin contractility can also generate force that enables cells to push their way through the ECM. Additionally, the tension created by this cortical actomyosin can lead to the formation of membrane blebs, which also contribute to migration [17, 19]. Therefore, cells that use an amoeboid mode of cell migration can move through the ECM by squeezing through spaces that are already present or by pushing their way through by force generated from cortical actomyosin and membrane blebs.

A mesenchymal mode of cell migration is used by cells such as neural crest cells and cancer cells [14, 17]. Mesenchymal migration is characterised by an elongated, spindle like morphology, the presence of actin stress fibres extending between the poles of the cell and high levels of adhesion to the ECM [10]. Cells that migrate in this way, move at speeds of 0.1 - 2 $\mu\text{m}/\text{minute}$, which is thought to be due to the high levels of adhesion to the ECM and the slow turnover of these [20]. There are a number of well defined steps that occur during mesenchymal cell migration. Firstly, an actin rich protrusion is formed at the front of the cell through which the cell adheres to the ECM and recruits adhesion molecules that lead to the formation of focal adhesions. Proteolytic enzymes are

also recruited to these focal adhesions to degrade the ECM, generating a path that the cell can move through. Loss of cell adhesions at the rear of the cell and contraction of actin stress fibres, by the activity of myosin proteins, results in the translocation of the cell [15]. This cycle then repeats and the cell moves forward. In contrast to amoeboid cell migration, cells that use a mesenchymal mode of cell migration move through the ECM by degrading and remodelling it to create paths that the cells can move through using their strong cell-matrix adhesions and contractile forces.

1.2.2 Collective cell migration

Collective cell migration occurs when groups of cells that are attached together move simultaneously. This type of migration is essential for many developmental processes for example the migration of *Drosophila* border cells, lateral line primordium cells in zebrafish and gastrulation in the embryo of multicellular organisms [5, 21, 22]. It is also necessary for wound healing and has been observed to occur during the invasion of cancer cells [6, 9]. In collective migration, cell-cell contacts are retained, unlike in individual cell migration, allowing cells to move as strands, sheets or clusters of cells (Figure 1-2) [10]. In these groups of cells it is only those at the leading edge that have properties similar to individually migrating cells such as generation of actin rich protrusions or blebs, formation of focal adhesions, and degradation and remodelling of the ECM [23, 24]. Cells at the rear of the group migrate passively due to their physical coupling to the cells at the front that are actively migrating [25].

1.2.3 Flexibility in cell migration modes

Although most cell types have a predominant mode of cell migration, it is now appreciated that cells can switch to an alternative type of migration under certain circumstances (Figure 1-2). Changes in the extracellular environment or properties of the cell that inhibits a particular mode of migration can result in the cell shifting to a different mode so that its movement is not stopped completely [11]. The ability to change the mode of cell migration is important for the maturation of macrophages and endothelial cells and has also been observed in the progression and invasion of cancer cells [10].

Epithelial to mesenchymal transition (EMT) occurs when cells lose cell-cell junctions while maintaining cell-matrix interactions, migratory and ECM remodelling capabilities. This enables them to break away from other cells and migrate in a mesenchymal mode. EMT is involved in many stages of development and thought to be a critical stage in the progression of cancers originating from epithelial tissues [3]. In a similar way, if a cell loses cell-matrix interactions in addition to cell-cell junctions, it will shift from a collective to amoeboid mode of migration. This is known as collective-amoeboid transition (CAT) and has been observed in melanoma explants [26]. The reverse of EMT and CAT can also occur if cell-cell adhesion is enhanced, resulting in cells migrating collectively rather than individually [27, 28].

The other shift in migration mode that has been observed to occur is between the two types of individual cell migration; amoeboid and mesenchymal. A key pathway determining whether an amoeboid or mesenchymal mode of cell migration is adopted is the balance between Rho and Rac signalling pathways. Increased Rho/Rho-associated coiled-coil containing kinase (ROCK) signalling leads to enhanced actomyosin contractility and an amoeboid type migration while increased Rac activity results in more cell protrusions and a mesenchymal type migration [17, 29]. Additionally, a decrease in cell-matrix interactions or loss of proteolytic activity at the leading edge can result in a mesenchymal to amoeboid transition (MAT) [30, 31]. Conversely, inhibition of Rho/ROCK signalling which results in an amoeboid to mesenchymal transition (AMT), causes an increase in cell-matrix interactions and proteolytic activity [32]. Transition between mesenchymal and amoeboid modes of cell migration is relatively rapid compared to EMT that involves a number of changes to gene transcription. It is thought this quick transition allows cells to respond promptly to changes in the environment so cell migration is not inhibited [15].

The range of migration modes used by cells and the transitions between them has been extensively studied in cancer cells. This flexibility in migration is likely to contribute to invasion and metastasis which requires cells to migrate and invade through many tissues that have very different physical properties and activate different signalling pathways within the cell.

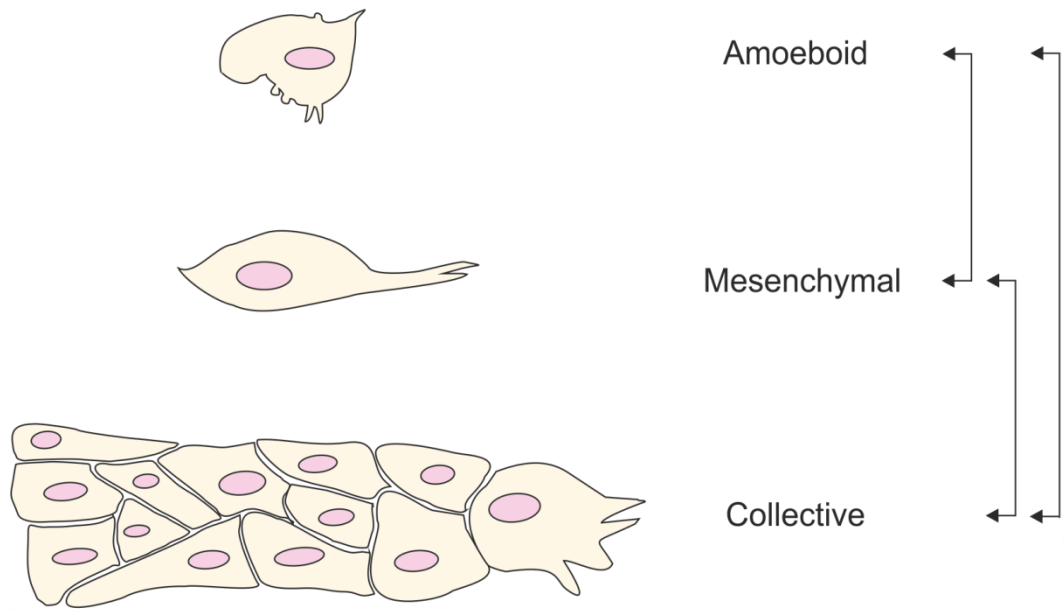


Figure 1-2 Different modes of cell migration

Diagram illustrating the different modes of cell migration that differ in morphology, organisation of the actin cytoskeleton, interaction with the extracellular matrix, method of moving through the ECM and speed. Arrows represent the transitions in cell migration modes that can occur. Figure adapted from [11].

1.3 Actin cytoskeleton dynamics in cell migration

The actin cytoskeleton consists of a network of actin filaments (F-actin) which are polymerised from actin monomers (G-actin). Each filament has a 'barbed' or 'plus' end where new monomers are constantly being added and a 'pointed' or 'minus' end that undergoes depolymerisation. Only adenosine triphosphate (ATP) loaded G-actin is added to the 'barbed' end, and over time the ATP is hydrolysed to adenosine diphosphate (ADP) and inorganic phosphate (Pi). The Pi is then released leaving ADP loaded F-actin which is depolymerised from the 'pointed' end. The ADP on the released actin monomer is exchanged for ATP and the ATP-G-actin is ready to be reincorporated into F-actin. This process is constantly occurring and is known as actin treadmilling. In addition to these continual changes to each filament, the actin cytoskeleton as a whole undergoes constant dynamic changes and this is particularly important during cell migration [33, 34]. There are a number of proteins that mediate these changes in the actin cytoskeleton but the main mediators and how they contribute to the formation of membrane protrusions involved in cell migration are summarised here (Figure 1-3).

The Arp2/3 complex binds to the sides of pre-existing actin filaments and initiates the formation of new filaments generating a branched actin network. It is activated through interactions with members of the WASP family of proteins [35]. The Arp2/3 complex is central to the formation of lamellipodia, which are flat sheet-like protrusions, and invadopodia which are actin rich protrusions that have the ability to degrade the ECM [36, 37]. In some situations it has also been found activated in filopodia, which are networks of parallel actin filaments [38]. Other well established actin regulators are members of the formin family of proteins. Formins can initiate the formation of new actin filaments as well as promoting elongation by binding to the barbed end of filaments and allowing the addition of new monomers while preventing capping proteins from blocking elongation [39]. Formins are major mediators of actin polymerisation that lead to the formation of actin stress fibres, filopodia, invadopodia and lamellipodia [40-43]. Members of the Ena/VASP family also promote filament elongation by preventing capping and therefore blocking of actin polymerisation and have been found in the leading edge of lamellipodia and required for the formation of

filopodia [44-46]. Additionally, the spire family of proteins can nucleate new actin filaments [47].

As well as proteins that directly increase actin filament nucleation and polymerisation, there are regulators that alter the structure of the actin cytoskeleton in different ways. Fascin can bundle actin filaments together, which has been shown to be important for the stability of filopodia and invadopodia [48]. Cofilin severs actin filaments, reducing the length of filaments in addition to providing new barbed ends for polymerisation and branching by other actin regulators. Cofilin is essential for both lamellipodia and invadopodia [49, 50]. Cortactin has been shown to activate the Arp2/3 complex and to stabilise branched actin networks and is important for the functions of both lamellipodia and invadopodia [51-53]. Profilin can bind to G-actin and has been described to promote both actin polymerisation and depolymerisation under different circumstances [54].

These mediators of actin cytoskeleton dynamics are tightly controlled in cells by a range of regulatory mechanisms. In particular, the Rho family of GTPases including Rho, Rac and Cdc42 are well known to be key regulators of the actin cytoskeleton, acting through proteins such as those described above [55]. Signalling through these and other pathways ensures that protrusions are generated and cells migrate only when necessary. Indeed, in invasive cancer cells many of these proteins and components of their upstream signalling pathways are upregulated, contributing to the migration, invasion and metastasis of cancer cells [56].

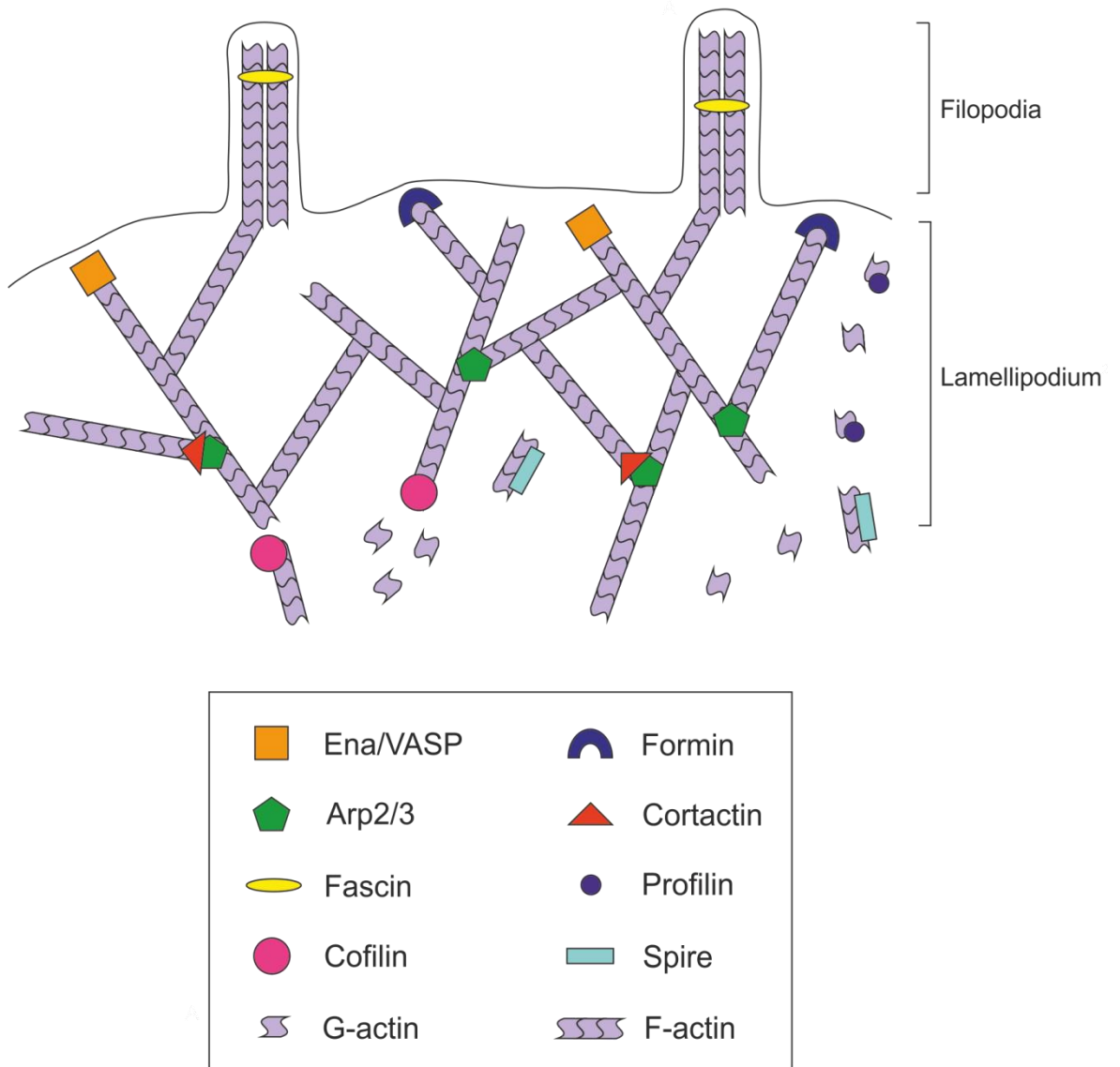


Figure 1-3 Proteins involved in mediating changes in the actin cytoskeleton

The actin cytoskeleton undergoes constant dynamic changes that are mediated by a number of proteins. This diagram illustrates the main proteins involved in altering the structure of the actin cytoskeleton. Figure adapted from [55] and [57].

1.4 ADF/cofilin family

The actin-depolymerising factor (ADF)/cofilin family of small actin binding (15-21 kDa) proteins have a characteristic three-dimensional (3D) fold known as the ADF-homology domain that binds to actin [58, 59]. This domain is also present in two structurally and functionally different families of proteins, twinfilins and debrin/Abp1s [60]. The ADF/cofilin family are ubiquitously expressed throughout eukaryotes, with unicellular eukaryotes such as yeast expressing just one protein and multicellular organisms producing several. In mammals there are three isoforms; ADF, cofilin-1 and cofilin-2 which have been shown to be expressed in different cell types. Cofilin-1 is the main isoform as it is expressed in most cells in both embryos and adult mice, with the exception of mature skeletal muscle, while cofilin-2 is restricted to muscle and ADF to epithelial and endothelial tissues [61, 62]. In addition to being differentially distributed in tissues, these three proteins have overlapping but also distinct roles in cells. This was observed in cell culture studies where the phenotype of cofilin-1 knockdown cells could be rescued by the overexpression of ADF and the reverse was also true [63]. Furthermore, loss of the yeast cofilin gene is lethal but can be rescued by both mammalian ADF and cofilin [64]. In contrast, knockout of cofilin-1 in mice is embryonic lethal and although the resultant ADF overexpression enables gastrulation to occur, it is not sufficient to rescue later stages of development [65]. In ADF knockout mice, there are no problems during development but shortly after birth they become blind due to hyperproliferation of the cornea epithelial cells, which is not rescued by the increased cofilin expression observed in these mice [66]. Additionally, cofilin-1 and cofilin-2 are both expressed in developing muscle but do not have the same affinity for F-actin and could therefore have different roles in muscle development [67].

As the focus of this project has been cofilin-1, from now on I will refer to this isoform as cofilin.

1.5 Cofilin regulation of actin dynamics

Cofilin can bind to both G-actin and F-actin [68]. There are two actin binding regions in cofilin, one that can bind both G-actin and F-actin and one that binds only F-actin. These were highlighted during systematic mutagenesis studies of

yeast cofilin and were modelled recently from the crystal structure of human cofilin [69, 70]. This modelling, in addition to previous electron cryomicroscopy experiments, revealed that cofilin binds to F-actin in a cooperative manner by binding to two actin monomers in a filament (Figure 1-4) [71]. Cofilin has a higher affinity for ADP-actin monomers than ATP-actin monomers and also preferentially binds to older actin filaments where ATP has been hydrolysed to ADP [72, 73]. The binding of cofilin to actin can have a number of different effects. When bound to F-actin, cofilin induces a conformational twist in the filament which reduces the crossover between adjacent actin subunits. This weakens the filaments and is proposed to result in severing of the filament [71, 74-76]. However, more recent studies suggest that the twist in the actin filament induced by cofilin is actually stabilised by the binding of cofilin to two monomers. In this model, it is the sites distant from cofilin binding that are weakened and are the points of severing [77]. Alternatively there is evidence supporting the hypothesis that cofilin severing occurs at the boundaries between the cofilin-bound and cofilin-unbound regions of F-actin [78, 79]. Although these studies suggest that cofilin severs F-actin at different sites, they all agree that severing of actin filaments is a major role of cofilin.

Cofilin has also been shown to increase the rate of actin monomer dissociation from the 'pointed' end [80]. Although it is highly debated as to whether this is indeed a function of cofilin, there are lines of evidence and models that support it. The destabilising effect of cofilin on actin filaments could extend to the weakening of interactions between actin subunits at the end of the filament, thereby increasing monomer dissociation [77]. Cofilin can also enhance the release of Pi after ATP bound to actin filaments is hydrolysed, thereby increasing the rate of filament maturation and consequently the dissociation of actin monomers from the 'pointed' end [81]. Additionally cofilin binds to ADP-actin and inhibits the exchange of ATP for ADP, therefore altering the concentration of ATP-actin available for incorporation into new filaments and consequently promoting dissociation [82]. In contrast to the involvement of cofilin in reducing F-actin levels by severing or monomer dissociation, it has been shown that cofilin can lead to the nucleation of G-actin and the formation of new filaments [72]. Furthermore cofilin has been found to promote the formation of actin rods, which are F-actin filaments that are bundled together [83, 84]. Cofilin can also

regulate the branching of actin filaments by competing with Arp2/3 and dissociating it and actin branches from filaments [85].

As it has been described, cofilin has a number of roles in the regulation of actin dynamics and at times these appear to be opposing. It is likely that the final outcome of cofilin activity is determined not just by cofilin alone but the presence of other actin regulatory proteins. For example, if there are high levels of capping proteins that block polymerisation, it is likely that cofilin severing of actin would result in an overall decrease in F-actin. In contrast, high formin, Arp2/3 complex and profilin levels could lead to increased polymerisation as cofilin would provide additional barbed ends for these proteins for the initiation of actin polymerisation. An additional level of control has become apparent more recently where the outcome of cofilin activity is dependent on its concentration [86]. At low concentrations, cofilin severs actin filaments while at high concentrations it promotes nucleation. It is proposed that at intermediate levels of cofilin, filaments are stabilised and not severed, which is in line with previous findings [77]. Furthermore, at excessively high levels of cofilin, actin rods form that are highly decorated with cofilin, sequestering it from performing any other functions [84].

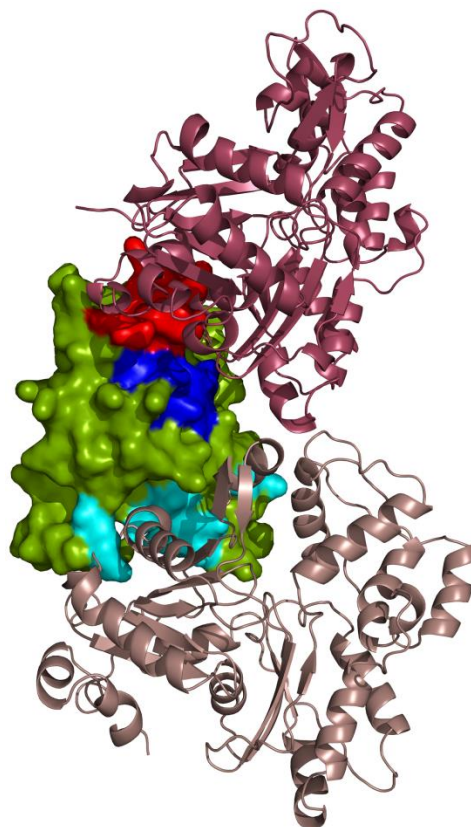


Figure 1-4 Model illustrating the regions of cofilin that interact with actin

The dark blue area highlights the region of cofilin (green) that interacts with G-actin or one actin subunit in F-actin (raspberry). The cyan area highlights the region of cofilin that interacts with a second actin subunit in F-actin (beige). The red area indicates a region of cofilin that would clash with actin, however this model predicts residues in this area would shift to allow an induced fit between cofilin and actin. Model taken from [70].

1.6 Cofilin functions unrelated to actin dynamics

It is now appreciated that cofilin has several roles that are not related to altering the structure of the actin cytoskeleton. One of these is in translocating actin to the nucleus. Actin has several functions in the nucleus including influencing the transcription activity of all three ribonucleic acid (RNA) polymerases and as a component of chromatin remodelling complexes and ribonucleoproteins; however, it has no nuclear localisation sequence (NLS) [87]. Consequently it must depend on binding to proteins that have an NLS, such as cofilin [88]. In support of this theory, ATP depletion in mast cells results in the nuclear translocation of actin that is dependent on cofilin [89]. In addition to chaperoning actin to the nucleus, cofilin has been implicated in RNA polymerase II transcription activity [90].

A second role of cofilin that is independent of actin is the induction of cell death by apoptosis and necrotic-like programmed cell death. Under conditions of oxidative stress, either directly from oxidants or through compounds that increase oxidant levels in cells, cofilin translocates to the mitochondria [91-93]. Here it mediates the opening of the permeability transition pore which enables the release of cytochrome c and consequently apoptosis [94].

A further actin independent cofilin function is the regulation of lipid metabolism. Cofilin can directly interact with and activate phospholipase D1 (PLD1), which hydrolyses phosphatidylcholine (PC) in cell membranes to phosphatidic acid (PA) [95]. PA is involved in a large number of cellular processes, suggesting that cofilin could therefore be involved in their regulation indirectly. [96, 97].

1.7 Regulation of cofilin activity

1.7.1 Phosphorylation of serine 3

The main way by which cofilin activity is regulated is through the phosphorylation status of its serine 3 residue (Figures 1-5 and 1-6). When phosphorylated on serine 3, cofilin is inactivated with respect to its actin modulating activities [98]. This phosphorylation prevents cofilin from binding to both G-actin and F-actin due to the negatively charged phosphate forming an

electrostatic interaction with two lysine residues (lysine 126 and lysine 127). These lysines are normally involved in cofilin binding to actin so when they interact with phosphorylated serine 3, binding is prevented [99, 100]. Cofilin also needs to be dephosphorylated to translocate to the mitochondria and induce apoptosis [93]. In contrast to this, phosphorylation of cofilin is required for it to activate PLD1 [95].

There are five kinases reported to phosphorylate and regulate the activity of cofilin; LIM domain kinases 1 and 2 (LIMK1 and LIMK2), testis-specific kinases 1 and 2 (TESK1 and TSK2) and Nck-interacting kinase-like embryo-specific kinase (NESK) (Figure 1-5) [101-106]. LIMK1 and 2 are activated by phosphorylation predominantly downstream of the Rho GTPases Rho, Rac and Cdc42. Rho and Cdc42 induce the phosphorylation of both LIMK1 and 2 through ROCK and myotonic dystrophy kinase-related Cdc42-binding kinase (MRCK) respectively [107-109]. Rac has been reported to induce the phosphorylation of LIMK1 downstream of p21-activated kinase (PAK) 1 and 4 [110, 111]. Furthermore LIMK1 can be phosphorylated and activated by kinases activated by adhesion to fibronectin and vascular endothelial growth factor (VEGF) signalling [112, 113]. LIMK1 can be dephosphorylated and inactivated by the phosphatase slingshot (SSH) [114].

In contrast to LIMK1 and 2, relatively little is known about the upstream regulators of TSK1 and 2, but their regulation is understood to mainly occur through integrin dependent adhesion. TSK1 is inhibited by binding to actopaxin and 14-3-3B but these interactions are dissociated by integrin binding to fibronectin [115, 116]. TSK1 is also inhibited by binding to sprouty-4 and spred1 [117, 118].

In addition to cellular kinases that phosphorylate cofilin, there are phosphatases that dephosphorylate it (Figure 1-5). Members of the SSH family, chronophin and the serine/threonine phosphatases protein phosphatase 1 (PP1) and protein phosphatase 2A (PP2A) are such enzymes [119-121]. As for the TSKs, little is known about the upstream regulators of these phosphatases. Association of the SSH family member SSH1L with F-actin enhances its activity [122]. SSH1L is also dephosphorylated and activated by increases in intracellular calcium (Ca^{2+}) through the phosphatase calcineurin [123]. Conversely SSH1L is inactivated by

PAK4 and protein kinase D (PKD) mediated phosphorylation [114, 124]. Phosphorylation of SSH1L by these enzymes results in it binding to the scaffolding protein 14-3-3 and consequently prevents it from binding to and being activated by F-actin [114, 122, 124]. Inhibition of SSH1L by 14-3-3 can be released by the oxidation of the cysteine residues of 14-3-3 [125]. The phosphatase chronophin is inhibited through its interaction with heat shock protein 90 (hsp90) but when ATP is depleted this interaction is disrupted, releasing chronophin and enabling it to dephosphorylate cofilin [126].

The many kinases and phosphatases that alter the phosphorylation status and activity of cofilin and the array of upstream signalling pathways that regulate these proteins highlights the central importance of cofilin phosphorylation as a mechanism of its regulation (Figure 1-5).

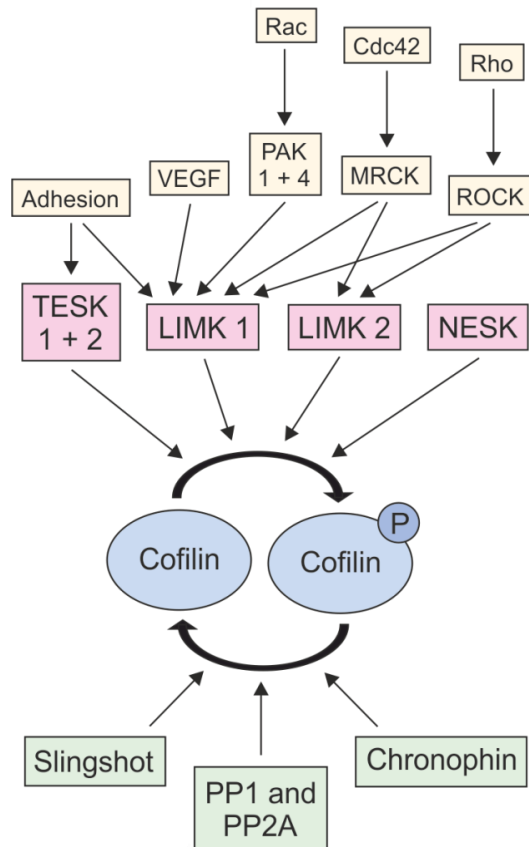


Figure 1-5 Regulation of cofilin phosphorylation status

Diagram showing the many kinases and phosphatases that can change the phosphorylation status and therefore activity of cofilin. Signalling pathways that are known to result in the activation of these enzymes are also shown.

1.7.2 pH and phosphatidylinositol (4,5) bisphosphate

It has been known for a number of years that phosphatidylinositol (4,5) bisphosphate (PIP₂) can bind to cofilin and prevent it from interacting with G-actin [127]. This is due to the fact that the PIP₂ and actin binding sites on cofilin overlap and therefore PIP₂ bound cofilin cannot interact simultaneously with actin [128, 129]. The hydrolysis of PIP₂ by phospholipase C (PLC) after epidermal growth factor (EGF) stimulation releases cofilin from its interaction with PIP₂ and allows it to bind to actin. Altering the kinetics of this process interferes with cofilin function [130, 131]. pH has also been shown to regulate cofilin activity both *in vitro* and *in vivo* with a higher pH increasing cofilin activity [132, 133]. Recent studies have highlighted that the pH and PIP₂ control of cofilin function are in fact not separate mechanisms but part of the same regulatory pathway, since PIP₂ binding to cofilin appears to be pH dependent with decreased binding at higher pH (Figure 1-6). It is suggested that the protonation of histidine 133 in cofilin is required for PIP₂ to bind and therefore at a higher pH this protonation is lost leading to a decrease in PIP₂ binding and consequent increase in cofilin activity [134].

1.7.3 Oxidation

The first evidence indicating that cofilin could be regulated by oxidation came from *in vitro* studies showing that cofilin formed dimers and oligomers, and that these multimers exhibited actin bundling rather than severing activity. The data suggested that oligomers are formed by disulphide bonds between cysteines 39 and 147 [135]. Shortly after this discovery, cell culture studies identified cofilin as one of the proteins that is glutathionylated (a product of oxidation) in oxidatively stressed T cells [136]. Furthermore, oxidation of cofilin is required for it to translocate to the mitochondria and mediate oxidant-induced apoptosis and necrotic-like programmed cell death. Both of these responses are suggested to be due to the formation of intramolecular disulphide bonds between cysteines 39 and 80 and cysteines 139 and 147 or just cysteines 39 and 80 respectively [91, 94]. Additionally, the altered actin dynamics observed in T cells during conditions of oxidative stress is attributed to oxidation of cofilin and the formation of an intramolecular disulphide bond between cysteines 39 and 80 (Figure 1-6) [137].

1.7.4 Regulation by other proteins

Tropomyosins are a large family of proteins consisting of more than 40 isoforms that bind to and stabilise actin filaments, preventing cofilin from disassembling them [68, 138, 139]. Due to the competitive binding of these proteins, it was thought that all tropomyosins would inhibit cofilin activity; however, one of the isoforms has now been found to associate with cofilin on the same actin filament (Figure 1-6) [140]. It is possible that with such a large number of tropomyosin isoforms, this is not the only one with a cooperative rather than competitive role. Actin interacting protein 1 (Aip1) is another actin binding protein that can modulate cofilin activity (Figure 1-6). Aip1 collaborates with cofilin to enhance its actin disassembling function by binding to barbed ends of filaments and blocking polymerisation [141, 142]. CAP/Srv2 is another protein that can enhance the filament disassembling function of cofilin by accelerating the release of cofilin from ADP-actin subunits allowing it to continue to sever more filaments (Figure 1-6) [143, 144]. Coronin can also alter cofilin activity depending on the nucleotide state and age of the F-actin. In new filaments, that are loaded with ATP or ADP+Pi, coronin blocks cofilin from severing them but in older, ADP loaded filaments, coronin amplifies cofilin severing (Figure 1-6) [145]. Finally cortactin can bind to cofilin and inhibit its actin severing function (Figure 1-6) [146].

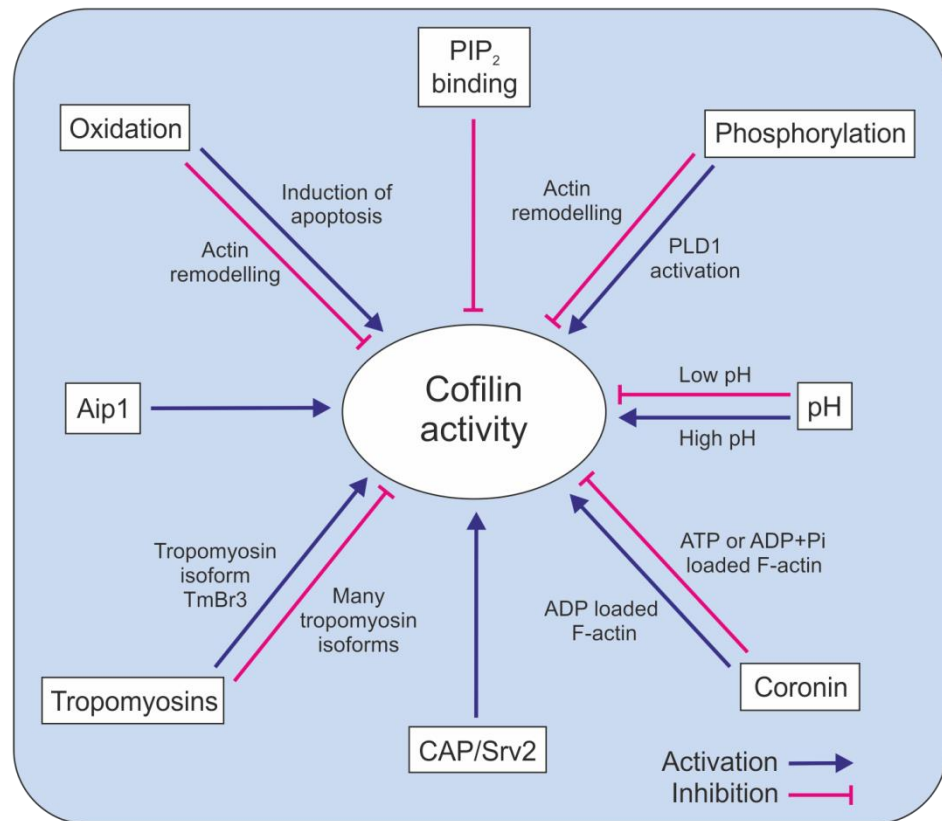


Figure 1-6 Regulation of cofilin activity

Diagram summarising the many ways in which cofilin activity can be activated and inhibited. Cofilin can be regulated by post translational modifications (phosphorylation and oxidation), proteins that compete with cofilin for actin binding (many tropomyosins and coronin), proteins that collaborate with cofilin to enhance actin filament severing and depolymerisation (Aip1, CAP/Srv2, tropomyosin isoform TmBr3 and coronin), phospholipids and pH.

1.8 Cofilin cellular functions

The number of mechanisms that exist to regulate cofilin activity, and the even greater diversity of signalling pathways that feed into these, highlights the central importance of cofilin in modulating cellular processes. As the predominant role of cofilin is in remodelling the actin cytoskeleton, cellular processes that require dynamic changes in actin structure are likely to involve cofilin. Indeed cofilin has been implicated in cell migration, cytokinesis, endocytosis, apoptosis and cell specific functions (Figure 1-7).

1.8.1 Cell migration

In order for cells to migrate they must first extend membrane protrusions, such as lamellipodia, filopodia, invadopodia and blebs at the leading edge of the cell. All these protrusions depend on dynamic changes in the actin cytoskeleton and both lamellipodia and invadopodia have been directly shown to require cofilin.

Development of lamellipodia depends on the activity of cofilin as inhibition of cofilin prevents lamellipod extension (Figure 1-7) [147, 148]. It was originally proposed that cofilin acted at the rear of the lamellipodia to disassemble actin, replenishing the pool of actin monomers required for polymerisation. This was based on the observation that cofilin preferentially bound to and disassembled filaments at the rear of the lamellipodia [149, 150]. Later studies supported this model, showing that cofilin promotes lamellipodium formation by depolymerising filaments and increasing G-actin levels [151, 152]. However, it has also been suggested that cofilin severs filaments generating additional barbed ends from which polymerisation can occur [130, 153, 154]. Furthermore, cofilin has been implicated in determining the direction of lamellipod growth by providing an initial burst of free barbed ends [155, 156]. Two models have been described that could explain these different roles of cofilin. In one, where cells are in continuous movement and availability of actin monomers is a limiting factor, cofilin disassembles filaments at the rear of protrusions to supply new monomers for polymerisation. In the other model, migration is stimulated for example by a chemoattractant such as EGF. In this situation cofilin enhances polymerisation and sets the direction of movement by severing actin filaments and generating a rapid increase in the available barbed ends for polymerisation [157]. In reality it

is possible that these two outcomes are not mutually exclusive and that a cell uses both at different stages of lamellipodia growth depending on local signalling and the presence of other actin remodelling proteins.

Cofilin has also been implicated in the maturation but not the initial assembly of invadopodia (Figure 1-7) [37]. The activity of cofilin is restricted to the core of the invadopodia by the RhoC GTPase which specifically induces the phosphorylation and inactivation of cofilin around the periphery of the invadopodia while leaving cofilin in the core active [158]. This results in filaments in the centre of the invadopodia being severed, creating new barbed ends and increasing G-actin levels for the polymerisation of new filaments resulting in the elongation of invadopodia [146, 159].

As cofilin was identified as one of the components required to recreate actin based motility *in vitro*, it is likely to be involved in the migration of all cells [160]. However, there are some specific cell types that have been proven directly to require cofilin for their migration. During development in mice, cofilin is essential for the polarisation and migration of neural crest cells to close the neural tube. This is the reason that cofilin knockout mice embryos do not survive past gastrulation [65]. Three different types of immune cells; macrophages, neutrophils and T cells, also depend on cofilin for migration [161-163]. Interestingly T cells require cofilin for migration in 3D but not in two-dimensional (2D) environments [162].

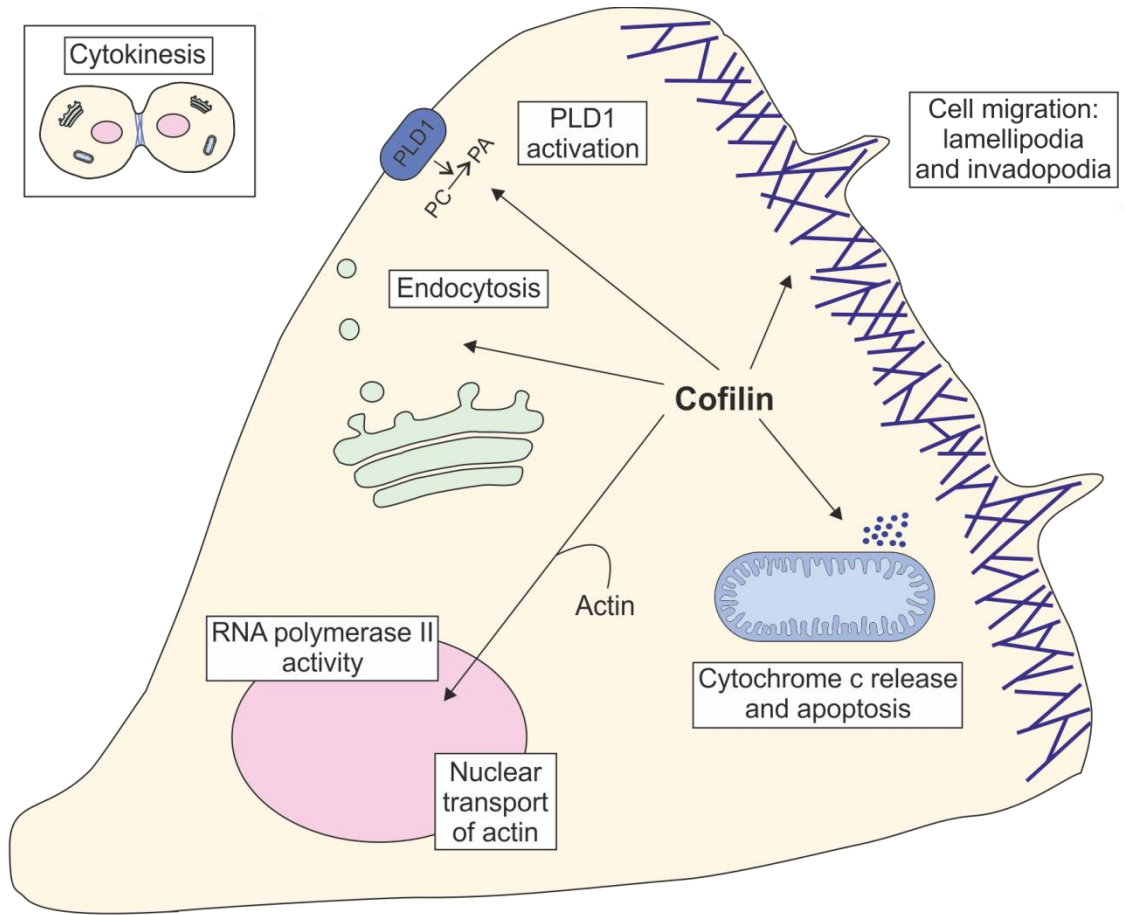


Figure 1-7 Cellular functions of cofilin

Diagram illustrating the many cellular functions of cofilin including those that involve dynamic changes in the actin cytoskeleton and those that are unrelated to actin dynamics. Figure adapted from [164].

1.8.2 Cytokinesis

Cofilin contributes to cytokinesis in several organisms including fission yeast, fruit flies, nematodes and frogs (Figure 1-7) [165-168]. It concentrates at the cleavage furrow in dividing cells and is required for the correct assembly of the contractile ring which constricts to separate the two daughter cells [169, 170].

1.8.3 Endocytosis

Cofilin is required for the disassembly of endocytic vesicles but not their assembly. It is proposed that cofilin binds to mature ADP loaded filaments at the membranes of internalised endocytic vesicles and depolymerises them thereby recycling actin monomers for the formation of other vesicles (Figure 1-7) [171].

1.8.4 Apoptosis

As has already been mentioned, cofilin is necessary for the induction of apoptosis under conditions of oxidative stress. During this process, cofilin translocates from the cytoplasm to the mitochondria where it causes mitochondrial swelling, opening of the permeability transition pore and release of cytochrome c (Figure 1-7) [93, 94]

1.8.5 Cell specific cofilin functions

In addition to being involved in processes common to all cells, cofilin is required for functions that are specific to certain cell types. Costimulation of T lymphocytes through accessory receptors such as CD2 and CD28 but not signalling through the T cell receptor alone results in the dephosphorylation of cofilin which subsequently interacts with actin and this is essential for T cell activation [172-174]. Presentation of antigens to T cells by macrophages is also dependent on cofilin [163]. The excitation and directional growth of neurites is an essential process for the development of the nervous system and depends on the remodelling of the actin cytoskeleton. Cofilin has recently been shown to be one of the actin regulatory proteins required for this process [175]. Myelination of neurons by Schwann cells is also dependent on cofilin activity [176].

1.9 Cofilin in disease

1.9.1 Cancer

Considering the many cellular processes that cofilin is involved in, it is not surprising that the cofilin pathway is implicated in cancer, predominantly in invasion and metastasis that depends heavily on cell migration. Cofilin expression is found altered in several cancer cell lines, being overexpressed in C6 rat glioblastoma, A549 human lung cancer and human pancreatic cancer cell lines and down-regulated in MHCC97-H hepatocellular carcinoma and ovarian surface epithelium cells from women with a family history of cancer and mutations in the BRCA1 gene [177-181]. The phosphorylation status of cofilin has also been observed to be decreased in cell lines from T cell lymphomas and carcinomas from the cervix, colon, liver and kidney [182]. Furthermore, elevated cofilin expression is seen in clinical samples from ovarian cancer, oral squamous cell carcinoma and renal cell carcinoma [183-185].

In addition to cofilin expression being altered, changes in the levels of proteins that modulate cofilin activity and therefore the outcome of the cofilin pathway have also been detected. LIMK1 is highly expressed in many cancer cell lines including those derived from breast, prostate, skin and ovarian cancers and SSH is upregulated in mouse mammary tumour cells [186-188].

Altering the expression of cofilin in cancer cell lines has also been shown to alter their invasiveness. Overexpression of cofilin in the H1299 human lung cancer cell line disrupted the actin cytoskeleton at the leading edge of the cells and inhibited their invasiveness [189]. Conversely, overexpression of wild type (WT) or non-phosphorylatable cofilin increased the migration and invasiveness of the K1735 melanoma cell line [190]. Additionally, the overexpression of cofilin and proteins that are part of pathways that regulate its activity was identified in an invasive subpopulation of cells from a mammary tumour [56]. Another study that regulated the output of the cofilin pathway by altering LIMK expression discovered that increasing or decreasing the activity of the cofilin pathway resulted in a respective increase or decrease in intravasation and metastasis of mammary tumours [191]. Furthermore, cofilin phosphorylation decreases with

colorectal cancer progression with the lowest levels observed in the most advanced primary tumours and lymph node metastases [192].

Although these studies do not agree on whether cofilin up- or down-regulation promotes cancer and most do not report on overall cofilin activity, it is clear that perturbations in the cofilin pathway and activity are commonly found in and enhance the progression of cancer. The involvement of cofilin in the invasion and metastasis of cancer is likely due to its central role in regulating the actin cytoskeleton and the formation of membrane protrusions required for cell migration that were described previously. Cofilin may also increase the chemotaxis of cancer cells towards a chemoattractant such as EGF. EGF signalling has been shown to positively correlate with the metastatic potential of cancer cells and tumour associated macrophages promote the invasion of carcinoma cells by expressing EGF [193-195]. Furthermore, the directional movement of carcinoma cells to EGF has been demonstrated to depend on cofilin [156]. Remodelling of the extracellular matrix may be an additional role of cofilin in the invasion of cancer cells. As was previously described, cofilin is involved in the maturation of invadopodia, which are often formed by invasive cancer cells [196]. Down-regulation of cofilin results in less stable invadopodia with reduced matrix degrading activity, while the expression of constitutively active cofilin leads to increased expression of matrix metalloproteinase (MMP) 2 and 14 that can degrade the extracellular matrix [37, 190].

1.9.2 Neurodegenerative diseases

Cofilin-actin rods are found in the hippocampal and cortical neurons in brains from Alzheimer's disease patients. Further to this, many signalling molecules that are known to induce neurodegeneration lead to the formation of cofilin-actin rods [84]. These aggregates of cofilin and actin contribute to the loss of synapses by blocking intracellular trafficking [197]. Accumulation of amyloid β peptide is a distinctive feature of Alzheimer's disease, and amyloid β dimers and trimers can directly induce the formation of cofilin-actin rods [198]. It has been suggested that these rods could promote the formation of larger amyloid β plaques by blocking vesicles containing amyloid precursor protein and enzymes that process this to amyloid β [199]. The development of cofilin-actin rods have

also been implicated in the progression of Huntington's disease, another neurodegenerative condition [200].

1.9.3 Other diseases

Actin rod-like structures containing cofilin and spherical aggregates of cofilin and actin were identified in the brains of twins with dystonia for which a genetic basis could not be found [201]. Cofilin is also found overexpressed in the endometria of patients with endometriosis and is linked to the malignant-like cell behaviours associated with this disease [202]. In human immunodeficiency virus (HIV), both the viral Nef and gp120 proteins inhibit the migration of infected T cells through pathways involving cofilin allowing the virus to evade the immune system and replicate [203, 204].

1.10 Reactive oxygen species

Reactive oxygen species (ROS) are highly reactive molecules that contain oxygen (O_2). They can be divided into two groups; free radical ROS which have one or more unpaired electrons in their outer electron layer and non-radical ROS which have no unpaired electrons in their outer electron layer but can be converted into free radical ROS. Examples of free radical ROS are superoxide (O_2^-) and hydroxyl radicals ($^{\cdot}OH$). Non-radical ROS include hydrogen peroxide (H_2O_2), ozone (O_3) and singlet oxygen (1O_2). Oxidants that contain nitrogen such as nitric oxide (NO) and peroxyxynitrate (HNO_4) are called reactive nitrogen species [205, 206].

There are two major sources of ROS in cells; the mitochondria and nicotinamide adenine dinucleotide phosphate oxidase (NOX) enzymes. During oxidative phosphorylation in the mitochondria, electrons are transferred through a series of protein complexes known collectively as the electron transfer chain. This generates a proton gradient that then powers the ATP synthetase to produce ATP for the cell [207]. However, this process is not always perfect as electrons can sometimes 'leak' out of the system leading to the incomplete reduction of O_2 to O_2^- . This 'leaking' can happen at complex I and complex III in the electron transfer chain [208]. In addition to ROS production during oxidative phosphorylation, there are seven other sites in the mitochondria where ROS are

produced, however less is known about these contributors than complex I and III [209].

The second major sources of ROS in cells are the NOX enzymes. Although NOX enzymes were originally identified in and thought to be restricted to phagocytic cells, it is now appreciated that they are expressed in many cells [210-212]. The NOX family of enzymes is currently known to consist of seven members NOX1-5 and dual oxidase (DUOX) 1 and 2. All isoforms are membrane bound and have a conserved function, which is to transfer electrons across membranes from nicotinamide adenine dinucleotide phosphate (NADPH), through flavin adenine dinucleotide (FAD) and haem groups, to O_2 creating O_2^- . In line with this, they have a core common structure of six transmembrane domains that can bind to two haem groups, and carboxy terminal NADPH and FAD binding sites [206]. Although they have a common function, the isoforms have different cellular localisations and regulatory subunits. NOX1 has been identified at the plasma membrane but also specifically at caveolae [213, 214]. Generation of O_2^- by NOX1 depends on the cytosolic regulatory subunits NOXO1 and NOXA1 and the membrane protein p22phox [215, 216]. There is also evidence that the GTPase Rac can regulate NOX1 activity [217, 218]. NOX2 localises to intracellular and plasma membranes and its activation requires the membrane protein p22phox, cytosolic proteins p47phox, p67phox and p40phox as well as Rac [219, 220]. At present, nothing is known about the subcellular localisation of NOX3 but its regulation is dependent on p22phox and NOXO1 [221, 222]. The involvement of NOXA1, p47phox, p67phox and Rac are under debate as contradictory studies have been published [221-223]. NOX4 has been detected at a number of subcellular localisations including the plasma membrane, endoplasmic reticulum and mitochondrial membranes as well as at focal adhesions and invadopodia [213, 224-227]. The activity of NOX4 requires p22phox but, unlike the other NOX enzymes, it does not depend on other cytosolic proteins or Rac [216, 228]. NOX5 is located at the plasma membrane and is activated through Ca^{2+} but not membrane or cytosolic regulatory subunits [229, 230]. DUOX1 and 2 have been identified in the apical membrane of certain epithelial cells and their activation, like NOX5, is regulated by Ca^{2+} and is independent of cytosolic or membrane factors [231-233].

In addition to mitochondrial and NOX enzyme produced ROS, there are other cellular enzymes that produce ROS as a by-product of their normal reactions. Cyclooxygenases that catalyse the formation of prostaglandins generate O_2^- during this process [234]. Endothelial nitric oxide synthetase that forms NO from L-arginine can also generate ROS in certain circumstances; for example when cofactors or substrate are in limited supply [235, 236]. Xanthine oxidase catalyses the oxidation of purines to urate and produces O_2^- as a by-product [237]. These are just a few examples of the many enzymes that produce ROS as a result of their normal chemical reaction or under certain circumstances.

It is clear that ROS are produced during normal cellular processes that are essential for cell survival, with ATP production in the mitochondria being the most obvious example. However, the highly reactive nature of some of the ROS means they readily react with and can damage proteins, DNA and lipids, and at very high levels can induce cell death [205]. The cell therefore has a range of protective mechanisms that maintain ROS homeostasis and avoid cell damage and death. Enzymatic antioxidants include superoxide dismutase (SOD), catalase and glutathione peroxidase (GPX). In humans there are three SOD enzymes; cytosolic Cu/Zn-SOD, mitochondrial Mn-SOD and extracellular SOD (EC-SOD) that all destroy O_2^- by converting it to H_2O_2 or O_2 . Catalase converts H_2O_2 to $H_2O + O_2$ very efficiently. GPX, of which there are five isoforms that differ in tissue expression, reduces H_2O_2 by catalysing the reaction with glutathione (GSH) to form H_2O and oxidised GSH [238]. GSH on its own is also a major cellular antioxidant as it directly reduces free radicals such as O_2^- and $^{\cdot}OH$ [239]. Additionally, GSH can reduce vitamin C and vitamin E back to their active forms which also act as cellular antioxidants [239-241]. The thioredoxin system consists of two enzymes, thioredoxin and thioredoxin reductase, which act together to reduce protein disulphide bonds formed by oxidation. Thioredoxin reduces the protein disulphide and becomes oxidised itself, while thioredoxin reductase reduces the oxidised thioredoxin so it can continue functioning. Thioredoxin reductase can also reduce other compounds and disulphide bonds in proteins other than thioredoxin [242]. Another family of antioxidant proteins are the peroxiredoxins. There are six mammalian isoforms that differ in subcellular localisation and the mechanism by which they are reduced. However, they all have the same basic catalytic mechanism whereby an active site cysteine

residue is oxidised while the substrate such as H_2O_2 or peroxynitrite are reduced [243].

1.11 Cell signalling by ROS

Although ROS were originally thought to only be detrimental to cells, there is now growing evidence that they are important for normal cellular functions due to their involvement in the regulation of a number of signalling pathways. This first came to light after the observation that both platelet-derived growth factor (PDGF) and EGF signalling were dependent on the production of H_2O_2 [244, 245]. The main way in which ROS exert their downstream effects is through the oxidation of proteins which consequently alters their activity.

1.11.1 Protein oxidation

The regulation of proteins by oxidation occurs through the oxidation of specific cysteine residues by H_2O_2 (Figure 1-8). Cysteine residues contain a thiol (R-SH) group which in free cysteine residues has a pKa between 8 and 9, however sometimes when incorporated into a protein the pKa drops to between 4 and 5. This means the hydrogen of the thiol group is more easily lost leaving an oxidation sensitive cysteine residue [246]. The first intermediate to form when a cysteine residue is oxidised is a sulfenic acid (R-SOH) that contains one oxygen atom. This is very unstable and so rapidly undergoes further oxidation and reactions to stabilise it. In high oxidation conditions, the sulfenic acid can go on to form sulfinic acid (R-SO₂H) that contains two oxygen atoms, or sulfonic acid (R-SO₃H) that contains three oxygen atoms (Figure 1-8). Both of these oxidised states have been observed in peroxiredoxin enzymes [247, 248]. Cysteine thiol groups in the sulfenic acid state can also be stabilised by the formation of an intramolecular disulphide bond as seen in the chemokine CCL18 or an intermolecular disulphide as with protein kinase G isoform 1 α where a disulphide bond forms between its two identical subunits (Figure 1-8) [249, 250]. Disulphide bonds can also form between the sulfenic acid and glutathione to form a glutathionylated protein as is seen in p21Ras (Figure 1-8) [251]. The final modification that can stabilise a thiol oxidised to the sulfenic acid state is nitrosylation, which occurs following reaction with reactive nitrogen species and is demonstrated in the protein parkin [252]. Although only a few examples of

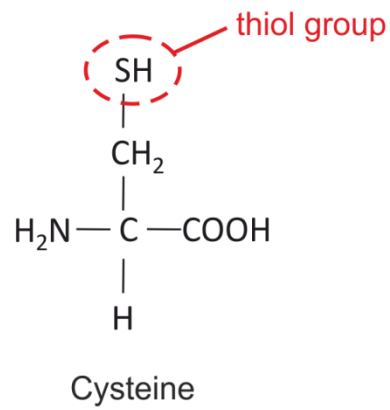
oxidised proteins have been given here, many other proteins have been proven to be modified by oxidation and computational analysis of protein sequences and large scale proteomic studies predict that more than 500 individual proteins have reactive cysteine residues that could potentially be modified by oxidation [253, 254]. Therefore, it is highly likely that there are a number of signalling pathways involving proteins that can be regulated by oxidation.

1.12 ROS and cell migration

1.12.1 Regulation of cell migration by ROS

One cellular function that is understood to be regulated by ROS is cell migration and there are several lines of evidence to support this. Treatment of vascular smooth muscle cells with antioxidants and ROS scavenging enzymes inhibited VEGF and PDGF stimulated migration [244, 255]. Furthermore, the migration of mouse and human endothelial cells and the chemotaxis of neutrophils was impaired by expressing antioxidant enzymes [256-258]. Conversely, the PDGF induced migration of mouse embryonic fibroblasts (MEFs) was increased when the antioxidant peroxiredoxin was removed from cells [259]. In addition to this *in vitro* evidence, *in vivo* studies have also confirmed an involvement of ROS in cell migration. Mice lacking both EC-SOD and Cu/Zn SOD showed decreased neovascularisation following ischemia, which was shown to be directly due, in part, to a decrease in migratory ability of cells in the Cu/Zn SOD knockout mice [260, 261]. The reverse of this has also been shown as the overexpression of EC-SOD by gene transfer resulted in increased angiogenesis, which is another process known to require cell migration [262]. In addition to endogenous ROS production being required for cell migration, exogenous H₂O₂ has also been shown to act as a chemoattractant. Mouse neutrophils *in vitro* migrated directly towards low levels of H₂O₂ [263]. The recruitment of leukocytes and hemocytes to wounds in zebrafish larvae and *Drosophila* embryos, respectively, also required H₂O₂ which acted as the chemoattractant [264, 265].

A



B

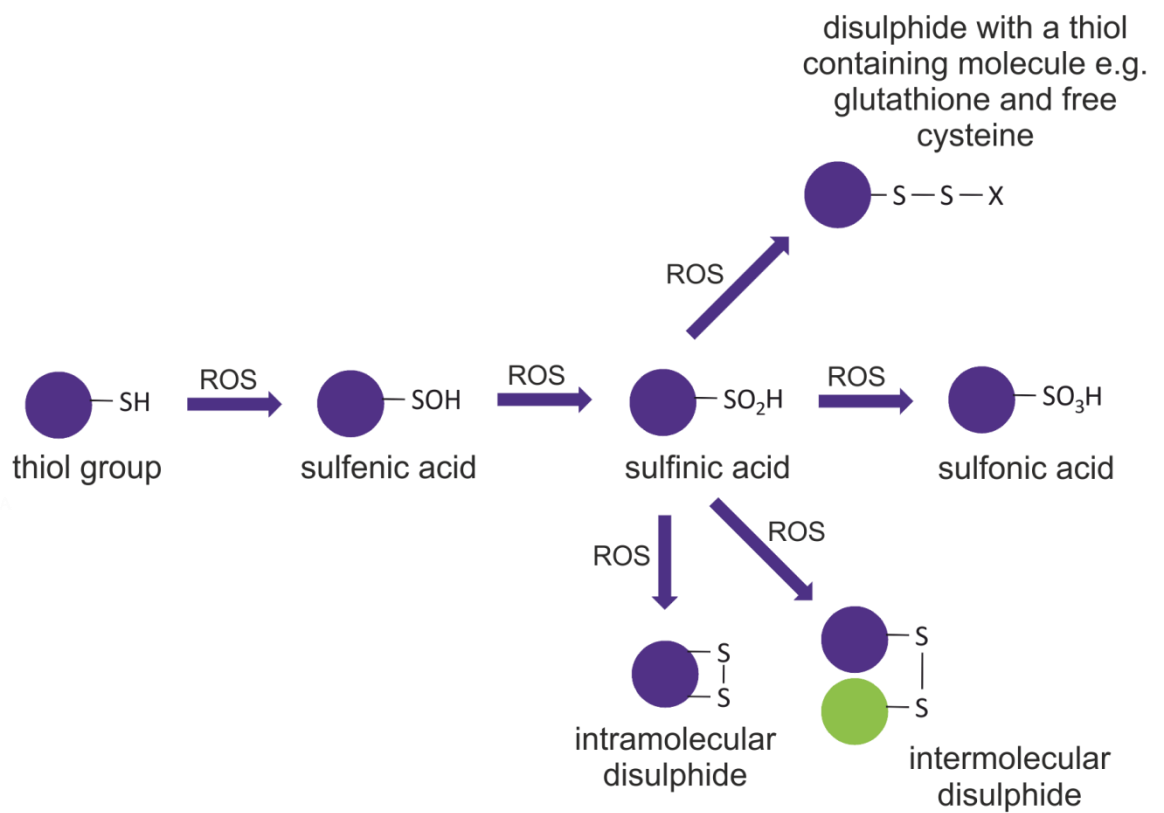


Figure 1-8 Potential protein products resulting from cysteine oxidation by ROS

A) Structure of the amino acid cysteine with oxidation sensitive thiol group highlighted. B) Schematic diagram showing the different stages and final protein products resulting from cysteine oxidation by ROS.

1.12.2 Sources of ROS in migrating cells

The predominant sources of ROS that induce the migration of cells are the NOX enzymes. This has been shown through a number of studies that either inhibit NOX enzymes or alter the expression of one or more of the NOX enzyme catalytic or regulatory subunits. The migration of human and mouse endothelial cells in response to VEGF, angiopoietin-1 and wounding was suppressed by the inhibition of NOX enzymes [257, 266, 267]. Directional migration of colon epithelial cells also depends on NOX1 generated ROS as knockdown of NOX1 inhibited migration [268]. Stimulation of vascular smooth muscle cell migration to PDGF is inhibited by a decrease in the levels of NOX1 and NOX4 and migration to fibroblast growth factor (FGF) by a decrease in NOX1 levels [269-271]. Conversely, vascular smooth muscle cell migration increases in response to PDGF when NOX1 is overexpressed [271]. Furthermore, a small molecule inhibitor screen to find regulators of neutrophil chemotaxis identified ROS produced by NOX enzymes as one such factor [272]. This study also confirmed the requirement of NOX in neutrophil migration *in vivo* by showing that neutrophils from mice with deleted NOX2 displayed impaired recruitment to sites of inflammation compared to WT mice. Another *in vivo* study highlighted the requirement of NOX2 in VEGF induced angiogenesis [273]. It is not surprising that NOX enzymes are activated and required for cell migration considering the small GTPase Rac that is often activated in migrating cells is also one of the regulatory subunits of some of the NOX enzymes.

Although NOX enzymes are the main source of ROS in migrating cells, recent studies have also implicated mitochondrial generated ROS. Induction of migration by MMP3 is mediated by ROS which was identified to originate from the mitochondria [274]. VEGF stimulation of human endothelial cells results in an increase in mitochondrial ROS production and cell migration which can be blocked by targeting the antioxidants vitamin E or catalase to the mitochondria [275].

1.12.3 Localisation of ROS in migrating cells

In order for cells to promote directional cell movement with ROS as a mediator of the signalling pathway, they need to spatially regulate ROS production and

evidence for how they do this is now growing. p47phox, the regulatory subunit of NOX2 is localised to the leading edge in migrating cells and both it and NOX translocate to the leading edge in VEGF-induced endothelial cell migration [276-279]. SOD that converts O_2^- to H_2O_2 , the ROS responsible for protein oxidation, is also localised to lipid rafts in VEGF stimulated endothelial cells [262]. Membrane associated peroxiredoxin 1, an antioxidant that could potentially reduce ROS levels and block ROS signalling, is phosphorylated and inactivated in response to growth factor and immune receptor activation and at the edges of healing wounds in mice [280]. This could allow a local increase in ROS for the purpose of promoting cell migration through ROS mediated signalling pathways.

1.12.4 Targets of ROS in migrating cells

Although the involvement and sources of ROS in cell migration are well established, very little is known about the downstream targets. Treatment of cells with H_2O_2 resulted in an increase in F-actin levels and establishment of stress fibres [281, 282]. This suggests that protein targets of ROS in migrating cells may be involved in rearranging the actin cytoskeleton as this is an important process for cell migration. Actin itself has been identified in an oxidised and glutathionylated state in oxidatively stressed T-lymphocytes, fibroblasts and gastric mucosal cells [136, 283, 284]. Actin is predominantly oxidised on cysteine 374 and when oxidised has a reduced stability and ability to polymerise, and increased ATPase activity [285, 286]. As was described previously, the actin binding protein cofilin is also a target of oxidation. Additionally, the actin cross-linking protein filamin translocates from the membrane to the cytosol when cells are treated with H_2O_2 , however the direct oxidation of filamin has not been shown [287, 288]. Although there is evidence that these proteins are targeted and regulated by ROS, there is no evidence that this has any involvement in cell migration.

The main class of proteins that have been proven to be directly oxidised by ROS in migrating cells are protein tyrosine phosphatases (PTPs). PTPs have a cysteine residue at their active site which is susceptible to oxidation and results in the reversible inhibition of these enzymes [289]. Phosphatases PTP1B and DEP1 were oxidised and inactivated in response to VEGF, which resulted in VEGF receptor phosphorylation that was shown to be required for endothelial cell migration

[262]. PTP-PEST was also oxidised and inhibited by NOX generated ROS and was necessary for endothelial cell migration [276]. Furthermore, Rac induced ROS production in migrating cells lead to the oxidation and inhibition of LMW-PTP. Consequently p190RhoGAP was phosphorylated, Rho activity decreased and lamellipodia were formed [290]. LMW-PTP was also inhibited by oxidation following the activation of integrin receptors, which resulted in focal adhesion kinase (FAK) phosphorylation and activation and the formation of focal adhesions and cell spreading [291].

It has yet to be determined if ROS produced in migrating cells mediate their effect entirely by the inhibition of PTPs, which can have a number of downstream targets, or if the activity of other proteins is also regulated by oxidation and contributes to cell migration. Recently a study reported that there were increased levels of protein oxidation at the leading edge of migrating cells and this colocalised with p47phox, a regulatory subunit of NOX2 and possibly NOX3. One of these proteins was identified as IQGAP1 but whether this oxidation alters its function is still unknown [278].

1.13 ROS and cancer

1.13.1 ROS levels in cancer

Cancer cell lines and tumour samples frequently exhibit higher levels of ROS compared to normal cells and tissues and this contributes to disease development and progression. ROS production was shown to be higher in prostate cancer cell lines compared to normal prostate cell lines [292]. A number of cancer cell lines derived from different tumour types including melanomas and ovarian tumours produced large amounts of H₂O₂ [293]. O₂⁻ levels were also elevated in melanoma cells and in the leukocytes from leukaemia patients compared to healthy individuals [294, 295]. The number of free, non-oxidised thiol groups was lower in oral squamous cell carcinoma compared to surrounding tissue indicating higher ROS levels were present in the cancerous tissue [296]. In renal cell carcinoma, mammary invasive ductal carcinoma, lung cancer and gliomas, levels of oxidised DNA, which result from damage by ROS, were also elevated [297-299]. Furthermore, lipid oxidation, another ROS induced damage, was increased in non-small cell lung cancer [300]. Not only are ROS

levels increased in cancer cells and tissues but they also correlate with disease aggressiveness and overall prognosis [292, 296, 299].

1.13.2 Sources of increased ROS in cancer

These increased ROS levels in cancer can originate from mitochondrial sources, NOX enzymes and from the altered expression of cellular antioxidants. Mitochondrial DNA, which codes for components of the electron transfer chain, is often found mutated in cancer resulting in an increase in ROS [301, 302]. Additionally, c-Myc, whose expression is associated with cell transformation, increases ROS production most likely due to an increase in oxidative phosphorylation in the mitochondria [303, 304]. Ras and p53, which are both frequently mutated in cancer, are involved in the expression of antioxidants, therefore loss of their function could result in increased ROS levels [305-307]. Furthermore, the expression of various NOX enzymes is elevated in cancer cell lines and tumour samples compared to the normal equivalents. NOX1 is increased in adenocarcinoma and prostate cancer cell lines and tumour samples, NOX2 in melanoma, NOX4 in thyroid cancer and NOX5 in malignant B cells [308-312].

1.13.3 ROS in cancer invasion and metastasis

ROS contribute to many stages of cancer development and progression through their ability to cause DNA damage and genetic instability, and their involvement in cell signalling pathways important in cancer. One of these areas is in promoting the invasion and metastasis of tumours. ROS generation is critical for the migratory and invasive phenotype of prostate cancer cells and conversely inhibition of NOX4 decreased the migration and metastasis of breast cancer cells [292, 313]. Altering cellular antioxidant levels had a similar effect, as a decrease in glutathione peroxidase increased lymph node metastasis of gastric carcinoma and injecting mice with catalase along with colon cancer cells, decreased the number of lung metastases [314, 315]. Mutations in mitochondrial DNA that are known to increase ROS levels also enhanced the metastatic potential of breast cancer cells [301, 316]. Furthermore, activation of the c-Met hepatocyte growth factor (HGF) and BLT2 leukotriene receptors and hypoxia promoted invasion and metastasis through ROS dependent signalling pathways [317-319]. These are just

a few examples of the signalling pathways and alterations in protein levels that have been shown to increase the migration, invasion and metastasis of cancer cells through ROS dependent processes. The involvement of ROS in this aspect of cancer progression is not surprising considering the participation of ROS in mediating cell migration, a key requirement for invasion and metastasis.

1.14 Project aims

Considering that cancer metastasis is so frequently the fatal stage in cancer progression, increasing our understanding of the underlying molecular mechanisms is key in developing successful therapeutic strategies to target it. It has become increasingly apparent, over the past decade in particular, that ROS have central roles in migration, invasion and metastasis. In addition to this, the involvement of ROS in cell signalling pathways, mediating its effects through the oxidation of target proteins has also become very clear. Despite this, surprisingly little is known about the direct protein targets of ROS in cells normally and more importantly in processes that contribute to cancer progression. Therefore, the aim of this project was to deepen our understanding in this area by, firstly, investigating the exact type and location of ROS produced in migrating cells and, secondly, identifying protein targets of this ROS that are oxidised and subsequently contribute to cell migration.

2 Materials and Methods

2.1 Materials

2.1.1 Reagents and chemicals

Table 2-1 List of reagents and chemicals

Reagent/Chemical	Supplier
Albumin standard (2 mg/ml)	Thermo Scientific
Ampicillin sodium salt	Sigma
<i>Bam HI</i>	Invitrogen
β -mercaptoethanol	Sigma
Bicinchoninic acid solution	Sigma
Biotin-iodoacetamide	Invitrogen
Catalase	Sigma
Copper (II) sulphate solution	Sigma
DCFDA (2',7'-dichlorofluorescein diacetate)	Sigma
Dimedone (5,5-dimethyl-1,3-cyclohexanedione)	Sigma
DMEM (Dulbecco's Modified Eagle Medium)	Gibco
DMEM (phenol red free)	Gibco
DMSO (dimethyl sulfoxide)	Sigma
dNTPs	Invitrogen
<i>E. coli</i> BL21 (DE3) pLys ^s cells	Agilent Technologies
<i>E. coli</i> DH5 α cells	Invitrogen
Ethidium bromide	Sigma
Fetal bovine serum	PAA
FuGENE transfection reagent	Promega
G418	Formedium
Glutathione Sepharose 4B	GE Healthcare
<i>Hin dIII</i>	Invitrogen
Hydrogen peroxide (30%, w/w)	Sigma
HyPerLadder I	Bioline
IPTG (Isopropyl β -D-1-thiogalactopyranoside)	Melford

L15 medium	Gibco
L-glutamine (200 mM)	Gibco
Lipofectamine LTX reagent	Invitrogen
Matrigel basement membrane matrix	BD Biosciences
NAC (N-acety-L-cysteine)	Sigma
NuPAGE 4-12% Bis-Tris gels	Invitrogen
NuPAGE LDS sample buffer (4x)	Invitrogen
NuPAGE MES SDS running buffer (20x)	Invitrogen
NuPAGE sample reducing agent (10x)	Invitrogen
NuPAGE transfer buffer (20x)	Invitrogen
One-Phor-All buffer	Amersham
Optimem I reduced serum medium	Gibco
<i>p</i> -aminobenzamidine	Sigma
PenStrep (penicillin and streptomycin)	Gibco
<i>PfuUltra</i> II Fusion HS DNA polymerase	Agilent Technologies
Precision Plus Protein™ all blue standards	Bio-Rad
Protein A Dynabeads	Invitrogen
Protein G Sepharose beads	Sigma
Protran™ nitrocellulose membrane	GE Healthcare
Pyrene labelled G-actin	Laura Machesky Lab
SimplyBlue™ SafeStain	Invitrogen
S.O.C. medium (Super Optimal broth with Catabolite repression)	Invitrogen
Streptavidin Alexa Fluor 680 conjugated	Invitrogen
T4 DNA ligase	Roche
T4 DNA ligase buffer (10x)	Roche
Thrombin	Sigma
Trypsin-EDTA (0.05%)	Gibco
<i>Xho</i> I	Roche

2.1.2 Kits

Table 2-2 List of kits

Kit	Supplier
CellTiter-Glo Luminescent Cell Viability Assay	Promega
Purelink HiPure Plasmid Filter Purification Kit	Invitrogen
QIAquick PCR Purification Kit	QIAGEN
QuikChange II XL Site-Directed Mutagenesis Kit	Agilent Technologies

2.1.3 Solutions

Table 2-3 List of solutions and their recipes

Solutions	Recipe
Agar plates	85 mM NaCl, 1% (w/v) bacto trypton, 0.5% (w/v) yeast extract, 1.5% (w/v) agarose, antibiotic (100 µg/ml ampicillin or 50 µg/ml kanamycin)
Annealing buffer	10 mM Tris-HCl pH 7.5, 1 mM EDTA, 50 mM NaCl
Bacterial lysis buffer	1x TBS, 2x complete protease inhibitor, 3 mM DTT, 1 mg/ml lysozyme
DNA loading buffer	20 mM EDTA, 0.05% (w/v) bromophenol blue, 50% (v/v) glycerol
F-buffer (10x)	20 mM Tris-HCl pH 8.0, 2 mM ATP, 5 mM DTT and 2 mM CaCl ₂ , 500 mM KCl, 20 mM MgCl ₂ , 1 mM EGTA
G-buffer	2 mM Tris-HCl pH 8.0, 0.2 mM ATP, 0.5 mM DTT, 0.2 mM CaCl ₂
IP lysis buffer	TBS, 1% Triton X-100, 1 mM EDTA, 0.2 mM Na ₃ VO ₄ , 20 mM NaF, 1x complete protease inhibitor, 1% (v/v) phenylmethylsulfonyl fluoride (PMSF)
L-broth	85 mM NaCl, 1% (w/v) bacto trypton, 0.5% (w/v) yeast extract
PBS	170 mM NaCl, 3.3 mM KCl, 1.8 mM Na ₂ HPO ₄ , 10.6 mM H ₂ PO ₄
PBS-T	PBS, 0.1% Triton X-100
RIPA lysis buffer	10 mM Tris-HCl pH 7.5, 5 mM EDTA, 150 mM NaCl, 40 mM NaPPi, 1 mM Na ₃ VO ₄ , 50 mM NaF, 1% NP40, 0.5% Na deoxycholate, 0.025% SDS, 1 mM PMSF, 1X complete protease inhibitor
SDS running buffer	25 mM Tris base, 192 mM glycine, 0.1% (w/v) SDS

SDS sample buffer	125 mM Tris-HCl pH 6.8, 6% (w/v) SDS, 30% glycerol, 225 mM DTT, 0.05% (w/v) bromophenol blue
SDS transfer buffer	192 mM glycine, 25 mM Tris base, 20% (v/v) methanol, 0.036% (w/v) SDS
TBE	89 mM Tris base, 89 mM boric acid, 2.5 mM EDTA
TBS	20 mM Tris-HCl pH 7.5, 136 mM NaCl
TBS-T	20 mM Tris-HCl pH 7.5, 136 mM NaCl, 0.1% Tween 20
Wash buffer 1	1x TBS, 3 mM DTT, 1 mM EDTA
Wash buffer 2	1x TBS, 1 mM MgCl ₂ , 1 mM CaCl ₂ , 3 mM DTT

2.1.4 Antibodies

Table 2-4 List of primary antibodies

Antigen	Species	Supplier	Catalogue no.
Cofilin	Mouse	Abcam	Ab75510
Cofilin	Rabbit	Abcam	Ab42824
Cofilin	Rabbit	Cytoskeleton	ACFL02-A
Dimedone (cysteine sulfenic acid)	Rabbit	Millipore	07-2139
DsRed (mCherry)	Rabbit	Clontech	632496
ERK2	Rabbit	Cell Signalling	91085
GFP	Mouse	Clontech	632380
Mouse IgG	Mouse	Jackson Immune Research	015-000-120

Table 2-5 List of secondary antibodies

Antibody	Supplier	Catalogue no.
Alexa Fluor 680 goat anti-mouse IgG	Invitrogen	A21076
DyLight 800 goat anti-mouse IgG	Perbio Science UK	35521
DyLight 800 goat anti-rabbit IgG	Perbio Science UK	35571

2.1.5 Plasticware

Table 2-6 List of plasticware

Plasticware	Supplier
35 mm glass bottom dishes	Mat Tek
96-well ImageLock™ plates	Essen Bioscience
96-well plates (black/clear bottom/sterile)	BD Falcon
96-well plates (clear/non-sterile)	Greiner Bio-One
96-well plates (white/non-sterile)	Fisher Scientific
Amicon Ultra 0.5 ml 10k centrifugal filters	Millipore
Cell strainers	BD Falcon
Cryogenic vials	Thermo Scientific
E plate 16	ACEA Biosciences
FACS tubes	BD Falcon
Falcon tubes for bacterial transformation (352059)	BD Falcon
Syringe filters	Gilson
Tissue culture flasks	Nunclon
Tissue culture dishes (10 cm and 6-well)	Corning
Tissue culture dishes (96-well)	Falcon

2.2 Molecular cloning

2.2.1 Plasmids

A list of plasmids and their sources or how they were made is detailed below (Table 2-7).

Table 2-7 List of plasmids and their sources

Plasmid	Source
pGEX-KG-hCofilin WT	Previously made in research group
pGEX-KG-hCofilin C39A	Made during this project by site-directed mutagenesis (SDM) from pGEX-KG-hCofilin WT
pGEX-KG-hCofilin C80A	Made during this project by SDM from pGEX-KG-hCofilin WT

pGEX-KG-hCofilin C139A	Made during this project by SDM from pGEX-KG-hCofilin WT
pGEX-KG-hCofilin C147A	Made during this project by SDM from pGEX-KG-hCofilin WT
pGEX-KG-hCofilin C39/80A	Made during this project by SDM from pGEX-KG-hCofilin WT
pGEX-KG-hCofilin C39/139A	Made during this project by SDM from pGEX-KG-hCofilin WT
pGEX-KG-hCofilin C39/147A	Made during this project by SDM from pGEX-KG-hCofilin WT
pGEX-KG-hCofilin C80/139A	Made during this project by SDM from pGEX-KG-hCofilin WT
pGEX-KG-hCofilin C80/147A	Made during this project by SDM from pGEX-KG-hCofilin WT
pGEX-KG-hCofilin C139/147A	Made during this project by SDM from pGEX-KG-hCofilin WT
pmCherry C1	Provided by Kurt Anderson's research group
pmCherry N1	Provided by Kurt Anderson's research group
pmCherry Cofilin WT	Made during this project by amplifying cofilin gene from pGEX-KG-hCofilin WT and inserting this into pmCherry C1
pmCherry Cofilin C139/147A	Made during this project by SDM from pmCherry Cofilin WT
pHyPer-cyto	Purchased from Evrogen
pHyPer-PM	Made during this project by annealing oligonucleotides for a CAAX motif and inserting this into pHyPer-cyto after removing the stop codon by SDM

2.2.2 Oligonucleotides and primers

Oligonucleotides and primers used in this project are listed below (Table 2-8).

Table 2-8 List of primers, their applications and sequences

Oligonucleotide	Application	Sequence (5'-3')
pGEX F	Sequencing pGEX plasmids	CTTTGCAGGGCTGGCAAG
pGEX R	Sequencing pGEX plasmids	GAGCTGCATGTGTCAGAGG

pGEX N	Sequencing pGEX plasmids	CACAAATTGATAAGTACTTG
Cofilin C39A F	SDM to make cofilin mutants	CGCAAGAAGGCGGTGCTCTTCGCG CTGAGTGAGGACAAG
Cofilin C39A R	SDM to make cofilin mutants	CTTGTCTCACTCAGCGCGAAGAGC ACCGCCTTCTTGCG
Cofilin C80A F	SDM to make cofilin mutants	GCTGCCAGATAAGGACGCGCGCTAT GCCCTCTATGATGCAACC
Cofilin C80A R	SDM to make cofilin mutants	GGTTGCATCATAGAGGGCATAGCG CGCGTCCTTATCTGGCAGC
Cofilin C139A F	SDM to make cofilin mutants	GAATTGCAAGCAAACGCGTACGAGG AGGTCAAGGACCGC
Cofilin C139A R	SDM to make cofilin mutants	GCGGTCCTTGACCTCCTCGTACGCG TTTGCTTGCAATTC
Cofilin C147A F	SDM to make cofilin mutants	GAGGAGGTCAAGGACCGCGCGACC CTGGCAGAGAAG
Cofilin C147A R	SDM to make cofilin mutants	CTTCTCTGCCAGGGTCGCGCGGTCC TTGACCTCTC
CMV-F	Sequencing pmCherry plasmids	CGCAAATGGGCGGTAGGCGTG
EGFP-C1-R	Sequencing pmCherry plasmids	AACCATTATAAGCTGCAATAAAC
mCh SEQ F	Sequencing pmCherry plasmids	CCCCGTAATGCAGAAGAAGA
mCh SEQ R3	Sequencing pmCherry plasmids	CCTTATCTGGCAGCATCTTGAC
<i>Xho I</i> Cofilin	Amplifying cofilin gene from pGEX-KG-hCofilin WT	TCTCGAGCTATGGCCTCCGGTGTG GCTGTC
Cofilin <i>Bam HI</i>	Amplifying cofilin gene from pGEX-KG-hCofilin WT	GCTGGATCCTCACAAAGGCTTGCCC TCCAG
pHyPer SEQ F	Sequencing pHyPer plasmids	CATTGACGTCAATGGGAGTTTG
pHyPer SEQ F2	Sequencing pHyPer plasmids	CAACCACTACCTGAGCTTCC
pHyPer SEQ F3	Sequencing pHyPer plasmids	CAAGGACGACGGCAACTACAAGAC
pHyPer SEQ F4	Sequencing pHyPer plasmids	CTGGTTTATCGTCCTGGCTCAC
pHyPer SEQ R1b	Sequencing pHyPer plasmids	CAACCCTATCTCGGTCTATTC

pHyPer SEQ R2	Sequencing pHyPer plasmids	GCTCCTGGACGTAGCCTTCG
pHyPer anti-TAA F	SDM to remove pHyPer-cyto stop codon	CAGGCGGTTGCAAAGCTTCGAATTC TGCAG
pHyPer anti-TAA R	SDM to remove pHyPer-cyto stop codon	CTGCAGAATTCGAAGCTTTGCAACCGCCTG
CAAX motif F	Oligonucleotides for annealing to generate CAAX insert	AGCTTAAAAAGATGAGCAAGGACGG CAAGAAGAAGAAGAAGAGCAAG ACAAAGTGTGTAATTATGTAAG
CAAX motif R	Oligonucleotides for annealing to generate CAAX insert	GATCCTTACATAATTACACACTTTGT CTTGCTCTTCTTCTTCTTCTTCTTGC CGTCCTTGCTCATCTTTTAA

2.2.3 Annealing oligonucleotides

3 µg each of CAAX forward and reverse oligonucleotides were diluted in annealing buffer to a total volume of 50 µl in a polymerase chain reaction (PCR) tube. This was placed in a MJ Research PTC-200 PCR machine that was set to heat the sample at 94°C for 4 minutes and then gradually reduce the temperature to 4°C over 1.5 hours.

2.2.4 PCR

50 µl PCR mix was set up in a PCR tube as detailed below:

Reagent	Volume (µl)
Nuclease free H ₂ O	36
10x <i>PfuUltra</i> buffer	5
dNTPs (2.5 mM)	5
Template DNA (100 ng/µl)	1
Primer 1 (<i>Xho I</i> Cofilin) (10 µM)	1
Primer 2 (Cofilin <i>Bam HI</i>) (10 µM)	1
<i>PfuUltra</i>	1
Total Volume	50

PCR mix was placed in a MJ Research PTC-200 PCR machine and the PCR programme was set up as detailed below:

Temperature	Time
95°C	7 minutes
30 cycles of: 95°C 60°C 72°C	40 seconds 30 seconds 2 minutes
72°C	7 minutes
4°C	∞

Amplification of PCR product was confirmed by agarose gel electrophoresis and purified as described below.

2.2.5 Restriction enzyme digestion

Digestion of DNA with restriction enzymes was carried out in One-Phor-All Buffer at 37°C for 2 hours (*Xho I* and *Hin dIII*) or 3 hours (*Bam HI*). 10 U of restriction enzyme was added per 1 µg of DNA and reactions were adjusted to a total volume of 30 µl for single digests and 50 µl for double digests. Digestion of DNA was confirmed by agarose gel electrophoresis and purified as described below.

2.2.6 DNA purification

DNA from restriction digests and PCR products was purified using the QIAquick PCR Purification Kit following the manufacturer's instructions. Briefly, 5 volumes of Buffer PB was added to 1 volume of PCR or restriction digest product in a QIAquick column. This was centrifuged in a collection tube in an Eppendorf 5417R centrifuge at 13,000 rpm for 1 minute at room temperature. The flow through was discarded, 750 µl Buffer PE added to the QIAquick column and centrifuged at 13,000 rpm for 1 minute at room temperature. Flow through was discarded and the QIAquick column centrifuged one more time at 13,000 rpm for 1 minute at room temperature. DNA was eluted by adding 50 µl Buffer EB to the middle of the QIAquick membrane and centrifuging at 13,000 rpm for 1 minute at room temperature in a new microfuge tube.

2.2.7 Determination of DNA concentration

Concentration of double stranded DNA was determined using an Eppendorf BioSpectrometer. DNA was diluted in nuclease free H₂O and absorbance at 260 nm measured.

2.2.8 Ligation of DNA

Ligation reactions were performed using T4 DNA ligase. The ligation reaction was prepared by adding a 1:3 molar ratio of restriction digested vector:insert and 1 µl of T4 DNA ligase to 1x T4 DNA ligase buffer. This was incubated at room temperature for 16 hours.

2.2.9 Agarose gel electrophoresis

1% agarose gels were prepared by adding 1 g agarose to 100 ml 1x TBE in a conical flask and heating in a microwave until all the agarose had dissolved. After the solution had cooled slightly, 2 µg/ml ethidium bromide was added and the gel poured into the gel caster. Once the gel had set it was placed into a Bio-Rad gel tank containing 1x TBE buffer. DNA samples were prepared by adding DNA loading buffer and then loaded on the gel alongside the DNA ladder, HyPerLadder I. Gels were run at 80-100 V and the DNA bands visualised using a Syngene Genius Bio Imaging System.

2.2.10 Bacterial transformation

An aliquot of *E. coli* DH5α competent cells was thawed on ice. 50 µl was then transferred to a pre-cooled Falcon tube (Falcon 352059) along with 2 µl plasmid DNA and incubated for 30 minutes on ice. Bacteria were heat shocked by placing the tubes in a 42°C water bath for 45 seconds followed by incubation on ice for 2 minutes. 200 µl S.O.C. medium was added and the cultures were incubated at 37°C for 1 hour in a shaking incubator. The transformation mixture was then spread on an agar plate containing the appropriate antibiotic for selection. After the liquid had been absorbed the plates were placed inverted in a 37°C incubator for at least 16 hours.

2.2.11 Site-directed mutagenesis

Site-directed mutagenesis was carried out using the QuikChange II XL Site-Directed Mutagenesis Kit following the manufacturer's instructions. Details of the oligonucleotide primers used for these experiments can be found in the table of oligonucleotides and primers (Table 2-8). Briefly, mutagenesis reactions were set up in PCR tubes as follows:

Reagent	Volume (μ l)
10x reaction buffer	5
Template DNA (2 ng/ μ l)	5
Primer 1 (125 ng/ μ l)	1
Primer 2 (125 ng/ μ l)	1
dNTP mix	1
QuikSolution	3
Nuclease free H ₂ O	33
<i>PfuUltra</i> HF DNA polymerase (2.5 U/ μ l)	1
Total volume	50

The mutagenesis mix was placed in a MJ Research PTC-200 PCR machine and the PCR programme was set up as detailed below:

Temperature	Time
95°C	1 minute
18 cycles of: 95°C 60°C 68°C	50 seconds 50 seconds 1 minute/kb of plasmid
68°C	7 minutes
4°C	∞

Parental DNA was digested by adding 10 U *Dpn I* restriction enzyme and incubating at 37°C for 1 hour. The remaining mutated plasmid DNA was transformed into *E. coli* XL10-Gold ultracompetent cells by adding 2 μ l to 45 μ l of the bacterial cells in a pre-cooled Falcon tube (Falcon 352059). The bacteria were then incubated on ice for 30 minutes before heat shocking at 42°C for 30

seconds. After incubating on ice for 2 minutes, 500 μ l S.O.C. medium was added and the cultures were incubated at 37°C for 1 hour in a shaking incubator. The transformation mixture was spread across two agar plates containing the appropriate antibiotic for selection. Once the liquid was absorbed, the plates were placed inverted in a 37°C incubator for at least 16 hours. Eight colonies were selected and successful mutagenesis confirmed by DNA sequencing of the insert region.

2.2.12 Plasmid preparation

2.2.12.1 Small scale plasmid preparation

5 ml cultures of *E. coli* DH5 α cells that had been transformed with the required plasmid were grown overnight at 37°C in a shaking incubator. Cultures were then centrifuged in a Beckman Coulter J6-M1 centrifuge at 2,000 rpm for 15 minutes and DNA isolated from the cell pellet using a Qiagen 8000 Robot. DNA isolation was carried out by the Beatson Molecular Technology Services.

2.2.12.2 Large scale plasmid preparation

250-500 ml cultures of *E. coli* DH5 α cells that had been transformed with the required plasmid were grown overnight at 37°C in a shaking incubator. Cells were then centrifuged in a Beckman Coulter J6-M1 centrifuge at 4,000 rpm for 20 minutes and DNA isolated from the cell pellet using the Invitrogen Purelink HiPure Plasmid Filter Purification Kit following the manufacturer's instructions. DNA isolation was carried out by the Beatson Molecular Technology Services.

2.2.13 DNA Sequencing

DNA sequencing of plasmids was performed on an Applied Biosystems 3130x1 (16 capillary) sequencer. DNA sequencing reactions were set up, prepared for loading into the sequencer and sequenced DNA precipitated following the Applied Biosystems (BigDye 3.1) DNA sequencing protocol. DNA sequencing was carried out by the Beatson Molecular Technology Services.

2.3 Recombinant proteins and *in vitro* assays

2.3.1 Recombinant protein production

For large scale protein production, six bacterial culture flasks containing 100 ml of L-broth with 150 µg/ml ampicillin were inoculated with *E. coli* BL21 (DE3) pLys^s cells containing the desired plasmid and grown overnight in a shaking incubator at 37°C. These starter cultures were transferred to larger flasks holding 1 l of L-broth, with 150 µg/ml ampicillin, and returned to the shaking incubator for ~1 hour until the OD₆₀₀ was between 0.6 and 1.0. Cultures were then induced with 100 µM IPTG and grown for a further 3 hours in the shaking incubator at 37°C. Bacterial cells were pelleted by centrifuging in a Beckman Coulter J6-M1 centrifuge at 4,000 rpm for 20 minutes at 4°C and then resuspended in 3 ml bacterial lysis buffer. Samples were incubated on ice for 30 minutes before being sonicated and then centrifuged in a Beckman Coulter Avanti J-25 centrifuge at 14,000 rpm for 30 minutes at 4°C. Meanwhile 10 ml glutathione Sepharose beads were washed twice in 50 ml TBS. The supernatant from the bacterial sample was transferred to the washed glutathione beads and incubated overnight at 4°C while rotating to allow the expressed GST tagged proteins to bind to the beads. Beads were washed with 500 ml wash buffer 1 followed by 500 ml wash buffer 2 and left resuspended in 15 ml of wash buffer 2 to which 50 U of thrombin was added. This was left to incubate overnight at 4°C while rotating to release the desired protein from the GST tag. The flow through was collected and incubated with 100 µl of pre-washed *p*-aminobenzamidide bead solution (50% v/v), for 30 minutes at 4°C while rotating. After allowing the *p*-aminobenzamidide beads to settle, the supernatant was collected and concentrated to around 1 ml in a Millipore Amicon Ultra 0.5 ml 10k centrifugal filter. The protein concentration was then determined and aliquots stored at -80°C. The purity of the expressed protein was assessed by SDS-PAGE and gel staining.

2.3.2 Oxidation of recombinant cofilin

50 µl recombinant cofilin and 450 µl TBS were added to a Millipore Amicon Ultra 0.5 ml 10K centrifugal filter unit and centrifuged in an Eppendorf 5417R centrifuge at 14,000 rpm for 8 minutes at 4°C. The flow through was removed

and an additional 450 μ l TBS added to the top of the filter unit and centrifuged as before. This was repeated three times. The filter unit was then placed inverted into a new tube and centrifuged in an Eppendorf 5417R centrifuge at 1,000 rpm for 2 minutes at 4°C to collect the dialysed and concentrated protein. 50 μ g of protein in a total volume of 4 μ l was transferred to a 1.5 ml microfuge tube. 20 μ l of H₂O₂ at the indicated concentration was then added and incubated for 1 hour on ice and in the dark. Any remaining H₂O₂ was quenched by the addition of 4 μ l catalase (2,000 U).

2.3.3 Biotin-iodoacetamide labelling of recombinant cofilin

Following oxidation of recombinant cofilin as described above, levels of oxidation could be monitored by labelling with biotin-iodoacetamide (IAA) as follows. 1 nmole of biotin-IAA was added to the recombinant cofilin and incubated for 20 minutes in the dark at room temperature. Following this β -mercaptoethanol was added to a final concentration of 30 mM to quench any remaining biotin-IAA. Biotin-IAA labelling of cofilin was assessed by SDS-PAGE and western blotting using Alexa Fluor 680 conjugated streptavidin.

2.3.4 Preparation of G-actin

20 ml G-buffer was mixed with each gram of muscle acetone powder (kindly provided by Laura Machesky) by stirring on ice for 30 mins in a fume hood. Insoluble material was pelleted by centrifugation in a Beckman Coulter Avanti J-25 centrifuge at 16,000 rpm for 30 minutes at 2°C. The supernatant was kept while the pellet was used to repeat the extraction in G-buffer step. The combined supernatants were stirred while KCl and MgCl₂ were added to final concentrations of 50 mM KCl and 2 mM MgCl₂. This was stirred gently at room temperature for 30 minutes and then on ice for 30 minutes. More KCl was added, while still stirring on ice, to reach a final concentration of 0.8 M and then stirred for a further 30 minutes. This was centrifuged in a Beckman Coulter Optima L-90k Ultracentrifuge at 35,000 rpm for 2 hours at 4°C. Pellets were resuspended in G-buffer, homogenized in a Dounce homogenizer and dialysed in G-buffer for 2 days. G-buffer was changed twice during dialysis and concentration was kept below 6 mg/ml. The dialysed material was then centrifuged for another 2 hours in a Beckman Coulter Optima L-90k Ultracentrifuge at 35,000 rpm at 4°C. The

top 2/3 of the supernatant was removed, concentration determined by measuring absorbance at 290 nm and aliquots stored at -80°C.

2.3.5 Actin depolymerisation assay

2 µM F-actin was prepared by adding 100 µl 10x F-buffer to 900 µl 2 µM G-actin (5% labelled with pyrene) (pyrene labelled actin kindly provided by Laura Machesky). This was left at room temperature to polymerise for 2-3 hours. Polymerisation was monitored by adding 50 µl of the polymerising actin to a glass cuvette and measuring the fluorescence (excitation wavelength = 339 nm; emission wavelength = 384 nm) on a spectrofluorimeter. 50 µl of the polymerised F-actin was then added to a glass cuvette, with or without 10 µM WT or mutant cofilin, and fluorescence measured for 300 seconds. Data were presented as change in fluorescence over time.

2.4 Cell culture techniques

2.4.1 Origin, maintenance and storage of cell lines

MDAMB231 and MCF7 cells are both adherent, epithelial cell lines that were originally extracted from human breast cancer metastases. MDAMB231 cells were used for the majority of experiments, however occasionally MCF7 cells were used. Both cell lines were grown in DMEM medium supplemented with 10% fetal bovine serum (FBS), 2 mM L-glutamine, 10 U/ml penicillin and 10 µg/ml streptomycin. Cells were kept at 37°C with 5% CO₂ in a humidified incubator and passaged every 3-4 days as follows. Culture medium was removed, cells were washed once with PBS and then incubated in 0.05% trypsin for a short time. Cells were then resuspended in fresh culture medium and an aliquot was transferred to a new tissue culture flask or dish.

MDAMB231 cell lines stably expressing HyPer-cyto, HyPer-PM, mCherry (mCh), mCh cofilin WT or mCh cofilin C139/147A were grown and maintained as described above with the exception that the culture medium was also supplemented with 400 µg/ml G418 to ensure the continued expression of the plasmids.

For long term storage, all cell lines were kept frozen in liquid nitrogen vapour phase tanks. To freeze cells down, a flask of healthy cells was harvested by trypsinisation as described above for the general passaging of cells. They were then centrifuged in an Eppendorf 5804R centrifuge at 1,200 rpm for 5 minutes, the cell pellet resuspended in FBS supplemented with 10% DMSO and aliquots transferred to cryogenic vials. Cells were stored in a polystyrene box at -80°C for 24 hours before being placed in the liquid nitrogen tank. To thaw cells, cryogenic vials containing cells were transferred directly from the liquid nitrogen tank to a 37°C water bath. As soon as they were thawed, cells were transferred to culture medium and centrifuged in an Eppendorf 5804R centrifuge at 1,200 rpm for 5 minutes. The cell pellet was then resuspended in fresh culture medium and transferred to a new tissue culture flask or plate.

2.4.2 Tissue culture treatments

Treatment of cells with N-acetylcysteine (NAC) was carried out as follows. Fresh culture medium containing NAC at the indicated concentration (0, 2.5, 5, 10, 25, 50 or 75 mM) was prepared and then filtered through a $0.2\ \mu\text{m}$ syringe filter. pH of the culture medium was adjusted by adding sodium hydroxide (NaOH) until the phenol red in the medium indicated that the pH was equivalent across all samples. Culture medium on the cells was removed and the fresh, pH adjusted medium containing NAC was added. Cells were incubated for up to 72 hours depending on the experiment.

Treatment of cells with H_2O_2 was carried out as follows. Fresh culture medium without FBS (serum free (SF) culture medium) containing H_2O_2 at the indicated concentration (0, 1, 3 or $10\ \mu\text{M}$) was prepared. Culture medium on cells was removed and cells were washed twice with SF culture medium before the fresh medium containing H_2O_2 was added. Cells were incubated for 5 hours before continuing with the remainder of the experiment.

2.4.3 Transfection of plasmid DNA

FuGENE HD transfection reagent was used to transfect MDAMB231 cells with pHyPer-cyto and pHyPer-PM plasmids as follows. MDAMB231 cells were seeded at 2×10^5 cells per well in 6-well plates 24 hours before transfection. FuGENE HD

transfection reagent, plasmid DNA and Optimem I Reduced Serum Medium (Optimem) were allowed to reach room temperature before starting transfections. pHyPer-cyto plasmid DNA (2 µg) or pHyPer-PM plasmid DNA (0.75 µg) was diluted in 100 µl of Optimem. 7 µl of FuGENE HD transfection reagent was then added to the diluted DNA and the contents mixed by vortexing before being incubated at room temperature for 15 minutes to allow transfection reagent:DNA complexes to form. Meanwhile culture medium on the cells was removed, cells were washed twice with antibiotic free culture medium and then 2 ml of fresh antibiotic free culture medium was added. The full volume of the transfection reagent:DNA complex solution was added to one well of a 6-well plate and mixed by rocking the plate back and forth to ensure the complexes were evenly distributed. This medium containing transfection complexes was removed after 24 hours and replaced with fresh culture medium with antibiotics.

Lipofectamine LTX transfection reagent was used to transfect MDAMB231 cells with pmCherry, pmCherry cofilin WT or pmCherry cofilin C139/147A plasmids as follows. MDAMB231 cells were seeded at 5×10^5 cells per well in 6-well plates 24 hours before transfection. Lipofectamine LTX transfection reagent, plasmid DNA and Optimem medium were allowed to reach room temperature before starting transfections. 2.5 µg of each plasmid DNA was diluted in 500 µl Optimem medium, mixed gently by vortexing and then incubated for 5 minutes at room temperature. 11.25 µl Lipofectamine LTX transfection reagent was then added to the diluted DNA and mixed gently by vortexing before incubating at room temperature for 30 minutes. Meanwhile culture medium on the cells was removed, cells were washed twice with antibiotic free culture medium and then 2 ml of fresh antibiotic free culture medium was added. The full volume of the transfection reagent:DNA complex solution was added to one well of a 6-well plate and mixed by rocking the plate back and forth to ensure the complexes were evenly distributed. This medium containing transfection complexes was removed after 24 hours and replaced with fresh culture medium with antibiotics.

2.4.4 Establishment of stable cell lines

MDAMB231 cells were transfected with pHyPer-cyto, pHyPer-PM, pmCherry, pmCherry cofilin WT or pmCherry cofilin C139/147A plasmids as described above. 48 hours after transfection cells were transferred to a 10 cm tissue

culture dish and 400 µg/ml G418 was added to the culture medium. Cells were cultured until all control cells were dead and cells expressing the plasmids were identified and selected for by FACS. From then on, cells were maintained in the presence of 400 µg/ml G418.

2.4.5 Fluorescence activated cell sorting (FACS)

Cells stably expressing HyPer-cyto, HyPer-PM, mCh, mCh cofilin WT or mCh cofilin C139/147A were identified and selected for by FACS on a FACSaria cell sorter. Cells were harvested by trypsinisation as described for the general passaging of cells. Cells were centrifuged in an Eppendorf 5804R centrifuge at 1,200 rpm for 5 minutes and then resuspended in serum free culture medium to a concentration of 4×10^6 cells/ml before being strained through a 40 µm cell strainer. Appropriate gates were set on the FACSaria cell sorter to ensure only cells expressing the required protein were selected. Cells were then transferred to a new tissue culture dish and maintained as normal.

2.4.6 Labelling and detection of oxidised proteins

Oxidised proteins in cells were labelled and detected using the chemical 5,5-dimethyl-1,3-cyclohexanedione (dimedone). 5 mM dimedone was prepared directly in serum free culture medium and was filtered through a 0.2 µm syringe filter before use. After the required treatment, cell culture medium was removed and cells washed twice with serum free culture medium. Culture medium containing 5 mM dimedone was then added and cells incubated at 37°C for between 1 and 3 hours depending on the experiment and cell type. Cells were then harvested and dimedone labelling of oxidised proteins determined by western blot analysis. The specific experiments carried out are detailed below.

2.4.6.1 Dimedone labelling following NAC treatment

Cells were treated with NAC at the indicated concentrations for 72 hours, as described in the tissue culture treatment section, and 5mM dimedone was added for the final 3 hours.

2.4.6.2 Dimedone labelling following H₂O₂ treatment

Cells were treated with H₂O₂ at the indicated concentrations for 6 hours, as described in the tissue culture treatment section, and 5mM dimedone was added for the final 1 hour.

2.4.6.3 Dimedone labelling following wounding

Between 20 and 30 wounds, depending on the experiment, were created through a confluent cell monolayer with a P10 pipette tip. Cells were washed gently twice with culture medium before fresh medium was added. After 3 hours to allow the cells to start migrating to close the wounds, 5 mM dimedone was added for 1 hour.

2.4.7 Measurement of ROS production

The production of ROS in cells was measured using the fluorescent probe 2',7'-dichlorofluorescein diacetate (DCFDA). MDAMB231 cells were seeded at 40,000 cells per well in a BD Falcon 96-well plate (black/clear bottom, sterile). After 24 hours cells were treated with NAC at the indicated concentrations for 6 hours. Cells were washed once with PBS before 100 µl of 5 µM DCFDA in serum and phenol red free DMEM was added. After incubation at 37°C for 30 minutes, cells were washed once with PBS and 100 ul serum and phenol red free medium added to each well. DCFDA fluorescence was measured on a Tecan Safire II microplate reader (excitation wavelength = 485 nm; emission wavelength = 528 nm; bandwidth = 5 nm).

2.4.8 Cell proliferation assay

Cells were seeded in a 96-well tissue culture plate at 5,000 cells per well. Number of cells at 24, 48, 72 and 96 hours was measured using the CellTiter-Glo Luminescent Cell Viability Assay as follows. CellTiter-Glo reagent and cells were left at room temperature for 30 minutes to equilibrate. 100 µl of CellTiter-Glo reagent was added to each well including control wells containing culture medium only and the plate placed on an orbital shaker for 2 minutes. After incubation at room temperature for 10 minutes, the contents of each well were transferred to a Fisherbrand white 96-well plate. Luminescence readings were

made on a Glomax 96 Microplate Luminometer. Relative cell numbers were reported using 24 hours as the reference point.

2.4.9 Cell adhesion/spreading assay

Cell adhesion/spreading was measured on the xCelligence Real-Time Cell Analyzer (RTCA) system. 50 µl culture medium was added to each well of an E-plate 16 and left to equilibrate in the RTCA analyser, which is situated in a standard tissue culture incubator, for 1 hour before the background measurement was taken. 10,000 cells in 100 µl culture medium were added to each well of the E-plate 16, the plate placed back in the RTCA analyser and measurements taken every 10 minutes for 3 hours. The RTCA software automatically subtracted the background from each measurement taken.

2.4.10 Cell adhesion assay

50 µl of culture medium was added to each well of a 96-well tissue culture plate and placed in a tissue culture incubator for 1 hour. 40,000 cells in 100 µl culture medium were added to each well and left to adhere for 3 hours in standard culture conditions. Wells were washed 4 times with PBS to remove any cells that had not adhered before 100 µl culture medium was added. Number of adherent cells was measured using the CellTiter-Glo Luminescent Cell Viability Assay as described for the cell proliferation assay.

2.4.11 Wound healing cell migration assay

Migration of cells was assessed using the Essen Bioscience CellPlayer™ 96-well cell migration assay. Cells were seeded at 40,000 cells per well in a 96-well ImageLock™ plate and cultured overnight to form a confluent monolayer. Wounds were then created through the monolayers using a WoundMaker™ tool, cells washed twice with medium and then 100 µl fresh culture medium was added. The plate was placed in the Incucyte™ machine, which is situated in a standard tissue culture incubator, and left to equilibrate for 10 minutes before starting image acquisition. Brightfield images of the wounds were taken every 2 hours for 24 hours and wound width at each time point measured by the Incucyte™ software.

2.4.12 Individual cell migration assay

Cells were seeded at a subconfluent density in a 6-well tissue culture plate which was then placed on a Nikon TE 2000 Timelapse microscope fitted with an incubation chamber set at 37°C with 5% CO₂. This was left for 1 hour to allow the cells to settle on the bottom of the dish and for the plastic to adjust to the conditions of the chamber. Brightfield images were then taken every 10 minutes for 4 hours with a 10x objective. Migration of individual cells was analysed using the manual tracking and chemotaxis tool plugins in Image J.

2.4.13 Cell invasion assay

Invasion of cells through a 3D matrix was assessed using the Essen Bioscience CellPlayer™ 96-well cell invasion assay. Cells were seeded at 40,000 cells per well in a 96-well ImageLock™ plate and cultured overnight to form a confluent monolayer. Wounds were created through the monolayers using a Woundmaker™ tool. Cells were washed twice with medium and overlaid with Matrigel™ (diluted 1:1 with PBS) which was then left in the tissue culture incubator for 30 minutes to set. An additional 100 µl of culture medium was added to each well and the plate left in the Incucyte™ machine to equilibrate for 10 minutes before starting image acquisition. Brightfield images of the wounds were taken every 2 hours for 10 hours and the relative wound density at each time point was measured by the Incucyte™ software.

2.5 Microscopy

2.5.1 Fluorescence lifetime imaging microscopy

All fluorescence lifetime imaging microscopy (FLIM) of the HyPer-cyto and HyPer-PM cells was carried out on a Nikon TE 2000 inverted microscope fitted with a Lambert Instruments FLIM Attachment (LIFA) and a Yokogawa CSU22 spinning disk unit using a x100 oil objective. The LIFA system was equipped with an Omicron 50 mW 445 nm laser for CFP lifetimes and a 60 mW 488 nm laser for GFP lifetimes. It is based on the frequency domain method for fluorescence lifetime imaging and allows the rapid acquisition and generation of lifetime images. Fluorescence lifetimes were measured using LI-FLIM software and the results presented in a box and whiskers plot where the box represents the upper

and lower quartiles and the middle line represents the median. The specific experiments carried out are described below.

2.5.1.1 Baseline fluorescence lifetime imaging

Cells were grown in 35 mm glass bottom dishes until 50% confluent. 24 hours before imaging, culture medium was changed to Optimem and 1 hour before imaging cells were transferred to L15 medium to help maintain physiological pH during imaging.

2.5.1.2 Fluorescence lifetime imaging following H₂O₂ treatment

Cells were grown in 35 mm glass bottom dishes until 50% confluent. 24 hours before imaging, culture medium was changed to Optimem and 1 hour before imaging cells were transferred to L15 medium to help maintain physiological pH during imaging. For experiments investigating a single dose of H₂O₂, the microscope software was set up to acquire images every 30 seconds for a total of 15 minutes. After 2 minutes of imaging, 100 µl 3 mM H₂O₂ was added to the dish in the area being imaged. For experiments investigating two sequential doses of H₂O₂, the microscope software was set up to acquire images every 30 seconds for a total of 30 minutes. After 2 minutes of imaging, the first dose of 100 µl 3 mM H₂O₂ was added to dish in the area being imaged. After the fluorescence lifetime had recovered to starting levels, a second dose of 100 µl 3 mM H₂O₂ was added to the dish in the area being imaged.

2.5.1.3 Fluorescence lifetime imaging of *in vitro* wound healing assay

Cells were grown in 35 mm glass bottom dishes until 100% confluent. A wound was then created through the middle of the cell monolayer using a P10 pipette tip. Cells were left for 1 hour to allow the cells at the wound edge to start migrating and then transferred to L15 medium for 1 hour before imaging. Cells that were migrating at the wound edge and cells that were stationary in the confluent monolayer area of the dish were imaged.

2.5.1.4 Fluorescence lifetime imaging of cell protrusions

Cells were grown in 35 mm glass bottom dishes until 100% confluent. A wound was then created through the middle of the cell monolayer using a P10 pipette

tip. Cells were left for 1 hour to allow the cells at the wound edge to start migrating and then transferred to L15 medium for 1 hour before imaging. Cells that were actively migrating at the wound edge and at the time of imaging had clear cell protrusions were imaged. The z-position of the microscope was carefully set for each cell to ensure that the image taken captured the tips of cell protrusions and the cell body.

2.6 Cellular protein extraction and analysis

2.6.1 Cell lysate preparation

After cells had been grown to the desired confluence or treated as required, they were lysed to extract proteins. Cell culture dishes were placed on ice, the culture medium removed and cells washed twice with ice cold PBS. RIPA lysis buffer was then added to the dish (100-150 μ l per well of a 6-well dish, depending on confluence; 400 μ l per 10 cm plate) and cell lysates collected by scraping. Lysates were then incubated on ice for 15 minutes before being centrifuged at 14,000 rpm for 15 minutes at 4°C. The supernatant was transferred to a new microfuge tube, protein concentration determined and samples stored at -20°C.

2.6.2 Protein concentration determination

Protein concentration of recombinant protein and cell lysates was determined using the bicinchoninic acid (BCA) assay. Protein standards (0.08, 0.1, 0.2, 0.4, 1 and 2 mg/ml) were prepared in the appropriate buffer (recombinant protein wash buffer or RIPA buffer for cell lysates) using a 2 mg/ml albumin standard stock solution. 10 μ l of blank (buffer alone), protein standards and samples were added to a Greiner Bio-One 96-well plate. 200 μ l of developing solution (50:1, bicinchoninic acid:copper sulphate solution) was added to each well and incubated at 37°C for 30-60 minutes. Absorbance was measured using a Molecular Devices microplate reader and sample concentrations determined from the standard curve.

2.6.3 Immunoprecipitation

For the immunoprecipitation of cofilin from MCF7 cells following NAC and dimedone treatment, the following method was used. Cells were lysed using RIPA buffer and protein concentration determined as described above. At every stage of this protocol, Dynabeads were separated from the supernatant using a magnetic tube rack. 50 μ l of protein A Dynabead solution per immunoprecipitation was washed twice with PBS-T by rotating for 10 minutes at 4°C. Beads were then resuspended in 200 μ l PBS-T containing 2 μ g anti-cofilin Ab (Abcam: ab42824) and incubated for 1 hour at 4°C while rotating. Bead-Ab complexes were washed 3 times in 1 ml PBS-T by rotating for 10 minutes at 4°C. These were then incubated with 500 μ g lysate, in a total volume of 500 μ l, at 4°C while rotating. Beads were then washed 5 times with 1 ml PBS, as done previously, before being transferred in 100 μ l PBS to a new microfuge tube and resuspended in 20 μ l NuPAGE LDS sample buffer. Samples were stored at -20°C for further analysis by SDS-PAGE and western blot.

For the immunoprecipitation of cofilin from MDAMB231 cells following wounding and dimedone treatment, the following method was used. At every stage of this protocol, protein G Sepharose beads were separated from the supernatant by centrifuging in an Eppendorf 5417R centrifuge at 3,600 rpm for 1 minute at 4°C. Cells were washed with ice cold PBS and then lysed in IP lysis buffer (1 ml per 6-well or 10 cm plate) and harvested by scraping. Lysates were placed in 1.5 ml microfuge tubes and incubated at 4°C for 20-30 minutes while rotating. During this time 200 μ l of protein G Sepharose bead solution was washed 3 times with 1 ml TBS. Cell lysates were then centrifuged in an Eppendorf 5417R centrifuge at 13,200 rpm for 10 minutes, the supernatant removed and protein concentration determined. Equivalent quantities of lysate from each condition were then incubated with 25 μ l of protein G Sepharose beads for 30 minutes on a rotating wheel to remove proteins that bound non-specifically to the beads. After centrifuging to remove the beads, the lysates were incubated with anti-cofilin antibody or mouse IgG at a 1:25 dilution overnight at 4°C on a rotating wheel. 25 μ l of protein G Sepharose bead solution, which had been washed in the same way as before, was added to each tube and incubated for 1 hour at 4°C while rotating. Beads were washed three times in 1 ml TBS before being resuspended in 25 μ l of prewarmed (95°C) 1% SDS and then heated at 95°C for 5 minutes.

Samples were centrifuged in an Eppendorf 5417R centrifuge at 3,600rpm for 2 minutes after which the supernatant was removed and SDS sample buffer added. Samples were stored at -20°C until they were analysed by SDS-PAGE and western blot.

2.6.4 SDS-polyacrylamide gel electrophoresis

SDS-polyacrylamide gel electrophoresis (PAGE) was used to separate protein samples based on molecular weight. Protein samples were first prepared in sample buffer. For 15% Tris-glycine gels (recipe below), protein samples were prepared in SDS sample buffer and heated at 100°C for 3 minutes. For 4-12% NuPAGE Bis-tris gels, protein samples were prepared in NuPAGE LDS sample buffer with NuPAGE reducing agent for reducing gels or without for non-reducing gels. In both cases samples were heated at 70°C for 10 minutes. After heating, samples were briefly centrifuged and loaded on the gels alongside Precision Plus Protein™ all blue molecular weight marker. In general, Tris-glycine gels were run in tanks containing 1x SDS running buffer at 120 V for approximately 2 hours. Both reducing and non-reducing NuPAGE Bis-tris gels were run in tanks containing 1x NuPAGE MES running buffer at 150 V for approximately 1 hour 15 minutes. Afterwards, gels were either stained or used for western blotting.

Reagent	Separating Gel	Stacking Gel
30% Acrylamide mix	15 ml	1.7 ml
1 M Tris pH 6.8	-	1.25 ml
1 M Tris pH 8.8	7.5 ml	-
10% SDS	300 µl	100 µl
H ₂ O	6.9 ml	6.8 ml
10% ammonium persulfate	300 µl	100 µl
TEMED	24 µl	50 µl

2.6.5 Gel staining

Following protein separation by SDS-PAGE some gels were stained to detect protein bands as follows. Gels were washed in distilled water (dH₂O) for 5

minutes and this was repeated three times. Gels were then incubated in SimplyBlue™ SafeStain for 1 hour at room temperature. Following this, gels were washed in dH₂O for 1 hour and then overnight. Images of stained gels were acquired on a LI-COR Odyssey® system.

2.6.6 Western blotting

Following protein separation by SDS-PAGE some gels were used for western blotting. Proteins were transferred to Protran™ nitrocellulose membrane using a Bio-Rad Mini Trans-Blot® Cell. Proteins from Tris-glycine gels were transferred in tanks containing 1x SDS transfer buffer while proteins from NuPAGE Bis-tris gels were transferred in tanks containing 1x NuPAGE transfer buffer. All transfers were run at 100 V for 1 hour. The nitrocellulose membrane was blocked with 5% (w/v) milk powder in TBS-T (TBS-TM) for 1 hour. Primary antibodies were diluted to the required concentration in TBS-TM and membranes incubated with these solutions for 1 hour at room temperature or 4°C overnight. This was followed by four washes in TBS-T for 5 minutes each. The membrane was then incubated with the secondary antibody that had been diluted to the required concentration in TBS-TM, for 30-60 minutes at room temperature. After the blot was washed in TBS-T three times for 5 minutes each, it was rinsed in dH₂O and protein bands visualised on the LI-COR Odyssey® system. Protein bands were quantified using Image Studio Lite Version 3.1. Antibodies used for western blotting and the concentrations used are listed below.

Antibody	Concentration
Cofilin (Ab75510)	1:2000
Cofilin (Ab42824)	1:1000
Cofilin (ACFL02-A)	1:2000
Dimedone	1:5000
DsRed	1:1000
ERK2	1:2000
GFP	1:2000
All secondary antibodies	1:5000

3 Reactive Oxygen Species and Cell Migration

3.1 Introduction

There are a number of *in vitro* and *in vivo* studies demonstrating that ROS are required for cell migration. These have mainly involved increasing or decreasing antioxidant or ROS scavenging enzymes, which resulted in an inhibition or enhancement of cell migration respectively [255-259]. Increased ROS levels in migrating cells have also been shown directly through the use of fluorescent ROS sensors. Additionally, these studies identified an accumulation of ROS at the leading edge of migrating cells and at membrane ruffles which are the regions of the cell undergoing the most dynamic changes in the actin cytoskeleton [266, 277]. However, which of the many ROS are specifically elevated in migrating cells has not yet been determined. Therefore, I set out to establish if the ROS, H₂O₂, was increased in migrating cells globally and within specific regions of the cell. The results from these investigations are presented in this chapter.

3.2 Results

3.2.1 NAC reduces cellular ROS levels in MDAMB231 cells

To better understand the relationship between cellular ROS levels and migration I first wanted to find a method by which I could reliably reduce cellular ROS levels in the MDAMB231 cell line. I decided to treat cells with the ROS scavenger NAC and determine its effect on cellular ROS levels using the ROS sensitive chemical DCFDA. DCFDA is cell permeable and not fluorescent, however when it enters cells, it is deacetylated by cellular esterases to form DCF. When DCF is oxidised by ROS in cells, it becomes highly fluorescent with maximum excitation and emission wavelengths of 485 nm and 528 nm respectively, and therefore cellular ROS levels can be determined by measuring the fluorescence.

MDAMB231 cells that had been seeded in a 96-well plate were treated with NAC at 0, 2.5, 5 or 10 mM for 3 hours followed by incubation with DCFDA. Fluorescence and therefore ROS levels were then measured using a fluorescence plate reader. These results revealed that, as expected, there was a concentration dependent decrease in relative ROS levels following NAC

treatment, with significantly lower levels observed with 10 mM NAC compared to control (0 mM NAC) (Figure 3-1).

3.2.2 Reducing cellular ROS levels decreases cell migration

Having confirmed that NAC was able to effectively reduce ROS levels in MDAMB231 cells, I next wanted to see if this had any effect on the ability of the cells to migrate. To address this I used the Essen Bioscience CellPlayer™ 96-well cell migration assay, which is based on a traditional wound healing assay. Wound healing assays are used as a simple way to measure cell migration and based on the finding that cells will migrate into the wound until new cell-cell contacts are made [320]. The benefits of the Essen Bioscience CellPlayer™ 96-well assay is that the wounds created are much more reproducible, as they are made using a device designed for this purpose rather than by hand, and it has a much higher throughput.

MDAMB231 cells were seeded in a 96-well ImageLock™ plate, a specialised plate that allows wounds to be located by the Incucyte™ software, and cultured overnight to form a confluent monolayer. Wounds were then created through the middle of the monolayer using the WoundMaker™, a device containing 96 pins that each produce a wound in the wells of a 96-well plate. After this, cells were treated with 0, 2.5, 5 or 10 mM NAC and the plate placed in the Incucyte™ machine, which was scheduled to acquire images of the wounds every 2 hours for a total of 24 hours. The Incucyte™ software automatically analyses the wound and reports three parameters for each time point; wound width (the average distance between the edges of the wound), wound confluence (percentage of initial wound area that is covered by cells) and relative wound density (a measure of the density of the wound region compared to the cell regions). As the edges of the wound with MDAMB231 cells remain relatively parallel to one another, I decided to use the wound width as a measure of cell migration. Treatment of cells with NAC resulted in a concentration dependent decrease in wound closure (Figure 3-2) that mirrored the decrease in ROS levels observed with the same concentrations of NAC (Figure 3-1).

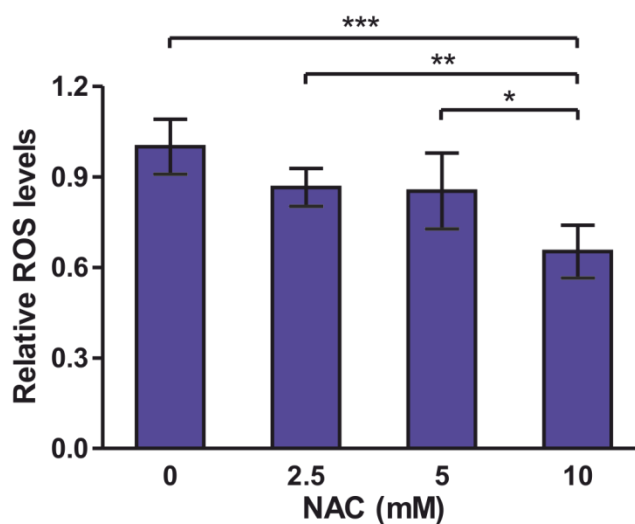


Figure 3-1 The antioxidant NAC reduces cellular ROS levels

MDAMB231 cells were seeded in a 96-well plate and allowed to adhere overnight. Cells were then treated with NAC at the indicated concentrations for 3 hours followed by measurement of cellular ROS levels using the cell permeable, ROS sensitive probe DCFDA. Graph indicates the mean relative ROS levels \pm standard error of the mean (SEM) measured across 4 independent experiments. Statistical significance of differences was determined by a one-way ANOVA followed by a Tukey Kramer multiple comparison test (*= $p < 0.05$, **= $p < 0.01$, ***= $p < 0.001$).

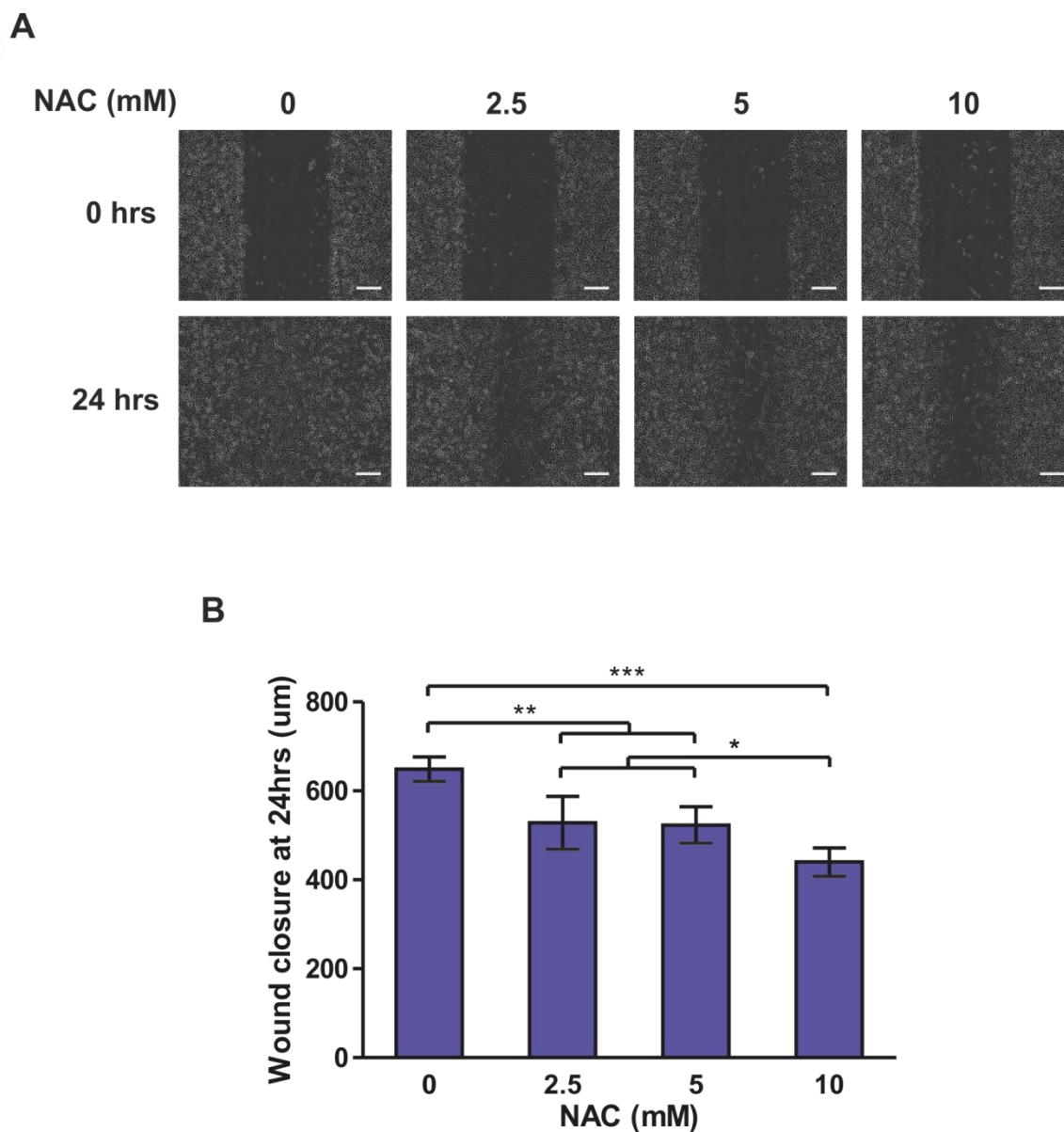


Figure 3-2 Decreasing cellular ROS levels with NAC reduces wound closure

MDAMB231 cells were seeded in a 96-well ImageLock™ plate and allowed to adhere overnight forming a confluent monolayer. Wounds were then created using a WoundMaker™ and cells treated with NAC at the indicated concentrations. Wound width was measured every 2 hours for a total of 24 hours using the Incucyte™ system. A) Representative images taken of the wounds at 0 and 24 hours. Scale bars = 200 μm. B) Graph indicates the mean wound closure at 24 hours +/- SEM measured across 3 independent experiments. Statistical significance of differences was determined by a one-way ANOVA followed by a Tukey Kramer multiple comparison test (*=p<0.05, **=p<0.01, ***=p<0.001).

3.2.3 Establishment of MDAMB231 cell line stably expressing HyPer-cyto

After finding that the presence of ROS was required for cell migration, I next wanted to know if I could directly see ROS being produced in migrating cells. To investigate this, I employed a fluorescent probe, HyPer, that can detect H_2O_2 , one of the ROS, in live cells. This was an attractive tool as it would allow me to image the production of H_2O_2 in real time in migrating cells. Additionally it can specifically detect H_2O_2 which, as described in Chapter 1, is a well established second messenger in cells and therefore a possible mediator of downstream responses in migrating cells. HyPer is composed of circularly permuted yellow fluorescent protein (YFP) inserted into the regulatory domain of the *E. coli* transcription factor OxyR. HyPer has two excitation peaks with maximums at 420 nm and 500 nm and one emission peak with a maximum of 516 nm. In the presence of H_2O_2 a disulphide bond forms between two cysteine residues (cysteine 199 and cysteine 208) in the OxyR part of HyPer that results in a conformational change [321]. This change in structure alters the excitation and emission spectra with a decrease in the excitation peak at 420 nm and a proportional increase in the excitation peak at 500 nm (Figure 3-3) [322]. The presence of H_2O_2 can therefore be measured by ratiometric confocal microscopy comparing the emission after excitation at 500 nm to that at 420 nm.

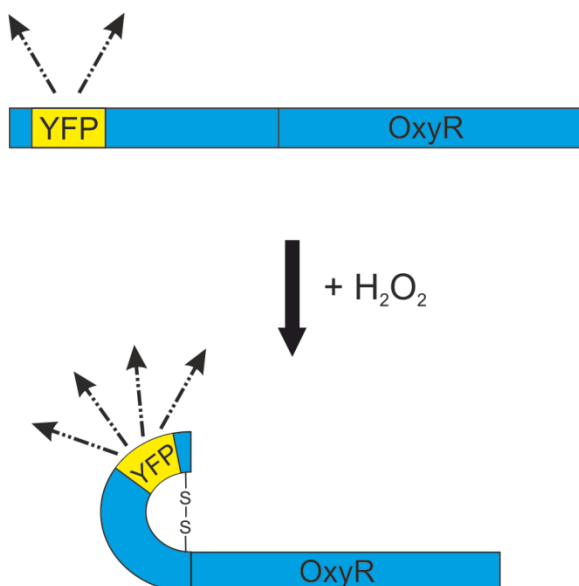


Figure 3-3 Schematic diagram of H_2O_2 sensing HyPer-cyto probe activation

HyPer is an H_2O_2 sensing fluorescent probe in which a derivative of YFP has been inserted into the regulatory domain of the bacterial OxyR protein. HyPer-cyto is a form of this probe that is expressed throughout the cell cytoplasm. In the presence of H_2O_2 , there is a conformational change in the probe resulting from the formation of a disulphide bond which leads to a change in the spectral properties of the probe.

I decided that the most efficient way to conduct my experiments using the HyPer-cyto probe (form of HyPer that is expressed throughout the cytoplasm) was to create a MDAMB231 cell line stably expressing the probe. To do this I transfected parental MDAMB231 cells with a plasmid expressing HyPer-cyto and a gene conferring resistance to G418. 48 hours after transfection, cells were transferred to G418 containing medium and cultured until all control cells that had not been transfected with the plasmid had died. The surviving cells expressing HyPer-cyto were selected by cell sorting using a FACSaria cell sorter and subdivided into populations expressing the probe at low, medium and high levels (Figure 3-4 A). The cells expressing HyPer-cyto at a medium level were then used for further experiments after confirming that the probe was expressed in these cells by western blot analysis using anti-green fluorescent protein (GFP) Ab capable of detecting HyPer (Figure 3-4 B). This population of cells was chosen because, out of the three subpopulations, they had the lowest level of HyPer-cyto expression that was still high enough for detection by microscopy.

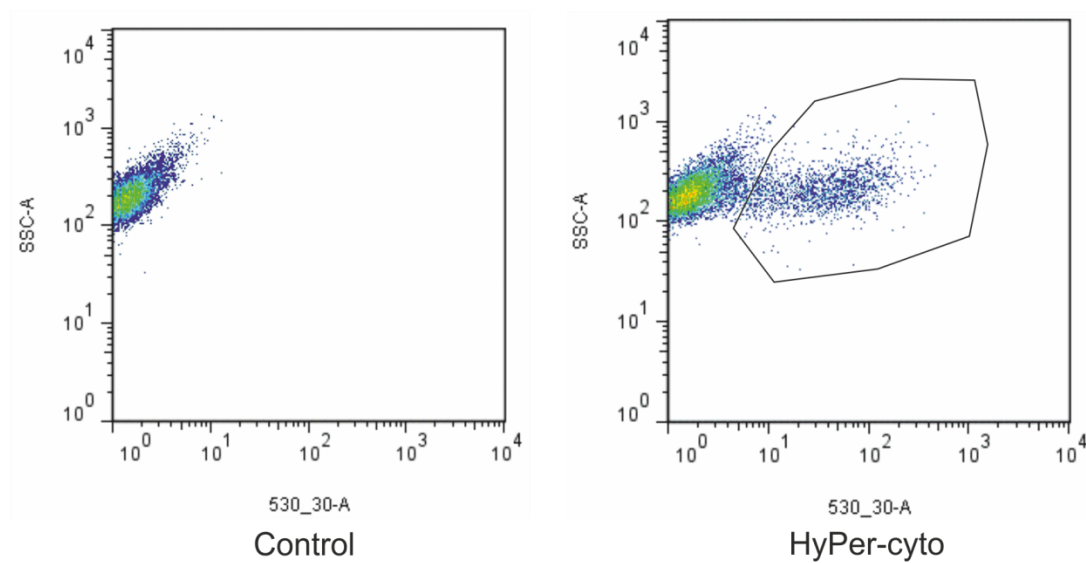
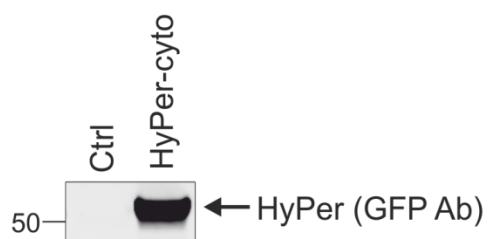
A**B**

Figure 3-4 Creation of MDAMB231 cell line stably expressing HyPer-cyto

A) FACS plots confirming a population of cells which positively expressed the HyPer-cyto probe. B) Western blot confirming the stable expression of HyPer-cyto in the MDAMB231 cell line. Membrane probed using anti-GFP Ab capable of detecting HyPer.

3.2.4 Baseline fluorescence lifetime of MDAMB231 HyPer-cyto cells

I wanted to extend the potential uses of HyPer-cyto by investigating if the presence of H_2O_2 could also be measured by fluorescence lifetime imaging microscopy (FLIM). The benefits of this are that only one wavelength image needs to be acquired allowing for faster data acquisition and less post acquisition analysis is required to determine H_2O_2 levels. The fluorescence lifetime measured is also independent of the concentration of the probe so slight cell to cell differences in expression will not affect the results.

Before investigating if H_2O_2 production could be monitored using FLIM, I wanted to know the fluorescence lifetime of HyPer-cyto in cells with basal H_2O_2 levels. Therefore, I imaged MDAMB231 HyPer-cyto cells using a microscope fitted with a LIFA system and measured the fluorescence lifetime using LI-FLIM software. The average fluorescence lifetime of these cells was 1.463 ns (Figure 3-5).

3.2.5 HyPer-cyto fluorescence lifetime decreases after the addition of H_2O_2

The next step of the investigation was to see how the fluorescence lifetime of HyPer-cyto changed with the addition of exogenous H_2O_2 . To test this, I cultured MDAMB231 HyPer-cyto cells in 35 mm glass bottom dishes to 50% confluence. Fields of view containing between one and four cells expressing HyPer-cyto were then imaged on a microscope fitted with a LIFA system every 30 seconds for a total of 15 minutes. After the 4th image had been acquired (around 2 minutes), 100 μl of 3 mM H_2O_2 was added to the dish. I found that the addition of H_2O_2 resulted in a significant decrease in HyPer-cyto fluorescence lifetime (Figure 3-6).

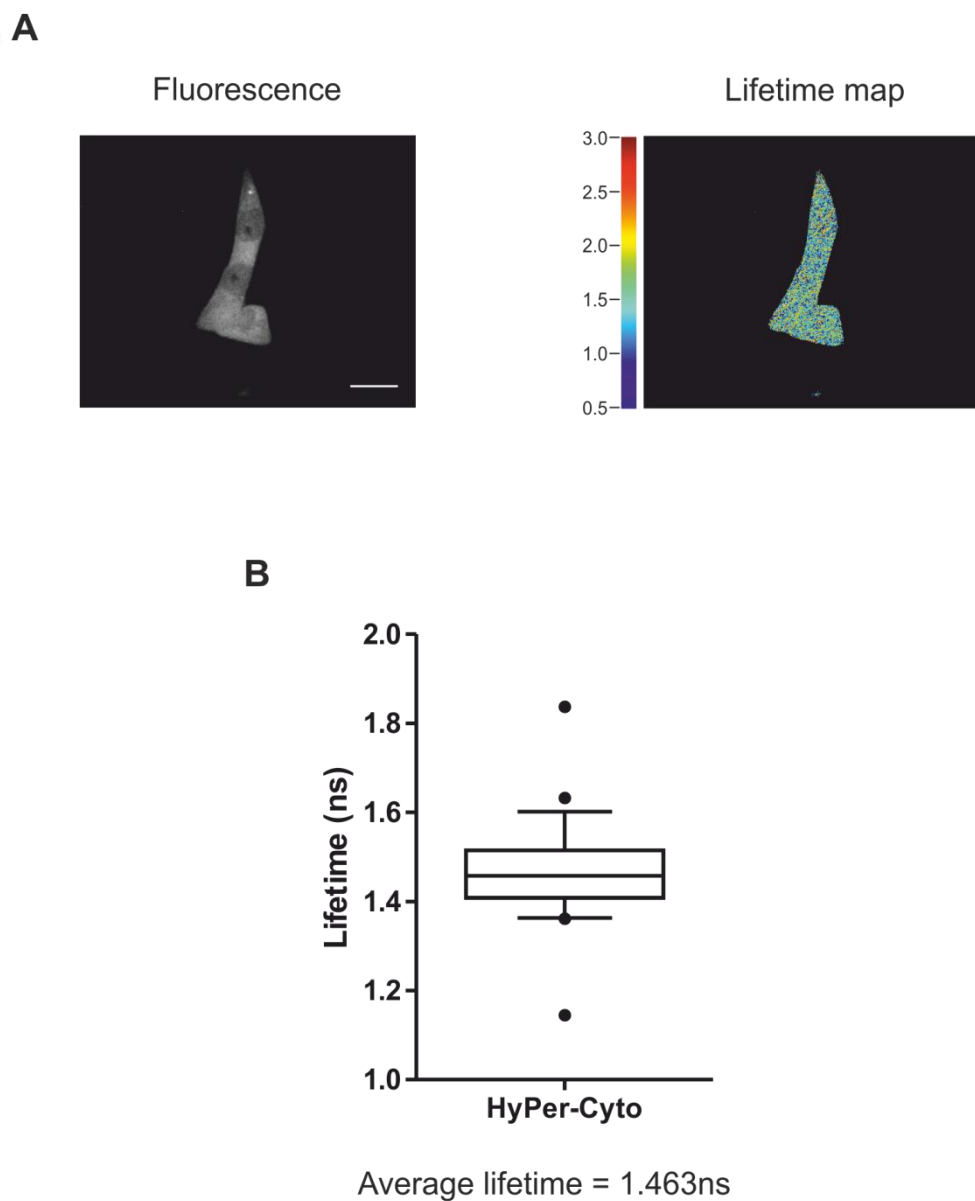
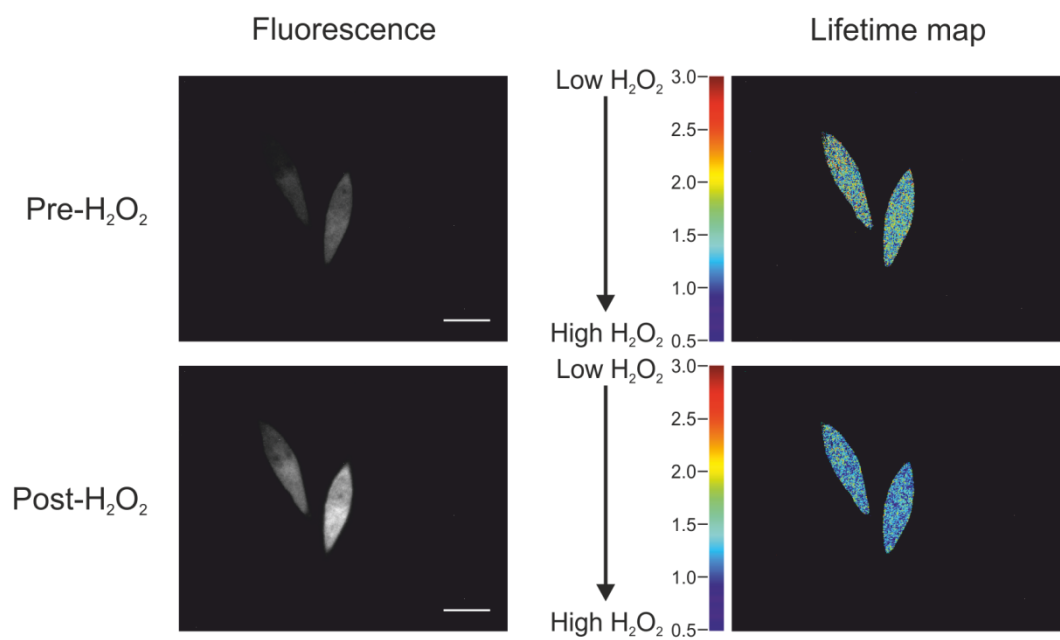
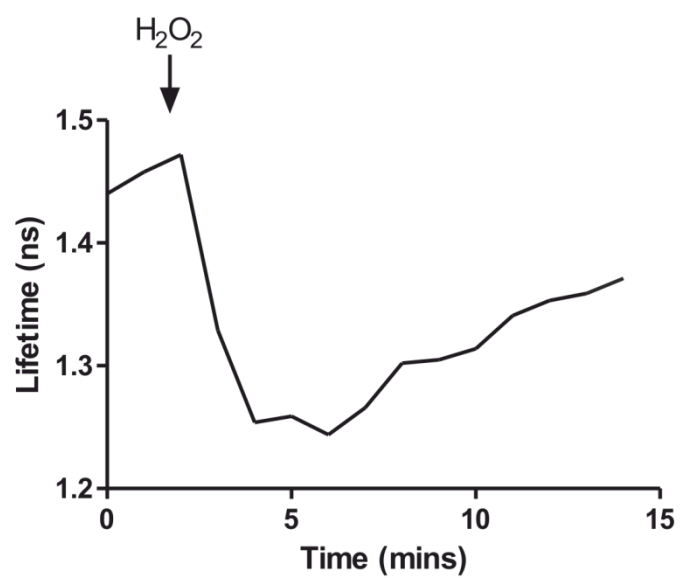
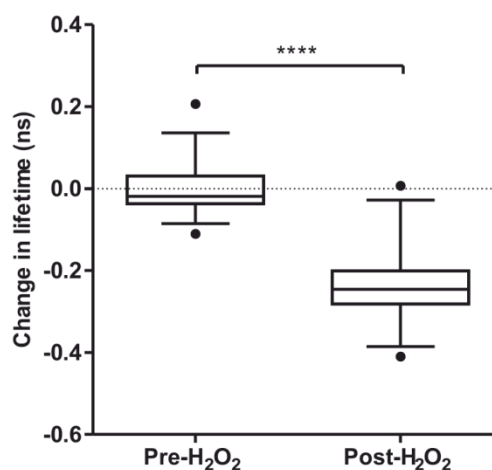


Figure 3-5 Expression and average fluorescence lifetime of HyPer-cyto

MDAMB231 HyPer-cyto cells were imaged on a microscope fitted with a LIFA system and fluorescence lifetime measured using LI-FLIM software. A) Representative fluorescence image and corresponding lifetime map of MDAMB231 HyPer-cyto cells. Scale bar = 20 μm . B) Box and whiskers plot (5-95 percentile) representing range of baseline fluorescence lifetimes observed in MDAMB231 HyPer-cyto cells with average fluorescence lifetime measured indicated. Results from 55 cells.

A**B**

C



D

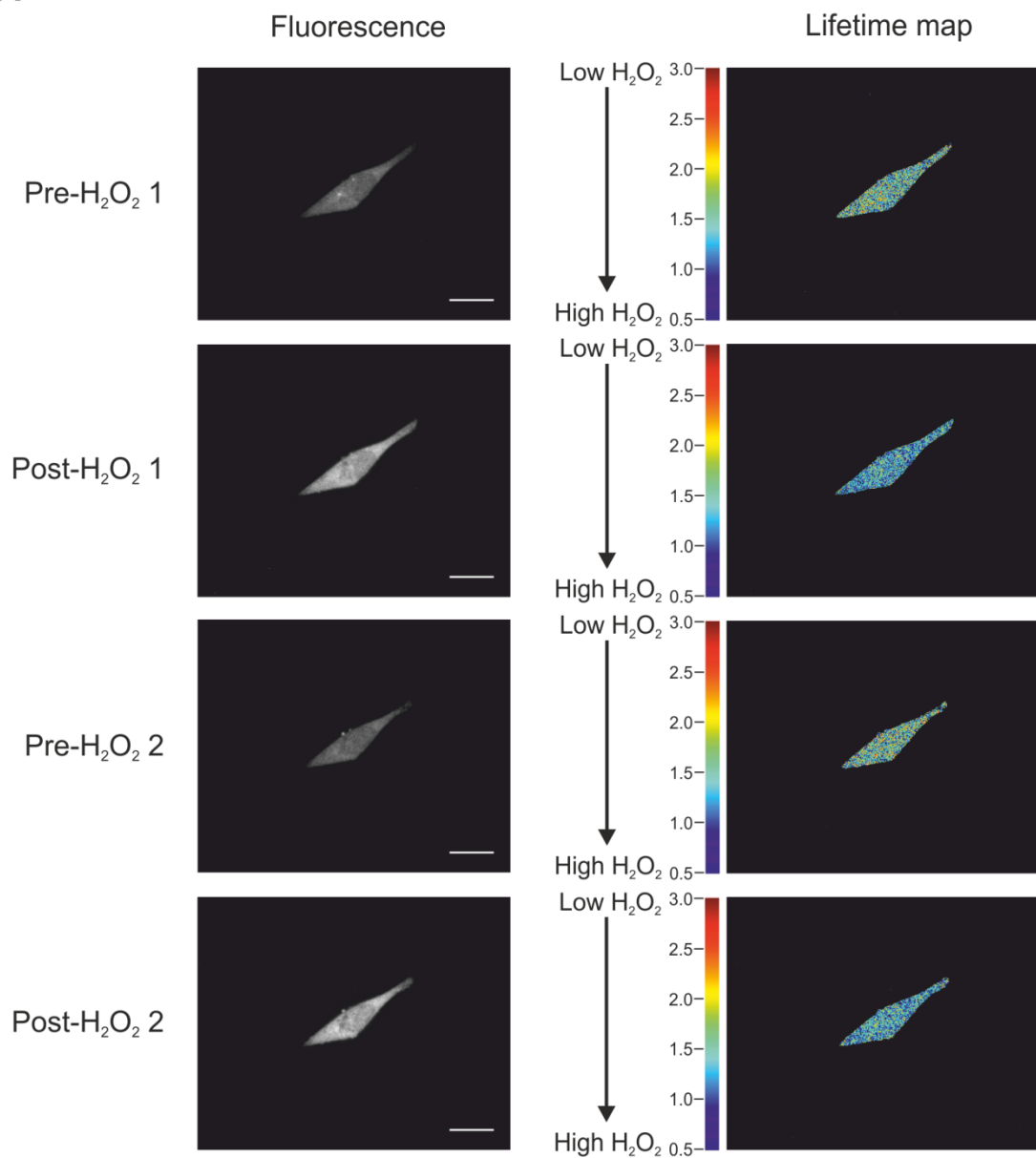
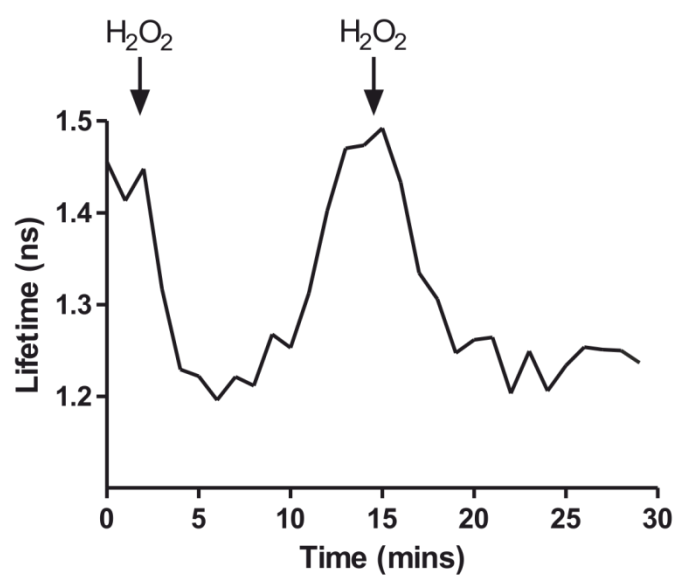
	Pre-H ₂ O ₂	Post-H ₂ O ₂
Average lifetime (ns)	1.472	1.241

Figure 3-6 HyPer-cyto fluorescence lifetime decreases after addition of H₂O₂

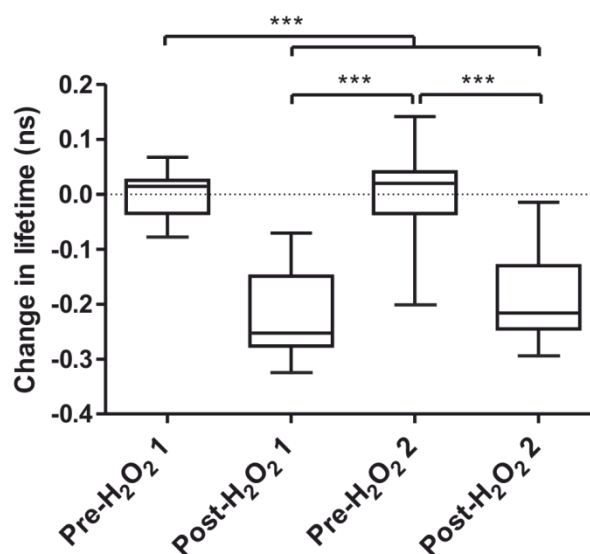
MDAMB231 HyPer-cyto cells were grown in 35 mm glass bottom dishes until ~50% confluent. Fields of view containing between one and four cells expressing HyPer-cyto were imaged on a microscope fitted with a LIFA system every 30 seconds for a total of 15 minutes with 100 μ l 3 mM H₂O₂ added at ~2 minutes. Fluorescence lifetime was measured in each cell over the time course using LI-FLIM software. A) Representative fluorescence images and corresponding lifetime maps of MDAMB231 HyPer-cyto cells before and after H₂O₂ treatment. Scale bar = 20 μ m. B) Graph showing change in fluorescence lifetime over a 15 minute period with the point of H₂O₂ addition indicated. Results displayed are average of 32 cells. C) Box and whiskers plot (5-95 percentile) indicating range of changes in fluorescence lifetimes observed after H₂O₂ addition. D) Table showing average fluorescence lifetimes measured before and after H₂O₂ treatment. Results from 32 cells. Statistical significance of differences determined by a paired t-test (****=p<0.0001).

3.2.6 Change in fluorescence lifetime of HyPer-cyto after the addition of H₂O₂ is reversible.

As changes in H₂O₂ levels in cells are likely to be transient events, I wanted to assess if the fluorescence lifetime of HyPer-cyto would return to normal levels after it is decreased by the addition of H₂O₂, and if at this point HyPer-cyto could be reactivated by a further addition of H₂O₂. For this reason I repeated the previous experiment, but this time continued to measure the fluorescence lifetime every 30 seconds for a total of 30 minutes. After the addition of the first dose of H₂O₂, I waited for the fluorescence lifetime to return to starting levels and then added a second dose of 100 µl 3 mM H₂O₂. These experiments revealed that with time, the decrease in fluorescence lifetime observed when H₂O₂ was added returned to starting levels. In addition, HyPer-cyto could be restimulated by a second dose of H₂O₂ again significantly decreasing the fluorescence lifetime. It was noted that there was no significant difference in the fluorescence lifetimes measured before the first and second doses of H₂O₂ nor between the fluorescence lifetimes after each H₂O₂ dose (Figure 3-7). This confirms that HyPer-cyto can fully recover after activation by H₂O₂ and is equally sensitive to a second increase in H₂O₂ of the same dose. These results are not unexpected as the change in lifetime occurs due to the formation of a disulphide bond which would be exposed to and reduced by the cells endogenous mechanisms to protect itself against oxidative damage. Consequently, the probe would be returned to its inactivated state and sensitive to subsequent activations.

A**B**

C



D

	Pre-H ₂ O ₂ 1	Post-H ₂ O ₂ 1	Pre-H ₂ O ₂ 2	Post-H ₂ O ₂ 2
Average lifetime (ns)	1.493	1.273	1.493	1.302

Figure 3-7 HyPer-cyto fluorescence lifetime recovers to baseline levels following H₂O₂ treatment and can be reactivated following further H₂O₂ addition

MDAMB231 HyPer-cyto cells were grown in 35 mm glass bottom dishes until ~50% confluent. Fields of view containing between one and four cells expressing HyPer-cyto were imaged on a microscope fitted with a LIFA system every 30 seconds for a total of 30 minutes with 100 μ l 3 mM H₂O₂ added after ~2 minutes and after fluorescence lifetime had returned to starting levels. Fluorescence lifetime was measured in each cell over the time course using LI-FLIM software. A) Representative fluorescence images and corresponding lifetime maps of MDAMB231 HyPer-cyto cells before and after first and second H₂O₂ treatments. Scale bar = 20 μ m. B) Graph showing change in fluorescence lifetime over a 30 minute period with the points of first and second H₂O₂ addition indicated. Results displayed are from a representative cell. C) Box and whiskers plot (5-95 percentile) indicating range of changes in fluorescence lifetimes observed before and after each H₂O₂ treatment. D) Table showing average fluorescence lifetimes measured before and after each H₂O₂ treatment. Results from 18 cells. Statistical significance of differences determined by a one-way ANOVA followed by a Tukey Kramer multiple comparison test (**= $p < 0.001$).

3.2.7 H₂O₂ levels are higher in migrating cells than stationary cells

Having validated the use of FLIM as a way to measure H₂O₂ levels with HyPer-cyto, I now wanted to determine if I could detect the production of H₂O₂ in migrating cells. To do this, I cultured MDAMB231 HyPer-cyto cells in 35 mm glass bottom dishes until they formed a confluent monolayer. Wounds were then created through the middle of the monolayer using a P10 pipette tip. Cells were then left for 1 hour to allow time for cells to start migrating to close the wound. Cells at the edge of the wound (classified as migrating) and those in the confluent areas of the dish (classified as stationary) were then imaged on a microscope fitted with a LIFA system and fluorescence lifetime measured using LI-FLIM software. I discovered that there was a significantly lower fluorescence lifetime and therefore higher H₂O₂ levels in cells that were migrating (Figure 3-8).

3.2.8 Establishment of MDAMB231 cell line stably expressing HyPer-PM

After finding that H₂O₂ levels were elevated globally in migrating compared to stationary cells, I next wanted to know if this was also the case at the plasma membrane of cells. My reason for asking this was due to the fact that the plasma membrane is where signals from outside the cell are received and processed and the area of the cell that undergoes the most dynamic changes when migrating [35, 55]. To address this, I modified the HyPer-cyto probe by the addition of a CAAX motif (full sequence can be found in Table 2-8) at the C terminus, localising it to cell membranes and called this version HyPer-PM (Figure 3-9). Proteins that have this motif at their C terminus are targeted by a series of enzymes that modify the protein to become hydrophobic and consequently integrated into cell membranes [323].

I made a MDAMB231 cell line stably expressing this probe by transfecting parental MDAMB231 cells with a plasmid expressing HyPer-PM and a gene conferring resistance to G418. 48 hours after transfection, cells were transferred to G418 containing medium and cultured until all control cells that had not been transfected with the plasmid died. Surviving cells expressing HyPer-PM were selected by cell sorting using a FACSaria cell sorter and subdivided into

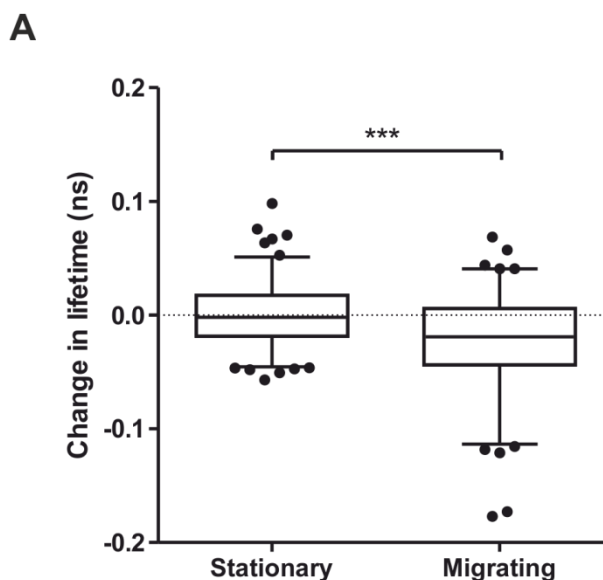
populations expressing the probe to low, medium and high levels (Figure 3-10 A). In this case the cells expressing HyPer-PM to the highest level were used for further experiments after confirming that the probe was expressed in these cells by western blot analysis using anti-GFP Ab capable of detecting HyPer (Figure 3-10 B). This population of cells was chosen as it was the only population that expressed HyPer-PM to a high enough level for detection by microscopy.

3.2.9 Baseline fluorescence lifetime of MDAMB231 HyPer-PM cells

Before investigating if HyPer-PM responded to H_2O_2 in the same way as HyPer-cyto, I wanted to know the fluorescence lifetime of HyPer-PM in cells with basal H_2O_2 levels. I therefore imaged MDAMB231 HyPer-PM cells using a microscope fitted with a LIFA system and measured the fluorescence lifetime using LI-FLIM software. The average fluorescence lifetime of these cells was 1.404 ns (Figure 3-11). This is slightly, but significantly, lower than was observed for HyPer-cyto (Figure 3-5) which could mean that the areas at cell membranes have higher levels of H_2O_2 than the cell as a whole or that the integration of the probe into the cell membrane slightly alters its fluorescence lifetime.

3.2.10 HyPer-PM fluorescence lifetime decreases upon the addition of H_2O_2

I next wanted to test whether HyPer-PM responded to the addition of H_2O_2 in the same way as HyPer-cyto to ensure that adding the CAAX motif and targeting the probe to the membrane had not changed its sensitivity. In the same way as I did for HyPer-cyto cells, I cultured MDAMB231 HyPer-PM cells in 35 mm glass bottom dishes until around 50% confluent. Fields of view containing between one and four cells expressing HyPer-PM were then imaged on a microscope fitted with a LIFA system every 30 seconds for a total of 15 minutes. After the 4th image had been acquired (around 2 minutes) 100 μ l of 3 mM H_2O_2 was added to the dish. As with HyPer-cyto, addition of H_2O_2 to the MDAMB231 HyPer-PM cells resulted in a significant decrease in the fluorescence lifetime of HyPer-PM (Figure 3-12).



B

	Stationary	Migrating
Average lifetime (ns)	1.403	1.382

Figure 3-8 H₂O₂ levels elevated in migrating compared to stationary cells

MDAMB231 HyPer-cyto cells were grown in 35 mm glass bottom dishes until they formed a confluent monolayer. A wound was then created through the middle of the monolayer and after 1 hour cells still in a confluent area of the dish (stationary cells) and those at the edge of the wound (migrating cells) were imaged on a microscope fitted with a LIFA system. Fluorescence lifetime was measured in each cell imaged using LI-FLIM software. A) Box and whiskers plot (5-95 percentile) showing the range of changes in fluorescence lifetimes observed in migrating cells compared to stationary cells. B) Table showing average lifetimes measured in stationary and migrating cells. Results from >102 cells. Statistical significance of differences determined by an unpaired t-test (**= $p < 0.001$).

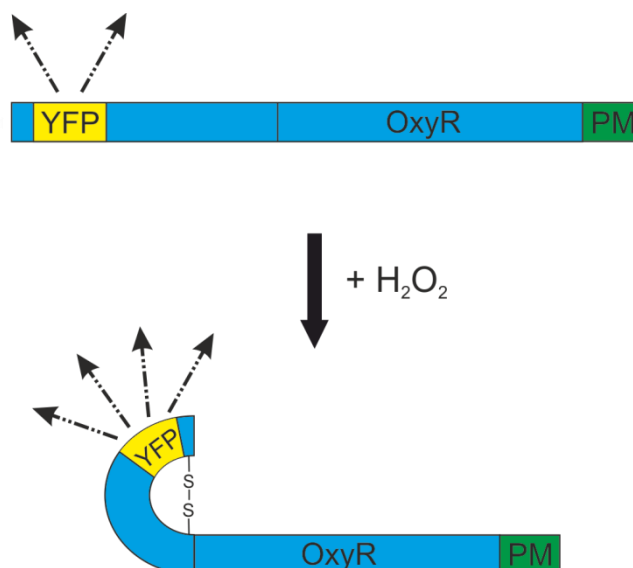
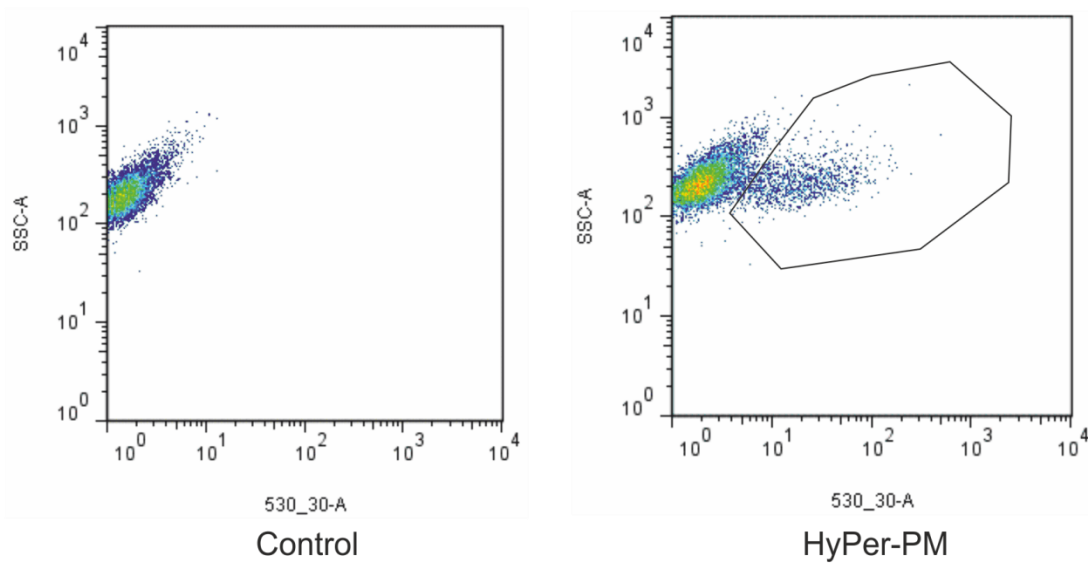
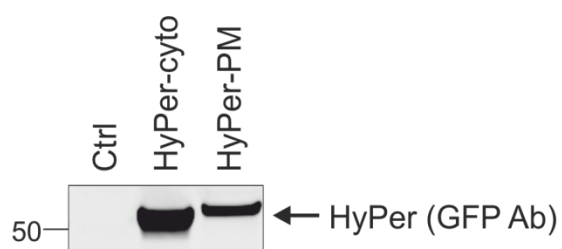


Figure 3-9 Schematic diagram of H₂O₂ sensing HyPer-PM probe activation

HyPer is an H₂O₂ sensing fluorescent probe in which a derivative of YFP has been inserted into the regulatory domain of the bacterial OxyR protein. HyPer-PM is a form of this probe that has been modified from the HyPer-cyto version by the addition of a CAAX motif (full sequence can be found in Table 2-8) (PM – green), localising it to the plasma membrane. In the presence of H₂O₂ there is a conformational change resulting from a disulphide bond being formed which leads to a change in the spectral properties of the probe.

A**B****Figure 3-10 Creation of MDAMB231 cell line stably expressing HyPer-PM**

A) FACS plots confirming a population of cells that positively expressed the HyPer-PM probe. B) Western blot confirming the stable expression of HyPer-PM and HyPer-cyto in MDAMB231 cell lines. Membrane was probed using anti-GFP Ab capable of detecting HyPer.

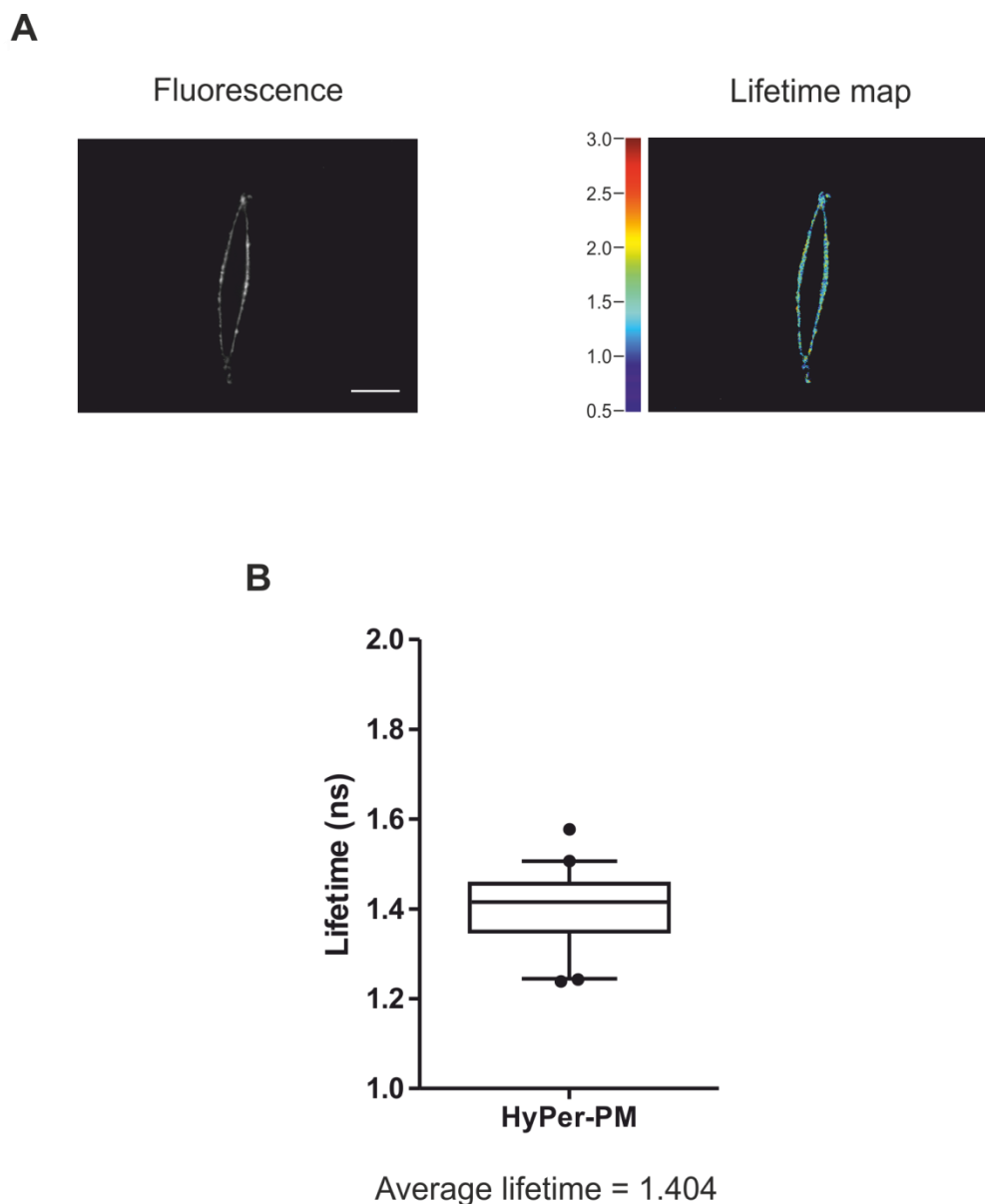
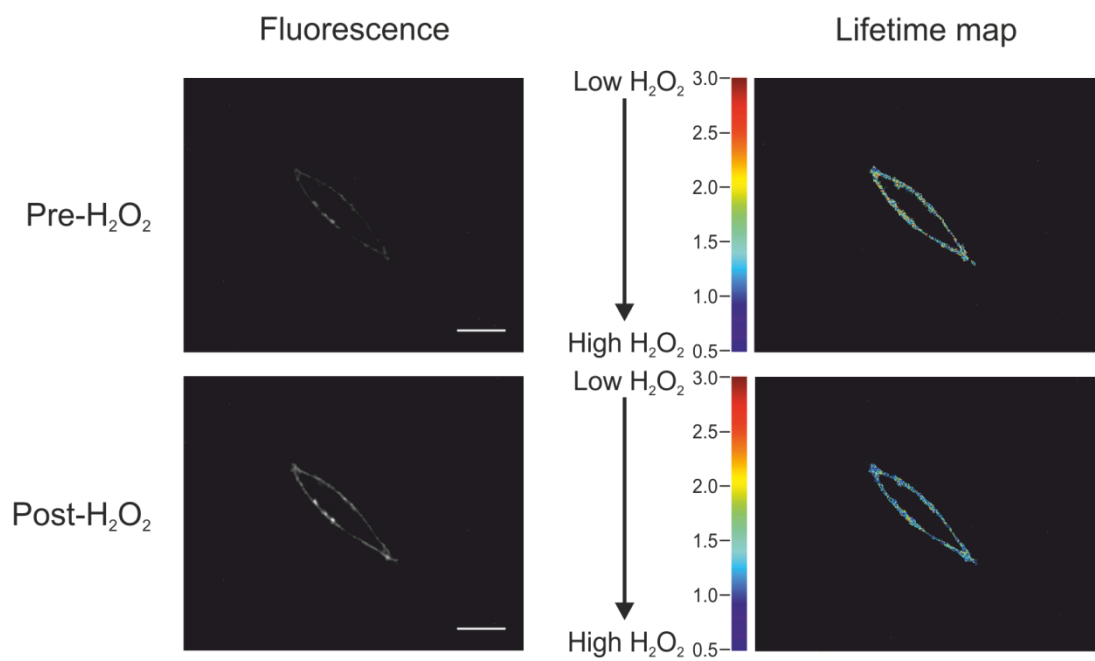
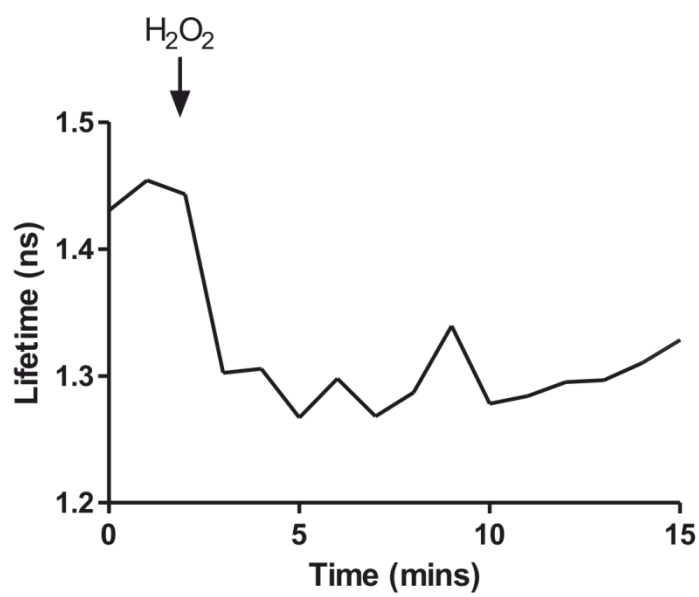
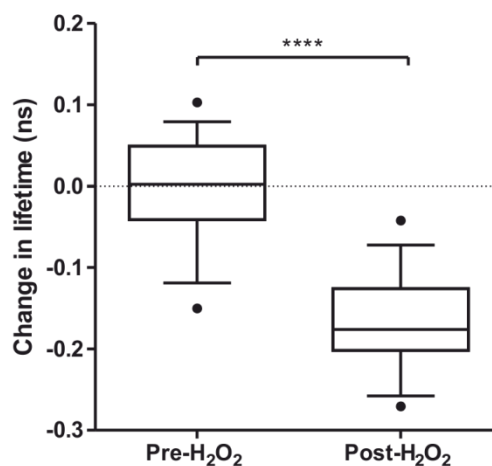


Figure 3-11 Expression and average fluorescence lifetime of HyPer-PM

MDAMB231 HyPer-PM cells were imaged on a microscope fitted with a LIFA system and fluorescence lifetime measured using LI-FLIM software. A) Representative fluorescence image and corresponding lifetime map of MDAMB231 HyPer-PM cell. Scale bar = 20 μm . B) Box and whiskers plot (5-95 percentile) representing range of baseline fluorescence lifetimes observed in MDAMB231 HyPer-PM cells with average fluorescence lifetime measured indicated. Results from 42 cells.

A**B**

C



D

	Pre-H ₂ O ₂	Post-H ₂ O ₂
Average lifetime (ns)	1.425	1.256

Figure 3-12 HyPer-PM fluorescence lifetime decreases after addition of H₂O₂

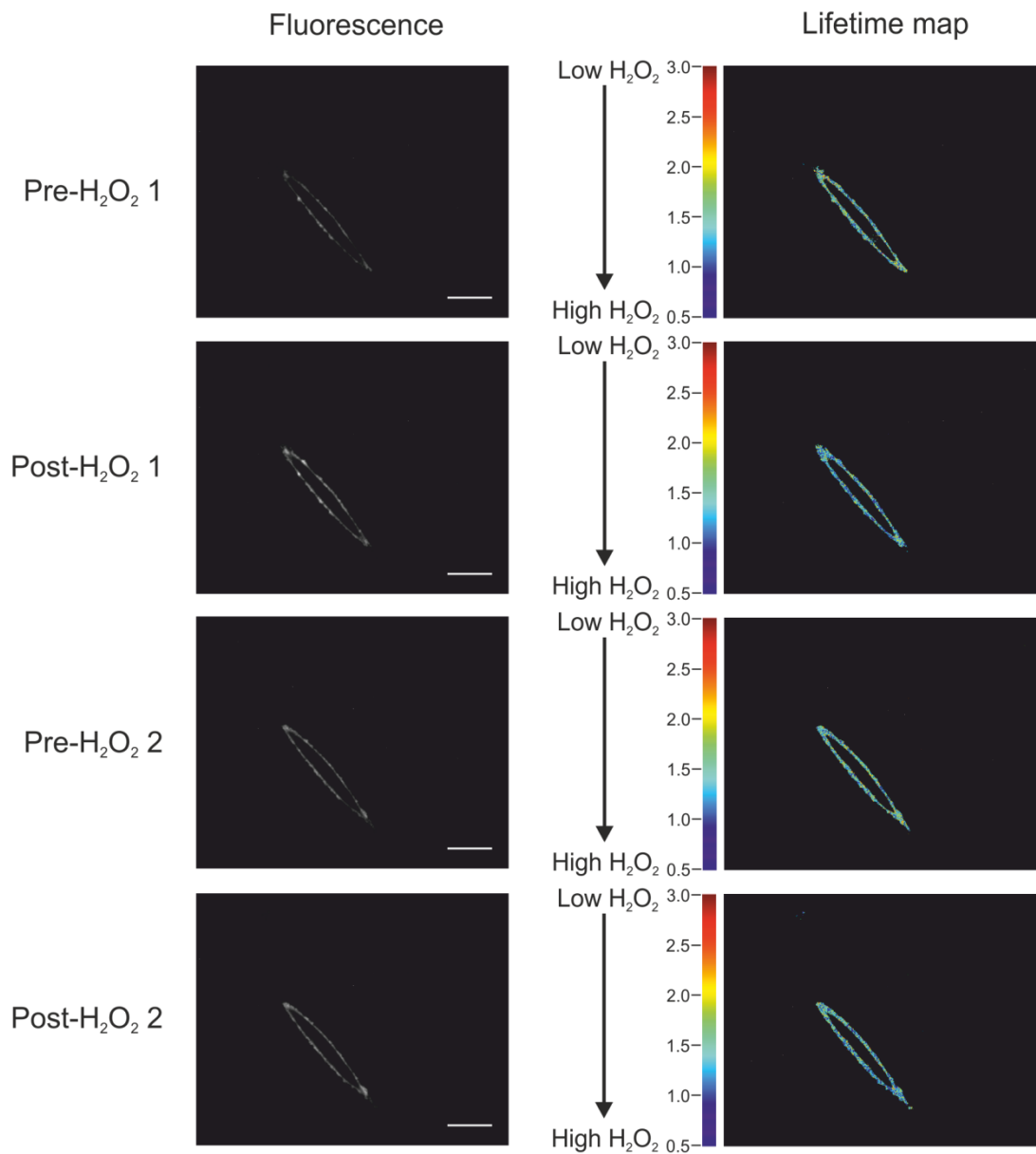
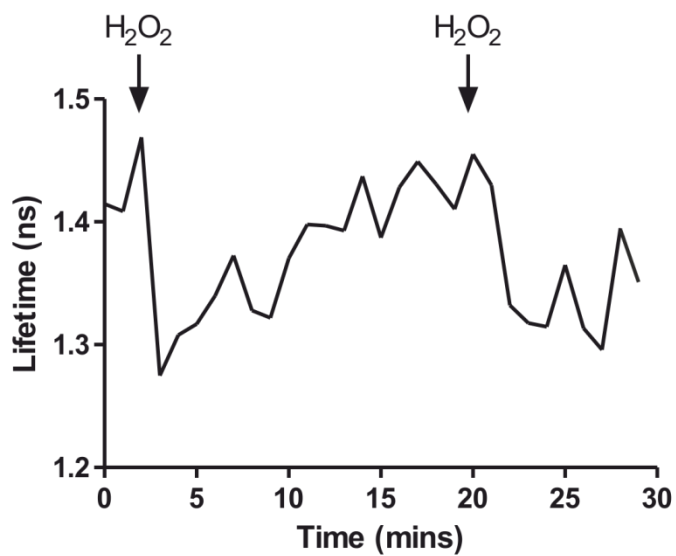
MDAMB231 HyPer-PM cells were grown in 35 mm glass bottom dishes until ~50% confluent. Fields of view containing between one and four cells expressing HyPer-PM were imaged on a microscope fitted with a LIFA system every 30 seconds for a total of 15 minutes with 100 μ l 3 mM H₂O₂ added at ~2 minutes. Fluorescence lifetime was measured in each cell over the time course using LI-FLIM software. A) Representative fluorescence images and corresponding lifetime maps of MDAMB231 HyPer-PM cells before and after H₂O₂ treatment. Scale bar = 20 μ m. B) Graph showing change in fluorescence lifetime over a 15 minute period with the point of H₂O₂ addition indicated. Results displayed are average of 5 cells. C) Box and whiskers plot (5-95 percentile) indicating range of changes in fluorescence lifetimes observed after H₂O₂ addition. D) Table showing average fluorescence lifetimes measured before and after H₂O₂ treatment. Results from 32 cells. Statistical significance of differences determined by a paired t-test (****=p<0.0001).

3.2.11 Change in fluorescence lifetime of HyPer-PM upon H₂O₂ addition is reversible

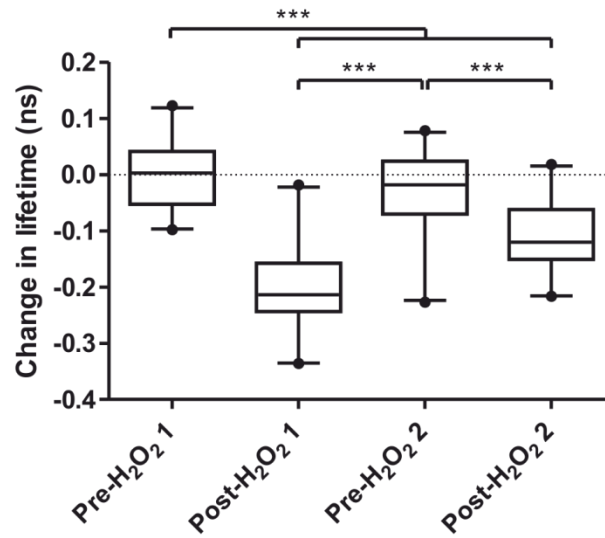
Along the same lines, I wanted to check if the fluorescence lifetime of HyPer-PM would return to starting levels after it was decreased by the addition of H₂O₂, and if the probe could then be reactivated by a further addition of H₂O₂. As for the HyPer-cyto probe, I repeated the previous experiment but this time continued to measure the fluorescence lifetime every 30 seconds for a total of 30 minutes. After addition of the first dose of H₂O₂, I waited for the fluorescence lifetime to return to starting levels and then added a second dose of 100 µl 3 mM H₂O₂. In a similar way to HyPer-cyto, with time the decrease in fluorescence lifetime of HyPer-PM observed when H₂O₂ is added recovers to starting levels. Additionally, HyPer-PM can be restimulated by a second dose of H₂O₂ exhibiting a significant decrease in fluorescence lifetime, although the decrease observed with the second H₂O₂ dose was not as large as that seen with the first H₂O₂ dose (Figure 3-13). As the decrease in fluorescence lifetime was still significant, this difference would not prevent HyPer-PM from detecting transient and repeated changes in H₂O₂ levels.

3.2.12 H₂O₂ levels are higher at the plasma membrane in migrating cells than stationary cells

After confirming that adding a CAAX motif to target HyPer-PM to the plasma membrane did not adversely affect the functioning of the probe, I then wanted to determine if H₂O₂ levels were higher at the plasma membrane in migrating cells compared to stationary cells. Therefore, I cultured MDAMB231 HyPer-PM cells in 35 mm glass bottom dishes until they formed a confluent monolayer. Wounds were then created through the middle of the monolayer using a P10 pipette tip and cells were left for 1 hour to allow cells to start migrating to close the wound. Cells that were at the edge of the wound (classified as migrating) and those still in confluent areas of the dish (classified as stationary) were then imaged on a microscope fitted with a LIFA system and fluorescence lifetime measured using LI-FLIM software. When all cells had been analysed there was a significantly lower fluorescence lifetime and therefore higher H₂O₂ levels at the plasma membrane in the migrating cells compared to the stationary cells (Figure 3-14).

A**B**

C

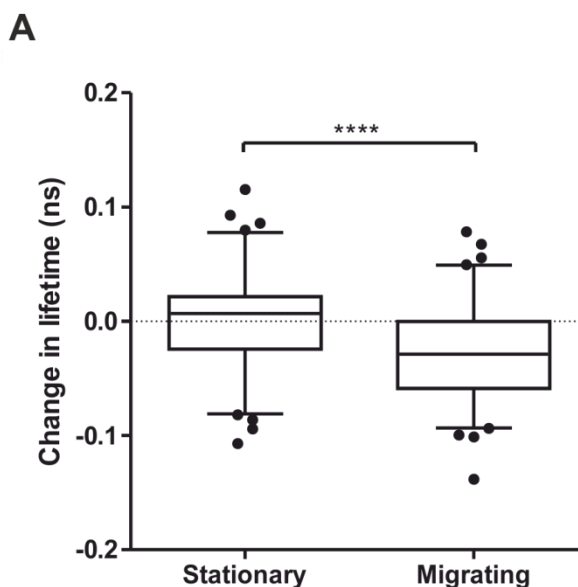


D

	Pre-H ₂ O ₂ 1	Post-H ₂ O ₂ 1	Pre-H ₂ O ₂ 2	Post-H ₂ O ₂ 2
Average lifetime (ns)	1.465	1.265	1.429	1.355

Figure 3-13 HyPer-PM lifetime recovers to baseline levels following H₂O₂ treatment and can be reactivated following further H₂O₂ addition

MDAMB231 HyPer-PM cells were grown in 35 mm glass bottom dishes until ~50% confluent. Fields of view containing between one and four cells expressing HyPer-PM were imaged on a microscope fitted with a LIFA system every 30 seconds for a total of 30 minutes with 100 μ l 3 mM H₂O₂ added after ~2 minutes and after fluorescence lifetime had returned to starting levels. Fluorescence lifetime was measured in each cell over the time course using LI-FLIM software. A) Representative fluorescence images and corresponding lifetime maps of MDAMB231 HyPer-PM cells before and after first and second H₂O₂ treatments. Scale bar = 20 μ m. B) Graph showing change in fluorescence lifetime over a 30 minute period with the points of first and second H₂O₂ addition indicated. Results displayed are from a representative cell. C) Box and whiskers plot (5-95 percentile) indicating range of changes in fluorescence lifetimes observed before and after each H₂O₂ treatment. D) Table showing average fluorescence lifetimes measured before and after each H₂O₂ treatment. Results from 21 cells. Statistical significance of differences determined by a one-way ANOVA followed by a Tukey Kramer multiple comparison test (**=p<0.001).



B

	Stationary	Migrating
Average lifetime (ns)	1.334	1.307

Figure 3-14 H₂O₂ levels elevated at plasma membrane in migrating compared to stationary cells

MDAMB231 HyPer-PM cells were grown in 35 mm glass bottom dishes until they formed a confluent monolayer. A wound was then created through the middle of the monolayer and after 1 hour cells still in a confluent area of the dish (stationary cells) and those at the edge of the wound (migrating cells) were imaged on a microscope fitted with a LIFA system. Fluorescence lifetime was measured in each cell imaged using LI-FLIM software. A) Box and whiskers plot (5-95 percentile) showing the range of changes in fluorescence lifetimes observed at the plasma membrane in migrating cells compared to stationary cells. B) Table showing average fluorescence lifetimes measured in stationary and migrating cells. Results from 83 cells. Statistical significance of differences determined by an unpaired t-test (****= $p < 0.0001$).

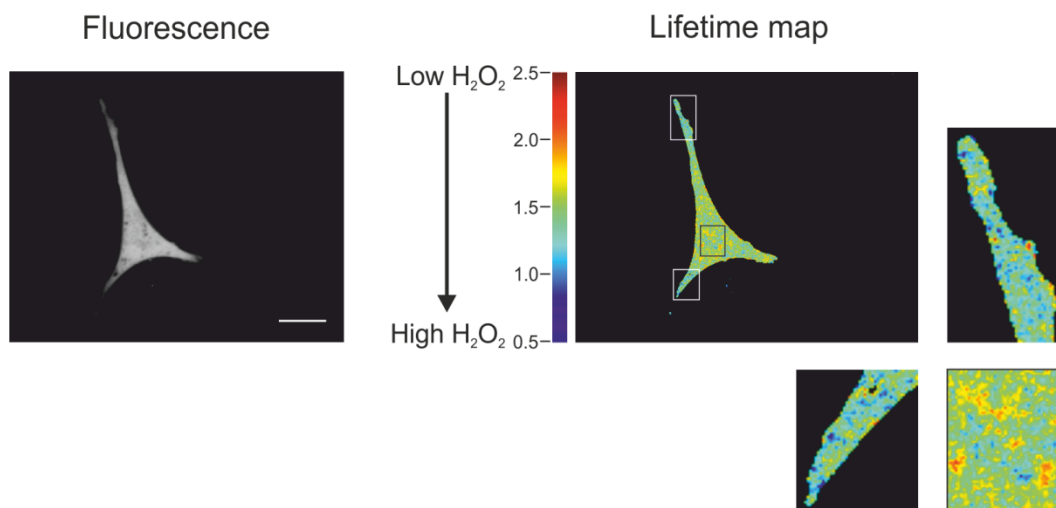
3.2.13 H₂O₂ levels are elevated at the tips of cell protrusions

While analysing data from the experiments investigating if there were increased H₂O₂ levels in migrating cells, I made an interesting observation. In some cells where cell protrusions had been captured in the image acquired, the tip of the protrusion was much more blue in the lifetime map, indicating higher H₂O₂ levels compared to the rest of the cell. I therefore decided to investigate this further by repeating the experiment undertaken to compare H₂O₂ levels in MDAMB231 HyPer-cyto cells that were stationary or migrating. However, this time the focus was on imaging migrating cells at the edge of the wound that at the time of image acquisition had obvious cell protrusions. The z-position of the microscope was carefully set for each cell to ensure that the image taken captured the tip of the cell protrusions and the cell body. Fluorescence lifetime of HyPer-cyto was then measured at the tip of the cell protrusion and in the cell body using LI-FLIM software. This confirmed my initial observations were correct, as I found there was a significantly lower fluorescence lifetime, indicating higher H₂O₂ levels, at the tips of cell protrusions compared to the cell body (Figure 3-15).

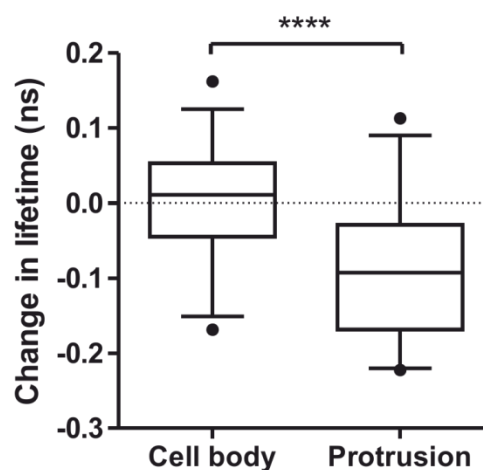
3.3 Conclusions

In this chapter I have presented results showing that the ROS scavenger, NAC, reduced ROS levels in MDAMB231 cells and that reducing ROS levels with NAC resulted in a corresponding decrease in cell migration. Not only are ROS required for migration but I also provided evidence that the ROS, H₂O₂, was present at higher levels in migrating cells than in stationary cells both throughout the cell and specifically at the cell membrane, an area that undergoes massive dynamic changes during cell migration. Further to this, I revealed that H₂O₂ levels were not uniform throughout a migrating cell with increased levels found at the tip of cell protrusions compared to the cell body.

A



B



C

	Cell body	Protrusion
Average lifetime (ns)	1.487	1.392

Figure 3-15 H_2O_2 levels elevated at tips of protrusions compared to cell bodies

MDAMB231 HyPer-cyto cells were grown in 35 mm glass bottom dishes until they formed a confluent monolayer. A wound was then created through the middle of the monolayer and after 1 hour cells at the edge of the wound which had well defined protrusions were imaged on a microscope fitted with a LIFA system ensuring that the z-position set captured the protrusion tip and cell body. Fluorescence lifetime in the protrusion tip and cell body were measured in each cell using LI-FLIM software. A) Representative fluorescence image and corresponding lifetime map of MDAMB231 HyPer-cyto cell with enlarged images of protrusion tips and selected area of cell body displayed. Scale bar = 20 μ m. B) Box and whiskers plot (5-95 percentile) showing the range of changes in the fluorescence lifetimes observed in the tips of cell protrusions compared to the cell body. C) Table showing average fluorescence lifetimes measured in the cell body and tips of cell protrusions. Results from >29 cells. Statistical significance of differences determined by a paired t-test(****= $p < 0.0001$).

4 Protein Oxidation and Cell Migration

4.1 Introduction

After finding that H_2O_2 levels were elevated in migrating cells, in particular at the tips of cell protrusions, and knowing that H_2O_2 can regulate cellular signalling pathways through the oxidation of proteins, I wanted to investigate if protein oxidation was also increased in migrating cells [244-246]. Global protein oxidation has been shown previously to be increased in cells stimulated with VEGF, a growth factor known to induce the migration of endothelial cells. In addition, a population of oxidised proteins was located at the leading edge in migrating cells in the presence of VEGF [278]. However, the direct oxidation of proteins in migrating cells has not yet been demonstrated. Moreover, there are only a few proteins, mainly protein tyrosine phosphatases, that have been found to be oxidised and to contribute to cell migration [262, 276, 290, 291]. Therefore, I set out to identify the direct oxidation of specific proteins in migrating cells. In this chapter I have presented results from my investigations into the global oxidation of proteins in migrating cells and the identification of a specific protein that is oxidised.

4.2 Results

4.2.1 Cellular protein oxidation increases with H_2O_2 treatment

In order to determine if the oxidation of proteins is increased in migrating cells, I needed to identify a reliable method to monitor levels of protein oxidation in cells. There are several commercially available options for this however, they each can have a number of drawbacks. Many are not completely specific for cysteine sulfenic acids and will cross-react with other cellular molecules and amino acids. Some also label oxidised proteins during cell lysis since the probes are unable to or inefficiently enter cells. As proteins can be easily oxidised during cell lysis and sample preparation steps, this may lead to an inaccurate representation of the actual oxidation state of proteins within cells. Additionally, some of the probes form modifications on the oxidised cysteine that are reversible and may be lost before they are detected and measured [324]. For these reasons I decided to use the chemical dimedone. Dimedone is a

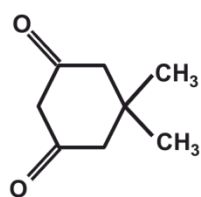
cell permeable chemical that forms a covalent bond with the sulfenic acid form of an oxidised protein (Figure 4-1) [325]. It therefore has the benefits that it monitors protein oxidation levels as they are in the cell and results are not affected by protein oxidation that could occur during cell lysis or sample preparation. Equally as important, since it forms an irreversible covalent bond with oxidised proteins, it will not be lost or reduced during cell lysis or sample preparation. A further advantage of dimedone is it can detect all proteins undergoing oxidation regardless of the final oxidation product as it reacts with sulfenic acid, the very first intermediate formed when a protein is oxidised (Figure 1-8).

Firstly, I wanted to validate the probe functioned correctly. To test this I treated MCF7 cells with 0, 1, 3 or 10 μM H_2O_2 for 6 hours. For the final 1 hour cells were also incubated with 5 mM dimedone and then harvested. The levels of protein oxidation, as indicated by dimedone labelling, were analysed by western blot. The membrane was probed with anti-dimedone Ab to detect oxidised proteins and anti-ERK2 Ab as a loading control. This confirmed the probe was behaving as expected as when cells were treated with H_2O_2 , I saw increased dimedone labelling and therefore oxidised protein levels (Figure 4-2).

4.2.2 Cellular protein oxidation decreases with NAC treatment

In a similar way, I wanted to investigate if dimedone was also sufficiently sensitive to detect decreased oxidation. For this I treated MDAMB231 cells with 0, 10, 25, 50 and 75 mM of the ROS scavenger NAC for 72 hours, again incubating them with 5 mM dimedone for the final 3 hours before harvesting. Protein oxidation was analysed by western blot with the membrane being probed with anti-dimedone Ab to detect oxidised proteins and anti-ERK2 Ab as a loading control. Again dimedone acted as expected with decreased levels of dimedone labelling of proteins, and therefore oxidised protein levels, when cells were treated with NAC (Figure 4-3).

A



dimedone

B

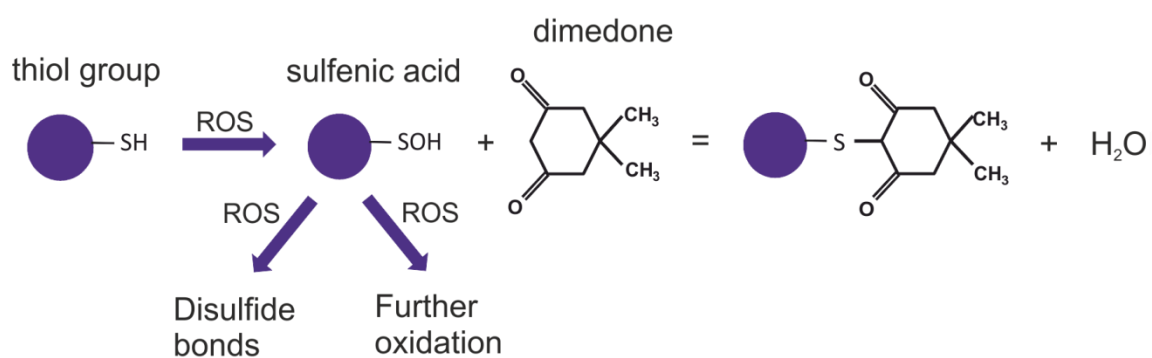


Figure 4-1 Dimedone irreversibly reacts with oxidised cysteine in its sulfenic acid state

A) Structure of chemical probe dimedone. B) Schematic diagram of the reaction of dimedone with oxidised cysteine residues.

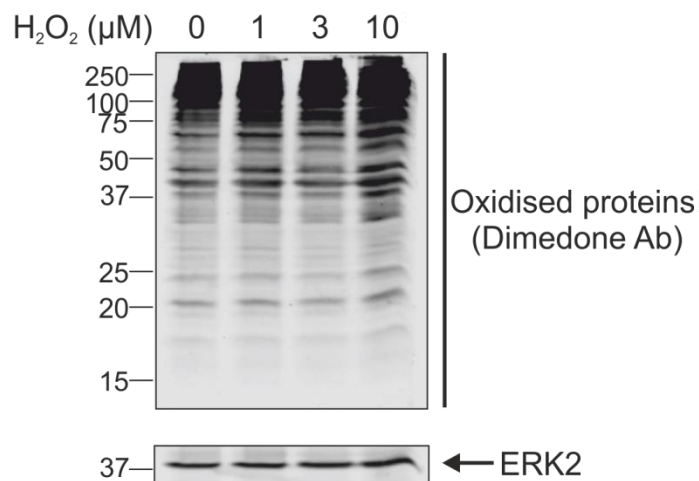


Figure 4-2 Cellular protein oxidation increases with H₂O₂ treatment

MCF7 cells were treated with H₂O₂ for 6 hours at the indicated concentrations and incubated with 5 mM dimedone for the final 1 hour before harvesting. Dimedone labelling of oxidised proteins was then assessed by western blot analysis. Membranes were probed with anti-dimedone Ab to detect oxidised proteins and anti-ERK2 Ab as a loading control. Western blot showing levels of protein oxidation present following treatment with indicated concentrations of H₂O₂.

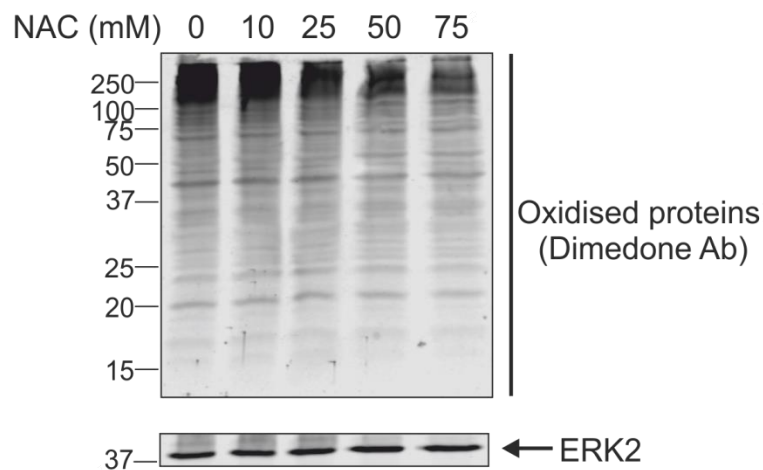


Figure 4-3 Cellular protein oxidation decreases with NAC treatment

MDAMB231 cells were treated with NAC for 72 hours at the indicated concentrations and incubated with 5 mM dimedone for the final 3 hours before harvesting. Dimedone labelling of oxidised proteins was then assessed by western blot analysis. Membranes were probed with anti-dimedone Ab to detect oxidised proteins and anti-ERK2 Ab as a loading control. A) Western blot showing levels of protein oxidation present following treatment with indicated concentrations of NAC.

4.2.3 Cellular protein oxidation is higher in migrating than stationary cells

After validating that dimedone could detect both increases and decreases in protein oxidation, I could continue with experiments to determine if oxidation of proteins was increased in cells that were migrating compared to those that were stationary. This was investigated by culturing MDAMB231 cells in a 6-well dish until they formed a confluent monolayer. Half of the wells were then wounded 20 times using a P10 pipette tip and the other half were left as a confluent monolayer. Cells were then left for 3 hours to allow those cells at the edge of the wounds to begin migrating to close the wounds. After a further 1 hour during which cells were incubated with 5 mM dimedone, cells were harvested. Levels of protein oxidation were then analysed by western blot with the membrane being probed with anti-dimedone Ab to detect oxidised proteins. A second set of samples from each condition was separated on a protein gel and stained to check for equal loading. From this it was discovered that oxidation of proteins is indeed increased in migrating compared to stationary cells (Figure 4-4). This was not unexpected as I had seen in the previous chapter that H_2O_2 is elevated in migrating cells and one of the downstream targets of H_2O_2 , as explained in the introduction, are proteins which become oxidised. Therefore in a situation where increased H_2O_2 is observed, you would also expect to see increased protein oxidation.

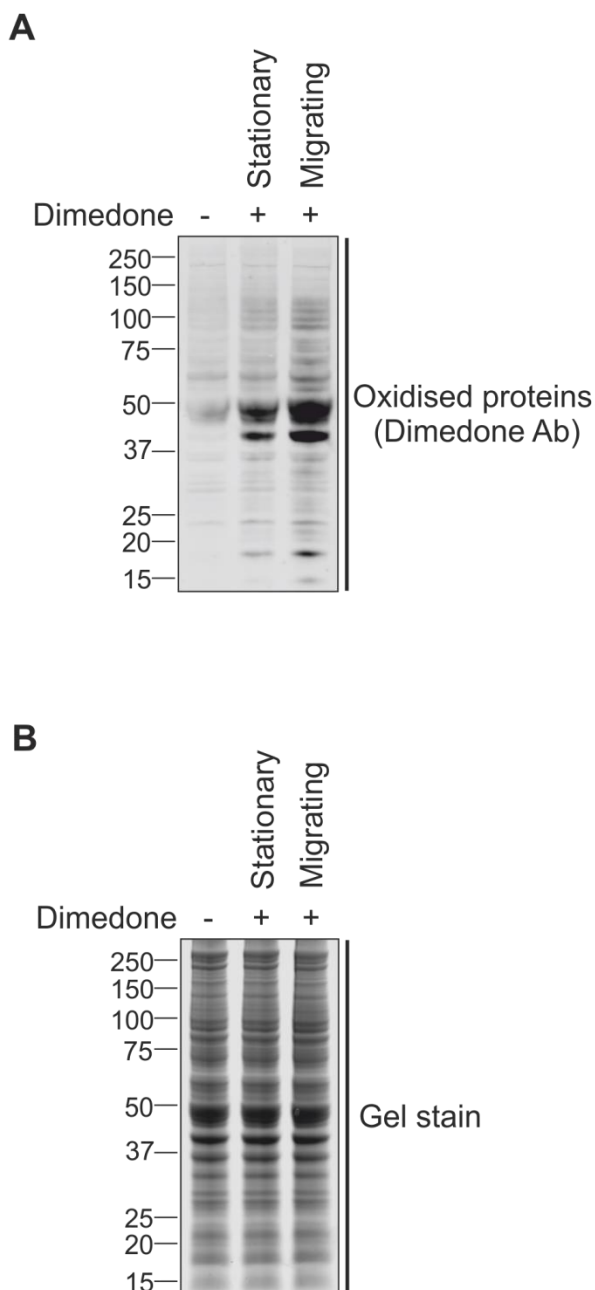


Figure 4-4 Protein oxidation is increased in migrating cells compared to stationary cells

MDAMB231 cells were cultured in a 6-well dish until they formed a confluent monolayer and then wounded 20 times (migrating) or left unwounded (stationary). After 3 hours cells were incubated with 5 mM dimedone for 1 hour before harvesting. Dimedone labelling of oxidised proteins was then assessed by western blot analysis. A) Representative western blot from 3 independent experiments showing levels of protein oxidation in migrating cells compared to stationary cells. Membrane probed with anti-dimedone Ab to detect oxidised proteins. B) Protein gel stained to confirm equal loading of samples.

4.2.4 Cofilin is identified as a protein oxidised in cells

Having found that overall protein oxidation was increased in migrating cells, I started to speculate about which proteins could be targets of this oxidation. Additionally, which of these proteins would have an altered activity as a result of this oxidation and could therefore be contributing to remodelling of the actin cytoskeleton to aid migration. As cofilin is a key regulator of actin cytoskeleton dynamics and its involvement in the induction of cell death and the reduced response of T cells under conditions of oxidative stress have recently been shown to be regulated by oxidation, it came up as an attractive candidate to investigate further [91, 94, 137].

I therefore set out to determine if I could detect oxidised cofilin in cells using dimedone. To do this I cultured MCF7 cells in the presence or absence of NAC for 72 hours with cells being incubated with 5 mM dimedone for the final 3 hours before harvesting. Cofilin was then immunoprecipitated from the cell lysates and analysed for dimedone labelling by western blot. Membranes were probed with anti-cofilin Ab to check total cofilin levels and anti-dimedone Ab to determine oxidised cofilin levels. From this I found that cofilin was indeed present in an oxidised form in cells as indicated by dimedone labelling. This was confirmed to be oxidised cofilin as in the presence of NAC, the level of dimedone labelling on cofilin decreased (Figure 4-5).

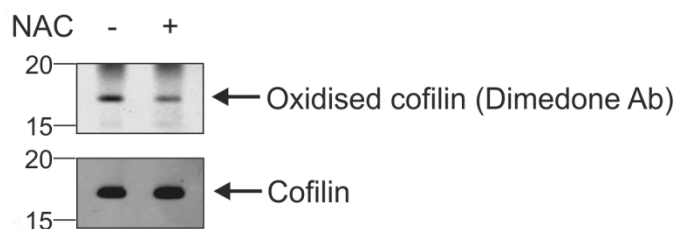


Figure 4-5 Cofilin identified in oxidised state in cells

MCF 7 cells treated with or without 25 mM NAC for 72 hours and with 5 mM dimedone for the final 3 hours before harvesting. Cofilin was then immunoprecipitated and dimedone incorporation assessed by western blot analysis. A) Western blot from preliminary experiment showing levels of oxidised cofilin and total cofilin in cells with and without NAC treatment. Membrane probed with anti-cofilin Ab and anti-dimedone Ab to detect oxidised cofilin.

4.2.5 Cofilin oxidation is higher in migrating than stationary cells

After establishing that cofilin was oxidised in cells, I next wanted to determine if cofilin was one of the proteins that exhibited increased oxidation in migrating cells compared to stationary cells. This was investigated by culturing MDAMB231 cells in a 6-well dish until they formed a confluent monolayer. Cell monolayers were then wounded 30 times using a P10 pipette tip or left unwounded. After 3 hours to allow those cells at the edge of the wounds to begin migrating to close the wounds, cells were incubated with 5 mM dimedone for 1 hour. Cells were then harvested, cofilin immunoprecipitated from lysates and levels of cofilin oxidation were analysed by western blot with the membrane being probed with anti-dimedone Ab to detected oxidised protein. From this it was established that cofilin oxidation was indeed increased in migrating cells compared to stationary cells (Figure 4-6).

4.3 Conclusions

In this chapter I have presented results confirming that the chemical dimedone can be used to reliably monitor levels of protein oxidation in cells, as shown by increases and decreases in dimedone labelling with H_2O_2 and NAC treatment respectively. Dimedone was then used to reveal that the oxidation of proteins was increased in migrating cells compared to stationary cells. Additionally, cofilin was identified in an oxidised state in cells and the level of cofilin oxidation was increased in migrating cells compared to stationary cells. Therefore, cofilin oxidation could alter its activity and contribute to the remodelling of the actin cytoskeleton required for cell migration.

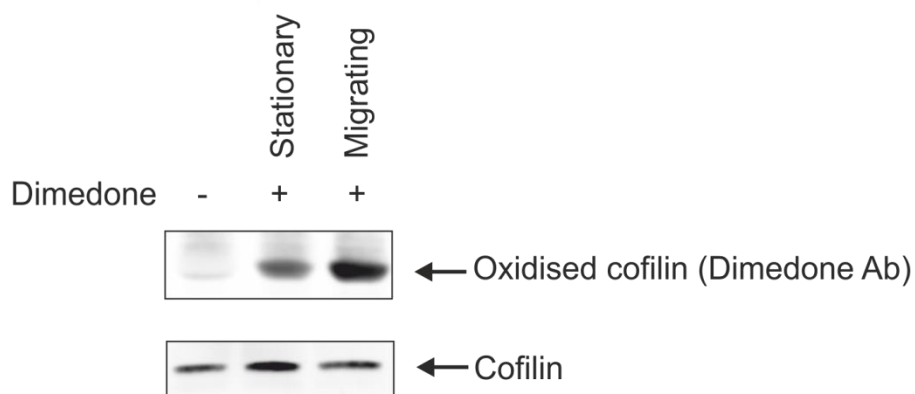


Figure 4-6 Cofilin oxidation increased in migrating cells compared to stationary cells

MDAMB231 cells were cultured until they formed a confluent monolayer and then wounded 30 times (migrating) or left unwounded (stationary). After 3 hours cells were incubated with 5 mM dimedone for 1 hour before harvesting. Cofilin was immunoprecipitated from lysates and dimedone labelling was then assessed by western blot analysis. Representative western blot from 3 independent experiments showing levels of cofilin oxidation in migrating cells compared to stationary cells. Membrane probed with anti-cofilin Ab and anti-dimedone Ab to detect oxidised protein. Figure courtesy of June Munro.

5 Cofilin Oxidation and Actin Dynamics

5.1 Introduction

The oxidation of cofilin has previously been reported to be required for some cellular processes. The induction of apoptosis and necrotic-like programmed cell death in response to oxidants is dependent on the oxidation of cofilin [91, 94]. Furthermore, cofilin oxidation has been implicated in the reduced response of T cells under conditions of oxidative stress [137]. Having established that cofilin was one of the proteins oxidised in migrating cells, I next wanted to determine if this oxidation was altering its activity and consequently contributing to cell migration. As cofilin has a central role in remodelling the actin cytoskeleton and this is essential for cell migration, I set out to identify if the oxidation of cofilin altered its ability to sever and depolymerise F-actin *in vitro*. In addition to this, as proteins are oxidised on cysteine residues, I wanted to establish which of the cysteine residues in cofilin were oxidised and contributing to any observed change in activity [246]. The results from these *in vitro* studies are presented in this chapter.

5.2 Results

5.2.1 Purification of actin and cofilin for *in vitro* actin depolymerisation assay

Having identified oxidised cofilin in cells I wanted to know if the oxidation of cofilin affected its ability to depolymerise F-actin. To assess this, I used an *in vitro* actin depolymerisation assay that used pyrene conjugated actin [326]. When pyrene conjugated actin is in a G-actin state, it has a low fluorescence; however, when it is incorporated into F-actin, its fluorescence increases. Changes in F-actin levels over time can therefore be monitored by measuring the change in pyrene actin fluorescence. To assess the ability of a protein of interest to depolymerise F-actin, a solution of G-actin is prepared in which 5% is conjugated to pyrene. Upon the addition of a high salt solution (polymerisation buffer), F-actin begins to form and eventually equilibrium between G-actin and F-actin levels is reached. The point at which equilibrium has been reached can be determined by measuring the fluorescence throughout the polymerisation; when fluorescence stops increasing and remains constant, equilibrium has been

achieved. A protein of interest can then be added and if it depolymerises F-actin a decrease in fluorescence will be observed due to a shifting of the equilibrium towards G-actin. In contrast, if the protein promotes further polymerisation there will be an increase in fluorescence due to a shifting of the equilibrium towards F-actin (Figure 5-1). In order to test the effect of cofilin oxidation on its actin depolymerisation activity in this assay, I purified bacterially expressed recombinant cofilin. The actin used for this assay was extracted and purified from rabbit skeletal muscle (Figure 5-2).

5.2.2 Oxidation of recombinant cofilin

Before investigating the effect of cofilin oxidation on its actin depolymerising activity, I wished to confirm that I could oxidise the recombinant cofilin. I decided to do this by incubating the recombinant cofilin with H_2O_2 of increasing concentrations between 0 and 10 mM for 1 hour. Residual H_2O_2 left at the end of the incubation time was quenched with catalase and then levels of cofilin oxidation measured using biotin conjugated iodoacetamide (biotin-IAA). IAA is a chemical that attaches to free, non-oxidised thiol groups on protein cysteine residues. It therefore binds to proteins that are not oxidised and the presence of the biotin tag on IAA allows its incorporation into non-oxidised proteins to be measured. I analysed the levels of non-oxidised cofilin in these samples by western blot, probing the membrane using Alexa Fluor 680 conjugated streptavidin. As streptavidin has a high affinity for biotin, this will detect biotin-IAA incorporation in proteins and therefore measure non-oxidised protein levels. I found that I could effectively oxidise recombinant cofilin by incubating it with H_2O_2 at concentrations greater than 1 mM as I observed a dose dependent decrease in non-oxidised cofilin with 1, 3, and 10 mM H_2O_2 (Figure 5-3).

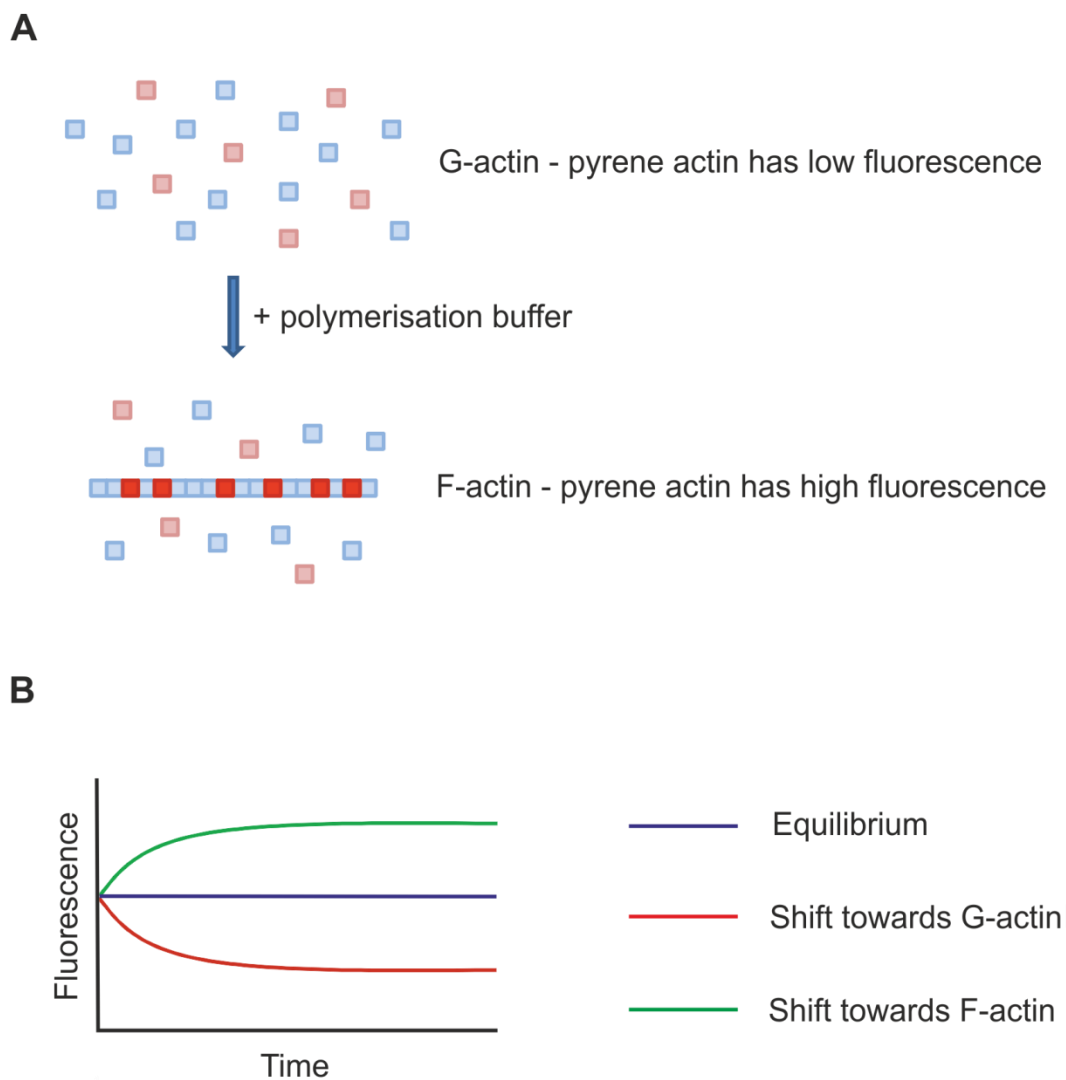


Figure 5-1 Schematic diagram of *in vitro* actin depolymerisation assay

A) Schematic diagram illustrating change in fluorescence seen when pyrene labelled G-actin is incorporated into F-actin. B) Graph illustrating potential changes in G-actin and F-actin levels and consequently the fluorescence that could result from the addition of a protein of interest.

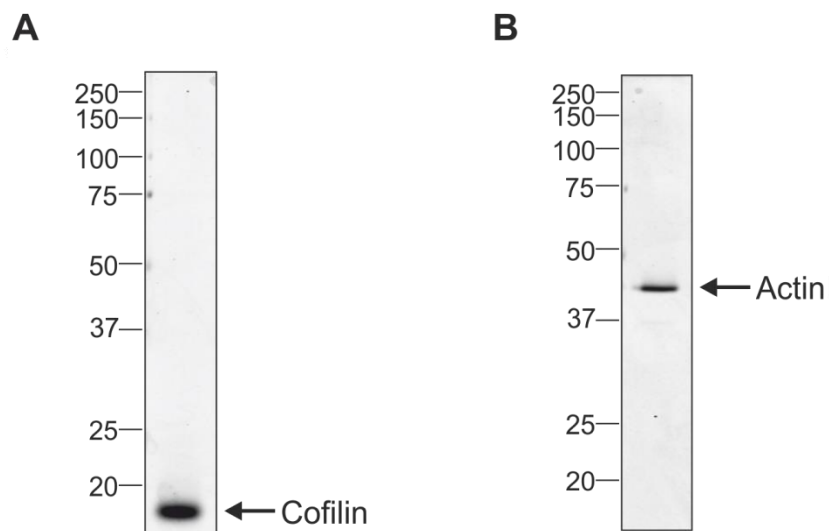


Figure 5-2 Purification of cofilin and actin for *in vitro* assay

A) Protein gel of purified recombinant cofilin expressed in bacteria. B) Protein gel of purified actin extracted from rabbit skeletal muscle.

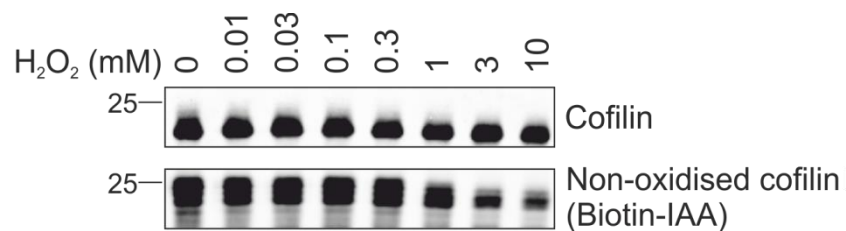


Figure 5-3 Oxidation of recombinant cofilin with H₂O₂

Recombinant cofilin was treated with H₂O₂ at the concentrations indicated. After quenching of residual H₂O₂, cofilin was incubated with biotin-IAA to detect non-oxidised cofilin. Biotin-IAA incorporation and therefore non-oxidised cofilin was assessed by western blot analysis. Membranes were probed with anti-cofilin Ab to detect total cofilin levels and Alexa Fluor 680 conjugated streptavidin to detect biotin-IAA and therefore non-oxidised cofilin. A) Western blot showing total cofilin and non-oxidised cofilin levels (as indicated by biotin-IAA) at the H₂O₂ concentrations indicated.

5.2.3 Oxidation of recombinant cofilin reduces its ability to decrease F-actin levels

Having established that I could oxidise recombinant cofilin *in vitro* I was then able to assess the ability of oxidised cofilin to decrease F-actin levels in the assay described at the start of this chapter. I incubated the recombinant cofilin with 0, 3, 5, 7 or 10 mM H₂O₂ for 1 hour as these concentrations were within the range in which I observed oxidation previously. Remaining H₂O₂ was quenched with catalase to prevent any further oxidation. These cofilin samples were then added to pyrene labelled actin that had reached a steady state level of F-actin following addition of polymerisation buffer to a G-actin solution. Fluorescence was measured over 5 minutes to monitor F-actin levels.

The results showed that the percentage fluorescence and therefore the F-actin levels at the endpoint of the assay were significantly higher when cofilin was treated with 5, 7 or 10 mM H₂O₂ compared to untreated cofilin. This demonstrates that the oxidation of cofilin inhibits it from decreasing F-actin levels in the depolymerisation assay and the degree of inhibition observed is dependent on the concentration of H₂O₂ with which the cofilin was oxidised (Figure 5-4).

5.2.4 Generation of cofilin cysteine to alanine mutants

As it was explained in the introduction, it is the cysteine residues in proteins that are targeted and oxidised by H₂O₂. As cofilin has four cysteine residues (Figure 5-5), I wanted to know which of these residues, when oxidised, was inhibiting cofilin from reducing F-actin levels. To do this I generated four cofilin mutants by site-directed mutagenesis in which each cysteine residue was independently mutated to alanine and therefore unable to be oxidised. These cofilin mutants were designated C39A, C80A, C139A and C147A depending on the position of the cysteine residue that had been mutated to alanine. These mutant cofilin proteins, as with the WT cofilin, were bacterially expressed and purified (Figure 5-6).

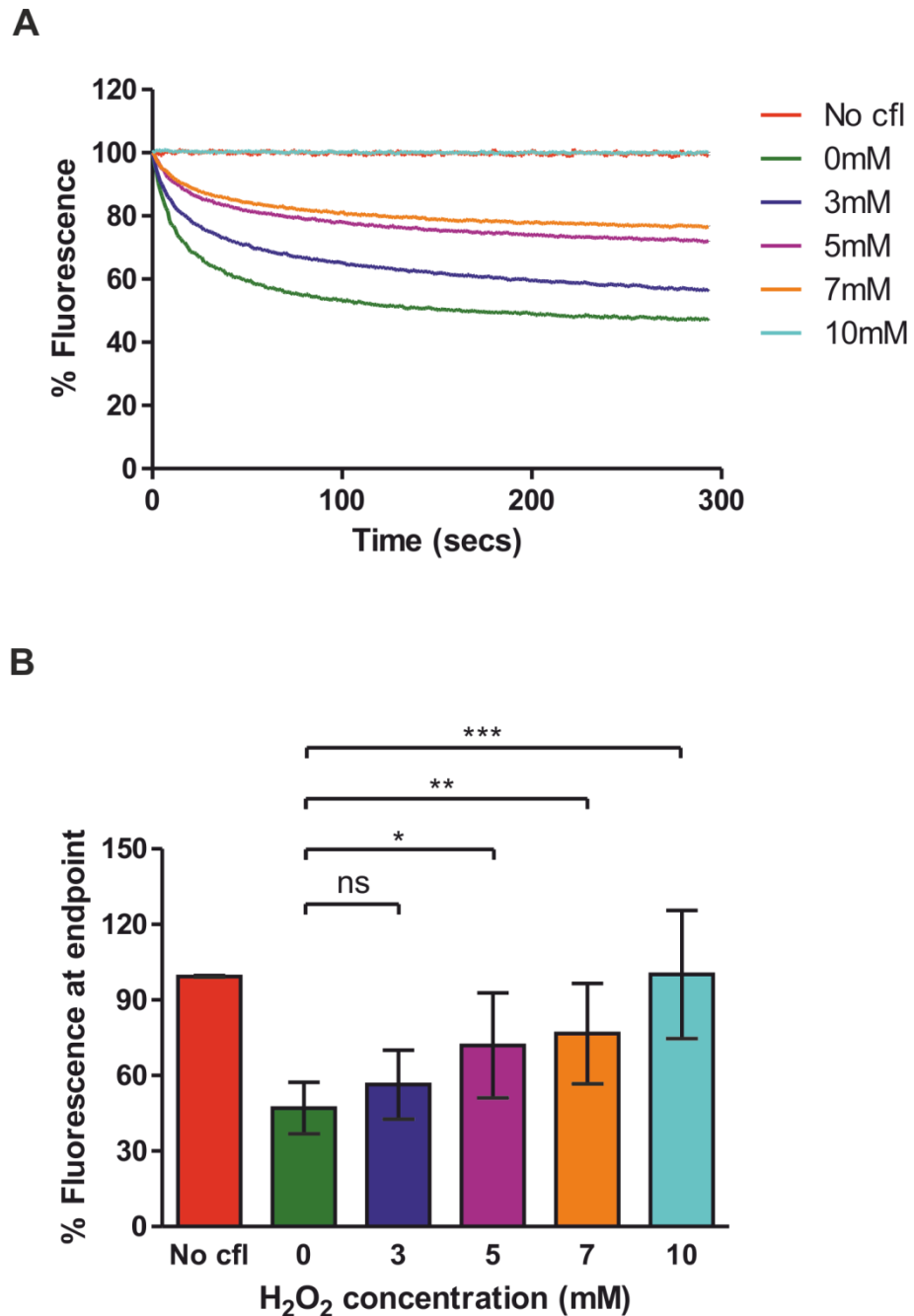


Figure 5-4 Oxidation of cofilin reduces its ability to decrease F-actin levels

Recombinant cofilin was oxidised with H₂O₂ at the concentrations indicated. Oxidised cofilin was then added to pyrene labelled actin which had already reached a steady state level of F-actin. Fluorescence was measured over 5 minutes to monitor changes in F-actin levels. A) Graph showing average changes in fluorescence over 5 minutes after addition of cofilin treated with indicated concentrations of H₂O₂. B) Graph showing mean percentage fluorescence +/- standard deviation (SD) at endpoint compared to start of experiment after addition of cofilin treated with indicated concentrations of H₂O₂. Statistical significance of differences determined by a one-way ANOVA followed by a Tukey Kramer multiple comparison test (ns=not significant, *=p<0.05, **=p<0.01, ***=p<0.001), n=9.

A

```

MASGVAVSDGVIKVFNDMKVRKSSTPEEVKKR
KKAVLFC39LSEDKKNIILEEGKEILVGDVGQTVDD
PYATFVKMLPDKDC80RYALYDATYETKESKKEDL
VFIFWAPESAPLKSKMIYASSKDAIKKKLTGIKH
ELQANC139YEEVKDR147TLAEKLGGSAVISLEGKPL

```

B

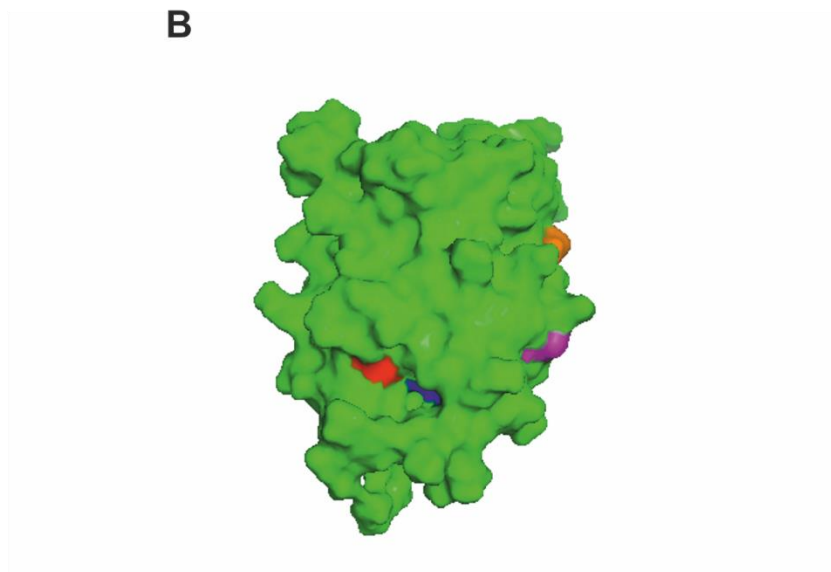


Figure 5-5 Cofilin has four cysteine residues

Cysteine 39 (red), cysteine 80 (blue), cysteine 139 (pink), cysteine 147 (orange). A) Position of cysteine residues in cofilin amino acid sequence. B) Position of cysteine residues in cofilin 3D structure. Model created in PyMol using NMR structure data (PDB ID: 1Q8G) [327].

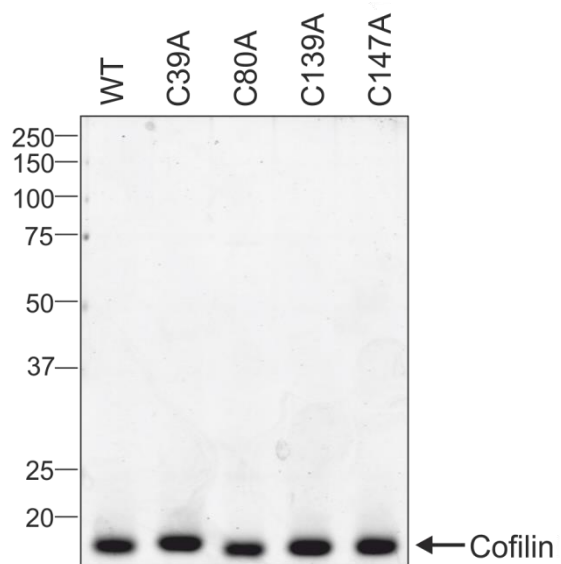


Figure 5-6 Purification of cofilin cysteine to alanine mutants used for *in vitro* assay

A) Protein gel of purified recombinant cofilin cysteine to alanine mutants expressed in bacteria.

5.2.5 Cofilin cysteine residues 139 and 147 are responsible for the reduced ability of cofilin to decrease F-actin levels when oxidised

Having generated these cofilin cysteine to alanine mutants, I wanted to test their ability to decrease F-actin levels in the actin depolymerisation assay when non-oxidised and oxidised. To do this, I incubated each of the cofilin mutants or WT protein with 10 mM H₂O₂ for 1 hour or left them untreated. 10 mM H₂O₂ was chosen as this was the concentration of H₂O₂ that showed the greatest inhibition of cofilin activity in the previous experiment. Any remaining H₂O₂ was quenched with catalase to prevent further oxidation. The cofilin WT and mutant samples were then added to pyrene labelled actin that had reached a steady state level of F-actin following addition of polymerisation buffer to a G-actin solution. Fluorescence was measured over 5 minutes to monitor F-actin levels.

These results indicated that in the absence of oxidation the cofilin cysteine to alanine mutants were able to decrease F-actin levels to the same degree as WT cofilin. However, when these mutants were oxidised, the C139A and C147A mutants were still able to decrease F-actin levels unlike oxidised WT cofilin. In fact when looking at the percentage fluorescence and therefore F-actin levels at the endpoint of this experiment, there was no significant difference seen between the non-oxidised and oxidised C139A and C147A mutants. This demonstrates that both cysteines 139 and 147 must be oxidised and contribute to the inhibition of cofilin activity observed in the actin depolymerisation assay when it was oxidised. Interestingly I also noticed that when the C39A and C80A mutants were oxidised they led to an increase in the F-actin levels at the endpoint of the assay compared to oxidised WT cofilin (Figure 5-7). It could be that when oxidised these mutants are causing F-actin filaments already present to bundle together forming actin rods and this is leading to an increased fluorescence. Alternatively, as the actin the proteins are added to is in a state of equilibrium where the rate of polymerisation and depolymerisation of F-actin are equal; these mutants when oxidised could be blocking or at least slowing the rate of depolymerisation while polymerisation continues at an unaltered rate and consequently causing a shift in the equilibrium towards F-actin, again explaining the increased fluorescence I observed. Although this was an interesting phenomenon, it was not within the scope of my study to investigate

this further as my primary interest was in which of the cysteine residues was inhibiting the ability of cofilin to decrease F-actin levels when oxidised.

5.2.6 Generation of cofilin double cysteine to alanine mutants

After discovering that cofilin cysteine residues 139 and 147 appeared to be the ones responsible for the inhibition of cofilin activity when oxidised, I next wanted to know if mutating either of these residues in combination with each of the other cysteine residues would also be able to rescue the inhibition of cofilin activity seen when it was oxidised. For this reason I generated cofilin mutants by site-directed mutagenesis in which every combination of two cysteine residues were mutated to alanine therefore creating cofilin proteins that could not be oxidised on two of the cysteine residues. These were named C39/80A, C39/139A, C39/147A, C80/139A, C80/147A and C139/147A depending on which two of the cysteine residues had been mutated to alanine. These cofilin double cysteine to alanine mutants, as with the WT and single cysteine to alanine mutants, were bacterially expressed and purified (Figure 5-8).

5.2.7 Cofilin cysteine residue 147 appears to be the cysteine residue predominantly responsible for the reduced ability of cofilin to decrease F-actin levels when oxidised

Having generated cofilin double cysteine to alanine mutants, I wanted to test their ability to reduce F-actin levels in the actin depolymerisation assay when non-oxidised and oxidised. To do this I incubated each of the cofilin mutants and WT protein with 10 mM H₂O₂ for 1 hour or left them untreated as was done with the cofilin single cysteine to alanine mutants. Remaining H₂O₂ was then quenched with catalase to prevent further oxidation. Cofilin WT and mutant proteins were then added to pyrene labelled actin that had reached a steady state level of F-actin following the addition of polymerisation buffer to a G-actin solution. Fluorescence was measured over 5 minutes to monitor F-actin levels.

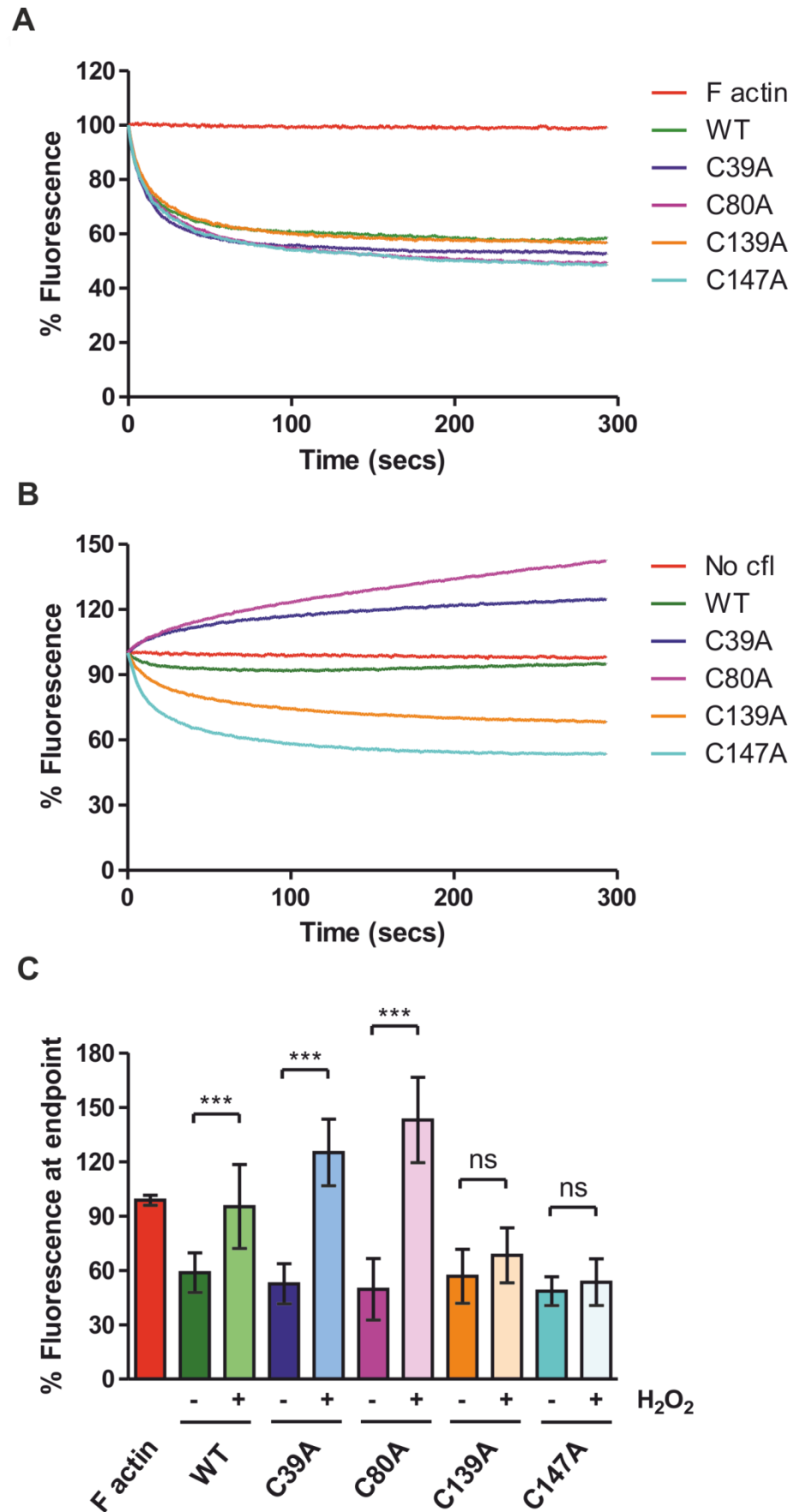


Figure 5-7 Cofilin cysteine residues 139 and 147 are responsible for the reduced ability of cofilin to decrease F-actin levels when oxidised

Recombinant cofilin cysteine to alanine mutants were oxidised with 10 mM H₂O₂ or left untreated. Non-oxidised and oxidised cofilin mutants were then added to pyrene labelled actin which had already reached a steady state level of F-actin. Fluorescence was measured over 5 minutes to

monitor changes in F-actin levels. A) Graph showing average changes in fluorescence over 5 minutes after addition of non-oxidised cofilin mutants. B) Graph showing average changes in fluorescence over 5 minutes after addition of oxidised cofilin mutants. C) Graph showing mean percentage fluorescence \pm SD at endpoint compared to start of experiment after addition of non-oxidised and oxidised cofilin mutants. Statistical significance of differences determined by a one-way ANOVA followed by a Tukey Kramer multiple comparison test (ns=not significant, ***= $p < 0.001$), $n > 12$.

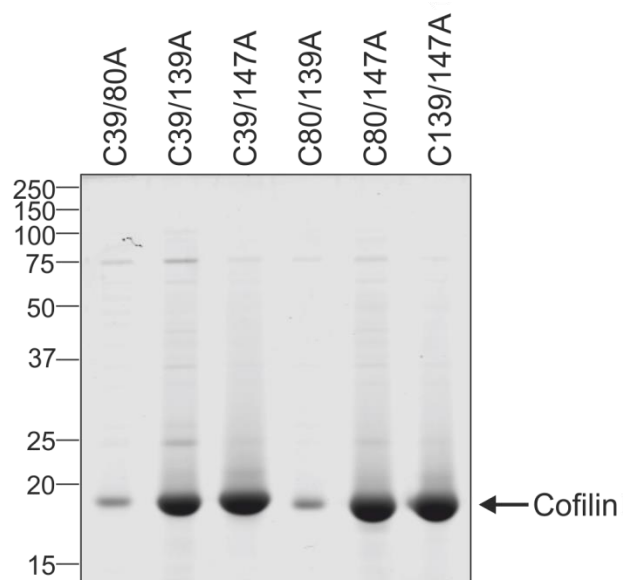


Figure 5-8 Purification of cofilin double cysteine to alanine mutants used for *in vitro* assay
Protein gel of purified recombinant cofilin double cysteine to alanine mutants expressed in bacteria.

By comparing results across all the mutants that contain cysteine 39 mutated to alanine (C39A, C39/80A, C39/139A and C39/147A), I determined that when these mutants were not oxidised, they were able to decrease F-actin levels to the same degree as WT as there was no significant difference between the percentage fluorescence and therefore F-actin levels at the endpoint of the assay. As I saw in the previous experiment, the C39A mutant was not able to rescue the inhibition of cofilin activity seen when WT cofilin was oxidised. Similarly with the double C39/80A and C39/139A mutants, there was no rescue in activity seen upon oxidation. However, when the C39/147A mutant was oxidised it was still able to decrease F-actin levels and no significant difference was observed between the percentage fluorescence and therefore F-actin levels at the endpoint of this assay between the non-oxidised and oxidised protein (Figure 5-9).

By comparing results across all mutants that contain cysteine 80 mutated to alanine (C80A, C39/80A, C80/139A and C80/147A) I saw that when these cofilin mutants were not oxidised, they were able to decrease F-actin levels to the same degree as WT as there was no significant difference between the percentage fluorescence and therefore F-actin levels at the endpoint of the assay. As I saw before, the C80A mutant was not able to rescue the inhibition of cofilin activity seen when WT cofilin was oxidised. I also found that none of the cofilin double cysteine to alanine mutants, namely C39/80A, C80/139A and C80/147A, were able to rescue cofilin activity when oxidised. Interestingly though, I observed a partial restoration of cofilin activity in the C80/147A mutant when it was oxidised as it was able to cause a decrease in the percentage fluorescence and therefore F-actin levels at the endpoint of the assay compared to all the other cofilin mutants involving the mutation of cysteine 80 which resulted in an increase in percentage fluorescence and F-actin levels (Figure 5-10).

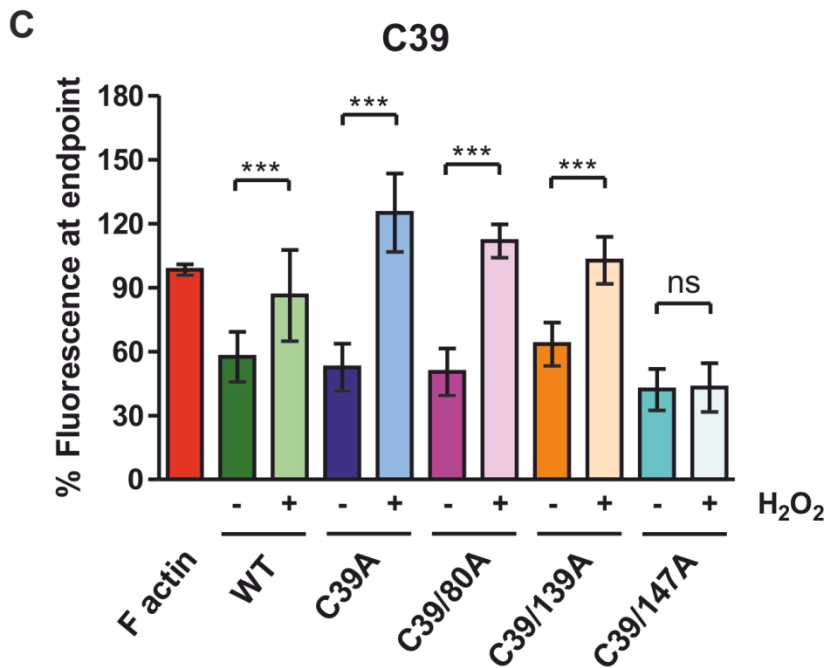
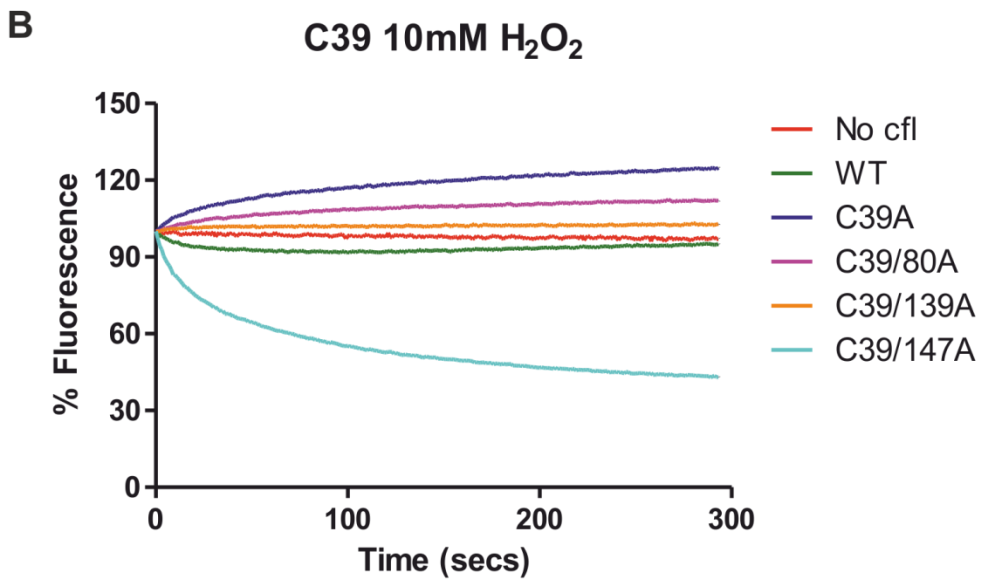
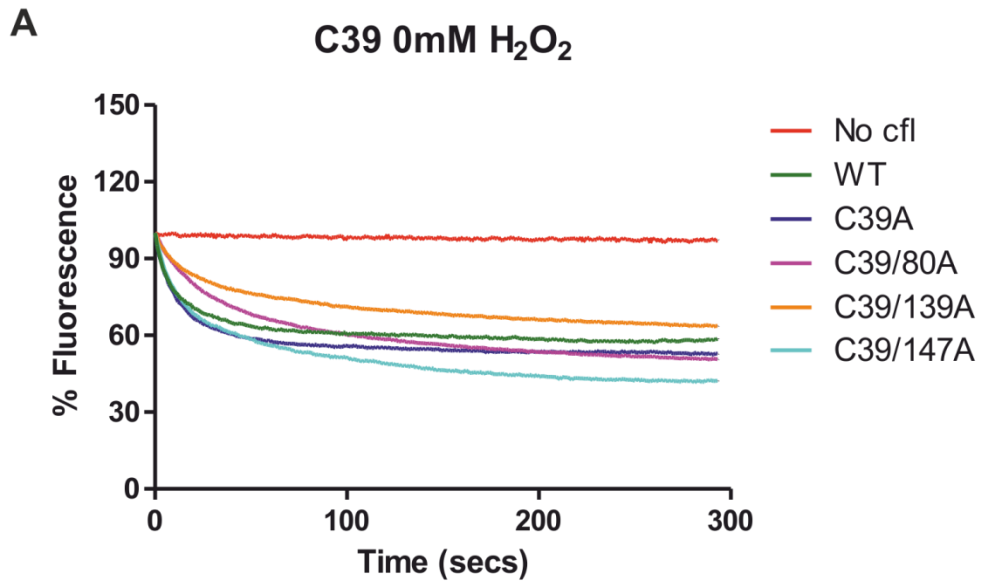


Figure 5-9 Cofilin C39/147A mutant can rescue the inhibition in the ability of cofilin to decrease F-actin levels when oxidised

Recombinant cofilin single and double cysteine to alanine mutants containing mutated cysteine 39 were oxidised with 10 mM H₂O₂ or left untreated. Non-oxidised and oxidised cofilin mutants were then added to pyrene labelled actin which had already reached a steady state level of F-actin. Fluorescence was measured over 5 minutes to monitor changes in F-actin levels. A) Graph showing average changes in fluorescence over 5 minutes after addition of non-oxidised cofilin mutants containing mutated cysteine 39. B) Graph showing average changes in fluorescence over 5 minutes after addition of oxidised cofilin mutants containing mutated cysteine 39. C) Graph showing mean percentage fluorescence +/- SD at endpoint compared to start of experiment after addition of non-oxidised or oxidised cofilin mutants containing mutated cysteine 39. Statistical significance of differences determined by a one-way ANOVA followed by a Tukey Kramer multiple comparison test (ns=not significant, ***=p<0.001), n>7.

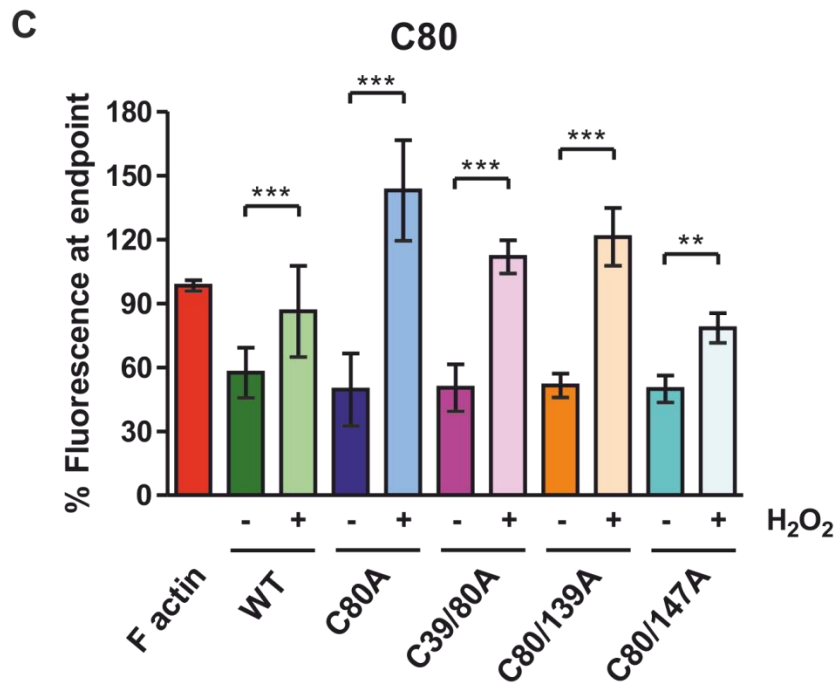
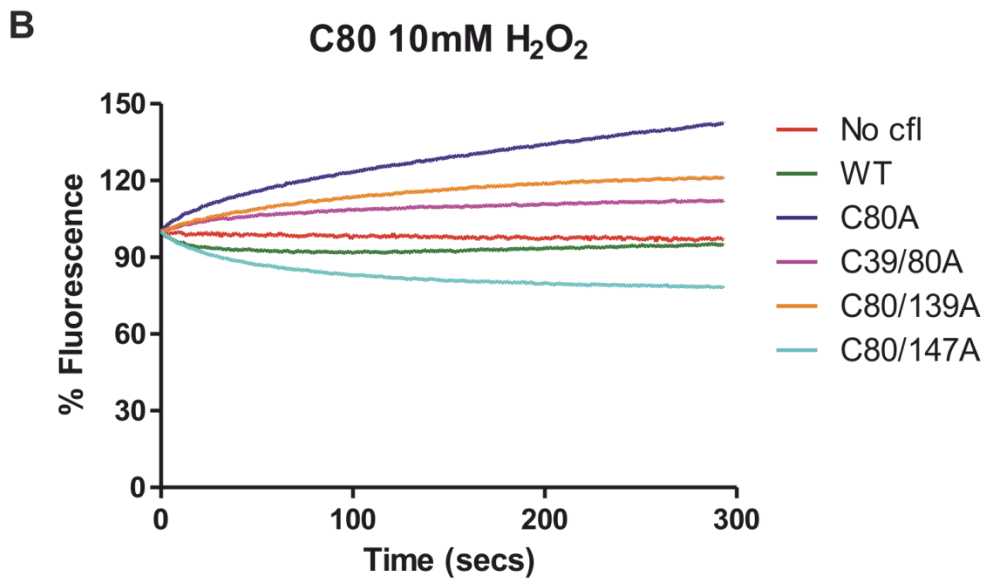
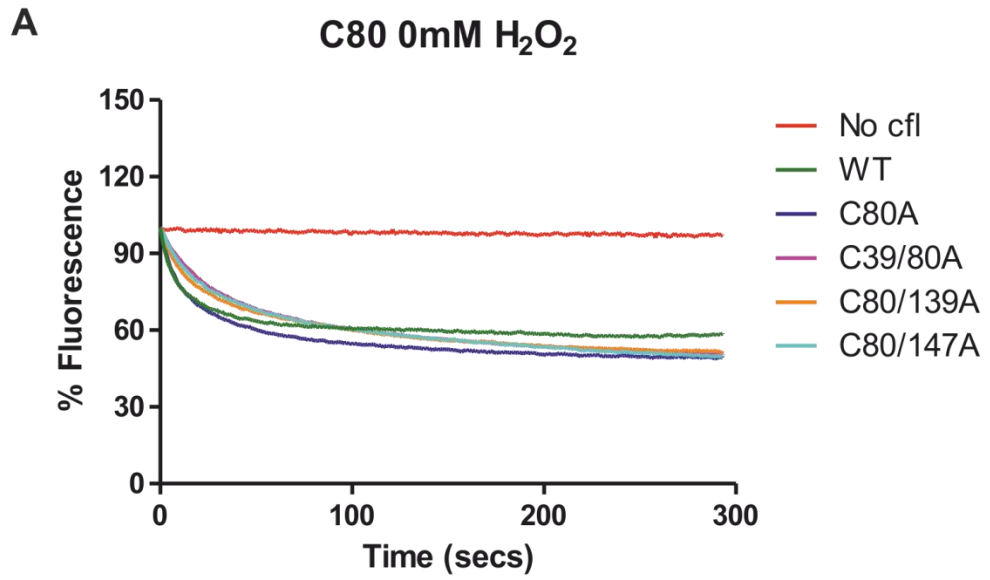


Figure 5-10 No cofilin cysteine to alanine mutants containing mutated cysteine 80 can rescue the inhibition in the ability of cofilin to decrease F-actin levels when oxidised

Recombinant cofilin single and double cysteine to alanine mutants containing mutated cysteine 80 were oxidised with 10 mM H₂O₂ or left untreated. Non-oxidised and oxidised cofilin mutants were then added to pyrene labelled actin which had already reached a steady state level of F-actin. Fluorescence was measured over 5 minutes to monitor changes in F-actin levels. A) Graph showing average changes in fluorescence over 5 minutes after addition of non-oxidised cofilin mutants containing mutated cysteine 80. B) Graph showing average changes in fluorescence over 5 minutes after addition of oxidised cofilin mutants containing mutated cysteine 80. C) Graph showing mean percentage fluorescence +/- SD at endpoint compared to start of experiment after addition of non-oxidised or oxidised cofilin mutants containing mutated cysteine 80. Statistical significance of differences determined by a one-way ANOVA followed by a Tukey Kramer multiple comparison test (**=p<0.01, ***=p<0.001), n>9.

By comparing results across all the mutants that contain cysteine 139 mutated to alanine (C139A, C39/139A, C80/139A and C139/147A) I saw that when these cofilin mutants were not oxidised, they were able to decrease F-actin levels to the same degree as WT as there was no significant difference between the percentage fluorescence and therefore F-actin levels at the endpoint of the assay. As seen previously, the C139A mutant was able to decrease F-actin levels when oxidised unlike WT cofilin. With the C39/139A and C80/139A mutants there was actually a loss of this effect as these mutants were unable to decrease F-actin levels. Although the mutation of cysteine 139 to alanine on its own was sufficient to rescue cofilin activity when oxidised, this was clearly not a strong enough effect to overcome the increase in F-actin levels observed when cysteine 39 or 80 were mutated independently. In contrast, the C139/147A mutant, when oxidised, could still decrease F-actin levels and to an even greater extent than C139A (Figure 5-11).

By comparing the results across all the mutants that contain cysteine 147 mutated to alanine (C147A, C39/147A, C80/147A and C139/147A) I saw that when these cofilin mutants were not oxidised, they were able to decrease F-actin levels to the same degree as WT as there is no significant difference between the percentage fluorescence and therefore F-actin levels at the endpoint of the assay. As was presented before, the C147A mutant when oxidised was able to decrease F-actin levels, rescuing the inhibition of activity seen when WT cofilin was oxidised. Indeed all cofilin single and double cysteine to alanine mutants that have cysteine 147 mutated to alanine, except C80/147A, were able to restore cofilin activity with no significant differences observed in the F-actin levels at the endpoint of the assay between the non-oxidised and oxidised forms of these mutants. Although the C80/147A mutant was not able to completely rescue cofilin activity when oxidised, it did result in a decrease in F-actin levels unlike the C80A mutant where an increase was seen (Figure 5-12).

All these results suggest that cysteine 147 appears to be the key cysteine residue that inhibits WT cofilin activity when oxidised. This is evident from the fact that all the cofilin single and double mutants containing cysteine 147 mutated were able to decrease F-actin levels to some degree when oxidised, with three out of the four being able to completely rescue the inhibition in the ability of cofilin to decrease F-actin levels that was seen with oxidised WT cofilin.

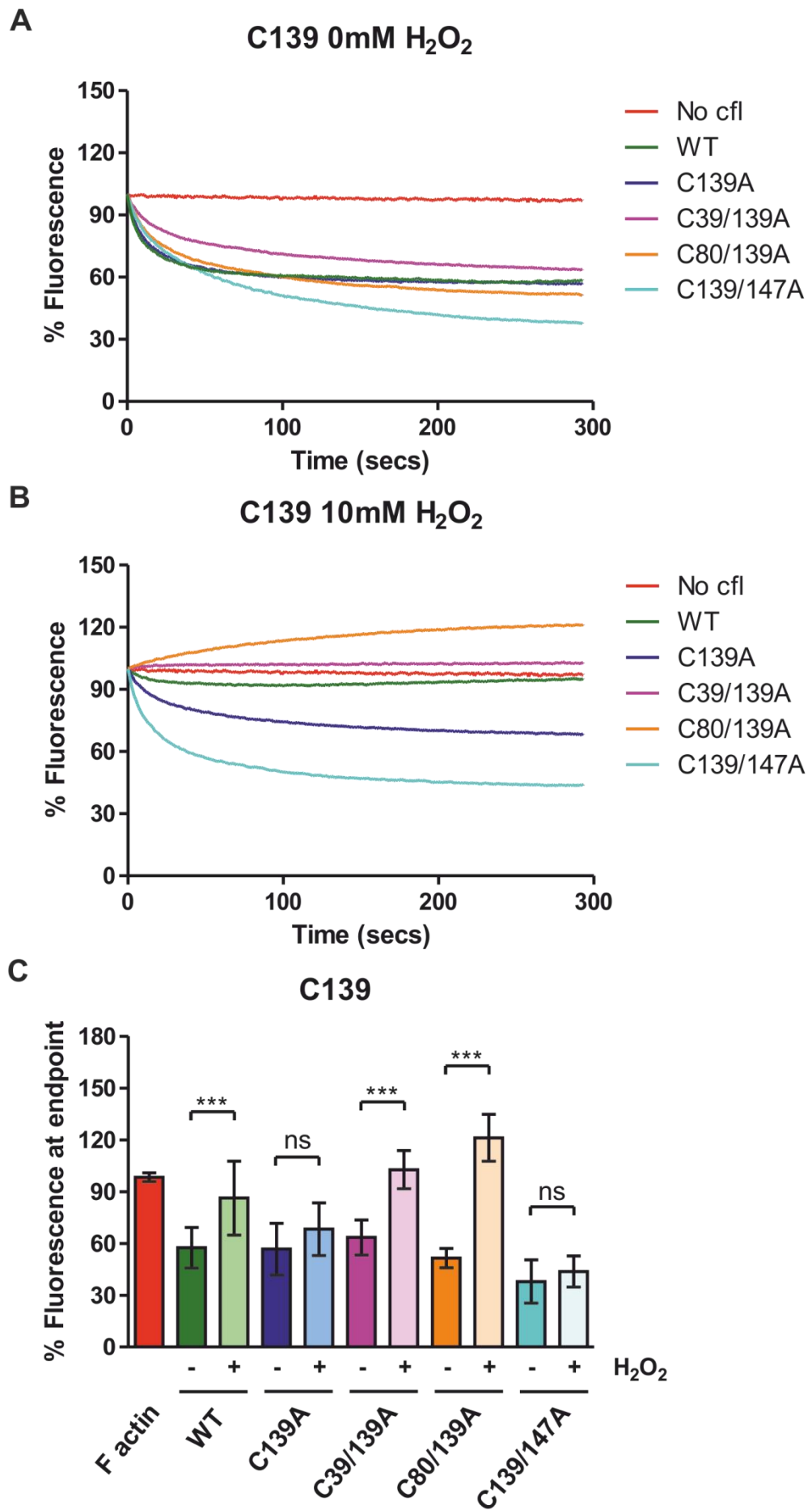


Figure 5-11 Cofilin C139A and C139/147A mutants can rescue the inhibition in the ability of cofilin to decrease F-actin levels when oxidised

Recombinant cofilin single and double cysteine to alanine mutants containing mutated cysteine 139 were oxidised with 10 mM H₂O₂ or left untreated. Non-oxidised and oxidised cofilin mutants were then added to pyrene labelled actin which had already reached a steady state level of F-actin. Fluorescence was measured over 5 minutes to monitor changes in F-actin levels. A) Graph showing average changes in fluorescence over 5 minutes after addition of non-oxidised cofilin mutants containing mutated cysteine 139. B) Graph showing average changes in fluorescence over 5 minutes after addition of oxidised cofilin mutants containing mutated cysteine 139. C) Graph showing mean percentage fluorescence +/- SD at endpoint compared to start of experiment after addition of non-oxidised or oxidised cofilin mutants containing mutated cysteine 139. Statistical significance of differences determined by a one-way ANOVA followed by a Tukey Kramer multiple comparison test (ns=not significant, ***=p<0.001), n>7.

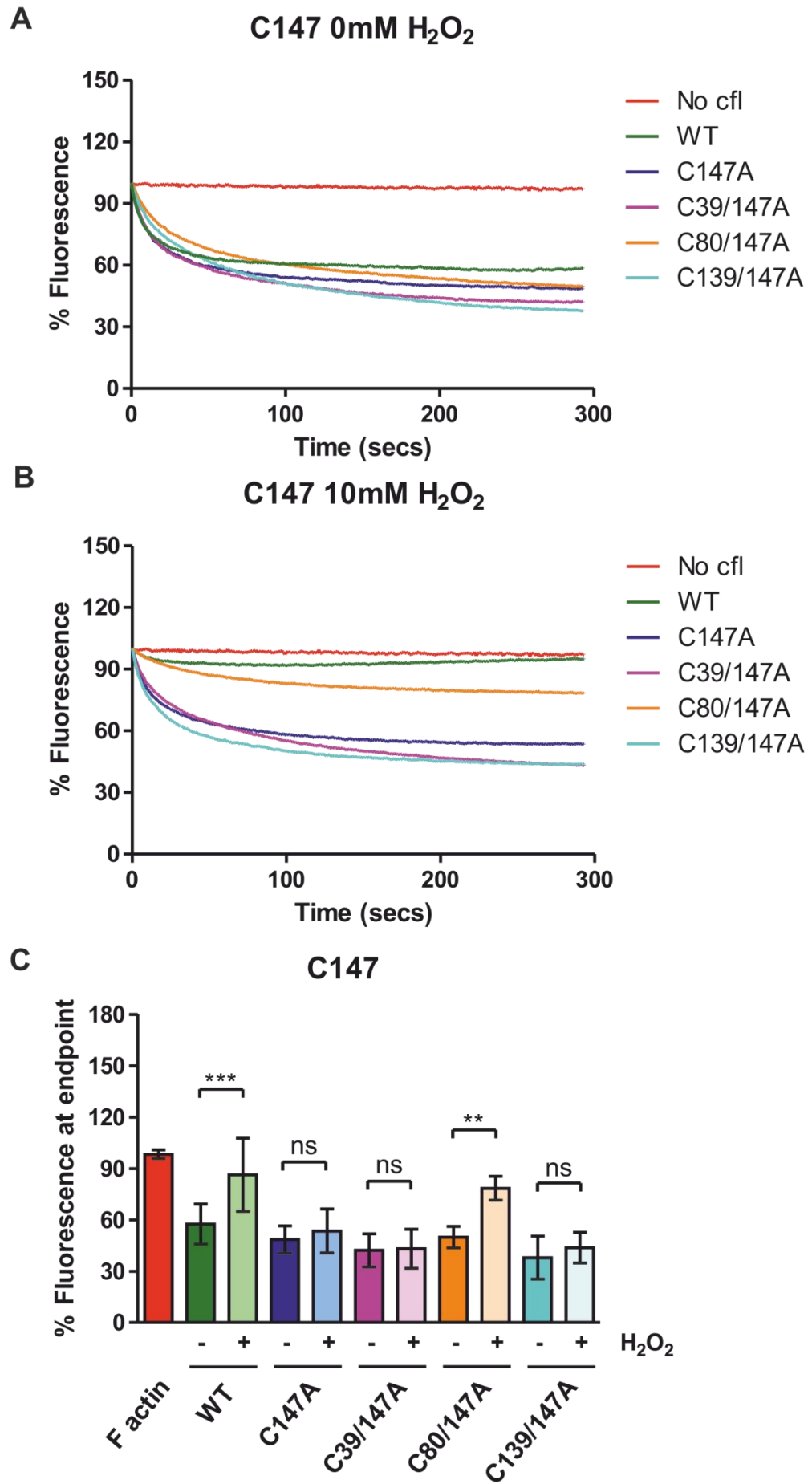


Figure 5-12 Cofilin C147A, C39/147A and C139/147A mutants can rescue the inhibition in the ability of cofilin to decrease F-actin levels when oxidised

Recombinant cofilin single and double cysteine to alanine mutants containing mutated cysteine 147 were oxidised with 10 mM H₂O₂ or left untreated. Non-oxidised and oxidised cofilin mutants were then added to pyrene labelled actin which had already reached a steady state level of F-actin. Fluorescence was measured over 5 minutes to monitor changes in F-actin levels. A) Graph showing average changes in fluorescence over 5 minutes after addition of non-oxidised cofilin mutants containing mutated cysteine 147. B) Graph showing average changes in fluorescence over 5 minutes after addition of oxidised cofilin mutants containing mutated cysteine 147. C) Graph showing mean percentage fluorescence +/- SD at endpoint compared to start of experiment after addition of non-oxidised or oxidised cofilin mutants containing mutated cysteine 147. Statistical significance of differences determined by a one-way ANOVA followed by a Tukey Kramer multiple comparison test (ns=not significant, **=p<0.01, ***=p<0.001), n>7.

5.2.8 Oxidation of recombinant cofilin results in a reduction in monomer levels and the formation of oligomers

As was detailed in the introduction, there are a number of different products that can form when a protein is oxidised (Figure 1-8). Since I was able to show that the oxidation of cofilin had an effect on its ability to reduce F-actin levels in the actin depolymerisation assay, I next wanted to establish if I could determine which oxidised cofilin product was being formed in the context of this assay. My first approach to address this was to separate the oxidised cofilin samples by non-reducing SDS-PAGE. The theory behind this was if any disulphide bonds were being formed within cofilin, a possibility considering the presence of more than one cysteine residue, a shift in the cofilin band may be observed as non-reducing gels preserve the integrity of disulphide bonds. I therefore incubated recombinant cofilin with 0, 3, 5, 7 or 10 mM H₂O₂ for 1 hour as I had done for the actin depolymerisation assay, quenching residual H₂O₂ at the end by the addition of catalase. Cofilin samples were then separated by non-reducing SDS-PAGE and cofilin assessed by western blot analysis with the membrane being probed with anti-cofilin Ab. Surprisingly and very interestingly what I observed was that when recombinant cofilin was treated with H₂O₂ there was a concentration dependent decrease in the levels of cofilin monomer and the appearance of a distinctive banding pattern in which each band corresponded to the expected molecular weight of cofilin oligomers. This trend observed was confirmed when the levels of cofilin monomer present at each concentration of H₂O₂ was quantified across four independent experiments (Figure 5-13).

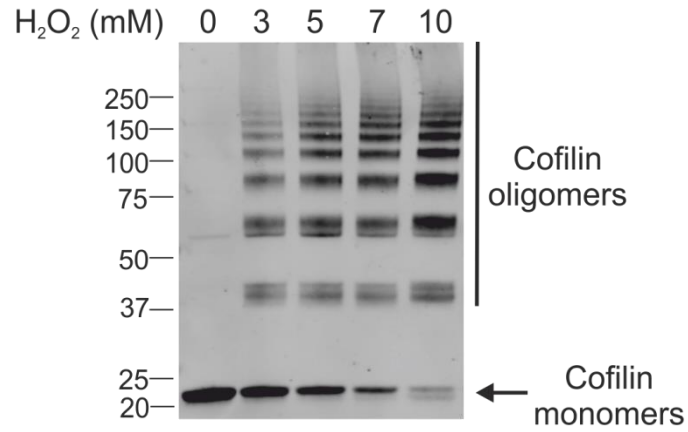
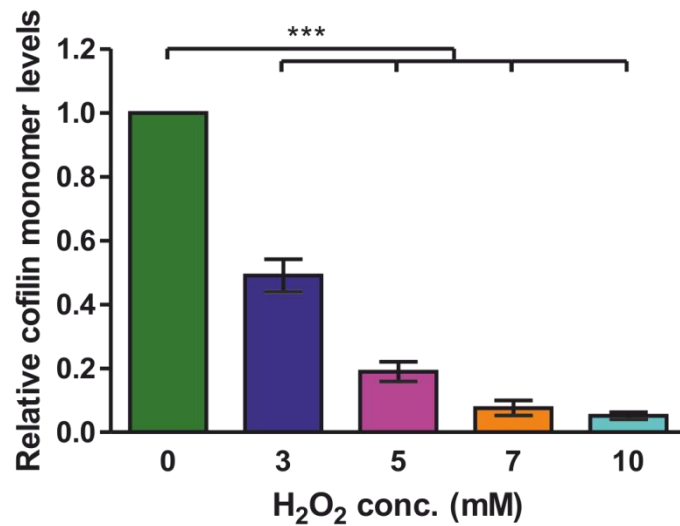
A**B**

Figure 5-13 Oxidation of recombinant cofilin results in a reduction in cofilin monomer levels and the formation of oligomers

Recombinant cofilin was oxidised with H₂O₂ at the concentrations stated. Samples were then separated by non-reducing SDS-PAGE and cofilin levels assessed by western blot analysis. Membrane probed with anti-cofilin Ab. A) Representative western blot showing cofilin monomer levels and oligomerisation. B) Graph showing mean cofilin monomer levels +/- SEM measured from 4 independent experiments. Statistical significance of differences determined by a one-way ANOVA followed by a Tukey Kramer multiple comparison test (**=p<0.01, ***=p<0.001).

5.2.9 Cofilin cysteine residue 147 is predominantly responsible for the reduction in monomer levels and oligomerisation of oxidised recombinant cofilin

After discovering that the oxidation of recombinant cofilin was leading to its oligomerisation and a decrease in monomer levels, I wanted to know what happened in the case of the cofilin single cysteine to alanine mutants I had generated. I therefore incubated cofilin WT, C39A, C80A, C139A and C147A with 10 mM H₂O₂ for 1 hour, as this was the concentration I used when testing these mutant cofilin proteins in the actin depolymerisation assay, or left them untreated. Residual H₂O₂ present at the end of the incubation time was quenched by catalase. Cofilin samples were then separated by non-reducing SDS-PAGE and cofilin assessed by western blot analysis with the membrane being probed with anti-cofilin Ab. The results from this experiment revealed that the levels of cofilin monomer present after oxidation of C39A and C80A was lower although not significantly than WT cofilin when oxidised. In contrast when C139A and C147A were oxidised, higher levels of cofilin monomer remained compared to oxidised WT cofilin. This increase in cofilin monomer levels was not classified as significant for the C139A mutant but was for the C147A cofilin mutant when quantified and analysed across three independent experiments (Figure 5-14). These results suggest that both cysteine 139 and 147 contribute to the formation of oligomers in oxidised cofilin but cysteine 147 has a greater and more important role than cysteine 139.

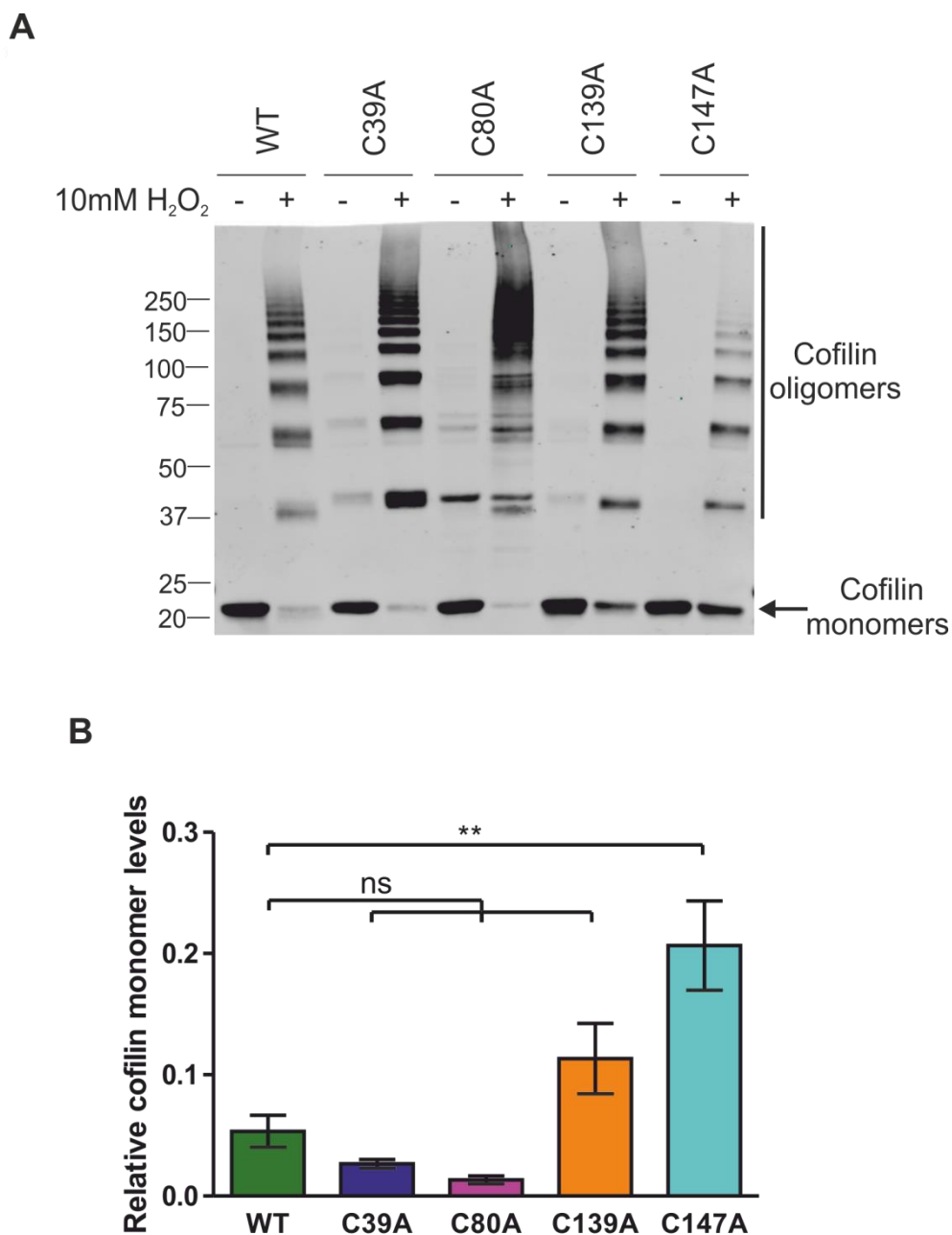


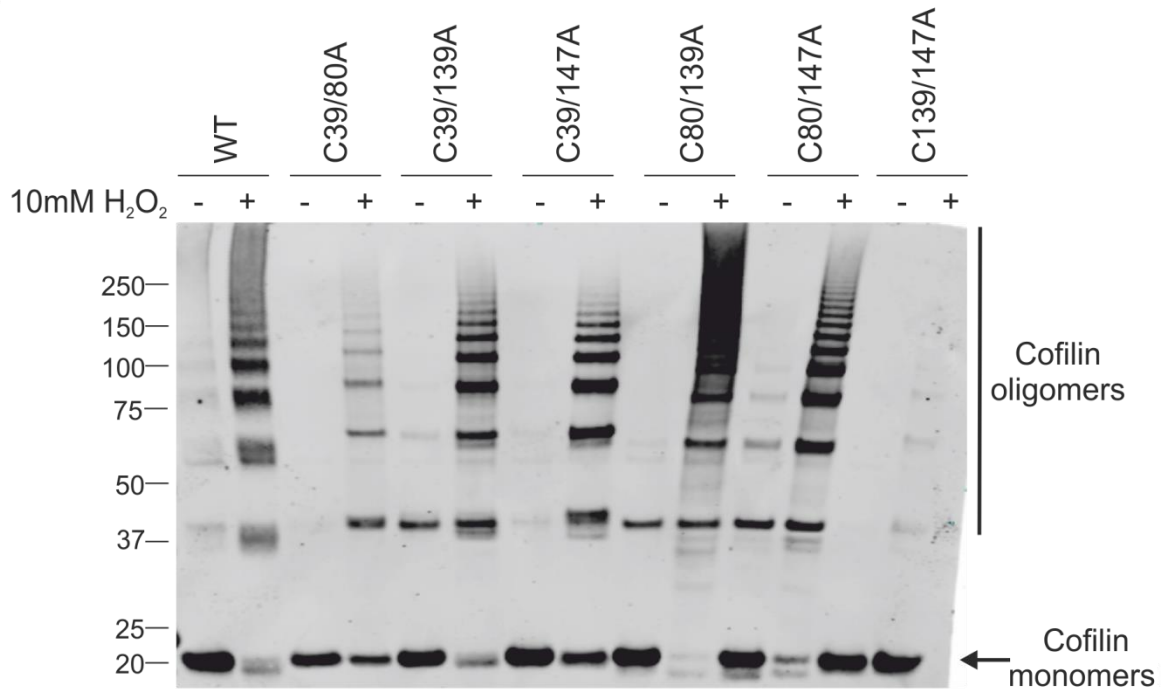
Figure 5-14 Monomer levels and oligomerisation before and following oxidation of cofilin cysteine to alanine mutants

Recombinant cofilin cysteine to alanine mutants were oxidised with 10 mM H₂O₂ or left untreated. Non-oxidised and oxidised cofilin mutant samples were then separated by non-reducing SDS-PAGE and cofilin levels assessed by western blot analysis. Membrane probed with anti-cofilin Ab. A) Representative western blot showing monomer levels and oligomerisation of cofilin mutants. B) Graph showing mean monomer levels +/- SEM of cofilin mutants measured from 3 independent experiments. Statistical significance of differences determined by a one-way ANOVA followed by a Tukey Kramer multiple comparison test (ns=not significant, **= $p < 0.01$).

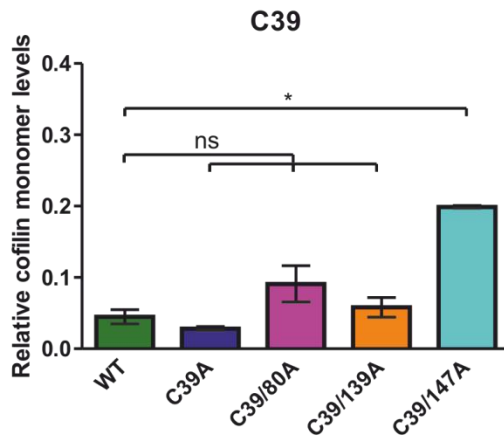
5.2.10 Cofilin cysteine residues 139 and 147 are almost completely responsible for the reduction in monomer levels and oligomerisation of oxidised recombinant cofilin

I also decided to investigate how cofilin monomer levels and oligomerisation were affected in the cofilin double cysteine to alanine mutants to see if I could learn any more about the oligomerisation of recombinant cofilin. I therefore incubated the cofilin double cysteine to alanine mutants (C39/80A, C39/139A, C39/147A, C80/139A, C80/147A and C139/147A) with 10 mM H₂O₂ for 1 hour, again as this was the concentration used for the actin depolymerisation assay, or left them untreated followed by quenching remaining H₂O₂ with catalase. Cofilin samples were then separated by non-reducing SDS-PAGE and cofilin assessed by western blot analysis with the membrane being probed with anti-cofilin Ab. Comparing the levels of cofilin monomer quantified across four independent experiments I found that of the cofilin cysteine to alanine mutants containing mutant cysteine 39, only cofilin C39/147A exhibited significantly increased levels of monomer compared to WT when oxidised (Figure 5-15 B). There was no significant difference identified between the cofilin monomer levels in any of the oxidised cofilin cysteine to alanine mutants containing cysteine 80 (Figure 5-15 C). Cofilin mutants which had cysteine 139 mutated to alanine showed a similar trend to those involving mutant cysteine 39 in that only the double mutant involving C147 (C139/147A) showed significantly increased monomer levels compared to WT when oxidised (Figure 5-15 D). Of the four cofilin cysteine to alanine mutants containing cysteine 147 mutated, three showed increased monomer levels when oxidised compared to WT (Figure 5-15 E). The greatest increase in cofilin monomer levels was seen in the C139/147A mutant; western blot of this sample revealed that virtually all oligomerisation of cofilin was prevented (Figure 5-15 A). These results indicate that cofilin cysteine residues 139 and 147 are responsible almost exclusively for the formation of intermolecular disulphide bonds and subsequent oligomerisation of cofilin.

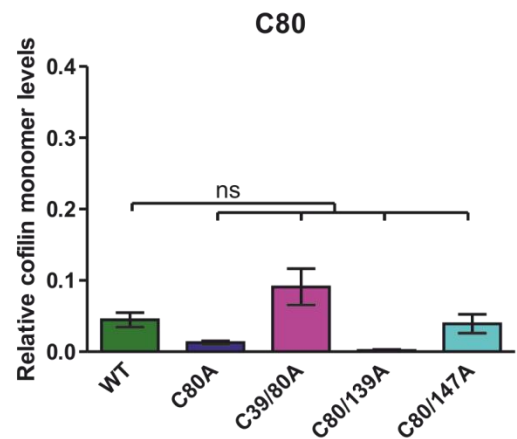
A



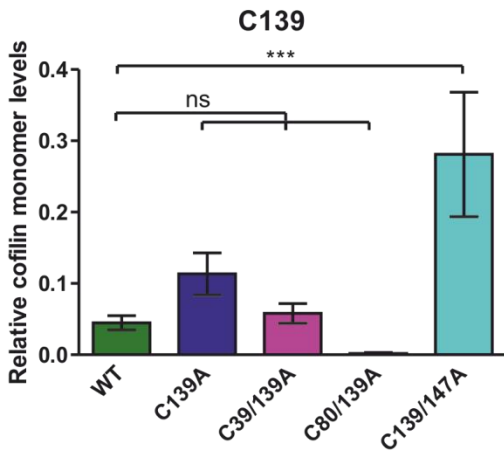
B



C



D



E

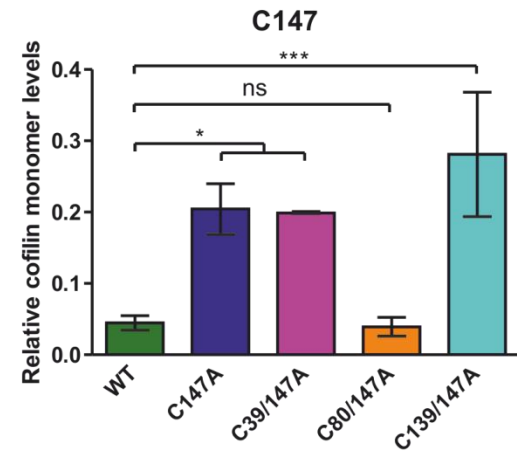


Figure 5-15 Monomer levels and oligomerisation before and following oxidation of cofilin double cysteine to alanine mutants

Recombinant cofilin double cysteine to alanine mutants were oxidised with 10 mM H₂O₂ or left untreated. Non-oxidised and oxidised cofilin mutant samples were then separated by non-reducing SDS-PAGE and cofilin levels assessed by western blot analysis. Membrane probed with anti-cofilin Ab. A) Representative western blot showing monomer levels and oligomerisation of cofilin mutants. B) Graph showing mean monomer levels of cofilin mutants containing cysteine 39 mutated +/- SEM measured from >3 independent experiments. C) Graph showing mean monomer levels of cofilin mutants containing cysteine 80 mutated +/- SEM measured from >3 independent experiments. D) Graph showing mean monomer levels of cofilin mutants containing cysteine 139 mutated +/- SEM measured from >3 independent experiments. E) Graph showing mean monomer levels of cofilin mutants containing cysteine 147 mutated +/- SEM measured from >3 independent experiments. Statistical significance of differences in B) - E) determined by a one-way ANOVA followed by a Tukey Kramer multiple comparison test (ns=not significant, *=p<0.05, ***=p<0.001).

5.3 Conclusions

In this chapter I have presented data showing that the oxidation of recombinant cofilin inhibited its activity as it had a reduced ability to decrease F-actin levels. Cofilin cysteine residues 139 and 147, but more notably cysteine 147, were the key cysteine residues responsible for this inhibition of activity observed with oxidised cofilin. Oxidation of recombinant cofilin also resulted in its oligomerisation and a corresponding reduction in monomer levels. Cofilin cysteine residues 139 and 147 were almost entirely responsible for this oligomerisation and reduction in monomer levels again with cysteine 147 having the predominant role.

6 Cofilin Oxidation and Cell Migration and Invasion

6.1 Introduction

Cofilin has been well documented to be involved in cell migration and invasion. Reports have been published highlighting that cofilin is required for the migration of neural crest cells, macrophages, neutrophils and T cells [65, 161-163]. Moreover, the overexpression of cofilin increased the migration and invasion of melanoma cells, while cofilin was identified to be overexpressed in an invasive subpopulation of mammary tumour cells [56, 190]. In addition to this, increasing or decreasing the activity of cofilin resulted in an increase or decrease in the invasiveness of mammary tumour cells, respectively [191]. Since I demonstrated that oxidation of cofilin inhibited its ability to reduce F-actin levels and that this was dependent on cysteine residues 139 and 147, I wanted to establish if the oxidation of cofilin on these residues was also required for cell migration and invasion, cellular processes that require dynamic changes in the actin cytoskeleton. In this chapter, the results from my investigations into the involvement of cofilin oxidation in cell migration and invasion are presented.

6.2 Results

6.2.1 Establishment of MDAMB231 cell lines stably expressing mCh, mCh cofilin WT or mCh cofilin C139/147A

After discovering through my *in vitro* studies that the oxidation of cofilin inhibited its ability to decrease F-actin levels and resulted in its oligomerisation and a reduction in monomer levels, I wanted to investigate how the oxidation of cofilin could affect its functioning in cells. To do this I created MDAMB231 cell lines stably expressing either mCh cofilin WT or mCh cofilin C139/147A which would be insensitive to oxidation on cysteine residues 139 and 147. I chose the cofilin C139/147A mutant as it was the one that was able to reduce F-actin levels to the same degree when oxidised and non-oxidised, and showed the greatest inhibition of oligomerisation *in vitro*. In addition to the cofilin expressing cell lines I also generated a mCh expressing cell line as a control. To create these cell lines, I transfected parental MDAMB231 cells with plasmids expressing mCh, mCh cofilin WT or mCh cofilin C139/147A and a gene conferring resistance to G418. 48 hours after transfection, cells were transferred to G418

containing medium and cultured until all control cells that had not been transfected with any of the plasmids had died. Surviving cells expressing mCh, mCh cofilin WT or mCh cofilin C139/147A were selected by cell sorting using a FACSAria cell sorter (Figure 6-1 A). These cells were then used for subsequent experiments after confirmation by western blot analysis that they were expressing the mCh control or cofilin proteins. Membranes were probed using both anti-cofilin Ab and anti-dsRed Ab capable of detecting mCh (Figure 6-1 B).

6.2.2 No difference in proliferation of MDAMB231 cell lines expressing mCh, mCh cofilin WT or mCh cofilin C139/147A

Before undertaking any further experiments with the newly generated cell lines, I wanted to check that their proliferation rates had not been affected by the expression of these proteins. To do this I seeded each cell line at 5,000 cells per well in a 96-well plate and then counted the cells at 24, 48, 72 and 96 hours using the CellTiter-Glo assay. From this I was able to confirm that there was no difference in the proliferation of the cell lines expressing mCh, mCh cofilin WT or mCh cofilin C139/147A compared to the parental MDAMB231 cells (Figure 6-2).

6.2.3 mCh cofilin WT and mCh cofilin C139/147A cells show slight decrease in migration

After establishing that; i) H_2O_2 levels were increased in migrating cells and ROS are necessary for migration, ii) cofilin oxidation was found increased in migrating cells and iii) that the oxidation of cofilin inhibits its activity, I wanted to know if the mCh cofilin C139/147A cells exhibited an altered ability to migrate compared to the mCh cofilin WT cells. To address this I again used the Essen Bioscience CellPlayerTM 96-well cell migration assay as described in chapter 3.

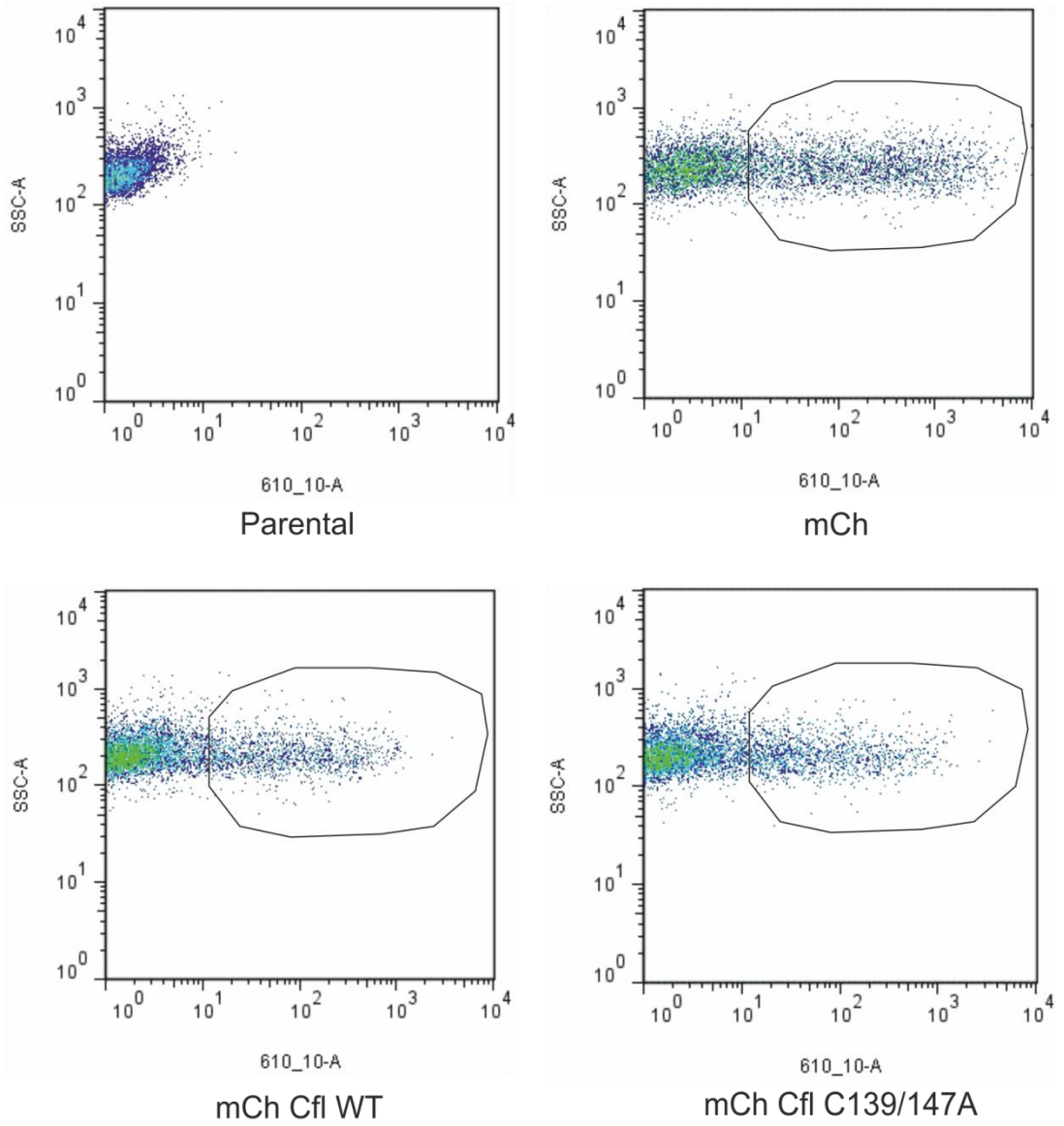
Cells were seeded in a 96-well ImageLockTM plate and cultured overnight to form a confluent monolayer. Wounds were then created through the monolayer using the WoundMakerTM after which the plate was placed in the IncucyteTM machine which was scheduled to acquire images of the wounds every 2 hours for 24 hours. Again as in chapter 3, wound width was used as a measure of cell migration. The results from this experiment showed that both the MDAMB231

cell lines expressing mCh cofilin WT and mCh cofilin C139/147A had a slightly reduced migration compared to the parental and mCh expressing cell lines but no difference was observed between the WT and C139/147A cofilin expressing cells (Figure 6-3). This was not unexpected as it has been reported that overexpressing cofilin within cells disrupts the actin cytoskeleton at the leading edge and this inhibits their invasiveness [189].

6.2.4 mCh cofilin C139/147A cells have reduced directionality

Having seen no difference in the migration between mCh cofilin WT and mCh cofilin C139/147A cells, I next wanted to investigate if cofilin oxidation was involved in particular aspects of cell migration. Such factors might not be detected in an assay that just measures overall migration, such as the one used previously, due to the fact that cells have a remarkable ability to switch the way in which they migrate as discussed in the introduction. One aspect of cell migration that cofilin has been implicated in is directionality, therefore it was decided to determine if cofilin oxidation was required for cell directionality [155, 156]. To investigate this, cells were seeded at a subconfluent density in a 6-well plate, allowed to settle to the bottom and then imaged on a timelapse microscope for 4 hours. Paths taken by individual cells were tracked and directionality determined using ImageJ. This revealed that the MDAMB231 cells expressing mCh cofilin C139/147A had a significantly lower directionality compared to the mCh and mCh cofilin WT expressing cells (Figure 6-4).

A



B

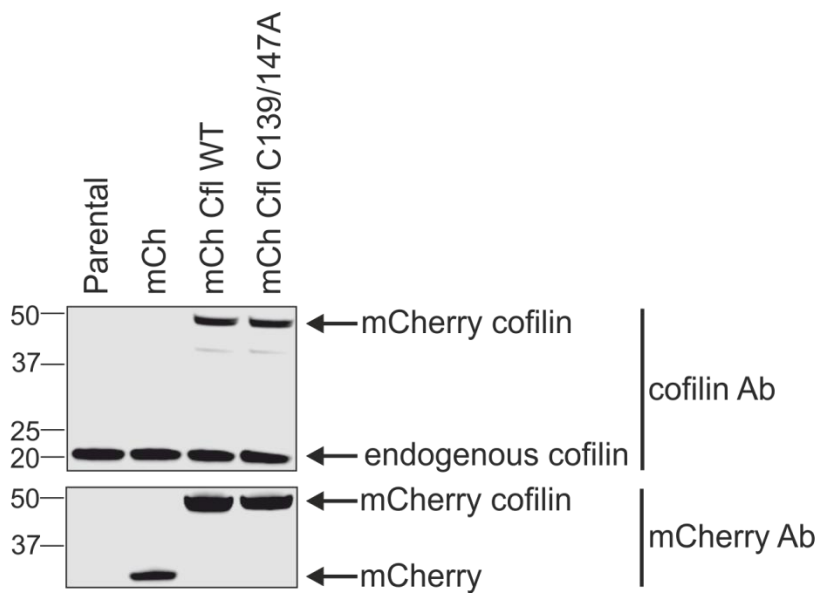


Figure 6-1 Creation of MDAMB231 cell lines stably expressing mCh, mCh cofilin WT or mCh cofilin C139/147A

A) FACS plots confirming a population of cells which positively expressed either mCh, mCh cofilin WT or mCh cofilin C139/147A. B) Western blot confirming the stable expression of mCh, mCh cofilin WT or mCh cofilin C139/147A in the MDAMB231 cell line. Membranes were probed using anti-cofilin Ab and anti-dsRed Ab capable of detecting mCh.

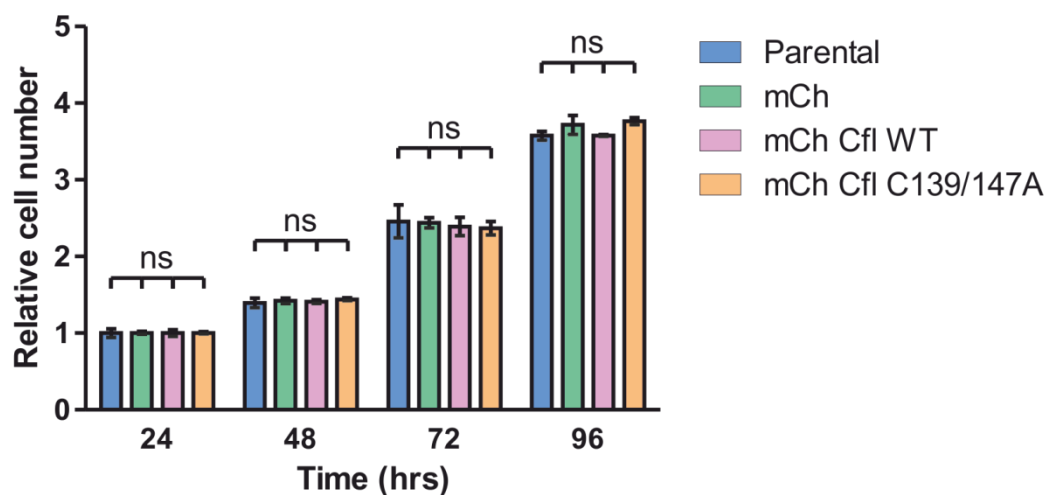


Figure 6-2 No difference in proliferation rate of stable cell lines expressing mCh, mCh cofilin WT or mCh cofilin C139/147A

Cells were seeded in a 96-well plate at 5,000 cells per well and at the time points indicated cells were counted using the CellTiter-Glo assay. A) Graph showing mean cell number \pm SEM relative to 24 hours measured across 3 independent experiments. Statistical significance of differences determined by a one-way ANOVA followed by a Tukey Kramer multiple comparison test (ns=not significant).

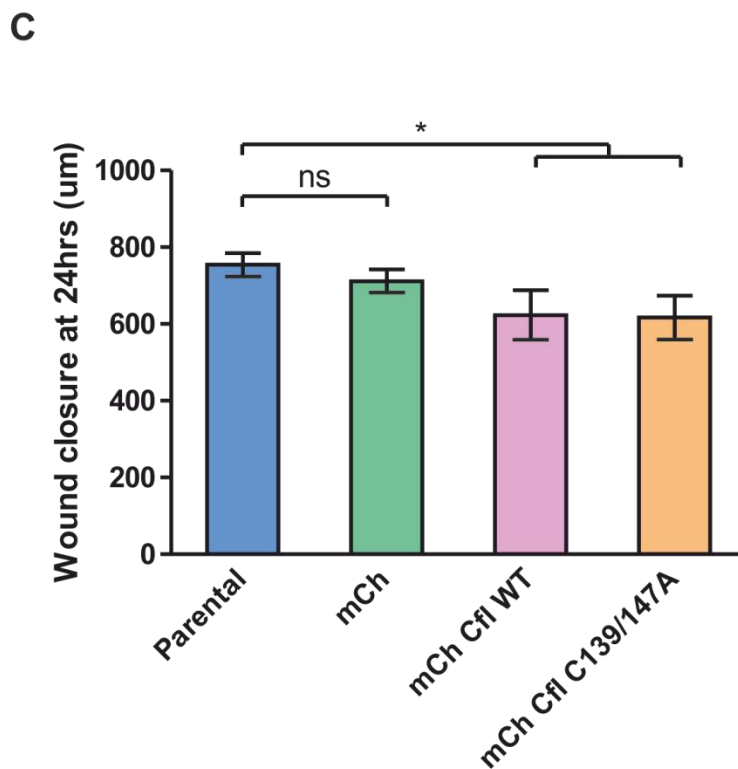
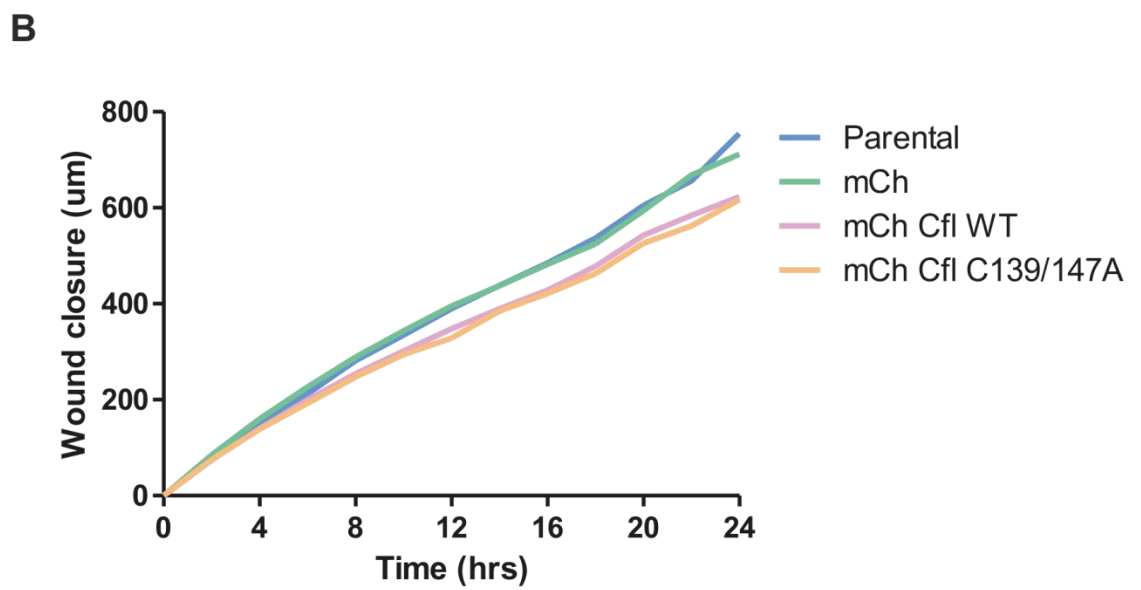
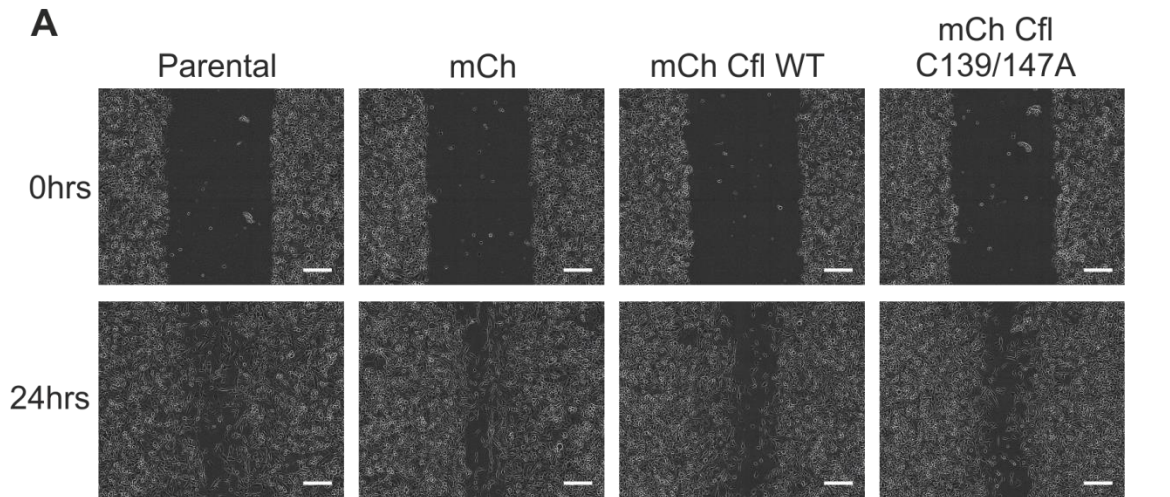


Figure 6-3 Expression of mCh cofilin WT or mCh cofilin C139/147A results in a small decrease in wound closure

Cells were cultured in ImageLock™ 96-well plates to form a confluent monolayer. Wounds were created using a WoundMaker™ and wound closure measured over 24 hours using the Incucyte™ system. A) Representative images of wounds at 0 and 24 hours. B) Graph showing wound closure over 24 hours. C) Graph showing mean wound closure at 24 hours +/- SEM measured across 3 independent experiments. Statistical significance of differences determined by a one-way ANOVA followed by a Tukey Kramer multiple comparison test (ns=not significant, * $p < 0.05$).

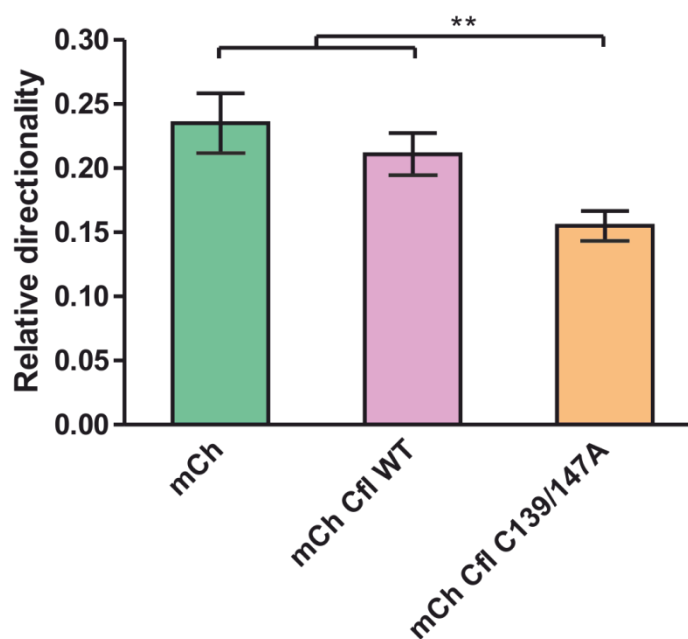


Figure 6-4 Cells expressing mCh cofilin C139/147A have reduced directionality

Cells were seeded subconfluently in 6-well dishes and images taken on a timelapse microscope every 10 minutes for 4 hours. Paths taken by individual cells were tracked and directionality determined using ImageJ. Graph shows mean relative directionality \pm SEM, $n=12$. Statistical significance of differences determined by a one-way ANOVA followed by a Tukey Kramer multiple comparison test (**= $p < 0.01$). Figure courtesy of Mike Olson.

6.2.5 mCh cofilin C139/147A cells have reduced spreading/adhesion as measured by xCelligence system

Having identified a difference in the directionality of the mCh cofilin C139/147A expressing cells, I next wanted to investigate if these cells exhibited any difference in adhesion and/or spreading. To address this I used the xCelligence system which can monitor changes in a number of different cell properties using special plates, called E-plates, which have electrodes at the base of the wells. When cells adhere to and spread on these plates there is a change in the electrical impedance measured and a read out of this called cell index is reported. This system can therefore be used to measure differences in the adhesion and spreading of cells.

I seeded cells in the E-plates at 10,000 per well and scheduled the xCelligence software to measure the electrical impedance every 10 minutes for 3 hours. I found that the spreading/adhesion of mCh cofilin C139/147A cells increased at a slower rate and was significantly lower at the end of the 3 hours compared to the mCh cofilin WT, mCh or parental cell lines (Figure 6-5).

6.2.6 mCh cofilin C139/147A cells have reduced adhesion

As the lower cell index measured in the mCh cofilin C139/147A cells could be the result of reduced cell adhesion and/or cell spreading, I decided to carry out experiments to investigate this finding further. Initially I wanted to know if the difference in cell index observed was due to adhesion. I therefore seeded cells in a 96-well plate at 40,000 cells per well. After 3 hours, I washed the wells multiple times to remove cells that had not fully adhered to the plate and counted the number of adherent cells using the CellTiter-Glo Assay. I discovered that the mCh cofilin C139/147A cells had significantly reduced cell adhesion compared to mCh cofilin WT and mCh cells (Figure 6-6). The reduction in relative adhesion measured was similar to the decrease in relative spreading/adhesion reported in the previous experiment. Reduced adhesion could therefore account in full or in part for the decreased cell index seen.

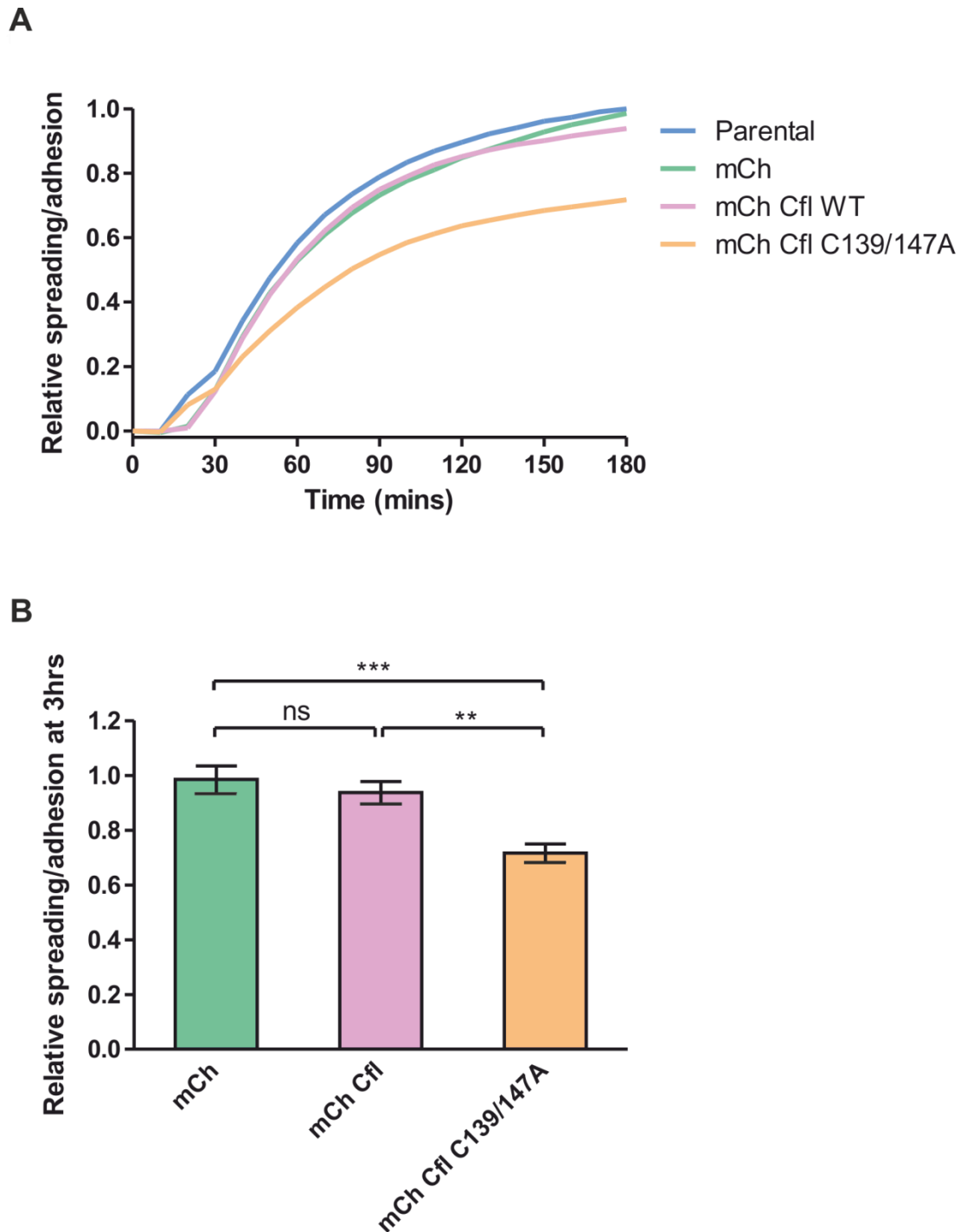


Figure 6-5 Cells expressing mCh cofilin C139/147A have reduced spreading/adhesion as measured by the xCelligence system

Cells were seeded in E-plates at 10,000 per well and spreading/adhesion (as indicated by cell index) measured over 3 hours on the xCelligence system. A) Graph showing spreading/adhesion relative to parental cell line measured over 3 hours from time of seeding. B) Graph showing mean spreading/adhesion \pm SEM relative to parental cell line at 3 hours measured across 3 independent experiments. Statistical significance of differences determined by a one-way ANOVA followed by a Tukey Kramer multiple comparison test (ns=not significant, **= $p < 0.01$, ***= $p < 0.001$).

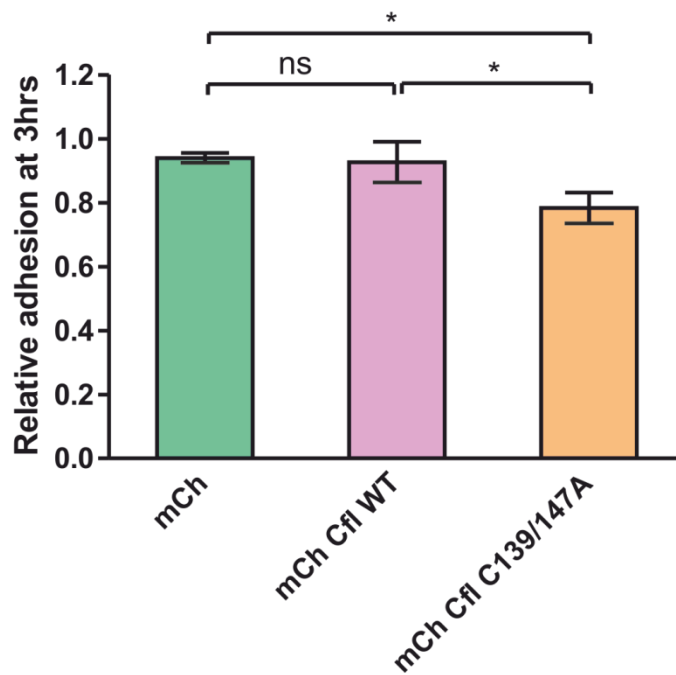


Figure 6-6 Cells expressing mCh cofilin C139/147A have reduced adhesion

Cells were seeded in 96-well plates at 40,000 cells per well. After 3 hours non-adherent cells were washed off and adherent cells counted using CellTiter-Glo assay. A) Graph showing mean percentage adhesion +/- SEM relative to parental cell line after 3 hours measured across 3 independent experiments. Statistical significance of differences determined by a one-way ANOVA followed by a Tukey Kramer multiple comparison test (ns=not significant, $*=p<0.05$).

6.2.7 mCh cofilin WT and mCh cofilin C139/147A cells show no difference in invasion

Having seen a decrease in the directionality and adhesion of the mCh cofilin C139/147A cells, I wanted to know if there was any difference in their rate of invasion. To do this, I used the Essen Bioscience CellPlayer™ 96-well cell invasion assay which follows a similar format to the cell migration assay except the cells have to invade through a layer of Matrigel in order to close the wound.

Cells were seeded in a 96-well ImageLock™ plate and cultured overnight to form a confluent monolayer and wounds then created through the monolayer using the WoundMaker™. Cells were then overlaid with a layer of Matrigel and the plate placed in the Incucyte™ machine which was scheduled to acquire images of the wounds every 2 hours. In this case relative cell density was used as a measure of cell invasion. Neither wound width or wound confluence could be used as a measure of invasion as the presence of the Matrigel and the way in which cells invade interferes with the integrated metrics that measure these factors. From this I discovered that there was no difference in the rate of invasion between the mCh cofilin WT and mCh cofilin C139/147A cells even with respect to the parental and mCh cell lines (Figure 6-7).

6.3 Conclusions

In this chapter I have presented results showing that cells expressing mCh cofilin WT and mCh cofilin C139/147A have no difference in proliferation compared to control parental and mCh cells. Both mCh cofilin WT and mCh cofilin C139/147A cells exhibit a decrease in migration compared to parental and mCh cells. In contrast mCh cofilin C139/147A cells have a decreased directionality and adhesion, compared to mCh cofilin WT, mCh and parental cells. Although these differences were observed in migration, directionality and adhesion, there was no change in the invasion of either mCh cofilin WT or mCh cofilin C139/147A cells compared to parental or mCh cells.

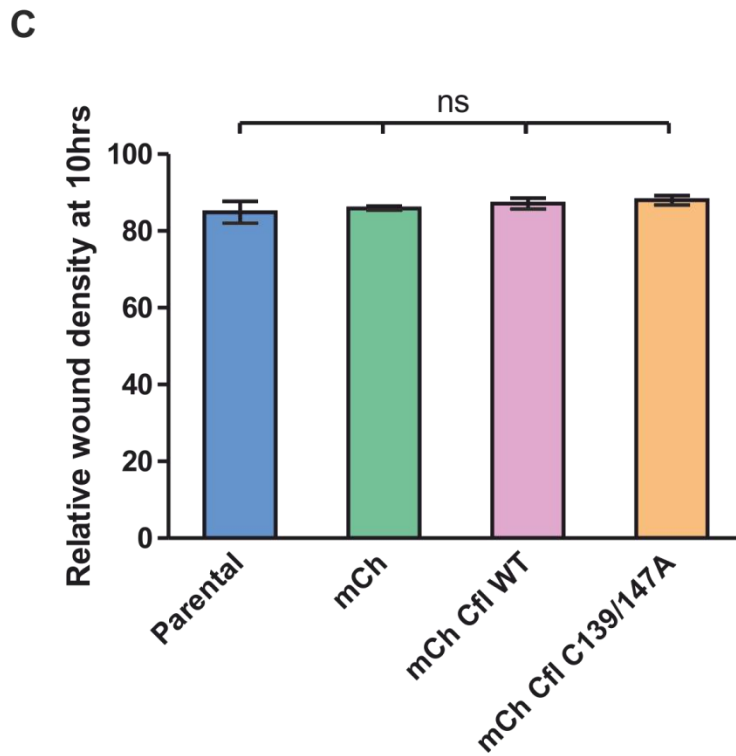
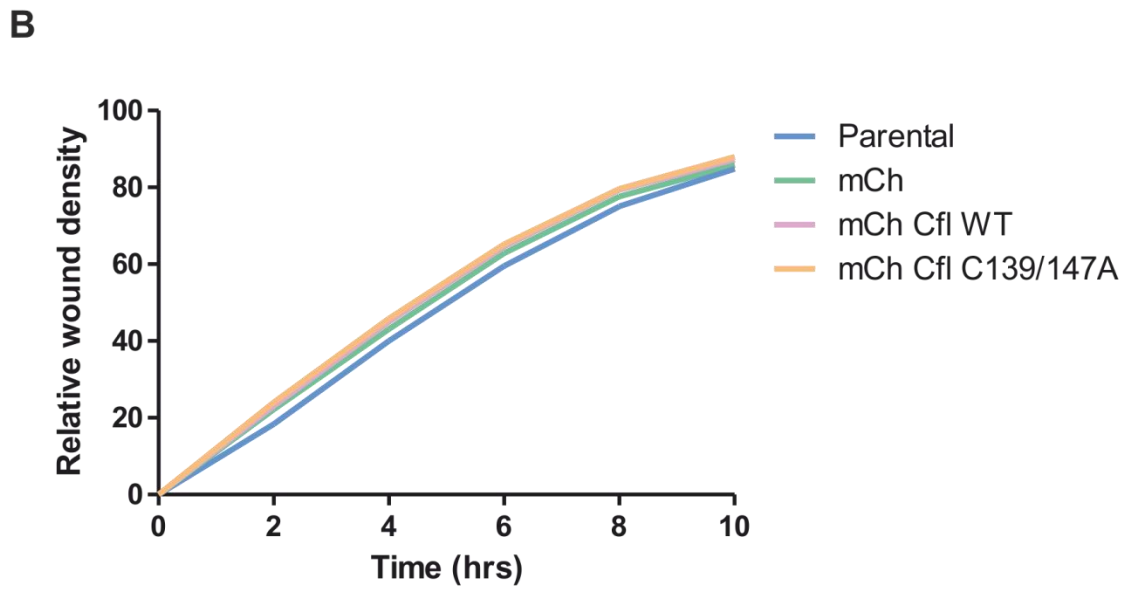
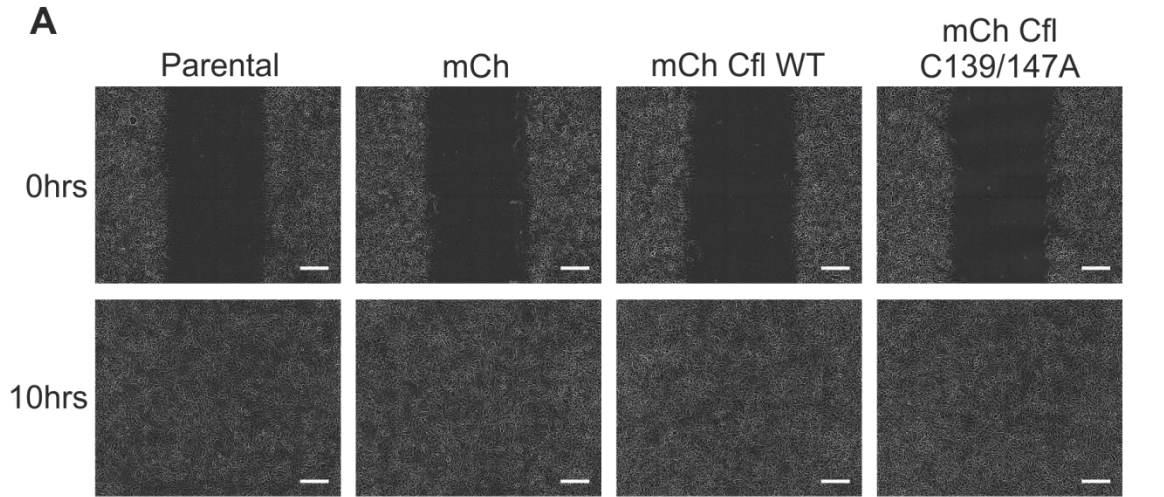


Figure 6-7 No difference in invasion observed in cells expressing mCh cofilin WT or mCh cofilin C139/147A

Cells were cultured in ImageLock™ 96-well plates to form a confluent monolayer. Wounds were created using a WoundMaker™ then overlaid with Matrigel. Invasion was measured over 10 hours by measuring relative wound density using the Incucyte™ system. A) Representative images of wounds at 0 and 10 hours. B) Graph showing relative wound density over 10 hours. C) Graph showing mean relative wound density at 10 hours +/- SEM measured across 3 independent experiments. Statistical significance of differences determined by a one-way ANOVA followed by a Tukey Kramer multiple comparison test (ns=not significant).

7 Discussion

As described in the introduction, ROS are frequently elevated in cancer cell lines and tissue samples. Increased ROS levels are also associated with a more aggressive disease and poorer prognosis. One of the hallmarks of cancer and aspects of disease progression that is known to be promoted by ROS is invasion and metastasis. Cell migration is an essential component of invasion and metastasis, and is also understood to be regulated by ROS. Although it is known that ROS exert their downstream effects primarily through the oxidation of proteins on key cysteine residues, very few proteins have been identified as direct targets of this oxidation and found to be involved in ROS mediated signalling in migrating cells. Here I have presented data showing that the ROS, H_2O_2 , is produced at increased levels in migrating cells, predominantly at the tips of protrusions. Additionally I have demonstrated that protein oxidation is increased in migrating cells and identified the actin binding protein cofilin as one of the oxidised proteins. Furthermore I established that, when oxidised, cofilin forms oligomers and has a reduced ability to decrease F-actin levels *in vitro*, which is dependent on the oxidation of cysteine residues 139 and 147. Moreover, the oxidation of these cysteine residues is required for directional cell migration and adhesion in cell culture.

7.1 ROS and cell migration

There is a wealth of *in vitro* and *in vivo* evidence demonstrating the involvement of ROS in cell migration. Most of these studies have shown this by increasing antioxidant or ROS scavenging enzyme levels, which results in a decrease in migration, or conversely reducing antioxidant levels which enhances cell migration [255-259]. These reports are supported by my own experiments showing that treatment of cells with the antioxidant NAC inhibits migration (Figure 3-2). Others have shown a direct increase in ROS levels in migrating cells using derivatives of the fluorescent ROS sensor, DCF. Some of these studies also identified an accumulation of ROS at membrane ruffles and the leading edge of migrating cells which are the areas undergoing the most dynamic changes in the actin cytoskeleton [266, 277]. However, the ROS sensors used in these experiments are not able to distinguish between different types of ROS. It would be of interest to know if H_2O_2 in particular was elevated as it is the ROS known

to act as a second messenger in signalling pathways and be responsible for protein oxidation [328]. To address this issue I employed a fluorescent probe, HyPer, that is sensitive specifically to H_2O_2 and can be used in live cell imaging [322]. Using this probe, I established that H_2O_2 levels are elevated in actively migrating cells (Figures 3-8 and 3-14). Moreover, this increase in H_2O_2 was particularly apparent at the tips of cell protrusions, which are the most motile areas of the cell (Figure 3-15). These results are consistent with the previously mentioned studies but, as far as I am aware, is the first time H_2O_2 levels have been specifically shown to be elevated in migrating cells and localised at the leading edge. As H_2O_2 is the ROS responsible for protein oxidation, this finding compliments and provides further insight into the observation that protein oxidation is increased at the leading edge of migrating cells [278].

Although my data clearly show that the concentration of H_2O_2 is higher in migrating cells, especially at the leading edge, one question still remains; what is the source of this H_2O_2 ? A possible answer to this question is the NOX enzymes. A number of studies where NOX enzymes were chemically inhibited reported a decrease in migration [257, 266, 267]. Similarly, knockdown of NOX1 and NOX4 lead to impaired migration and conversely, overexpressing NOX1 increased migration [268-271]. Additionally, NOX2 and its regulatory subunit, p47phox, have been identified at the leading edge in VEGF-induced migrating cells and NOX4 in focal adhesions and invadopodia, both structures that are associated with the leading edge in migrating cells [213, 227, 277, 278]. Although the ROS produced by NOX enzymes is O_2^- , this is very unstable and so will rapidly convert to H_2O_2 either spontaneously or by the action of enzymes such as SOD [206, 329]. Interestingly, SOD has also been found localised at specific regions of the membrane in VEGF stimulated cells but the colocalisation of SOD and NOX enzymes has yet to be shown [262]. In further support of this hypothesis is the fact that cells at wound margins in zebrafish larvae and *Drosophila* embryos produce H_2O_2 to attract leukocytes and hemocytes respectively to wounds, which is dependent on DUOX, a member of the NOX family of proteins [264, 265]. Nevertheless a direct involvement of NOX in the production of H_2O_2 at the leading edge of migrating cells remains to be confirmed by the use of NOX inhibitors or the knockdown of NOX in cells.

7.2 Protein oxidation and cell migration

Global protein oxidation has previously been shown to be increased in human umbilical vein endothelial cells (HUVEC) stimulated with VEGF, a growth factor that is known to induce the migration of endothelial cells [278]. This study also reported that a population of oxidised proteins was located at the leading edge in migrating cells in the presence of VEGF. However, the results I have presented are the first directly demonstrating that protein oxidation is increased in migrating cells (Figure 4-4). Due to observations by myself and others that ROS are required for cell migration, it is likely that the oxidation of some of these proteins alters their activity in order to aid migration. In addition to showing that there was a population of oxidised proteins at the leading edge in migrating cells, Kaplan et al. also highlighted that this population colocalised with F-actin [278]. I therefore hypothesised that some of the proteins oxidised in migrating cells would be involved in remodelling the actin cytoskeleton at the leading edge where it is undergoing constant dynamic changes.

With this in mind, I started to speculate about which proteins could be targets of the H_2O_2 produced in migrating cells. One attractive candidate was the actin binding protein cofilin, which is known to be enriched at the leading edge of migrating cells and has previously been reported to be oxidised in T cells treated with H_2O_2 and in cells undergoing apoptosis induced by the oxidant taurine chloramine (TnCl) [94, 137, 153]. With the use of the chemical probe dimedone, I established that cofilin is oxidised in cells under normal resting conditions and the level of oxidation is increased during migration (Figures 4-5 and 4-6). This is the first report of cofilin oxidation in cells under physiological conditions (resting state and during migration) rather than following treatment with oxidants. The only proteins previously identified to be oxidised and to contribute to cell migration were the protein tyrosine phosphatases PTP1B, DEP1, PTP-PEST and LMW-PTP [262, 276, 290, 291]. These were all shown to be oxidised following the activation of signalling pathways that induce and contribute to cell migration. In addition to these, the scaffolding protein IQGAP1 is oxidised following stimulation of cells with VEGF, however whether this has a role in VEGF-induced migration is still unclear [278]. Therefore, my results are the first to detect the oxidation of a specific protein in migrating cells, and provide a direct link

between increased ROS levels at the leading edge and the dynamic changes in the actin cytoskeleton that take place here.

7.3 Cofilin oxidation and actin dynamics

Having established that cofilin was oxidised in migrating cells, I wanted to determine if this altered its activity to aid cell migration. As a starting point, I tested the effect of cofilin oxidation on actin dynamics *in vitro* using a pyrene conjugated actin depolymerisation assay which revealed that the oxidation of cofilin inhibited it from severing or depolymerising actin filaments to reduce F-actin levels (Figure 5-4). This is consistent with data published from another group who also reported that the oxidation of recombinant cofilin reduced its ability to decrease F-actin levels *in vitro* [137]. During the process of confirming that the recombinant cofilin was oxidised, I discovered that cofilin oxidation resulted in the formation of cofilin oligomers (Figure 5-13). A previous study also demonstrated, based on results using cross linking agents, a natural tendency of cofilin to form oligomers [135]. However, the data I have presented confirms this using a physiologically relevant source of oxidation and cross linking through disulphide bonds. Pfannstiel et al., also show that cofilin monomers and oligomers have different activities when it comes to regulating actin structures. While monomers sever and depolymerise F-actin, oligomers induce actin bundling [135]. This difference in the activities of monomers and oligomers could explain the results I obtained in the actin depolymerisation assay. The inhibition in the ability of cofilin to reduce F-actin levels as the concentration of H₂O₂ was increased could be due to a reduction in monomers acting to depolymerise the F-actin and an increase in oligomers promoting the bundling of F-actin. However, if this were the case, I would have expected at the highest concentration of H₂O₂ (10 mM), where virtually all of the cofilin was present as oligomers, that F-actin would be predominantly bundled with negligible amounts of depolymerisation, leading to an increase in pyrene actin fluorescence. An alternative explanation is that the cofilin monomers depolymerise and sever F-actin while the oligomers cannot bind to F-actin at all or they bind to F-actin but do not depolymerise or sever it. There is conflicting evidence supporting both sides of this hypothesis. One *in vitro* study reported that oxidised cofilin retains its actin binding activity while a different cell culture study demonstrated that cofilin loses its affinity for actin when oxidised under conditions of oxidative

stress [94, 137]. However, the *in vitro* experiments I completed with the cofilin cysteine to alanine mutants provides further insight into this apparently conflicting data and will be addressed later.

As the present literature published on cofilin oxidation is not in agreement about which cysteine residues in cofilin are oxidised and potentially involved in intramolecular and intermolecular disulphide bonds, I undertook experiments to answer these discrepancies. For this purpose, I created cofilin mutants in which one or two of the cysteine residues in cofilin were mutated to alanine and therefore could not be oxidised and tested their abilities to reduce F-actin levels and form oligomers. From these experiments, I concluded that cysteine residues 139 and 147, but predominantly 147, are oxidised and responsible for the inhibition of cofilin activity in the F-actin depolymerisation assay and the oligomerisation of cofilin (Figures 5-7, 5-9, 5-10, 5-11, 5-12, 5-14 and 5-15). Previous studies that had implicated cofilin oxidation in the induction of cell death and T-cell hyporesponsiveness suggested an intramolecular disulphide bond forms between cysteine residues 39 and 80 and is required for these cellular functions [94, 137]. My findings do not exclude a cysteine 39 to 80 intramolecular disulphide bond as a possibility, but if it does form it is not involved in inhibiting cofilin from reducing F-actin levels or forming oligomers. One of these studies also proposed a cysteine 139 to 147 intramolecular disulphide bond forms but based on the 3D structure of cofilin this would be unlikely [70, 94, 327]. Another *in vitro* study suggested cofilin oligomers form through intermolecular disulphide bonds between cysteine 39 and 147 [135]. Again my data do not disagree with this possibility as the C39/147A cofilin mutant was able to rescue the inhibition of cofilin activity seen with oxidised WT cofilin and partially prevent oligomerisation (Figures 5-9 and 5-15). It also confirmed my conclusion that cysteine 147 is one of the cysteine residues oxidised and responsible for the oligomerisation and inhibition of cofilin activity when WT cofilin is oxidised. However, my results suggest that cysteine 139 is the second residue that is sensitive to oxidation and contributes to the formation of oligomers and the inhibition of cofilin activity when WT cofilin is oxidised.

My conclusion that cofilin cysteine residues 139 and 147 are the most sensitive to oxidation is also feasible based on the position of these two residues compared to cysteines 39 and 80 in the 3D structure of cofilin [70, 327] (Figure 5-5). As

cysteine residues 39 and 80 appear to be tucked away in a small pocket within cofilin, it makes sense that these residues would be less accessible to oxidants and therefore less likely to be oxidised. Also based on their proximity to each other, if one did become oxidised it is possible that they would form an intramolecular disulphide bond with each other, as has previously been suggested, rather than partaking in an intermolecular disulphide bond. In contrast, cysteine residues 139 and 147 are externally positioned and exposed on the surface of cofilin and therefore easily accessible to cellular oxidants and well placed to be involved in the formation of intermolecular disulphide bonds.

Consulting a model of cofilin interacting with actin provides further information about how the oxidation of cysteines 139 and 147 could prevent cofilin from severing and depolymerising F-actin (Figure 7-1). The model was created based on the crystal structure of the C147A cofilin mutant and the crystallised complex of G-actin and the C-terminal domain of twinfilin [70, 330]. This model predicts that cysteine residues 139 and 147 lie at the interface between cofilin and actin. Therefore, if these residues were involved in forming a disulphide bond with another cofilin molecule, or any other thiol containing molecule e.g. glutathione, actin binding would be blocked. However, what would happen if the cysteine residues were oxidised to the sulfinic or sulfonic acid states rather than forming intermolecular disulphide bonds? Charges and radii of each of the atoms of reduced and oxidised cofilin and actin were calculated using PDB2PQR with the exception of the oxidised cysteine residues which were calculated using a developmental version of PRODRG [331, 332]. This modelling proposes that the radii of cysteines 139 and 147 oxidised to the sulfinic acid state are much greater than the reduced cysteine residues. Therefore oxidation of cysteine residues 139 and 147 to sulfinic or sulfonic acids could sterically interfere with the actin binding interface due to an increase in size. This seems particularly relevant for cysteine 139 (the upper residue) which sits much closer to actin at the interface. In addition to this, based on the electrostatic surface potential of actin and the reduced and oxidised cofilin which were calculated using APBS, there could be an electrostatic interference between actin and oxidised cofilin [333]. Electrostatic surface potential mapping suggests that actin has a very negatively charged area around the site that interacts with the cofilin cysteine 147 residue (the lower residue). In addition to this, as the cysteine residues are

oxidised to sulfinic and sulfonic acids, the whole area immediately around them becomes more negatively charged. Therefore, as cofilin is oxidised there could be repulsive forces acting to disrupt the cofilin actin interaction, particularly around cysteine 147.

My data clearly demonstrate that the cysteine residues on cofilin that are sensitive to oxidation and responsible for the formation of oligomers and the inhibition of cofilin severing and depolymerising activity *in vitro* are cysteines 139 and 147. Based on modelling of the interaction between cofilin and actin, I hypothesise that the oxidation of cofilin on these residues prevents it from binding to F-actin and severing or depolymerising it. This could be due to electrostatic or steric interference if sulfinic or sulfonic acids are the product of cofilin oxidation. Alternatively cofilin oxidation could result in its oligomerisation, which has not been observed in cells but has been suggested could occur in regions of high cofilin oxidation, or the formation of intermolecular disulphide bonds with other thiol containing molecules such as glutathione, which has been observed in cells [135, 136]. In this situation the cofilin actin interface would be completely blocked preventing cofilin binding to and severing or depolymerising F-actin. However, to confirm this hypothesis actin binding studies *in vitro* and in cell culture with WT and the cysteine to alanine cofilin mutants would need to be carried out.

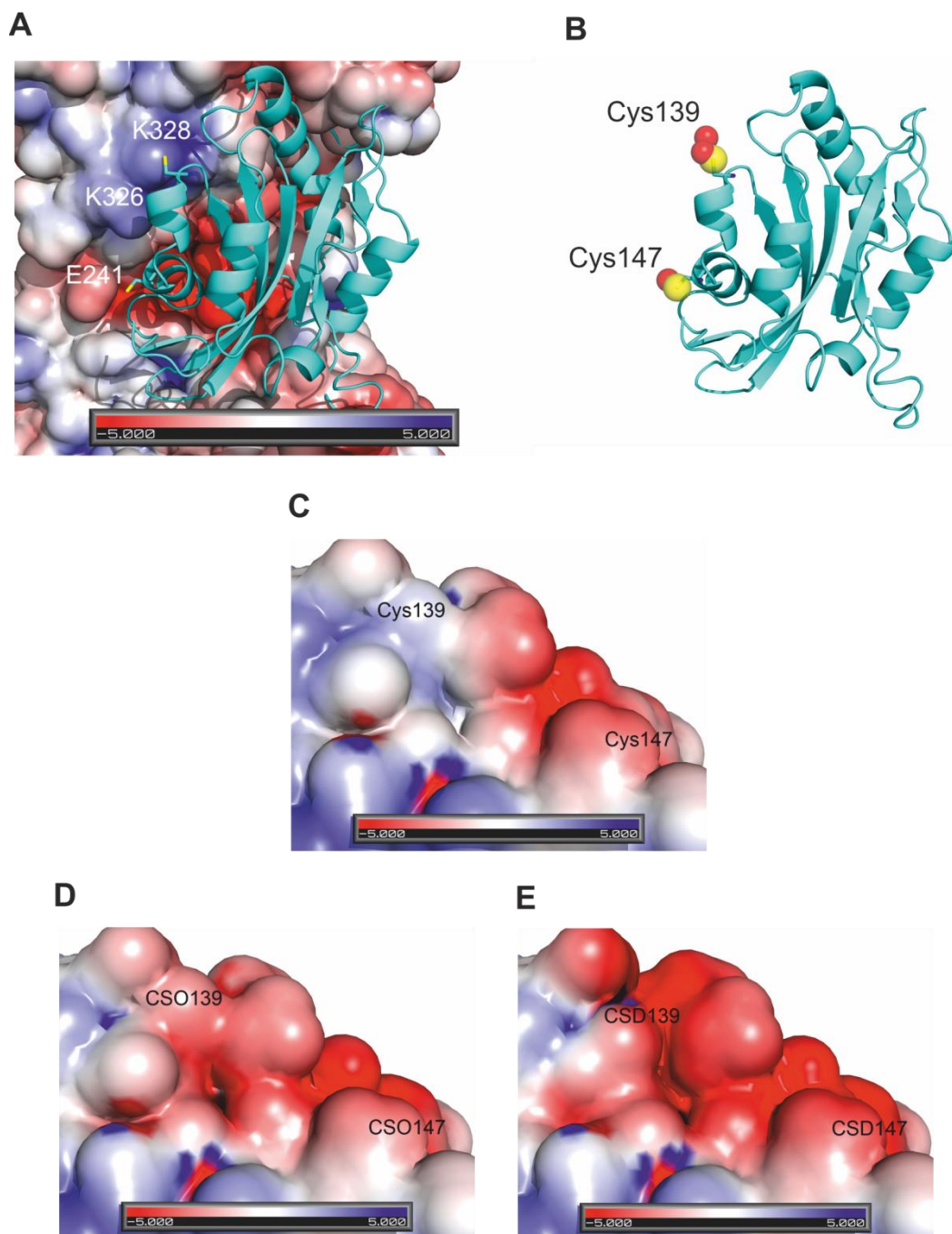


Figure 7-1 Modelling of the interaction between oxidised cofilin and actin

Model based on crystal structure of the C147A cofilin mutant and the crystallised complex of G-actin with the C-terminal domain of twinfilin [70, 330]. Charges and radii of each of the atoms of reduced and oxidised cofilin and actin were calculated using PDB2PQR with the exception of the oxidised cysteine residues which were calculated using a developmental version of PRODRG [331, 332]. Electrostatic surface potentials were calculated using APBS [333]. Figures were created in PyMOL. A) Actin, represented as an electrostatic surface potential map, interacting with cofilin, shown in cyan. Sulphur atoms of cysteine 139 (upper residue) and 147 (lower residue) residues shown in yellow. B) Model showing increased radii of cysteine residues when oxidised. Sulphur atoms shown in yellow and oxygen atoms shown in red. Cofilin in same position and orientation as in A). C) – E) Electrostatic surface potential maps of areas around cysteine residues 139 and 147 when reduced (C) or in sulfenic (D) or sulfinic (E) acid states. Figure courtesy of Mads Gabrielsen.

7.4 Cofilin oxidation and cell migration and invasion

Cofilin is well known to be required for cell migration both under normal circumstances and in the context of cancer [65, 161-163, 190]. Since I have demonstrated that H₂O₂ levels are increased in migrating cells particularly at the leading edge, cofilin oxidation is increased in migrating cells and the oxidation of cofilin inhibits its ability to reduce F-actin levels, I next wanted to determine if the oxidation of cofilin was involved in regulating its activity with respect to cell migration. For this reason I expressed either WT or C139/147A mutant cofilin in cells and measured their ability to migrate. I found that in both cases cell migration was impaired (Figure 6-3). This is not surprising as the overexpression of cofilin has previously been shown to disrupt the actin cytoskeleton at the leading edge and to decrease migration [189]. Although the C139/147A cofilin could not be regulated by oxidation it would still be subject to regulation by other mechanisms such as phosphorylation and therefore largely act as normal.

As there are many factors, for example protrusion development and cell adhesion, that contribute to the overall migration of cells it was decided to interrogate if cofilin oxidation contributed specifically to some of these factors. An involvement of cofilin oxidation in particular aspects of cell migration might not be detected in an assay that just measures overall migration such as the one used previously since, as explained in the introduction, cells have a remarkable ability to switch migration modes so that migration is not prevented. As cofilin has been implicated in the directional migration of cells and in determining the direction of lamellipod growth, it was decided to investigate if cofilin oxidation was required for establishing cell directionality [155, 156]. By tracking the movement of individual WT and C139/147A cofilin expressing cells migrating randomly on a 2D surface it was discovered that the C139/147A cofilin cells moved in a less directional manner than the WT cofilin or control cells (Figure 6-4). It has been reported that cofilin is required for the directional migration of carcinoma cells towards EGF, and EGF has also been shown to induce the production of ROS in cells [156, 245]. Combining this information with the data I have presented indicating that cofilin oxidation contributes to directional migration, it is reasonable to hypothesise that EGF induces an increase in ROS in

cells, this oxidises cofilin which contributes to the directional migration towards the source of EGF.

However in what way does cofilin oxidation actually contribute to directional cell migration? The extension of membrane protrusions, such as lamellipodia, is the first step that must occur in order for cells to migrate. Cofilin has been shown to be required for the development of lamellipodia and particularly for the initial production of actin barbed ends that initiate protrusion growth and sets the direction of cell movement [147, 148, 155, 156]. The continued activity of cofilin has also been suggested to be necessary to maintain the supplies of G-actin and barbed ends needed for the growth of the lamellipodia [151-154]. I hypothesise that while cofilin activity is required for the events I have described, the inhibition of cofilin nearer the front of the lamellipodia and directly at the leading edge would prevent it severing and depolymerising actin filaments enabling more efficient actin polymerisation, lamellipod growth and cell migration. The oxidation of cofilin by H_2O_2 at the leading edge of cells migrating at a wound edge or in response to a chemoattractant, such as EGF, could provide the local inhibition of cofilin activity required for this to occur. The localised control of cofilin activity has already been demonstrated to occur in invadopodia where cofilin is inactivated around the edge of invadopodia by phosphorylation through a RhoC activated pathway but remains unphosphorylated and active in the core of the invadopodia [158]. Therefore it is not inconceivable that cofilin activity is also tightly controlled and restricted to specific regions in cell protrusions by oxidation.

Another aspect of cell migration that I investigated to establish whether it required cofilin oxidation was cell adhesion. I determined that the C139/147A cofilin expressing cells had reduced adhesion compared to WT cofilin and control cells (Figure 6-6). The assembly of nascent adhesions is known to require actin polymerisation and is proportional to the rate of lamellipodial protrusion [57, 334]. Therefore, the reduced level of adhesion I observed could also be explained by the hypothesis I proposed above. If cofilin oxidation is required to allow efficient actin polymerisation and growth of cell protrusions, preventing its oxidation could inhibit the extension of protrusions at the same time as impairing the assembly of nascent adhesions. However reports have also been published suggesting that cofilin is involved in endocytosis and receptor

trafficking and so the reduced adhesion could be the result of a defect in the recycling or transport of adhesion receptors and components of focal adhesions [171, 335]. Additional research would be required to explore this preliminary hypothesis, firstly to establish if cofilin was involved in such cellular processes and then if this was influenced by cofilin oxidation.

After finding that cells expressing C139/147A cofilin had impaired directionality and adhesion, I anticipated that they might also have an altered ability to invade into a 3D matrix since these two factors are involved in invasion and cofilin has been implicated in cell invasion [56, 189, 190]. However, results from the invasion assays I carried out indicated that there was no difference in the invasion of WT or C139/147A cofilin expressing cells compared to control cells (Figure 6-7). As in the migration experiments, it is possible that differences would only be seen if investigating individual aspects of cell invasion such as invadopodia stability or matrix degradation. In addition, carrying out an invasion assay in which cells are fully embedded in matrix rather than just overlaid might also reveal a requirement for cofilin oxidation in cell invasion. So although initial experiments suggest cofilin oxidation is not required for cell invasion, I believe further investigation into particular aspects of cell invasion such as those discussed above would be important to fully explore this possibility.

7.5 Final conclusions

In conclusion I have shown that the ROS, H_2O_2 , is found at elevated levels in migrating cells and in particular is localised to the tips of cell protrusions. Additionally, I demonstrated that protein oxidation is increased in migrating cells and identified one of these oxidised proteins as the actin binding protein cofilin. From *in vitro* experiments I determined that the oxidation of cofilin results in its oligomerisation and inhibits its ability to reduce F-actin levels, which is dependent on cofilin cysteine residues 139 and 147. Furthermore, the oxidation of cofilin in cells is important for migration to determine directionality and for adhesion.

I therefore propose that H_2O_2 levels are increased at the leading edge of cells whether through the activation of NOX enzymes by growth factors, cytokines or adhesion receptor pathways or by H_2O_2 acting directly as a chemoattractant. As

a result, cofilin is oxidised in this region of the cell preventing it from binding to and severing or depolymerising F-actin, enhancing actin polymerisation near the front of the protrusion and promoting protrusion growth. Meanwhile cofilin further back from the front of the protrusion can remain active, supplying G-actin and barbed ends required to fuel the continued growth of the protrusion. This localised control of cofilin activity would therefore allow cell protrusions to develop as quickly and efficiently as possible to facilitate cell migration (Figure 7-2).

ROS are known to enhance cancer progression in particular by promoting migration, invasion and metastasis. Additionally EGF signalling, which has been shown to positively correlate with the metastatic potential of cancer cells has also been reported to induce intracellular ROS production. As these cellular processes have been demonstrated to depend on cofilin, the mechanism I have proposed where the local inhibition of cofilin by oxidation contributes to cell migration could be utilised by cancer cells to enhance migration, invasion and metastasis. Although much more work is required to fully understand how cofilin oxidation is involved in directional cell migration and whether it contributes to invasion and metastasis, such studies could potentially highlight new ways to target this stage of cancer progression and other diseases in which cofilin has been implicated. Furthermore, I believe this work highlights the importance of studying how the oxidation of specific proteins can regulate cellular processes. At present this is an area that is very poorly understood but has the potential to reveal new ways of treating a number of human diseases.

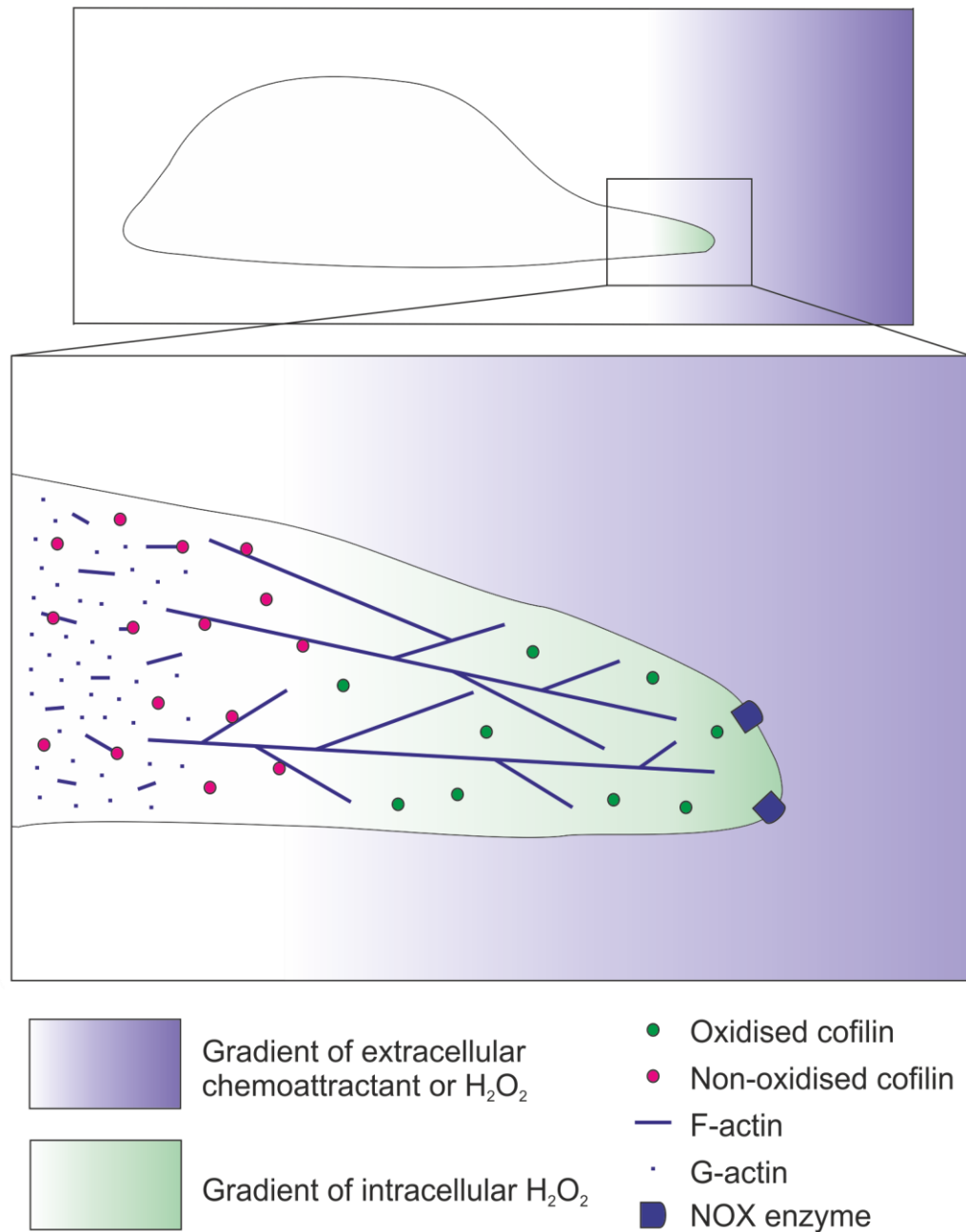


Figure 7-2 Proposed model for the involvement of cofilin oxidation in cell migration

H_2O_2 acting directly as a chemoattractant or produced by activated NOX enzymes in response to chemoattractants, such as EGF, oxidises cofilin at the leading edge of cells. Consequently cofilin is prevented from binding to and severing or depolymerising F-actin, enhancing actin polymerisation. Meanwhile cofilin further back from the front of the protrusion remains active, supplying G-actin and barbed ends required to fuel the continued growth of the protrusion. This localised control of cofilin activity therefore facilitates cell migration by allowing protrusions to develop as quickly and efficiently as possible.

References

1. Hanahan, D. and R.A. Weinberg, *The hallmarks of cancer*. Cell, 2000. **100**(1): p. 57-70.
2. Hanahan, D. and R.A. Weinberg, *Hallmarks of cancer: the next generation*. Cell, 2011. **144**(5): p. 646-74.
3. Yang, J. and R.A. Weinberg, *Epithelial-mesenchymal transition: at the crossroads of development and tumor metastasis*. Dev Cell, 2008. **14**(6): p. 818-29.
4. Gupta, G.P. and J. Massague, *Cancer metastasis: building a framework*. Cell, 2006. **127**(4): p. 679-95.
5. Keller, R., *Cell migration during gastrulation*. Curr Opin Cell Biol, 2005. **17**(5): p. 533-41.
6. Farooqui, R. and G. Fenteany, *Multiple rows of cells behind an epithelial wound edge extend cryptic lamellipodia to collectively drive cell-sheet movement*. J Cell Sci, 2005. **118**(Pt 1): p. 51-63.
7. Muller, W.A., *Mechanisms of transendothelial migration of leukocytes*. Circ Res, 2009. **105**(3): p. 223-30.
8. Woollard, K.J., *Immunological aspects of atherosclerosis*. Clin Sci (Lond), 2013. **125**(5): p. 221-35.
9. Alexander, S., G.E. Koehl, M. Hirschberg, E.K. Geissler, and P. Friedl, *Dynamic imaging of cancer growth and invasion: a modified skin-fold chamber model*. Histochem Cell Biol, 2008. **130**(6): p. 1147-54.
10. Friedl, P., *Prespecification and plasticity: shifting mechanisms of cell migration*. Curr Opin Cell Biol, 2004. **16**(1): p. 14-23.
11. Friedl, P. and K. Wolf, *Plasticity of cell migration: a multiscale tuning model*. J Cell Biol, 2010. **188**(1): p. 11-9.
12. Sahai, E., *Illuminating the metastatic process*. Nat Rev Cancer, 2007. **7**(10): p. 737-749.
13. Friedl, P., S. Borgmann, and E.B. Brocker, *Amoeboid leukocyte crawling through extracellular matrix: lessons from the Dictyostelium paradigm of cell movement*. J Leukoc Biol, 2001. **70**(4): p. 491-509.
14. Kuriyama, S. and R. Mayor, *Molecular analysis of neural crest migration*. Philos Trans R Soc Lond B Biol Sci, 2008. **363**(1495): p. 1349-62.
15. Pankova, K., D. Rosel, M. Novotny, and J. Brabek, *The molecular mechanisms of transition between mesenchymal and amoeboid invasiveness in tumor cells*. Cell Mol Life Sci, 2010. **67**(1): p. 63-71.

16. Friedl, P., F. Entschladen, C. Conrad, B. Niggemann, and K.S. Zanker, *CD4⁺ T lymphocytes migrating in three-dimensional collagen lattices lack focal adhesions and utilize B1 integrin-independent strategies for polarization, interaction with collagen fibers and locomotion*. Eur J Immunol, 1998. **28**(8): p. 2331-43.
17. Sahai, E. and C.J. Marshall, *Differing modes of tumour cell invasion have distinct requirements for Rho/ROCK signalling and extracellular proteolysis*. Nat Cell Biol, 2003. **5**(8): p. 711-9.
18. Friedl, P., P.B. Noble, E.D. Shields, and K.S. Zanker, *Locomotor phenotypes of unstimulated CD45RA^{high} and CD45RO^{high} CD4⁺ and CD8⁺ lymphocytes in three-dimensional collagen lattices*. Immunology, 1994. **82**(4): p. 617-24.
19. Mandeville, J.T., M.A. Lawson, and F.R. Maxfield, *Dynamic imaging of neutrophil migration in three dimensions: mechanical interactions between cells and matrix*. J Leukoc Biol, 1997. **61**(2): p. 188-200.
20. Friedl, P., K.S. Zanker, and E.B. Brocker, *Cell migration strategies in 3-D extracellular matrix: differences in morphology, cell matrix interactions, and integrin function*. Microsc Res Tech, 1998. **43**(5): p. 369-78.
21. Geisbrecht, E.R. and D.J. Montell, *Myosin VI is required for E-cadherin-mediated border cell migration*. Nat Cell Biol, 2002. **4**(8): p. 616-20.
22. Ghysen, A. and C. Dambly-Chaudiere, *Development of the zebrafish lateral line*. Curr Opin Neurobiol, 2004. **14**(1): p. 67-73.
23. Nabeshima, K., T. Inoue, Y. Shimao, Y. Okada, Y. Itoh, M. Seiki, and M. Koono, *Front-Cell-specific Expression of Membrane-Type 1 Matrix Metalloproteinase and Gelatinase A during Cohort Migration of Colon Carcinoma Cells Induced by Hepatocyte Growth Factor/Scatter Factor*. Cancer Res, 2000. **60**(13): p. 3364-3369.
24. Friedl, P. and D. Gilmour, *Collective cell migration in morphogenesis, regeneration and cancer*. Nat Rev Mol Cell Biol, 2009. **10**(7): p. 445-457.
25. Ganz, A., M. Lambert, A. Saez, P. Silberzan, A. Buguin, R.M. Mège, and B. Ladoux, *Traction forces exerted through N-cadherin contacts*. Biology of the Cell, 2006. **98**(12): p. 721-730.
26. Hegerfeldt, Y., M. Tusch, E.-B. Bröcker, and P. Friedl, *Collective Cell Movement in Primary Melanoma Explants: Plasticity of Cell-Cell Interaction, B1-Integrin Function, and Migration Strategies*. Cancer Res, 2002. **62**(7): p. 2125-2130.
27. Kraus, A.C., I. Ferber, S.O. Bachmann, H. Specht, A. Wimmel, M.W. Gross, J. Schlegel, G. Suske, and M. Schuermann, *In vitro chemo- and radio-resistance in small cell lung cancer correlates with cell adhesion and constitutive activation of AKT and MAP kinase pathways*. Oncogene, 2002. **21**(57): p. 8683-95.

28. Davies, J.A., *Mesenchyme to epithelium transition during development of the mammalian kidney tubule*. Acta Anat (Basel), 1996. **156**(3): p. 187-201.
29. Sanz-Moreno, V., G. Gadea, J. Ahn, H. Paterson, P. Marra, S. Pinner, E. Sahai, and C.J. Marshall, *Rac activation and inactivation control plasticity of tumor cell movement*. Cell, 2008. **135**(3): p. 510-23.
30. Wolf, K., I. Mazo, H. Leung, K. Engelke, U.H. von Andrian, E.I. Deryugina, A.Y. Strongin, E.B. Brocker, and P. Friedl, *Compensation mechanism in tumor cell migration: mesenchymal-amoeboid transition after blocking of pericellular proteolysis*. J Cell Biol, 2003. **160**(2): p. 267-77.
31. Daryab, N., J. Moeller, C. Brakebusch, J. Eble, E.-B. Brocker, and P. Friedl, *Plasticity of tumor invasion: Mesenchymal-amoeboid transition in melanoma cells after blocking of B1 integrins*. AACR Meeting Abstracts, 2004. **2004**(1): p. 1133-d-1134.
32. Carragher, N.O., S.M. Walker, L.A. Scott Carragher, F. Harris, T.K. Sawyer, V.G. Brunton, B.W. Ozanne, and M.C. Frame, *Calpain 2 and Src dependence distinguishes mesenchymal and amoeboid modes of tumour cell invasion: a link to integrin function*. Oncogene, 2006. **25**(42): p. 5726-40.
33. Olson, M.F. and E. Sahai, *The actin cytoskeleton in cancer cell motility*. Clin Exp Metastasis, 2009. **26**(4): p. 273-87.
34. Le Clainche, C. and M.F. Carlier, *Regulation of actin assembly associated with protrusion and adhesion in cell migration*. Physiol Rev, 2008. **88**(2): p. 489-513.
35. Insall, R.H. and L.M. Machesky, *Actin dynamics at the leading edge: from simple machinery to complex networks*. Dev Cell, 2009. **17**(3): p. 310-22.
36. Lai, F.P., M. Szczodrak, J. Block, J. Faix, D. Breitsprecher, H.G. Mannherz, T.E. Stradal, G.A. Dunn, J.V. Small, and K. Rottner, *Arp2/3 complex interactions and actin network turnover in lamellipodia*. EMBO J, 2008. **27**(7): p. 982-92.
37. Yamaguchi, H., M. Lorenz, S. Kempiak, C. Sarmiento, S. Coniglio, M. Symons, J. Segall, R. Eddy, H. Miki, T. Takenawa, and J. Condeelis, *Molecular mechanisms of invadopodium formation: the role of the N-WASP-Arp2/3 complex pathway and cofilin*. J Cell Biol, 2005. **168**(3): p. 441-52.
38. Johnston, S.A., J.P. Bramble, C.L. Yeung, P.M. Mendes, and L.M. Machesky, *Arp2/3 complex activity in filopodia of spreading cells*. BMC Cell Biol, 2008. **9**: p. 65.
39. Chesarone, M.A., A.G. DuPage, and B.L. Goode, *Unleashing formins to remodel the actin and microtubule cytoskeletons*. Nat Rev Mol Cell Biol, 2010. **11**(1): p. 62-74.

40. Tominaga, T., E. Sahai, P. Chardin, F. McCormick, S.A. Courtneidge, and A.S. Alberts, *Diaphanous-related formins bridge Rho GTPase and Src tyrosine kinase signaling*. Mol Cell, 2000. **5**(1): p. 13-25.
41. Schirenbeck, A., T. Bretschneider, R. Arasada, M. Schleicher, and J. Faix, *The Diaphanous-related formin dDia2 is required for the formation and maintenance of filopodia*. Nat Cell Biol, 2005. **7**(6): p. 619-25.
42. Lizarraga, F., R. Poincloux, M. Romao, G. Montagnac, G. Le Dez, I. Bonne, G. Rigaille, G. Raposo, and P. Chavrier, *Diaphanous-related formins are required for invadopodia formation and invasion of breast tumor cells*. Cancer Res, 2009. **69**(7): p. 2792-800.
43. Yang, C., L. Czech, S. Gerboth, S. Kojima, G. Scita, and T. Svitkina, *Novel roles of formin mDia2 in lamellipodia and filopodia formation in motile cells*. PLoS Biol, 2007. **5**(11): p. e317.
44. Rottner, K., B. Behrendt, J.V. Small, and J. Wehland, *VASP dynamics during lamellipodia protrusion*. Nat Cell Biol, 1999. **1**(5): p. 321-2.
45. Krause, M., E.W. Dent, J.E. Bear, J.J. Loureiro, and F.B. Gertler, *Ena/VASP proteins: regulators of the actin cytoskeleton and cell migration*. Annu Rev Cell Dev Biol, 2003. **19**: p. 541-64.
46. Lebrand, C., E.W. Dent, G.A. Strasser, L.M. Lanier, M. Krause, T.M. Svitkina, G.G. Borisy, and F.B. Gertler, *Critical role of Ena/VASP proteins for filopodia formation in neurons and in function downstream of netrin-1*. Neuron, 2004. **42**(1): p. 37-49.
47. Quinlan, M.E., J.E. Heuser, E. Kerkhoff, and R.D. Mullins, *Drosophila Spire is an actin nucleation factor*. Nature, 2005. **433**(7024): p. 382-8.
48. Machesky, L.M. and A. Li, *Fascin: Invasive filopodia promoting metastasis*. Commun Integr Biol, 2010. **3**(3): p. 263-70.
49. van Rheenen, J., J. Condeelis, and M. Glogauer, *A common cofilin activity cycle in invasive tumor cells and inflammatory cells*. J Cell Sci, 2009. **122**(Pt 3): p. 305-11.
50. Oser, M. and J. Condeelis, *The cofilin activity cycle in lamellipodia and invadopodia*. J Cell Biochem, 2009. **108**(6): p. 1252-62.
51. Bryce, N.S., E.S. Clark, J.L. Leysath, J.D. Currie, D.J. Webb, and A.M. Weaver, *Cortactin promotes cell motility by enhancing lamellipodial persistence*. Curr Biol, 2005. **15**(14): p. 1276-85.
52. Clark, E.S., A.S. Whigham, W.G. Yarbrough, and A.M. Weaver, *Cortactin is an essential regulator of matrix metalloproteinase secretion and extracellular matrix degradation in invadopodia*. Cancer Res, 2007. **67**(9): p. 4227-35.
53. MacGrath, S.M. and A.J. Koleske, *Cortactin in cell migration and cancer at a glance*. J Cell Sci, 2012. **125**(7): p. 1621-1626.

54. Yarmola, E.G. and M.R. Bubb, *Profilin: emerging concepts and lingering misconceptions*. Trends Biochem Sci, 2006. **31**(4): p. 197-205.
55. Ridley, A.J., *Life at the leading edge*. Cell, 2011. **145**(7): p. 1012-22.
56. Wang, W., S. Goswami, K. Lapidus, A.L. Wells, J.B. Wyckoff, E. Sahai, R.H. Singer, J.E. Segall, and J.S. Condeelis, *Identification and testing of a gene expression signature of invasive carcinoma cells within primary mammary tumors*. Cancer Res, 2004. **64**(23): p. 8585-94.
57. Parsons, J.T., A.R. Horwitz, and M.A. Schwartz, *Cell adhesion: integrating cytoskeletal dynamics and cellular tension*. Nat Rev Mol Cell Biol, 2010. **11**(9): p. 633-643.
58. Lappalainen, P., M.M. Kessels, M.J.T.V. Cope, and D.G. Drubin, *The ADF Homology (ADF-H) Domain: A Highly Exploited Actin-binding Module*. Mol Biol Cell, 1998. **9**(8): p. 1951-1959.
59. Van Troys, M., L. Huyck, S. Leyman, S. Dhaese, J. Vandekerckhove, and C. Ampe, *Ins and outs of ADF/cofilin activity and regulation*. Eur J Cell Biol, 2008. **87**(8-9): p. 649-667.
60. Bamburg, J.R., *PROTEINS OF THE ADF/COFILIN FAMILY: Essential Regulators of Actin Dynamics*. Annu Rev Cell Dev Biol, 1999. **15**(1): p. 185-230.
61. Mohri, K., H. Takano-Ohmuro, K. Nakashima, K. Hayakawa, T. Endo, K. Hanaoka, and T. Obinata, *Expression of cofilin isoforms during development of mouse striated muscles*. Journal of Muscle Research & Cell Motility, 2000. **21**(1): p. 49-57.
62. Vartiainen, M.K., T. Mustonen, P.K. Mattila, P.J. Ojala, I. Thesleff, J. Partanen, and P. Lappalainen, *The Three Mouse Actin-depolymerizing Factor/Cofilins Evolved to Fulfill Cell-Type-specific Requirements for Actin Dynamics*. Mol Biol Cell, 2002. **13**(1): p. 183-194.
63. Hotulainen, P., E. Paunola, M.K. Vartiainen, and P. Lappalainen, *Actin-depolymerizing Factor and Cofilin-1 Play Overlapping Roles in Promoting Rapid F-Actin Depolymerization in Mammalian Nonmuscle Cells*. Mol Biol Cell, 2005. **16**(2): p. 649-664.
64. Kazuko, I., M. Kenji, M. Seiji, K. Hiroshi, N. Eisuke, and Y. Ichiro, *Isolation of a yeast essential gene, COF1, that encodes a homologue of mammalian cofilin, a low-M_r actin-binding and depolymerizing protein*. Gene, 1993. **124**(1): p. 115-120.
65. Gurniak, C.B., E. Perlas, and W. Witke, *The actin depolymerizing factor n-cofilin is essential for neural tube morphogenesis and neural crest cell migration*. Dev Biol, 2005. **278**(1): p. 231-241.
66. Ikeda, S., L.A. Cunningham, D. Boggess, C.D. Hobson, J.P. Sundberg, J.K. Naggert, R.S. Smith, and P.M. Nishina, *Aberrant actin cytoskeleton leads to accelerated proliferation of corneal epithelial cells in mice deficient*

- for destrin (actin depolymerizing factor)*. Human Molecular Genetics, 2003. **12**(9): p. 1029-1036.
67. Nakashima, K., N. Sato, T. Nakagaki, H. Abe, S. Ono, and T. Obinata, *Two Mouse Cofilin Isoforms, Muscle-Type (MCF) and Non-Muscle Type (NMCF), Interact with F-Actin with Different Efficiencies*. Journal of Biochemistry, 2005. **138**(4): p. 519-526.
 68. Nishida, E., S. Maekawa, and H. Sakai, *Cofilin, a protein in porcine brain that binds to actin filaments and inhibits their interactions with myosin and tropomyosin*. Biochemistry, 1984. **23**(22): p. 5307-5313.
 69. Lappalainen, P., E.V. Fedorov, A.A. Fedorov, S.C. Almo, and D.G. Drubin, *Essential functions and actin-binding surfaces of yeast cofilin revealed by systematic mutagenesis*. EMBO J, 1997. **16**(18): p. 5520-5530.
 70. Klejnot, M., M. Gabrielsen, J. Cameron, A. Mleczak, S.K. Talapatra, F. Kozielski, A. Pannifer, and M.F. Olson, *Analysis of the human cofilin 1 structure reveals conformational changes required for actin binding*. Acta Crystallographica Section D, 2013. **69**(9): p. 1780-1788.
 71. McGough, A., B. Pope, W. Chiu, and A. Weeds, *Cofilin Changes the Twist of F-Actin: Implications for Actin Filament Dynamics and Cellular Function*. J Cell Biol, 1997. **138**(4): p. 771-781.
 72. Yeoh, S., B. Pope, H.G. Mannherz, and A. Weeds, *Determining the differences in actin binding by human ADF and cofilin*. Journal of Molecular Biology, 2002. **315**(4): p. 911-925.
 73. Michelot, A., J. Berro, C. Guérin, R. Boujemaa-Paterski, C.J. Staiger, J.-L. Martiel, and L. Blanchoin, *Actin-Filament Stochastic Dynamics Mediated by ADF/Cofilin*. Current Biology, 2007. **17**(10): p. 825-833.
 74. Tsuda, Y., H. Yasutake, A. Ishijima, and T. Yanagida, *Torsional rigidity of single actin filaments and actin-actin bond breaking force under torsion measured directly by in vitro micromanipulation*. Proceedings of the National Academy of Sciences, 1996. **93**(23): p. 12937-12942.
 75. Maciver, S.K., *How ADF/cofilin depolymerizes actin filaments*. Curr Opin Cell Biol, 1998. **10**(1): p. 140-144.
 76. McGough, A. and W. Chiu, *ADF/Cofilin weakens lateral contacts in the actin filament*. Journal of Molecular Biology, 1999. **291**(3): p. 513-519.
 77. Bobkov, A.A., A. Muhlrads, D.A. Pavlov, K. Kokabi, A. Yilmaz, and E. Reisler, *Cooperative Effects of Cofilin (ADF) on Actin Structure Suggest Allosteric Mechanism of Cofilin Function*. Journal of Molecular Biology, 2006. **356**(2): p. 325-334.
 78. McCullough, Brannon R., Elena E. Grintsevich, Christine K. Chen, H. Kang, Alan L. Hutchison, A. Henn, W. Cao, C. Suarez, J.-L. Martiel, L. Blanchoin, E. Reisler, and E.M. De La Cruz, *Cofilin-Linked Changes in Actin Filament*

- Flexibility Promote Severing*. Biophysical Journal, 2011. **101**(1): p. 151-159.
79. Suarez, C., J. Roland, R. Boujemaa-Paterski, H. Kang, Brannon R. McCullough, A.-C. Reymann, C. Guérin, J.-L. Martiel, Enrique M. De La Cruz, and L. Blanchoin, *Cofilin Tunes the Nucleotide State of Actin Filaments and Severs at Bare and Decorated Segment Boundaries*. Current Biology, 2011. **21**(10): p. 862-868.
 80. Carlier, M.-F., V. Laurent, J. Santolini, R. Melki, D. Didry, G.-X. Xia, Y. Hong, N.-H. Chua, and D. Pantaloni, *Actin Depolymerizing Factor (ADF/Cofilin) Enhances the Rate of Filament Turnover: Implication in Actin-based Motility*. J Cell Biol, 1997. **136**(6): p. 1307-1322.
 81. Blanchoin, L. and T.D. Pollard, *Mechanism of Interaction of Acanthamoeba Actophorin (ADF/Cofilin) with Actin Filaments*. Journal of Biological Chemistry, 1999. **274**(22): p. 15538-15546.
 82. Nishida, E., *Opposite effects of cofilin and profilin from porcine brain on rate of exchange of actin-bound adenosine 5'-triphosphate*. Biochemistry, 1985. **24**(5): p. 1160-1164.
 83. Minamide, L.S., S. Maiti, J.A. Boyle, R.C. Davis, J.A. Coppinger, Y. Bao, T.Y. Huang, J. Yates, G.M. Bokoch, and J.R. Bamburg, *Isolation and Characterization of Cytoplasmic Cofilin-Actin Rods*. Journal of Biological Chemistry, 2010. **285**(8): p. 5450-5460.
 84. Minamide, L.S., A.M. Striegl, J.A. Boyle, P.J. Meberg, and J.R. Bamburg, *Neurodegenerative stimuli induce persistent ADF/cofilin-actin rods that disrupt distal neurite function*. Nat Cell Biol, 2000. **2**(9): p. 628-636.
 85. Chan, C., C.C. Beltzner, and T.D. Pollard, *Cofilin Dissociates Arp2/3 Complex and Branches from Actin Filaments*. Current Biology, 2009. **19**(7): p. 537-545.
 86. Andrianantoandro, E. and T.D. Pollard, *Mechanism of Actin Filament Turnover by Severing and Nucleation at Different Concentrations of ADF/Cofilin*. Mol Cell, 2006. **24**(1): p. 13-23.
 87. Zheng, B., M. Han, M. Bernier, and J.-k. Wen, *Nuclear actin and actin-binding proteins in the regulation of transcription and gene expression*. FEBS Journal, 2009. **276**(10): p. 2669-2685.
 88. Iida, K., S. Matsumoto, and I. Yahara, *The KKRKK Sequence is Involved in Heat Shock-Induced Nuclear Translocation of the 18-kDa Actin-Binding Protein, Cofilin*. Cell Structure and Function, 1992. **17**(1): p. 39-46.
 89. Pendleton, A., B. Pope, A. Weeds, and A. Koffer, *Latrunculin B or ATP Depletion Induces Cofilin-dependent Translocation of Actin into Nuclei of Mast Cells*. Journal of Biological Chemistry, 2003. **278**(16): p. 14394-14400.

90. Obrdlik, A. and P. Percipalle, *The F-actin severing protein cofilin-1 is required for RNA polymerase II transcription elongation*. Nucleus, 2011. 2(1): p. 72-79.
91. Wabnitz, G.H., C. Goursot, B. Jahraus, H. Kirchgessner, A. Hellwig, M. Klemke, M.H. Konstandin, and Y. Samstag, *Mitochondrial translocation of oxidized cofilin induces caspase-independent necrotic-like programmed cell death of T cells*. Cell Death and Dis, 2010. 1: p. e58.
92. Hsieh, Y.-C., Y.K. Rao, C.-C. Wu, C.-Y.F. Huang, M. Geethangili, S.-L. Hsu, and Y.-M. Tzeng, *Methyl Antcinate A from Antrodia camphorata Induces Apoptosis in Human Liver Cancer Cells through Oxidant-Mediated Cofilin- and Bax-Triggered Mitochondrial Pathway*. Chem Res Toxicol, 2010. 23(7): p. 1256-1267.
93. Chua, B.T., C. Volbracht, K.O. Tan, R. Li, V.C. Yu, and P. Li, *Mitochondrial translocation of cofilin is an early step in apoptosis induction*. Nat Cell Biol, 2003. 5(12): p. 1083-1089.
94. Klamt, F., S. Zdanov, R.L. Levine, A. Pariser, Y. Zhang, B. Zhang, L.-R. Yu, T.D. Veenstra, and E. Shacter, *Oxidant-induced apoptosis is mediated by oxidation of the actin-regulatory protein cofilin*. Nat Cell Biol, 2009. 11(10): p. 1241-1246.
95. Han, L., M.B. Stope, M.L. de Jesus, P.A. Oude Weernink, M. Urban, T. Wieland, D. Roskopf, K. Mizuno, K.H. Jakobs, and M. Schmidt, *Direct stimulation of receptor-controlled phospholipase D1 by phospho-cofilin*. EMBO J, 2007. 26(19): p. 4189-4202.
96. Ktistakis, N.T., C. Delon, M. Manifava, E. Wood, I. Ganley, and J.M. Sugars, *Phospholipase D1 and potential targets of its hydrolysis product, phosphatidic acid*. Biochem Soc Trans, 2003. 31(Pt 1): p. 94-7.
97. Exton, J.H., *Phospholipase D—Structure, regulation and function*, in *Reviews of Physiology, Biochemistry and Pharmacology*. 2002, Springer Berlin Heidelberg. p. 1-94.
98. Moriyama, K., K. Iida, and I. Yahara, *Phosphorylation of Ser-3 of cofilin regulates its essential function on actin*. Genes to Cells, 1996. 1(1): p. 73-86.
99. Wriggers, W., J.X. Tang, T. Azuma, P.W. Marks, and P.A. Janmey, *Cofilin and gelsolin segment-1: molecular dynamics simulation and biochemical analysis predict a similar actin binding mode*. Journal of Molecular Biology, 1998. 282(5): p. 921-932.
100. Pope, B.J., K.M. Zierler-Gould, R. Kühne, A.G. Weeds, and L.J. Ball, *Solution Structure of Human Cofilin: ACTIN BINDING, pH SENSITIVITY, AND RELATIONSHIP TO ACTIN-DEPOLYMERIZING FACTOR*. Journal of Biological Chemistry, 2004. 279(6): p. 4840-4848.
101. Arber, S., F.A. Barbayannis, H. Hanser, C. Schneider, C.A. Stanyon, O. Bernard, and P. Caroni, *Regulation of actin dynamics through*

- phosphorylation of cofilin by LIM-kinase*. Nature, 1998. **393**(6687): p. 805-809.
102. Yang, N., O. Higuchi, K. Ohashi, K. Nagata, A. Wada, K. Kangawa, E. Nishida, and K. Mizuno, *Cofilin phosphorylation by LIM-kinase 1 and its role in Rac-mediated actin reorganization*. Nature, 1998. **393**(6687): p. 809-812.
 103. Sumi, T., K. Matsumoto, Y. Takai, and T. Nakamura, *Cofilin Phosphorylation and Actin Cytoskeletal Dynamics Regulated by Rho- and Cdc42-Activated Lim-Kinase 2*. J Cell Biol, 1999. **147**(7): p. 1519-1532.
 104. Toshima, J., J.Y. Toshima, T. Amano, N. Yang, S. Narumiya, and K. Mizuno, *Cofilin Phosphorylation by Protein Kinase Testicular Protein Kinase 1 and Its Role in Integrin-mediated Actin Reorganization and Focal Adhesion Formation*. Mol Biol Cell, 2001. **12**(4): p. 1131-1145.
 105. Toshima, J., J.Y. Toshima, K. Takeuchi, R. Mori, and K. Mizuno, *Cofilin Phosphorylation and Actin Reorganization Activities of Testicular Protein Kinase 2 and Its Predominant Expression in Testicular Sertoli Cells*. Journal of Biological Chemistry, 2001. **276**(33): p. 31449-31458.
 106. Nakano, K., M. Kanai-Azuma, Y. Kanai, K. Moriyama, K. Yazaki, Y. Hayashi, and N. Kitamura, *Cofilin phosphorylation and actin polymerization by NRK/NESK, a member of the germinal center kinase family*. Exp Cell Res, 2003. **287**(2): p. 219-227.
 107. Ohashi, K., K. Nagata, M. Maekawa, T. Ishizaki, S. Narumiya, and K. Mizuno, *Rho-associated Kinase ROCK Activates LIM-kinase 1 by Phosphorylation at Threonine 508 within the Activation Loop*. Journal of Biological Chemistry, 2000. **275**(5): p. 3577-3582.
 108. Sumi, T., K. Matsumoto, and T. Nakamura, *Specific Activation of LIM kinase 2 via Phosphorylation of Threonine 505 by ROCK, a Rho-dependent Protein Kinase*. Journal of Biological Chemistry, 2001. **276**(1): p. 670-676.
 109. Sumi, T., K. Matsumoto, A. Shibuya, and T. Nakamura, *Activation of LIM Kinases by Myotonic Dystrophy Kinase-related Cdc42-binding Kinase a*. Journal of Biological Chemistry, 2001. **276**(25): p. 23092-23096.
 110. Edwards, D.C., L.C. Sanders, G.M. Bokoch, and G.N. Gill, *Activation of LIM-kinase by Pak1 couples Rac/Cdc42 GTPase signalling to actin cytoskeletal dynamics*. Nat Cell Biol, 1999. **1**(5): p. 253-259.
 111. Dan, C., A. Kelly, O. Bernard, and A. Minden, *Cytoskeletal Changes Regulated by the PAK4 Serine/Threonine Kinase Are Mediated by LIM Kinase 1 and Cofilin*. Journal of Biological Chemistry, 2001. **276**(34): p. 32115-32121.
 112. Leisner, T.M., M. Liu, Z.M. Jaffer, J. Chernoff, and L.V. Parise, *Essential role of CIB1 in regulating PAK1 activation and cell migration*. J Cell Biol, 2005. **170**(3): p. 465-476.

113. Kobayashi, M., M. Nishita, T. Mishima, K. Ohashi, and K. Mizuno, *MAPKAPK-2-mediated LIM-kinase activation is critical for VEGF-induced actin remodeling and cell migration*. EMBO J, 2006. **25**(4): p. 713-726.
114. Soosairajah, J., S. Maiti, O.N. Wiggan, P. Sarmiere, N. Moussi, B. Sarcevic, R. Sampath, J.R. Bamburg, and O. Bernard, *Interplay between components of a novel LIM kinase-slingshot phosphatase complex regulates cofilin*. EMBO J, 2005. **24**(3): p. 473-486.
115. LaLonde, D.P., M.C. Brown, B.P. Bouverat, and C.E. Turner, *Actopaxin Interacts with TESK1 to Regulate Cell Spreading on Fibronectin*. Journal of Biological Chemistry, 2005. **280**(22): p. 21680-21688.
116. Toshima, J.Y., J. Toshima, T. Watanabe, and K. Mizuno, *Binding of 14-3-3 β Regulates the Kinase Activity and Subcellular Localization of Testicular Protein Kinase 1*. Journal of Biological Chemistry, 2001. **276**(46): p. 43471-43481.
117. Johne, C., D. Matenia, X.-y. Li, T. Timm, K. Balusamy, and E.-M. Mandelkow, *Spred1 and TESK1—Two New Interaction Partners of the Kinase MARKK/TAO1 That Link the Microtubule and Actin Cytoskeleton*. Mol Biol Cell, 2008. **19**(4): p. 1391-1403.
118. Tsumura, Y., J. Toshima, O.C. Leeksa, K. Ohashi, and K. Mizuno, *Sprouty-4 negatively regulates cell spreading by inhibiting the kinase activity of testicular protein kinase*. Biochem. J., 2005. **387**(3): p. 627-637.
119. Niwa, R., K. Nagata-Ohashi, M. Takeichi, K. Mizuno, and T. Uemura, *Control of Actin Reorganization by Slingshot, a Family of Phosphatases that Dephosphorylate ADF/Cofilin*. Cell, 2002. **108**(2): p. 233-246.
120. Gohla, A., J. Birkenfeld, and G.M. Bokoch, *Chronophin, a novel HAD-type serine protein phosphatase, regulates cofilin-dependent actin dynamics*. Nat Cell Biol, 2005. **7**(1): p. 21-29.
121. Oleinik, N.V., N.I. Krupenko, and S.A. Krupenko, *ALDH1L1 inhibits cell motility via dephosphorylation of cofilin by PP1 and PP2A*. Oncogene, 2010. **29**(47): p. 6233-6244.
122. Nagata-Ohashi, K., Y. Ohta, K. Goto, S. Chiba, R. Mori, M. Nishita, K. Ohashi, K. Kousaka, A. Iwamatsu, R. Niwa, T. Uemura, and K. Mizuno, *A pathway of neuregulin-induced activation of cofilin-phosphatase Slingshot and cofilin in lamellipodia*. J Cell Biol, 2004. **165**(4): p. 465-71.
123. Wang, Y., F. Shibasaki, and K. Mizuno, *Calcium Signal-induced Cofilin Dephosphorylation Is Mediated by Slingshot via Calcineurin*. Journal of Biological Chemistry, 2005. **280**(13): p. 12683-12689.
124. Eiseler, T., H. Doppler, I.K. Yan, K. Kitatani, K. Mizuno, and P. Storz, *Protein kinase D1 regulates cofilin-mediated F-actin reorganization and cell motility through slingshot*. Nat Cell Biol, 2009. **11**(5): p. 545-556.

125. Kim, J.S., T.Y. Huang, and G.M. Bokoch, *Reactive oxygen species regulate a slingshot-cofilin activation pathway*. *Mol Biol Cell*, 2009. **20**(11): p. 2650-60.
126. Huang, T.Y., L.S. Minamide, J.R. Bamburg, and G.M. Bokoch, *Chronophin Mediates an ATP-Sensing Mechanism for Cofilin Dephosphorylation and Neuronal Cofilin-Actin Rod Formation*. *Dev Cell*, 2008. **15**(5): p. 691-703.
127. Yonezawa, N., Y. Homma, I. Yahara, H. Sakai, and E. Nishida, *A short sequence responsible for both phosphoinositide binding and actin binding activities of cofilin*. *Journal of Biological Chemistry*, 1991. **266**(26): p. 17218-17221.
128. Gorbatyuk, V.Y., N.J. Nosworthy, S.A. Robson, N.P.S. Bains, M.W. Maciejewski, C.G. dos Remedios, and G.F. King, *Mapping the Phosphoinositide-Binding Site on Chick Cofilin Explains How PIP₂ Regulates the Cofilin-Actin Interaction*. *Mol Cell*, 2006. **24**(4): p. 511-522.
129. Van Troys, M., D. Dewitte, J.-L. Verschelde, M. Goethals, J. Vandekerckhove, and C. Ampe, *The Competitive Interaction of Actin and PIP₂ with Actophorin Is Based on Overlapping Target Sites: Design of a Gain-of-Function Mutant*. *Biochemistry*, 2000. **39**(40): p. 12181-12189.
130. van Rheenen, J., X. Song, W. van Roosmalen, M. Cammer, X. Chen, V. DesMarais, S.-C. Yip, J.M. Backer, R.J. Eddy, and J.S. Condeelis, *EGF-induced PIP₂ hydrolysis releases and activates cofilin locally in carcinoma cells*. *J Cell Biol*, 2007. **179**(6): p. 1247-1259.
131. Leyman, S., M. Sidani, L. Ritsma, D. Waterschoot, R. Eddy, D. Dewitte, O. Debeir, C. Decaestecker, J. Vandekerckhove, J. van Rheenen, C. Ampe, J. Condeelis, and M. Van Troys, *Unbalancing the Phosphatidylinositol-4,5-bisphosphate-Cofilin Interaction Impairs Cell Steering*. *Mol Biol Cell*, 2009. **20**(21): p. 4509-4523.
132. Bernstein, B.W., W.B. Painter, H. Chen, L.S. Minamide, H. Abe, and J.R. Bamburg, *Intracellular pH modulation of ADF/cofilin proteins*. *Cell Motility and the Cytoskeleton*, 2000. **47**(4): p. 319-336.
133. Yonezawa, N., E. Nishida, and H. Sakai, *pH control of actin polymerization by cofilin*. *Journal of Biological Chemistry*, 1985. **260**(27): p. 14410-14412.
134. Frantz, C., G. Barreiro, L. Dominguez, X. Chen, R. Eddy, J. Condeelis, M.J.S. Kelly, M.P. Jacobson, and D.L. Barber, *Cofilin is a pH sensor for actin free barbed end formation: role of phosphoinositide binding*. *J Cell Biol*, 2008. **183**(5): p. 865-879.
135. Pfannstiel, J., M. Cyrklaff, A. Habermann, S. Stoeva, G. Griffiths, R. Shoeman, and H. Faulstich, *Human Cofilin Forms Oligomers Exhibiting Actin Bundling Activity*. *Journal of Biological Chemistry*, 2001. **276**(52): p. 49476-49484.

136. Fratelli, M., H. Demol, M. Puype, S. Casagrande, I. Eberini, M. Salmona, V. Bonetto, M. Mengozzi, F. Duffieux, E. Miclet, A. Bachi, J. Vandekerckhove, E. Gianazza, and P. Ghezzi, *Identification by redox proteomics of glutathionylated proteins in oxidatively stressed human T lymphocytes*. Proc Natl Acad Sci U S A, 2002. **99**(6): p. 3505-10.
137. Klemke, M., G.H. Wabnitz, F. Funke, B. Funk, H. Kirchgessner, and Y. Samstag, *Oxidation of Cofilin Mediates T Cell Hyporesponsiveness under Oxidative Stress Conditions*. Immunity, 2008. **29**(3): p. 404-413.
138. Gunning, P.W., G. Schevzov, A.J. Kee, and E.C. Hardeman, *Tropomyosin isoforms: divining rods for actin cytoskeleton function*. Trends in Cell Biology, 2005. **15**(6): p. 333-341.
139. Ono, S. and K. Ono, *Tropomyosin inhibits ADF/cofilin-dependent actin filament dynamics*. J Cell Biol, 2002. **156**(6): p. 1065-1076.
140. Bryce, N.S., G. Schevzov, V. Ferguson, J.M. Percival, J.J.-C. Lin, F. Matsumura, J.R. Bamburg, P.L. Jeffrey, E.C. Hardeman, P. Gunning, and R.P. Weinberger, *Specification of Actin Filament Function and Molecular Composition by Tropomyosin Isoforms*. Mol Biol Cell, 2003. **14**(3): p. 1002-1016.
141. Rodal, A.A., J.W. Tetreault, P. Lappalainen, D.G. Drubin, and D.C. Amberg, *Aip1p Interacts with Cofilin to Disassemble Actin Filaments*. J Cell Biol, 1999. **145**(6): p. 1251-1264.
142. Okada, K., L. Blanchoin, H. Abe, H. Chen, T.D. Pollard, and J.R. Bamburg, *Xenopus Actin-interacting Protein 1 (XAip1) Enhances Cofilin Fragmentation of Filaments by Capping Filament Ends*. Journal of Biological Chemistry, 2002. **277**(45): p. 43011-43016.
143. Moriyama, K. and I. Yahara, *Human CAP1 is a key factor in the recycling of cofilin and actin for rapid actin turnover*. J Cell Sci, 2002. **115**(8): p. 1591-1601.
144. Balcer, H.I., A.L. Goodman, A.A. Rodal, E. Smith, J. Kugler, J.E. Heuser, and B.L. Goode, *Coordinated Regulation of Actin Filament Turnover by a High-Molecular-Weight Srv2/CAP Complex, Cofilin, Profilin, and Aip1*. Current Biology, 2003. **13**(24): p. 2159-2169.
145. Gandhi, M., V. Achard, L. Blanchoin, and B.L. Goode, *Coronin Switches Roles in Actin Disassembly Depending on the Nucleotide State of Actin*. Mol Cell, 2009. **34**(3): p. 364-374.
146. Oser, M., H. Yamaguchi, C.C. Mader, J.J. Bravo-Cordero, M. Arias, X. Chen, V. DesMarais, J. van Rheenen, A.J. Koleske, and J. Condeelis, *Cortactin regulates cofilin and N-WASp activities to control the stages of invadopodium assembly and maturation*. J Cell Biol, 2009. **186**(4): p. 571-587.
147. Zebda, N., O. Bernard, M. Bailly, S. Welte, D.S. Lawrence, and J.S. Condeelis, *Phosphorylation of Adf/Cofilin Abolishes Egf-Induced Actin*

- Nucleation at the Leading Edge and Subsequent Lamellipod Extension.* J Cell Biol, 2000. **151**(5): p. 1119-1128.
148. Dawe, H.R., L.S. Minamide, J.R. Bamburg, and L.P. Cramer, *ADF/Cofilin Controls Cell Polarity during Fibroblast Migration.* Current Biology, 2003. **13**(3): p. 252-257.
 149. Svitkina, T.M. and G.G. Borisy, *Arp2/3 Complex and Actin Depolymerizing Factor/Cofilin in Dendritic Organization and Treadmilling of Actin Filament Array in Lamellipodia.* J Cell Biol, 1999. **145**(5): p. 1009-1026.
 150. Pantaloni, D., C.L. Clainche, and M.-F. Carlier, *Mechanism of Actin-Based Motility.* Science, 2001. **292**(5521): p. 1502-1506.
 151. Kiuchi, T., K. Ohashi, S. Kurita, and K. Mizuno, *Cofilin promotes stimulus-induced lamellipodium formation by generating an abundant supply of actin monomers.* J Cell Biol, 2007. **177**(3): p. 465-476.
 152. Vitriol, E.A., A.L. Wise, M.E. Berginski, J.R. Bamburg, and J.Q. Zheng, *Instantaneous inactivation of cofilin reveals its function of F-actin disassembly in lamellipodia.* Mol Biol Cell, 2013. **24**(14): p. 2238-2247.
 153. Chan, A.Y., M. Bailly, N. Zebda, J.E. Segall, and J.S. Condeelis, *Role of Cofilin in Epidermal Growth Factor-Stimulated Actin Polymerization and Lamellipod Protrusion.* J Cell Biol, 2000. **148**(3): p. 531-542.
 154. Ghosh, M., X. Song, G. Mouneimne, M. Sidani, D.S. Lawrence, and J.S. Condeelis, *Cofilin Promotes Actin Polymerization and Defines the Direction of Cell Motility.* Science, 2004. **304**(5671): p. 743-746.
 155. DesMarais, V., F. Macaluso, J. Condeelis, and M. Bailly, *Synergistic interaction between the Arp2/3 complex and cofilin drives stimulated lamellipod extension.* J Cell Sci, 2004. **117**(16): p. 3499-3510.
 156. Mouneimne, G., L. Soon, V. DesMarais, M. Sidani, X. Song, S.-C. Yip, M. Ghosh, R. Eddy, J.M. Backer, and J. Condeelis, *Phospholipase C and cofilin are required for carcinoma cell directionality in response to EGF stimulation.* J Cell Biol, 2004. **166**(5): p. 697-708.
 157. DesMarais, V., M. Ghosh, R. Eddy, and J. Condeelis, *Cofilin takes the lead.* J Cell Sci, 2005. **118**(1): p. 19-26.
 158. Bravo-Cordero, Jose J., M. Oser, X. Chen, R. Eddy, L. Hodgson, and J. Condeelis, *A Novel Spatiotemporal RhoC Activation Pathway Locally Regulates Cofilin Activity at Invadopodia.* Current Biology, 2011. **21**(8): p. 635-644.
 159. Magalhaes, M.A.O., D.R. Larson, C.C. Mader, J.J. Bravo-Cordero, H. Gil-Henn, M. Oser, X. Chen, A.J. Koleske, and J. Condeelis, *Cortactin phosphorylation regulates cell invasion through a pH-dependent pathway.* J Cell Biol, 2011. **195**(5): p. 903-920.

160. Loisel, T.P., R. Boujemaa, D. Pantaloni, and M.-F. Carrier, *Reconstitution of actin-based motility of Listeria and Shigella using pure proteins*. Nature, 1999. **401**(6753): p. 613-616.
161. Hirayama, A., R. Adachi, S. Otani, T. Kasahara, and K. Suzuki, *Cofilin plays a critical role in IL-8-dependent chemotaxis of neutrophilic HL-60 cells through changes in phosphorylation*. J Leukoc Biol, 2007. **81**(3): p. 720-728.
162. Klemke, M., E. Kramer, M.H. Konstandin, G.H. Wabnitz, and Y. Samstag, *An MEK-cofilin signalling module controls migration of human T cells in 3D but not 2D environments*. EMBO J, 2010. **29**(17): p. 2915-2929.
163. Jönsson, F., C.B. Gurniak, B. Fleischer, G. Kirfel, and W. Witke, *Immunological Responses and Actin Dynamics in Macrophages Are Controlled by N-Cofilin but Are Independent from ADF*. PLoS One, 2012. **7**(4): p. e36034.
164. Bernstein, B.W. and J.R. Bamburg, *ADF/cofilin: a functional node in cell biology*. Trends Cell Biol, 2010. **20**(4): p. 187-95.
165. Nakano, K. and I. Mabuchi, *Actin-depolymerizing Protein Adf1 Is Required for Formation and Maintenance of the Contractile Ring during Cytokinesis in Fission Yeast*. Mol Biol Cell, 2006. **17**(4): p. 1933-1945.
166. Gunsalus, K.C., S. Bonaccorsi, E. Williams, F. Verni, M. Gatti, and M.L. Goldberg, *Mutations in twinstar, a Drosophila gene encoding a cofilin/ADF homologue, result in defects in centrosome migration and cytokinesis*. J Cell Biol, 1995. **131**(5): p. 1243-1259.
167. Ono, K., M. Parast, C. Alberico, G.M. Benian, and S. Ono, *Specific requirement for two ADF/cofilin isoforms in distinct actin-dependent processes in Caenorhabditis elegans*. J Cell Sci, 2003. **116**(10): p. 2073-2085.
168. Abe, H., T. Obinata, L.S. Minamide, and J.R. Bamburg, *Xenopus laevis actin-depolymerizing factor/cofilin: a phosphorylation-regulated protein essential for development*. J Cell Biol, 1996. **132**(5): p. 871-885.
169. Nagaoka, R., H. Abe, K.-I. Kusano, and T. Obinata, *Concentration of cofilin, a small actin-binding protein, at the cleavage furrow during cytokinesis*. Cell Motility and the Cytoskeleton, 1995. **30**(1): p. 1-7.
170. Chen, Q. and T.D. Pollard, *Actin filament severing by cofilin is more important for assembly than constriction of the cytokinetic contractile ring*. J Cell Biol, 2011. **195**(3): p. 485-98.
171. Okreglak, V. and D.G. Drubin, *Cofilin recruitment and function during actin-mediated endocytosis dictated by actin nucleotide state*. J Cell Biol, 2007. **178**(7): p. 1251-1264.
172. Samstag, Y., C. Eckerskorn, S. Wesselborg, S. Henning, R. Wallich, and S.C. Meuer, *Costimulatory signals for human T-cell activation induce*

nuclear translocation of pp19/cofilin. Proceedings of the National Academy of Sciences, 1994. **91**(10): p. 4494-4498.

173. Lee, K.-H., S.C. Meuer, and Y. Samstag, *Cofilin: a missing link between T cell co-stimulation and rearrangement of the actin cytoskeleton*. Eur J Immunol, 2000. **30**(3): p. 892-899.
174. Eibert, S.M., K.-H. Lee, R. Pipkorn, U. Sester, G.H. Wabnitz, T. Giese, S.C. Meuer, and Y. Samstag, *Cofilin peptide homologs interfere with immunological synapse formation and T cell activation*. Proc Natl Acad Sci U S A, 2004. **101**(7): p. 1957-1962.
175. Figge, C., G. Loers, M. Schachner, and T. Tilling, *Neurite outgrowth triggered by the cell adhesion molecule L1 requires activation and inactivation of the cytoskeletal protein cofilin*. Molecular and Cellular Neuroscience, 2012. **49**(2): p. 196-204.
176. Sparrow, N., M.E. Manetti, M. Bott, T. Fabianac, A. Petrilli, M.L. Bates, M.B. Bunge, S. Lambert, and C. Fernandez-Valle, *The Actin-Severing Protein Cofilin Is Downstream of Neuregulin Signaling and Is Essential For Schwann Cell Myelination*. The Journal of Neuroscience, 2012. **32**(15): p. 5284-5297.
177. Gunnensen, J.M., V. Spirkoska, P.E. Smith, R.A. Danks, and S.-S. Tan, *Growth and migration markers of rat C6 glioma cells identified by serial analysis of gene expression*. Glia, 2000. **32**(2): p. 146-154.
178. Keshamouni, V.G., G. Michailidis, C.S. Grasso, S. Anthwal, J.R. Strahler, A. Walker, D.A. Arenberg, R.C. Reddy, S. Akulapalli, V.J. Thannickal, T.J. Standiford, P.C. Andrews, and G.S. Omenn, *Differential Protein Expression Profiling by iTRAQ-2DLC-MS/MS of Lung Cancer Cells Undergoing Epithelial-Mesenchymal Transition Reveals a Migratory/Invasive Phenotype*. Journal of Proteome Research, 2006. **5**(5): p. 1143-1154.
179. Sinha, P., G. Hutter, E. Kottgen, M. Dietel, D. Schadendorf, and H. Lage, *Increased expression of epidermal fatty acid binding protein, cofilin, and 14-3-3- σ (stratifin) detected by two-dimensional gel electrophoresis, mass spectrometry and microsequencing of drug-resistant human adenocarcinoma of the pancreas*. Electrophoresis, 1999. **20**(14): p. 2952-60.
180. Ding, S.-J., Y. Li, X.-X. Shao, H. Zhou, R. Zeng, Z.-Y. Tang, and Q.-C. Xia, *Proteome analysis of hepatocellular carcinoma cell strains, MHCC97-H and MHCC97-L, with different metastasis potentials*. PROTEOMICS, 2004. **4**(4): p. 982-994.
181. Smith-Beckerman, D.M., K.W. Fung, K.E. Williams, N. Auersperg, A.K. Godwin, and A.L. Burlingame, *Proteome changes in ovarian epithelial cells derived from women with BRCA1 mutations and family histories of cancer*. Mol Cell Proteomics, 2005. **4**(2): p. 156-68.

182. Nebl, G., S.C. Meuer, and Y. Samstag, *Dephosphorylation of Serine 3 Regulates Nuclear Translocation of Cofilin*. Journal of Biological Chemistry, 1996. **271**(42): p. 26276-26280.
183. Turhani, D., K. Krapfenbauer, D. Thurnher, H. Langen, and M. Fountoulakis, *Identification of differentially expressed, tumor-associated proteins in oral squamous cell carcinoma by proteomic analysis*. Electrophoresis, 2006. **27**(7): p. 1417-1423.
184. Unwin, R.D., R.A. Craven, P. Harnden, S. Hanrahan, N. Totty, M. Knowles, I. Eardley, P.J. Selby, and R.E. Banks, *Proteomic changes in renal cancer and co-ordinate demonstration of both the glycolytic and mitochondrial aspects of the Warburg effect*. PROTEOMICS, 2003. **3**(8): p. 1620-1632.
185. Martoglio, A.M., B.D. Tom, M. Starkey, A.N. Corps, D.S. Charnock-Jones, and S.K. Smith, *Changes in tumorigenesis- and angiogenesis-related gene transcript abundance profiles in ovarian cancer detected by tailored high density cDNA arrays*. Mol Med, 2000. **6**(9): p. 750-65.
186. Davila, M., A.R. Frost, W.E. Grizzle, and R. Chakrabarti, *LIM kinase 1 is essential for the invasive growth of prostate epithelial cells: implications in prostate cancer*. J Biol Chem, 2003. **278**(38): p. 36868-75.
187. Yoshioka, K., V. Foletta, O. Bernard, and K. Itoh, *A role for LIM kinase in cancer invasion*. Proc Natl Acad Sci U S A, 2003. **100**(12): p. 7247-52.
188. Wang, W., J.B. Wyckoff, S. Goswami, Y. Wang, M. Sidani, J.E. Segall, and J.S. Condeelis, *Coordinated regulation of pathways for enhanced cell motility and chemotaxis is conserved in rat and mouse mammary tumors*. Cancer Res, 2007. **67**(8): p. 3505-11.
189. Lee, Y.J., D.J. Mazzatti, Z. Yun, and P.C. Keng, *Inhibition of invasiveness of human lung cancer cell line H1299 by over-expression of cofilin*. Cell Biol Int, 2005. **29**(11): p. 877-83.
190. Dang, D., J.R. Bamburg, and D.M. Ramos, *avβ3 integrin and cofilin modulate K1735 melanoma cell invasion*. Exp Cell Res, 2006. **312**(4): p. 468-477.
191. Wang, W., G. Mouneimne, M. Sidani, J. Wyckoff, X. Chen, A. Makris, S. Goswami, A.R. Bresnick, and J.S. Condeelis, *The activity status of cofilin is directly related to invasion, intravasation, and metastasis of mammary tumors*. J Cell Biol, 2006. **173**(3): p. 395-404.
192. Lourenco, F.C., J. Munro, J. Brown, J. Cordero, R. Stefanatos, K. Strathdee, C. Orange, S.M. Feller, O.J. Sansom, M. Vidal, G.I. Murray, and M.F. Olson, *Reduced LIMK2 expression in colorectal cancer reflects its role in limiting stem cell proliferation*. Gut, 2013.
193. Kaufmann, A., K. Khazaie, M. Wiedemuth, B. Rohdeschulz, A. Ullrich, V. Schirmacher, and R. Lichtner, *Expression of epidermal growth-factor receptor correlates with metastatic potential of 13762NF rat mammary adenocarcinoma cells*. Int J Oncol, 1994. **4**(6): p. 1149-55.

194. Lichtner, R.B., A.M. Kaufmann, A. Kittmann, B. Rohde-Schulz, J. Walter, L. Williams, A. Ullrich, V. Schirmacher, and K. Khazaie, *Ligand mediated activation of ectopic EGF receptor promotes matrix protein adhesion and lung colonization of rat mammary adenocarcinoma cells*. *Oncogene*, 1995. **10**(9): p. 1823-32.
195. Goswami, S., E. Sahai, J.B. Wyckoff, M. Cammer, D. Cox, F.J. Pixley, E.R. Stanley, J.E. Segall, and J.S. Condeelis, *Macrophages Promote the Invasion of Breast Carcinoma Cells via a Colony-Stimulating Factor-1/Epidermal Growth Factor Paracrine Loop*. *Cancer Res*, 2005. **65**(12): p. 5278-5283.
196. Stylli, S.S., A.H. Kaye, and P. Lock, *Invadopodia: At the cutting edge of tumour invasion*. *Journal of Clinical Neuroscience*, 2008. **15**(7): p. 725-737.
197. Cichon, J., C. Sun, B. Chen, M. Jiang, X.A. Chen, Y. Sun, Y. Wang, and G. Chen, *Cofilin Aggregation Blocks Intracellular Trafficking and Induces Synaptic Loss in Hippocampal Neurons*. *Journal of Biological Chemistry*, 2012. **287**(6): p. 3919-3929.
198. Davis, R., I. Marsden, M. Maloney, L. Minamide, M. Podlisny, D. Selkoe, and J. Bamberg, *Amyloid beta dimers/trimers potently induce cofilin-actin rods that are inhibited by maintaining cofilin-phosphorylation*. *Molecular Neurodegeneration*, 2011. **6**(1): p. 10.
199. Maloney, M.T., L.S. Minamide, A.W. Kinley, J.A. Boyle, and J.R. Bamberg, *B-secretase-cleaved amyloid precursor protein accumulates at actin inclusions induced in neurons by stress or amyloid B: a feedforward mechanism for Alzheimer's disease*. *J Neurosci*, 2005. **25**(49): p. 11313-21.
200. Munsie, L., N. Caron, R.S. Atwal, I. Marsden, E.J. Wild, J.R. Bamberg, S.J. Tabrizi, and R. Truant, *Mutant huntingtin causes defective actin remodeling during stress: defining a new role for transglutaminase 2 in neurodegenerative disease*. *Human Molecular Genetics*, 2011. **20**(10): p. 1937-1951.
201. Gearing, M., J.L. Juncos, V. Procaccio, C.-A. Gutekunst, E.M. Marino-Rodriguez, K.A. Gyure, S. Ono, R. Santoianni, N.S. Krawiecki, D.C. Wallace, and B.H. Wainer, *Aggregation of actin and cofilin in identical twins with juvenile-onset dystonia*. *Annals of Neurology*, 2002. **52**(4): p. 465-476.
202. Xu, Y.-L., D.-B. Wang, Q.-F. Liu, Y.-H. Chen, and Z. Yang, *Silencing of cofilin-1 gene attenuates biological behaviours of stromal cells derived from eutopic endometria of women with endometriosis*. *Human Reproduction*, 2010. **25**(10): p. 2480-2488.
203. Stolp, B., M. Reichman-Fried, L. Abraham, X. Pan, S.I. Giese, S. Hannemann, P. Goulimari, E. Raz, R. Grosse, and O.T. Fackler, *HIV-1 Nef Interferes with Host Cell Motility by Deregulation of Cofilin*. *Cell Host & Microbe*, 2009. **6**(2): p. 174-186.

204. Trushin, S.A., G.D. Bren, and A.D. Badley, *CXCR4 Tropic HIV-1 gp120 Inhibition of SDF-1 α -Induced Chemotaxis Requires Lck and is Associated with Cofilin Phosphorylation*. *Open Virol J*, 2010. 4: p. 157-62.
205. Trachootham, D., J. Alexandre, and P. Huang, *Targeting cancer cells by ROS-mediated mechanisms: a radical therapeutic approach?* *Nat Rev Drug Discov*, 2009. 8(7): p. 579-591.
206. Bedard, K. and K.-H. Krause, *The NOX Family of ROS-Generating NADPH Oxidases: Physiology and Pathophysiology*. *Physiological Reviews*, 2007. 87(1): p. 245-313.
207. Elliot, W.H. and D.C. Elliot, *Glycolysis, the citric acid cycle, and the electron transport system*, in *Biochemistry and Molecular Biology*. 2005, Oxford University Press Inc.: New York, US. p. 211-217.
208. Cadenas, E., A. Boveris, C.I. Ragan, and A.O.M. Stoppani, *Production of superoxide radicals and hydrogen peroxide by NADH-ubiquinone reductase and ubiquinol-cytochrome c reductase from beef-heart mitochondria*. *Arch Biochem Biophys*, 1977. 180(2): p. 248-257.
209. Brand, M.D., *The sites and topology of mitochondrial superoxide production*. *Exp Gerontol*, 2010. 45(7-8): p. 466-472.
210. Royer-Pokora, B., L.M. Kunkel, A.P. Monaco, S.C. Goff, P.E. Newburger, R.L. Baehner, F.S. Cole, J.T. Curnutte, and S.H. Orkin, *Cloning the gene for an inherited human disorder--chronic granulomatous disease--on the basis of its chromosomal location*. *Nature*, 1986. 322(6074): p. 32-38.
211. Teahan, C., P. Rowe, P. Parker, N. Totty, and A.W. Segal, *The X-linked chronic granulomatous disease gene codes for the β -chain of cytochrome b₂₄₅*. *Nature*, 1987. 327(6124): p. 720-1.
212. Aguirre, J. and J.D. Lambeth, *Nox enzymes from fungus to fly to fish and what they tell us about Nox function in mammals*. *Free Radical Biology and Medicine*, 2010. 49(9): p. 1342-1353.
213. Hilenski, L.L., R.E. Clempus, M.T. Quinn, J.D. Lambeth, and K.K. Griending, *Distinct Subcellular Localizations of Nox1 and Nox4 in Vascular Smooth Muscle Cells*. *Arteriosclerosis, Thrombosis, and Vascular Biology*, 2004. 24(4): p. 677-683.
214. Cheng, G. and J.D. Lambeth, *NOXO1, Regulation of Lipid Binding, Localization, and Activation of Nox1 by the Phox Homology (PX) Domain*. *Journal of Biological Chemistry*, 2004. 279(6): p. 4737-4742.
215. Bánfi, B., R.A. Clark, K. Steger, and K.-H. Krause, *Two Novel Proteins Activate Superoxide Generation by the NADPH Oxidase NOX1*. *Journal of Biological Chemistry*, 2003. 278(6): p. 3510-3513.
216. Ambasta, R.K., P. Kumar, K.K. Griending, H.H.H.W. Schmidt, R. Busse, and R.P. Brandes, *Direct Interaction of the Novel Nox Proteins with*

- p22phox* Is Required for the Formation of a Functionally Active NADPH Oxidase. *Journal of Biological Chemistry*, 2004. **279**(44): p. 45935-45941.
217. Cheng, G., B.A. Diebold, Y. Hughes, and J.D. Lambeth, *Nox1-dependent Reactive Oxygen Generation Is Regulated by Rac1*. *Journal of Biological Chemistry*, 2006. **281**(26): p. 17718-17726.
218. Miyano, K., N. Ueno, R. Takeya, and H. Sumimoto, *Direct Involvement of the Small GTPase Rac in Activation of the Superoxide-producing NADPH Oxidase Nox1*. *Journal of Biological Chemistry*, 2006. **281**(31): p. 21857-21868.
219. Borregaard, N., J.M. Heiple, E.R. Simons, and R.A. Clark, *Subcellular localization of the b-cytochrome component of the human neutrophil microbicidal oxidase: translocation during activation*. *J Cell Biol*, 1983. **97**(1): p. 52-61.
220. Groemping, Y., K. Lapouge, S.J. Smerdon, and K. Rittinger, *Molecular Basis of Phosphorylation-Induced Activation of the NADPH Oxidase*. *Cell*, 2003. **113**(3): p. 343-355.
221. Ueno, N., R. Takeya, K. Miyano, H. Kikuchi, and H. Sumimoto, *The NADPH Oxidase Nox3 Constitutively Produces Superoxide in a p22phox-dependent Manner: ITS REGULATION BY OXIDASE ORGANIZERS AND ACTIVATORS*. *Journal of Biological Chemistry*, 2005. **280**(24): p. 23328-23339.
222. Cheng, G., D. Ritsick, and J.D. Lambeth, *Nox3 Regulation by NOXO1, p47phox, and p67phox*. *Journal of Biological Chemistry*, 2004. **279**(33): p. 34250-34255.
223. Ueyama, T., M. Geiszt, and T.L. Leto, *Involvement of Rac1 in Activation of Multicomponent Nox1- and Nox3-Based NADPH Oxidases*. *Mol Cell Biol*, 2006. **26**(6): p. 2160-2174.
224. von Löhneysen, K., D. Noack, A.J. Jesaitis, M.C. Dinauer, and U.G. Knaus, *Mutational Analysis Reveals Distinct Features of the Nox4-p22phox Complex*. *Journal of Biological Chemistry*, 2008. **283**(50): p. 35273-35282.
225. Block, K., Y. Gorin, and H.E. Abboud, *Subcellular localization of Nox4 and regulation in diabetes*. *Proceedings of the National Academy of Sciences*, 2009. **106**(34): p. 14385-14390.
226. Van Buul, J.D., M. Fernandez-Borja, E.C. Anthony, and P.L. Hordijk, *Expression and localization of NOX2 and NOX4 in primary human endothelial cells*. *Antioxid Redox Signal*, 2005. **7**(3-4): p. 308-17.
227. Diaz, B., G. Shani, I. Pass, D. Anderson, M. Quintavalle, and S.A. Courtneidge, *Tks5-Dependent, Nox-Mediated Generation of Reactive Oxygen Species Is Necessary for Invadopodia Formation*. *Sci. Signal.*, 2009. **2**(88): p. ra53.

228. Martyn, K.D., L.M. Frederick, K. von Loehneysen, M.C. Dinauer, and U.G. Knaus, *Functional analysis of Nox4 reveals unique characteristics compared to other NADPH oxidases*. *Cell Signal*, 2006. **18**(1): p. 69-82.
229. Bánfi, B., G. Molnár, A. Maturana, K. Steger, B. Hegedűs, N. Demaurex, and K.-H. Krause, *A Ca²⁺-activated NADPH Oxidase in Testis, Spleen, and Lymph Nodes*. *Journal of Biological Chemistry*, 2001. **276**(40): p. 37594-37601.
230. Serrander, L., V. Jaquet, K. Bedard, O. Plastre, O. Hartley, S. Arnaudeau, N. Demaurex, W. Schlegel, and K.-H. Krause, *NOX5 is expressed at the plasma membrane and generates superoxide in response to protein kinase C activation*. *Biochimie*, 2007. **89**(9): p. 1159-1167.
231. De Deken, X., D. Wang, M.-C. Many, S. Costagliola, F. Libert, G. Vassart, J.E. Dumont, and F. Miot, *Cloning of Two Human Thyroid cDNAs Encoding New Members of the NADPH Oxidase Family*. *Journal of Biological Chemistry*, 2000. **275**(30): p. 23227-23233.
232. De Deken, X., D. Wang, J.E. Dumont, and F. Miot, *Characterization of ThOX Proteins as Components of the Thyroid H₂O₂-Generating System*. *Exp Cell Res*, 2002. **273**(2): p. 187-196.
233. Ameziane-El-Hassani, R., S. Morand, J.-L. Boucher, Y.-M. Frapart, D. Apostolou, D. Agnandji, S. Gnidehou, R. Ohayon, M.-S. Noël-Hudson, J. Francon, K. Lalaoui, A. Virion, and C. Dupuy, *Dual Oxidase-2 Has an Intrinsic Ca²⁺-dependent H₂O₂-generating Activity*. *Journal of Biological Chemistry*, 2005. **280**(34): p. 30046-30054.
234. Kukreja, R.C., H.A. Kontos, M.L. Hess, and E.F. Ellis, *PGH synthase and lipoxygenase generate superoxide in the presence of NADH or NADPH*. *Circ Res*, 1986. **59**(6): p. 612-9.
235. Belik, J., M. Jerkic, B.A.S. McIntyre, J. Pan, J. Leen, L.X. Yu, R.M. Henkelman, M. Toporsian, and M. Letarte, *Age-dependent endothelial nitric oxide synthase uncoupling in pulmonary arteries of endoglin heterozygous mice*. *American Journal of Physiology - Lung Cellular and Molecular Physiology*, 2009. **297**(6): p. L1170-L1178.
236. Konduri, G.G., I. Bakhutashvili, A. Eis, and K. Pritchard, *Oxidant stress from uncoupled nitric oxide synthase impairs vasodilation in fetal lambs with persistent pulmonary hypertension*. *American Journal of Physiology - Heart and Circulatory Physiology*, 2007. **292**(4): p. H1812-H1820.
237. Meneshian, A. and G.B. Bulkeley, *The Physiology of Endothelial Xanthine Oxidase: From Urate Catabolism to Reperfusion Injury to Inflammatory Signal Transduction*. *Microcirculation*, 2002. **9**(3): p. 161-175.
238. Matés, J.M., C. Pérez-Gómez, and I.N. De Castro, *Antioxidant enzymes and human diseases*. *Clinical Biochemistry*, 1999. **32**(8): p. 595-603.
239. Masella, R., R. Di Benedetto, R. Vari, C. Filesi, and C. Giovannini, *Novel mechanisms of natural antioxidant compounds in biological systems:*

- involvement of glutathione and glutathione-related enzymes*. The Journal of Nutritional Biochemistry, 2005. **16**(10): p. 577-586.
240. Padayatty, S.J., A. Katz, Y. Wang, P. Eck, O. Kwon, J.-H. Lee, S. Chen, C. Corpe, A. Dutta, S.K. Dutta, and M. Levine, *Vitamin C as an Antioxidant: Evaluation of Its Role in Disease Prevention*. Journal of the American College of Nutrition, 2003. **22**(1): p. 18-35.
 241. Traber, M.G. and J. Atkinson, *Vitamin E, antioxidant and nothing more*. Free Radical Biology and Medicine, 2007. **43**(1): p. 4-15.
 242. Nordberg, J. and E.S.J. Arnér, *Reactive oxygen species, antioxidants, and the mammalian thioredoxin system*. Free Radical Biology and Medicine, 2001. **31**(11): p. 1287-1312.
 243. Wood, Z.A., E. Schröder, J. Robin Harris, and L.B. Poole, *Structure, mechanism and regulation of peroxiredoxins*. Trends Biochem Sci, 2003. **28**(1): p. 32-40.
 244. Sundaresan, M., Z.X. Yu, V.J. Ferrans, K. Irani, and T. Finkel, *Requirement for generation of H₂O₂ for platelet-derived growth factor signal transduction*. Science, 1995. **270**(5234): p. 296-9.
 245. Bae, Y.S., S.W. Kang, M.S. Seo, I.C. Baines, E. Tekle, P.B. Chock, and S.G. Rhee, *Epidermal growth factor (EGF)-induced generation of hydrogen peroxide. Role in EGF receptor-mediated tyrosine phosphorylation*. J Biol Chem, 1997. **272**(1): p. 217-21.
 246. Finkel, T., *Signal transduction by reactive oxygen species*. J Cell Biol, 2011. **194**(1): p. 7-15.
 247. Turner-Ivey, B., Y. Manevich, J. Schulte, E. Kistner-Griffin, A. Jezierska-Drutel, Y. Liu, and C.A. Neumann, *Role for Prdx1 as a specific sensor in redox-regulated senescence in breast cancer*. Oncogene, 2013. **32**(45): p. 5302-5314.
 248. Yang, K.-S., S.W. Kang, H.A. Woo, S.C. Hwang, H.Z. Chae, K. Kim, and S.G. Rhee, *Inactivation of Human Peroxiredoxin I during Catalysis as the Result of the Oxidation of the Catalytic Site Cysteine to Cysteine-sulfinic Acid*. Journal of Biological Chemistry, 2002. **277**(41): p. 38029-38036.
 249. Burgoyne, J.R., M. Madhani, F. Cuello, R.L. Charles, J.P. Brennan, E. Schröder, D.D. Browning, and P. Eaton, *Cysteine Redox Sensor in PKG α Enables Oxidant-Induced Activation*. Science, 2007. **317**(5843): p. 1393-1397.
 250. Legendre, B., C. Tokarski, Y. Chang, N. De Freitas Caires, H. Lortat-Jacob, P.D. Nadai, C. Rolando, C. Duez, A. Tsicopoulos, and P. Lassalle, *The disulfide bond between cysteine 10 and cysteine 34 is required for CCL18 activity*. Cytokine, 2013. **64**(1): p. 463-70.
 251. Clavreul, N., T. Adachi, D.R. Pimental, Y. Ido, C. Schöneich, and R.A. Cohen, *S-glutathiolation by peroxynitrite of p21ras at cysteine-118*

- mediates its direct activation and downstream signaling in endothelial cells.* The FASEB Journal, 2006.
252. Sunico, C., T. Nakamura, E. Rockenstein, M. Mante, A. Adame, S. Chan, T. Newmeyer, E. Masliah, N. Nakanishi, and S. Lipton, *S-Nitrosylation of parkin as a novel regulator of p53-mediated neuronal cell death in sporadic Parkinson's disease.* Molecular Neurodegeneration, 2013. **8**(1): p. 29.
 253. Fomenko, D.E., W. Xing, B.M. Adair, D.J. Thomas, and V.N. Gladyshev, *High-Throughput Identification of Catalytic Redox-Active Cysteine Residues.* Science, 2007. **315**(5810): p. 387-389.
 254. Weerapana, E., C. Wang, G.M. Simon, F. Richter, S. Khare, M.B.D. Dillon, D.A. Bachovchin, K. Mowen, D. Baker, and B.F. Cravatt, *Quantitative reactivity profiling predicts functional cysteines in proteomes.* Nature, 2010. **468**(7325): p. 790-795.
 255. Wang, Z., M.R. Castresana, and W.H. Newman, *Reactive Oxygen and NF- κ B in VEGF-Induced Migration of Human Vascular Smooth Muscle Cells.* Biochem Biophys Res Commun, 2001. **285**(3): p. 669-674.
 256. Qian, Y., J. Luo, S.S. Leonard, G.K. Harris, L. Millecchia, D.C. Flynn, and X. Shi, *Hydrogen Peroxide Formation and Actin Filament Reorganization by Cdc42 Are Essential for Ethanol-induced in Vitro Angiogenesis.* Journal of Biological Chemistry, 2003. **278**(18): p. 16189-16197.
 257. Harfouche, R., N.A. Abdel-Malak, R.P. Brandes, A. Karsan, K. Irani, and S.N.A. Hussain, *Roles of reactive oxygen species in angiopoietin-1/tie-2 receptor signaling.* The FASEB Journal, 2005. **19**(12): p. 1728-1730.
 258. Kato, T., T. Terui, O. Iizawa, and H. Tagami, *Lucigenin-Induced Chemiluminescence in Human Neutrophils in the Process of Chemotactic Migration Measured in a Modified Boyden Chamber.* Dermatology, 1989. **179**(1): p. 113-115.
 259. Choi, M.H., I.K. Lee, G.W. Kim, B.U. Kim, Y.-H. Han, D.-Y. Yu, H.S. Park, K.Y. Kim, J.S. Lee, C. Choi, Y.S. Bae, B.I. Lee, S.G. Rhee, and S.W. Kang, *Regulation of PDGF signalling and vascular remodelling by peroxiredoxin II.* Nature, 2005. **435**(7040): p. 347-353.
 260. Kim, H.W., A. Lin, R.E. Guldborg, M. Ushio-Fukai, and T. Fukai, *Essential Role of Extracellular SOD in Reparative Neovascularization Induced by Hindlimb Ischemia.* Circ Res, 2007. **101**(4): p. 409-419.
 261. Groleau, J., S. Dussault, P. Haddad, J. Turgeon, C. Ménard, J.S. Chan, and A. Rivard, *Essential Role of Copper-Zinc Superoxide Dismutase for Ischemia-Induced Neovascularization Via Modulation of Bone Marrow-Derived Endothelial Progenitor Cells.* Arteriosclerosis, Thrombosis, and Vascular Biology, 2010. **30**(11): p. 2173-2181.
 262. Oshikawa, J., N. Urao, H.W. Kim, N. Kaplan, M. Razvi, R. McKinney, L.B. Poole, T. Fukai, and M. Ushio-Fukai, *Extracellular SOD-Derived H₂O₂*

- Promotes VEGF Signaling in Caveolae/Lipid Rafts and Post-Ischemic Angiogenesis in Mice.* PLoS One, 2010. **5**(4): p. e10189.
263. Klyubin, I.V., K.M. Kirpichnikova, and I.A. Gamaley, *Hydrogen peroxide-induced chemotaxis of mouse peritoneal neutrophils.* Eur J Cell Biol, 1996. **70**(4): p. 347-51.
264. Niethammer, P., C. Grabher, A.T. Look, and T.J. Mitchison, *A tissue-scale gradient of hydrogen peroxide mediates rapid wound detection in zebrafish.* Nature, 2009. **459**(7249): p. 996-999.
265. Moreira, S., B. Stramer, I. Evans, W. Wood, and P. Martin, *Prioritization of Competing Damage and Developmental Signals by Migrating Macrophages in the Drosophila Embryo.* Current Biology, 2010. **20**(5): p. 464-470.
266. Moldovan, L., N.I. Moldovan, R.H. Sohn, S.A. Parikh, and P.J. Goldschmidt-Clermont, *Redox Changes of Cultured Endothelial Cells and Actin Dynamics.* Circ Res, 2000. **86**(5): p. 549-557.
267. Abid, M.R., Z. Kachra, K.C. Spokes, and W.C. Aird, *NADPH oxidase activity is required for endothelial cell proliferation and migration.* FEBS Letters, 2000. **486**(3): p. 252-256.
268. Sadok, A., A. Pierres, L. Dahan, C. Prévôt, M. Lehmann, and H. Kovacic, *NADPH Oxidase 1 Controls the Persistence of Directed Cell Migration by a Rho-Dependent Switch of $\alpha 2/\alpha 3$ Integrins.* Mol Cell Biol, 2009. **29**(14): p. 3915-3928.
269. Lyle, A.N., N.N. Deshpande, Y. Taniyama, B. Seidel-Rogol, L. Pounkova, P. Du, C. Papaharalambus, B. Lassègue, and K.K. Griendling, *Poldip2, a Novel Regulator of Nox4 and Cytoskeletal Integrity in Vascular Smooth Muscle Cells.* Circ Res, 2009. **105**(3): p. 249-259.
270. Schröder, K., I. Helmcke, K. Palfi, K.-H. Krause, R. Busse, and R.P. Brandes, *Nox1 Mediates Basic Fibroblast Growth Factor-Induced Migration of Vascular Smooth Muscle Cells.* Arteriosclerosis, Thrombosis, and Vascular Biology, 2007. **27**(8): p. 1736-1743.
271. Lee, M.Y., A.S. Martin, P.K. Mehta, A.E. Dikalova, A.M. Garrido, S.R. Datla, E. Lyons, K.-H. Krause, B. Banfi, J.D. Lambeth, B. Lassègue, and K.K. Griendling, *Mechanisms of Vascular Smooth Muscle NADPH Oxidase 1 (Nox1) Contribution to Injury-Induced Neointimal Formation.* Arteriosclerosis, Thrombosis, and Vascular Biology, 2009. **29**(4): p. 480-487.
272. Hattori, H., K.K. Subramanian, J. Sakai, Y. Jia, Y. Li, T.F. Porter, F. Loison, B. Sarraj, A. Kasorn, H. Jo, C. Blanchard, D. Zirkle, D. McDonald, S.-Y. Pai, C.N. Serhan, and H.R. Luo, *Small-molecule screen identifies reactive oxygen species as key regulators of neutrophil chemotaxis.* Proceedings of the National Academy of Sciences, 2010. **107**(8): p. 3546-3551.

273. Ushio-Fukai, M., Y. Tang, T. Fukai, S.I. Dikalov, Y. Ma, M. Fujimoto, M.T. Quinn, P.J. Pagano, C. Johnson, and R.W. Alexander, *Novel Role of gp91phox-Containing NAD(P)H Oxidase in Vascular Endothelial Growth Factor-Induced Signaling and Angiogenesis*. *Circ Res*, 2002. **91**(12): p. 1160-1167.
274. Radisky, D.C., D.D. Levy, L.E. Littlepage, H. Liu, C.M. Nelson, J.E. Fata, D. Leake, E.L. Godden, D.G. Albertson, M. Angela Nieto, Z. Werb, and M.J. Bissell, *Rac1b and reactive oxygen species mediate MMP-3-induced EMT and genomic instability*. *Nature*, 2005. **436**(7047): p. 123-127.
275. Wang, Y., Q.S. Zang, Z. Liu, Q. Wu, D. Maass, G. Dulan, P.W. Shaul, L. Melito, D.E. Frantz, J.A. Kilgore, N.S. Williams, L.S. Terada, and F.E. Nwariaku, *Regulation of VEGF-induced endothelial cell migration by mitochondrial reactive oxygen species*. *American Journal of Physiology - Cell Physiol*, 2011. **301**(3): p. C695-C704.
276. Wu, R.F., Y.C. Xu, Z. Ma, F.E. Nwariaku, G.A. Sarosi, and L.S. Terada, *Subcellular targeting of oxidants during endothelial cell migration*. *J Cell Biol*, 2005. **171**(5): p. 893-904.
277. Ikeda, S., M. Yamaoka-Tojo, L. Hilenski, N.A. Patrushev, G.M. Anwar, M.T. Quinn, and M. Ushio-Fukai, *IQGAP1 Regulates Reactive Oxygen Species-Dependent Endothelial Cell Migration Through Interacting With Nox2*. *Arteriosclerosis, Thrombosis, and Vascular Biology*, 2005. **25**(11): p. 2295-2300.
278. Kaplan, N., N. Urao, E. Furuta, S.J. Kim, M. Razvi, Y. Nakamura, R.D. McKinney, L.B. Poole, T. Fukai, and M. Ushio-Fukai, *Localized cysteine sulfenic acid formation by vascular endothelial growth factor: role in endothelial cell migration and angiogenesis*. *Free Radic Res*, 2011. **45**(10): p. 1124-35.
279. Wu, R.F., Y. Gu, Y.C. Xu, F.E. Nwariaku, and L.S. Terada, *Vascular Endothelial Growth Factor Causes Translocation of p47phox to Membrane Ruffles through WAVE1*. *Journal of Biological Chemistry*, 2003. **278**(38): p. 36830-36840.
280. Woo, H.A., S.H. Yim, D.H. Shin, D. Kang, D.-Y. Yu, and S.G. Rhee, *Inactivation of Peroxiredoxin I by Phosphorylation Allows Localized H₂O₂ Accumulation for Cell Signaling*. *Cell*, 2010. **140**(4): p. 517-528.
281. Omann, G.M., J.M. Harter, J.M. Burger, and D.B. Hinshaw, *H₂O₂-Induced Increases in Cellular F-Actin Occur without Increases in Actin Nucleation Activity*. *Arch Biochem Biophys*, 1994. **308**(2): p. 407-412.
282. Zhao, Y. and H.W. Davis, *Hydrogen peroxide-induced cytoskeletal rearrangement in cultured pulmonary endothelial cells*. *J Cell Physiol*, 1998. **174**(3): p. 370-379.
283. Pastore, A., G. Tozzi, L.M. Gaeta, E. Bertini, V. Serafini, S.D. Cesare, V. Bonetto, F. Casoni, R. Carrozzo, G. Federici, and F. Piemonte, *Actin Glutathionylation Increases in Fibroblasts of Patients with Friedreich's*

Ataxia: A POTENTIAL ROLE IN THE PATHOGENESIS OF THE DISEASE.
Journal of Biological Chemistry, 2003. **278**(43): p. 42588-42595.

284. Rokutan, K., R.B. Johnston, and K. Kawai, *Oxidative stress induces S-thiolation of specific proteins in cultured gastric mucosal cells.* American Journal of Physiology - Gastrointestinal and Liver Physiology, 1994. **266**(2): p. G247-G254.
285. Drewes, G. and H. Faulstich, *The enhanced ATPase activity of glutathione-substituted actin provides a quantitative approach to filament stabilization.* Journal of Biological Chemistry, 1990. **265**(6): p. 3017-21.
286. Stournaras, C., G. Drewes, H. Blackholm, I. Merkler, and H. Faulstich, *Glutathionyl(cysteine-374) actin forms filaments of low mechanical stability.* Biochimica et Biophysica Acta (BBA) - Protein Structure and Molecular Enzymology, 1990. **1037**(1): p. 86-91.
287. Hastie, L.E., W.F. Patton, H.B. Hechtman, and D. Shepro, *Filamin Redistribution in an Endothelial Cell Reoxygenation Injury Model.* Free Radical Biology and Medicine, 1997. **22**(6): p. 955-966.
288. Hastie, L.E., W.F. Patton, H.B. Hechtman, and D. Shepro, *Metabolites of the phospholipase D pathway regulate H₂O₂-induced filamin redistribution in endothelial cells.* J Cell Biochem, 1998. **68**(4): p. 511-524.
289. Tonks, N.K., *Redox redux: revisiting PTPs and the control of cell signaling.* Cell, 2005. **121**(5): p. 667-70.
290. Nimnual, A.S., L.J. Taylor, and D. Bar-Sagi, *Redox-dependent downregulation of Rho by Rac.* Nat Cell Biol, 2003. **5**(3): p. 236-241.
291. Chiarugi, P., G. Pani, E. Giannoni, L. Taddei, R. Colavitti, G. Raugei, M. Symons, S. Borrello, T. Galeotti, and G. Ramponi, *Reactive oxygen species as essential mediators of cell adhesion: the oxidative inhibition of a FAK tyrosine phosphatase is required for cell adhesion.* J Cell Biol, 2003. **161**(5): p. 933-944.
292. Kumar, B., S. Koul, L. Khandrika, R.B. Meacham, and H.K. Koul, *Oxidative Stress Is Inherent in Prostate Cancer Cells and Is Required for Aggressive Phenotype.* Cancer Res, 2008. **68**(6): p. 1777-1785.
293. Szatrowski, T.P. and C.F. Nathan, *Production of Large Amounts of Hydrogen Peroxide by Human Tumor Cells.* Cancer Res, 1991. **51**(3): p. 794-798.
294. Bittinger, F., J.L. González-García, C.L. Klein, C. Brochhausen, F. Offner, and C.J. Kirkpatrick, *Production of superoxide by human malignant melanoma cells.* Melanoma Research, 1998. **8**(5): p. 381-387.
295. Devi, G.S., M.H. Prasad, I. Saraswathi, D. Raghu, D.N. Rao, and P.P. Reddy, *Free radicals antioxidant enzymes and lipid peroxidation in*

- different types of leukemias*. Clinica Chimica Acta, 2000. **293**(1-2): p. 53-62.
296. Patel, B.P., U.M. Rawal, T.K. Dave, R.M. Rawal, S.N. Shukla, P.M. Shah, and P.S. Patel, *Lipid Peroxidation, Total Antioxidant Status, and Total Thiol Levels Predict Overall Survival in Patients With Oral Squamous Cell Carcinoma*. Integrative Cancer Therapies, 2007. **6**(4): p. 365-372.
297. Toyokuni, S., K. Okamoto, J. Yodoi, and H. Hiai, *Persistent oxidative stress in cancer*. FEBS Letters, 1995. **358**(1): p. 1-3.
298. Jaruga, P., T.H. Zastawny, J. Skokowski, M. Dizdaroglu, and R. Olinski, *Oxidative DNA base damage and antioxidant enzyme activities in human lung cancer*. FEBS Letters, 1994. **341**(1): p. 59-64.
299. Iida, T., A. Furuta, M. Kawashima, J.-i. Nishida, Y. Nakabeppu, and T. Iwaki, *Accumulation of 8-oxo-2'-deoxyguanosine and increased expression of hMTH1 protein in brain tumors*. Neuro-Oncology, 2001. **3**(2): p. 73-81.
300. Tsao, S.-M., M.-C. Yin, and W.-H. Liu, *Oxidant Stress and B Vitamins Status in Patients With Non-Small Cell Lung Cancer*. Nutrition and Cancer, 2007. **59**(1): p. 8-13.
301. Ishikawa, K., K. Takenaga, M. Akimoto, N. Koshikawa, A. Yamaguchi, H. Imanishi, K. Nakada, Y. Honma, and J.-I. Hayashi, *ROS-Generating Mitochondrial DNA Mutations Can Regulate Tumor Cell Metastasis*. Science, 2008. **320**(5876): p. 661-664.
302. Indo, H.P., M. Davidson, H.-C. Yen, S. Suenaga, K. Tomita, T. Nishii, M. Higuchi, Y. Koga, T. Ozawa, and H.J. Majima, *Evidence of ROS generation by mitochondria in cells with impaired electron transport chain and mitochondrial DNA damage*. Mitochondrion, 2007. **7**(1-2): p. 106-118.
303. Vafa, O., M. Wade, S. Kern, M. Beeche, T.K. Pandita, G.M. Hampton, and G.M. Wahl, *c-Myc Can Induce DNA Damage, Increase Reactive Oxygen Species, and Mitigate p53 Function: A Mechanism for Oncogene-Induced Genetic Instability*. Mol Cell, 2002. **9**(5): p. 1031-1044.
304. Dang, C.V., A. Le, and P. Gao, *MYC-Induced Cancer Cell Energy Metabolism and Therapeutic Opportunities*. Clinical Cancer Research, 2009. **15**(21): p. 6479-6483.
305. Kopnin, P.B., L.S. Agapova, B.P. Kopnin, and P.M. Chumakov, *Repression of Sestrin Family Genes Contributes to Oncogenic Ras-Induced Reactive Oxygen Species Up-regulation and Genetic Instability*. Cancer Res, 2007. **67**(10): p. 4671-4678.
306. Hussain, S.P., P. Amstad, P. He, A. Robles, S. Lupold, I. Kaneko, M. Ichimiya, S. Sengupta, L. Mechanic, S. Okamura, L.J. Hofseth, M. Moake, M. Nagashima, K.S. Forrester, and C.C. Harris, *p53-Induced Up-Regulation of MnSOD and GPx but not Catalase Increases Oxidative Stress and Apoptosis*. Cancer Res, 2004. **64**(7): p. 2350-2356.

307. Tan, M., S. Li, M. Swaroop, K. Guan, L.W. Oberley, and Y. Sun, *Transcriptional Activation of the Human Glutathione Peroxidase Promoter by p53*. *Journal of Biological Chemistry*, 1999. **274**(17): p. 12061-12066.
308. Kamiguti, A.S., L. Serrander, K. Lin, R.J. Harris, J.C. Cawley, D.J. Allsup, J.R. Slupsky, K.-H. Krause, and M. Zuzel, *Expression and Activity of NOX5 in the Circulating Malignant B Cells of Hairy Cell Leukemia*. *The Journal of Immunology*, 2005. **175**(12): p. 8424-8430.
309. Fukuyama, M., K. Rokutan, T. Sano, H. Miyake, M. Shimada, and S. Tashiro, *Overexpression of a novel superoxide-producing enzyme, NADPH oxidase 1, in adenoma and well differentiated adenocarcinoma of the human colon*. *Cancer Lett*, 2005. **221**(1): p. 97-104.
310. Lim, S.D., C. Sun, J.D. Lambeth, F. Marshall, M. Amin, L. Chung, J.A. Petros, and R.S. Arnold, *Increased Nox1 and hydrogen peroxide in prostate cancer*. *The Prostate*, 2005. **62**(2): p. 200-207.
311. Weyemi, U., B. Caillou, M. Talbot, R. Ameziane-El-Hassani, L. Lacroix, O. Lagent-Chevallier, A. Al Ghuzlan, D. Roos, J.-M. Bidart, A. Virion, M. Schlumberger, and C. Dupuy, *Intracellular expression of reactive oxygen species-generating NADPH oxidase NOX4 in normal and cancer thyroid tissues*. *Endocrine-Related Cancer*, 2010. **17**(1): p. 27-37.
312. Brar, S.S., T.P. Kennedy, A.B. Sturrock, T.P. Huecksteadt, M.T. Quinn, A.R. Whorton, and J.R. Hoidal, *An NAD(P)H oxidase regulates growth and transcription in melanoma cells*. *American Journal of Physiology - Cell Physiolog*, 2002. **282**(6): p. C1212-C1224.
313. Zhang, B., Z. Liu, and X. Hu, *Inhibiting cancer metastasis via targeting NADPH oxidase 4*. *Biochemical Pharmacology*, 2013. **86**(2): p. 253-266.
314. Peng, D.-F., T.-L. Hu, B.G. Schneider, Z. Chen, Z.-K. Xu, and W. El-Rifai, *Silencing of Glutathione Peroxidase 3 through DNA Hypermethylation Is Associated with Lymph Node Metastasis in Gastric Carcinomas*. *PLoS One*, 2012. **7**(10): p. e46214.
315. Nishikawa, M., A. Tamada, H. Kumai, F. Yamashita, and M. Hashida, *Inhibition of experimental pulmonary metastasis by controlling biodistribution of catalase in mice*. *International Journal of Cancer*, 2002. **99**(3): p. 474-479.
316. Ishikawa, K., H. Imanishi, K. Takenaga, and J.-I. Hayashi, *Regulation of metastasis; mitochondrial DNA mutations have appeared on stage*. *Journal of Bioenergetics and Biomembranes*, 2012. **44**(6): p. 639-644.
317. Kim, E.-Y., J.-M. Seo, C. Kim, J.-E. Lee, K.-M. Lee, and J.-H. Kim, *BLT2 promotes the invasion and metastasis of aggressive bladder cancer cells through a reactive oxygen species-linked pathway*. *Free Radical Biology and Medicine*, 2010. **49**(6): p. 1072-1081.

318. Ferraro, D., S. Corso, E. Fasano, E. Panieri, R. Santangelo, S. Borrello, S. Giordano, G. Pani, and T. Galeotti, *Pro-metastatic signaling by c-Met through RAC-1 and reactive oxygen species (ROS)*. *Oncogene*, 2006. **25**(26): p. 3689-3698.
319. Fitzgerald, J.P., B. Nayak, K. Shanmugasundaram, W. Friedrichs, S. Sudarshan, A.A. Eid, T. DeNapoli, D.J. Parekh, Y. Gorin, and K. Block, *Nox4 Mediates Renal Cell Carcinoma Cell Invasion through Hypoxia-Induced Interleukin 6- and 8- Production*. *PLoS One*, 2012. **7**(1): p. e30712.
320. Liang, C.C., A.Y. Park, and J.L. Guan, *In vitro scratch assay: a convenient and inexpensive method for analysis of cell migration in vitro*. *Nat Protoc*, 2007. **2**(2): p. 329-33.
321. Zheng, M., F. Aslund, and G. Storz, *Activation of the OxyR transcription factor by reversible disulfide bond formation*. *Science*, 1998. **279**(5357): p. 1718-21.
322. Belousov, V.V., A.F. Fradkov, K.A. Lukyanov, D.B. Staroverov, K.S. Shakhbazov, A.V. Terskikh, and S. Lukyanov, *Genetically encoded fluorescent indicator for intracellular hydrogen peroxide*. *Nat Methods*, 2006. **3**(4): p. 281-6.
323. Wright, L.P. and M.R. Philips, *Thematic review series: lipid posttranslational modifications. CAAX modification and membrane targeting of Ras*. *J Lipid Res*, 2006. **47**(5): p. 883-91.
324. Eaton, P., *Protein thiol oxidation in health and disease: techniques for measuring disulfides and related modifications in complex protein mixtures*. *Free Radic Biol Med*, 2006. **40**(11): p. 1889-99.
325. Allison, W.S., *Formation and reactions of sulfenic acids in proteins*. *Acc Chem Res*, 1976. **9**(8): p. 293-299.
326. Cooper, J., S. Walker, and T. Pollard, *Pyrene actin: documentation of the validity of a sensitive assay for actin polymerization*. *Journal of Muscle Research & Cell Motility*, 1983. **4**(2): p. 253-262.
327. Pope, B.J., K.M. Zierler-Gould, R. Kuhne, A.G. Weeds, and L.J. Ball, *Solution structure of human cofilin: actin binding, pH sensitivity, and relationship to actin-depolymerizing factor*. *J Biol Chem*, 2004. **279**(6): p. 4840-8.
328. Poole, L.B. and K.J. Nelson, *Discovering mechanisms of signaling-mediated cysteine oxidation*. *Curr Opin Chem Biol*, 2008. **12**(1): p. 18-24.
329. Block, K. and Y. Gorin, *Aiding and abetting roles of NOX oxidases in cellular transformation*. *Nat Rev Cancer*, 2012. **12**(9): p. 627-37.
330. Paavilainen, V.O., E. Oksanen, A. Goldman, and P. Lappalainen, *Structure of the actin-depolymerizing factor homology domain in complex with actin*. *J Cell Biol*, 2008. **182**(1): p. 51-9.

331. Dolinsky, T.J., J.E. Nielsen, J.A. McCammon, and N.A. Baker, *PDB2PQR: an automated pipeline for the setup of Poisson-Boltzmann electrostatics calculations*. *Nucleic Acids Res*, 2004. **32**(2): p. W665-7.
332. Schuttelkopf, A.W. and D.M. van Aalten, *PRODRG: a tool for high-throughput crystallography of protein-ligand complexes*. *Acta Crystallogr D Biol Crystallogr*, 2004. **60**(8): p. 1355-63.
333. Baker, N.A., D. Sept, S. Joseph, M.J. Holst, and J.A. McCammon, *Electrostatics of nanosystems: application to microtubules and the ribosome*. *Proc Natl Acad Sci U S A*, 2001. **98**(18): p. 10037-41.
334. Albiges-Rizo, C., O. Destaing, B. Fourcade, E. Planus, and M.R. Block, *Actin machinery and mechanosensitivity in invadopodia, podosomes and focal adhesions*. *J Cell Sci*, 2009. **122**(17): p. 3037-49.
335. Gu, J., C.W. Lee, Y. Fan, D. Komlos, X. Tang, C. Sun, K. Yu, H.C. Hartzell, G. Chen, J.R. Bamberg, and J.Q. Zheng, *ADF/cofilin-mediated actin dynamics regulate AMPA receptor trafficking during synaptic plasticity*. *Nat Neurosci*, 2010. **13**(10): p. 1208-1215.

